Geochemistry International, Vol. 42, Suppl. 1, 2004, pp. S1–S157.

COMAGMAT: Development of a Magma Crystallization Model and Its Petrological Applications

A. A. Ariskin and G. S. Barmina

Vernadsky Institute of Geochemistry and Analytical Chemistry, Russian Academy of Sciences, ul. Kosygina 19, Moscow, 119991 Russia

Received April 10, 2003

Abstract—This publication summarizes the results of petrologic studies aimed at the development and application of computer models simulating equilibrium and fractional crystallization in igneous systems of mafic to intermediate composition. The empiric and thermodynamic basis for the mineral-melt equilibria calculations is given in detail, including descriptions of the algorithm used in the COMAGMAT program to simulate both perfect and partial magma fractionation. New techniques are presented for the genetic interpretation of igneous rocks from large layered intrusions and Siberian sills and volcanic rocks from the Mid-Atlantic Ridge and Eastern Kamchatka. Using the COMAGMAT crystallization model, a set of low-pressure phase equilibria calculations (called *Geochemical Thermometry*) was conducted for the most primitive rocks from the Marginal Series and the Lower Zones of differentiated intrusions (Partridge River and Talnakh) and large layered complexes, such as Skaergaard, Kiglapait, and Yoko-Dovyren. This allowed us to define the range of initial temperatures (1165–1230°C) and the intercumulus melt compositions intrinsic to the original crystal mush from which the contact rocks crystallized. Simultaneously, we estimated the original mineral–melt proportions for the parental intrusive magmas. These modal proportions indicate that the magmatic suspensions could contain from a few percent (Siberian traps) to 15–25% (Talnakh and Kiglapait) and even 50–60% crystals (Yoko-Dovyren and Partridge River intrusions). Moreover, an impressive potential of a special sort of *Geochemical Thermometry* was demonstrated, which was designed for the interpretation of differentiated intrusion rocks. Based on the results of the modeling of phase equilibria for 65 rocks from the Layered Series of the Skaergaard intrusion, the first evaluations were obtained for the range of the intercumulus liquid temperatures (1145 to 1085°C) and oxygen fugacities (from 1–1.5 log units above QFM to slightly below QFM). The calculated average major-element compositions of the residual liquids demonstrate a trend of continual enrichment in FeO (up to ~18 wt %) and TiO_2 (up to ~5.5 wt %) with only minor variations in the SiO_2 contents (48 to 50 wt %) for the rocks from LZa to UZa. Using the ability of COMAGMAT-3.5 to calculate more accurately the crystallization of magnetite and ilmenite, the effect of oxygen fugacity on basalt magma fractionation trends was studied numerically. The application of this program to the tholeiitic series of Chazhma Sill in Eastern Kamchatka, Russia, points to an oxygen fugacity near NNO + 0.5. The numerical simulation of the fractional crystallization of an iron-enriched basaltic andesite parent under these oxidizing conditions accurately reproduced the FeO–SiO_2 relations observed in the Chazhma suite. Another example of the modeling of basalt magma fractionation includes polybaric calculations simulating the formation of tholeiitic glasses from the Mid-Atlantic Ridge. A decompression version of COMAGMAT was applied to the genetic interpretation of the volcanic suite of Klyuchevskoi volcano, Kamchatka. To identify the processes responsible for the origin of the suite, which is composed of rocks ranging from high-magnesia to high-alumina basalts, we used the model to simulate the isobaric crystallization of a parental HMB magma at a variety of pressures and conducted a separate set of simulations assuming fractionation during continuous magma ascent from a depth of 60 km. These results provide evidence that the Klyuchevskoi trend could be caused by ~40% fractionation of the *Ol–Aug*–Sp ± *Opx* assemblage during the ascent of the parental HMB magma within a pressure range of 19–7 kbar at 1350–1110°C. The decompression rate was estimated at 0.33 kbar/% crystallized, with ~2 wt % H_2O in the initial melt and ~3 wt % H_2O in the resultant high-Al basalt.

CONTENTS

EDITOR'S PREFACE

This publication is devoted to the problems of basaltic magma differentiation and the methods proposed to assay the role of these processes in the formation of a diversity of igneous rocks. These problems involve the identification of the principal differentiation mechanisms in magmatic systems and the evaluation of the thermodynamic and dynamic conditions under which these processes occur. In solving these problems, principal importance should be attached to the possibilities of calculating melt–mineral equilibria in systems corresponding to the original (parental) and derivative melts. Progress in this field is closely related to the application of modern magma crystallization models to igneous petrology problems (COMAGMAT, MELTS, MINXFRAC, and other computer programs). These models enable simulating changes in the phase proportions and the chemistry of minerals in the process of fractional and equilibrium crystallization of natural melts, which, in turn, makes it possible to quantify the effects of external factors on the chemical evolution of the melts. When a program for the calculation of melt–mineral equilibria can be combined with the description of the melt differentiation dynamics, the possibility arises of directly simulating the succession of formation and the inner structures of magmatic bodies. This puts forth new problems of theoretical and applied petrology, including the analysis of various dynamic regimes of fractionation, principles of elaboration and calibration of crystallization models, tuning of methodical approaches to the use of computer programs, and interpretation of the modeling results.

Studies in this field were launched in the 1970s by a research team at the Vernadsky Institute of Geochemistry and Analytical Chemistry, Russian Academy of Sciences, and the Department of Geochemistry at Moscow State University, which dealt with the differentiation mechanisms of basaltic magmas. Over the years that have elapsed since this time, these researchers have traveled an arduous path from developing, analyzing, and the first attempts of applying simplified models for the crystallization of basalts to the development of a comprehensive system for modeling magmatic processes. Now this system is represented in the form of a package of computer programs, including a database of experimental results on melt–crystal equilibria in igneous rocks (INFOREX), calibrating procedures of mineral–melt thermometers, numerical models for crystallization processes, and algorithms for modeling crystallization dynamics in the chamber. Simultaneously new techniques were developed for genetic interpretations of volcanic and intrusive rocks on the basis of these models. This publication presents a generalized experience in their application to diverse rocks and objects of magmatic origin.

In this publication, much attention is paid to the fundamentals of the development and methodical approaches to handling the COMAGMAT computer model. This program has received wide recognition among petrologists and is currently actively used at many research centers both in Russia and abroad. For about 15 years, the COMAGMAT program has been employed for the teaching of students and postgraduates majoring in geochemistry and petrology at Moscow State University. Starting in 1996, the program has also been utilized as an aid in the educational course *Modeling of Magmatic Systems* at Novosibirsk State University. The active practical application of this computational model inevitably poses questions as to whether its usage is justified for a given compositional range, what the accuracy of the estimated crystallization parameters is, and how reliable the petrological interpretations are. The illustrative examples of genetic reconstructions presented below for a variety of intrusive and volcanic basites offer answers to many of these questions.

I.D. Ryabchikov

NOTATION

Indices Used Frequently in the Text

i chemical element (n is the number of components)

j mineral (m is the number of minerals)

r end member

s general designation of the solid phase

l melt

Intensive Parameters

T temperature of equilibrium (crystallization) in the system

T^j_{dry} temperature of equilibrium between melt and mineral j in a dry system

$T^j_{H_2O}$ temperature of equilibrium between melt and mineral j in a hydrous system

P pressure

f_{O_2} oxygen fugacity

C_i weight concentration of element i (with superscript indices j, s, or l)

$x_i^{l/s}$ weight or molar concentration of element (component) i

C_{H_2O} weight concentration of water in melt

Some Extensive Parameters

$W^{l/s}$ mass of melt or solid phase

F^s_j bulk weight proportions of mineral phases in the system

F_l weight fraction of melt in the system

F^0_j, F^0_l original (primary) proportions of minerals and melt

f_j^s weight proportions of crystallizing minerals

Partition and Equilibrium Constants

D_i^j weight partition coefficient of element *i* between mineral *j* and melt

K_i^j molar partition coefficient of element *i*

K_i weighted mean (bulk) partition coefficient of element *i* between the solid phase and melt

K_D exchange equilibrium constant (co-crystallization coefficient)

K_{eq} equilibrium constant of a chemical reaction

K_r^j equilibrium constant of the crystallization reaction of component *r* in mineral *j*

Empirical Parameters

A_r^j, B_r^j regression coefficients of mineral–melt geothermometers

β_r^j coefficients accounting for the pressure effect on the crystallization temperatures

λ_j proportionality coefficients accounting for the effect of H_2O

Thermodynamic Notation

ϕ phases of the system (Φ is the total number of phases)

G Gibbs free energy

ΔG difference in the Gibbs free energy of the system in a reaction

ΔH difference in the enthalpy of the system in a reaction

ΔS difference in the entropy of the system in a reaction

ΔV difference in the volume in a crystallization reaction

R gas constant

$\nu_{i(r)}^j$ stoichiometric coefficients of a crystallization reaction for component *r* in mineral *j*

$a_{i/r}^{l/j}$ activities of components in melt or minerals

$x_{i/r}^{l/j}$ concentrations of components in melt or minerals

$\gamma_{i/r}^{l/j}$ activity coefficients of components

$\mu_{i/r}^{l/j}$ chemical potentials of components in melt or mineral

$N_{i/r}^{l/j}$ numbers of moles of components of melt or mineral

N_l number of melt moles

N_j number of moles of mineral *j* in the system

x_j^s mole proportions of crystallization of minerals

T_r^j predicted temperature of equilibrium with melt for component *r* in mineral *j*

ε_T accuracy of temperature calculation with the COMAGMAT model

ε_i^l accuracy of the calculation of the melt composition with the COMAGMAT model

Minerals and Components of Solid Solutions

Pl plagioclase (*Or*—orthoclase, *Ab*—albite, and *An*—anorthite)

Ol olivine (*Fa*—fayalite and *Fo*—forsterite)

Px1 high-Ca pyroxene (for early crystallization models)

Px2 low-Ca pyroxene (for early crystallization models)

Px general designation for pyroxenes

Cpx clinopyroxene (*Di*—diopside)

Aug augite (*Fs*—ferrosilite, *En*—enstatite, and *Wo*—wollastonite)

Pig pigeonite

Opx orthopyroxene

Sp spinel (chromite)

Mt magnetite (*Mag*—Fe_3O_4 and *Ulv*—Fe_2TiO_4)

Ilm ilmenite (*Hem*—Fe_2O_3 and *Il*—$FeTiO_3$)

Characteristics of Fractionation Processes

f^s melt fractionation factor

φ_{cr} degree of fractionation (crystallization) of melt

$\Delta\varphi_{cr}$ fractionation increment

$\partial P/\partial\varphi$ decompression rate of crystallizing melt

F_{mag} magma crystallinity

F_{cum} bulk fraction of primary cumulus minerals

$(1 - F_{cum})$ cumulus porosity

Other Symbols

NF network-forming components

NM network-modifying components

MGN Mg number = $100 \times MgO/(MgO + Fe^{2+}O)$

OLIV, PLAG, QTZ, CPX, AN, AB components used in projecting melt (system) compositions into phase diagrams

$Fe_{ox} = Fe^{3+}/(Fe^{3+} + Fe^{2+})$ bulk degree of Fe oxidation in melt

$Fe(II) = Fe^{2+}/(Fe^{3+} + Fe^{2+})$ bulk degree of Fe reduction in melt

IW, WM, QFM, NNO oxygen buffers

CHAPTER 1. PRINCIPLES OF DESIGNING MODELS TO SIMULATE MAGMA CRYSTALLIZATION

1.1. Understanding the Concepts of Magma and Magmatic Melt

The term *magma* is often defined in the reference literature as "…a molten hot substance (commonly of silicate composition) that is produced in the Earth's crust or upper mantle and gives rise to igneous rocks upon its solidification." [*Geological Dictionary*, 1978]. This definition highlights three aspects concerning the composition, state, and rock-forming role of magma in geological processes. The geological role of magmas is of a principal character and was emphasized by most researchers. Some disagreements pertain only to the phase composition and rheology of these complicated natural materials. Kuznetsov [1990] noted that magmas can be physically homogeneous (silicate melt ± dissolved volatile components) or, more often, heterogeneous (melt + crystals) systems, whose "characteristic feature is massive fluidity, a characteristic attained when the mixture contains more than 25% liquid." Modern discussions about the state of magmas are focused on the permissible proportions of crystals and melt that predetermine the fluidity of magma [Sharapov *et al.*, 1997].

The heterogeneity of the phase composition of magma is manifested as an uneven distribution of crystalline material from the solidification boundary inward the magma conduit or magma chamber, which makes it possible to subdivide the contact zone into at least two parts [Sinton *et al.*, 1992; Jaupart and Tait, 1995]. Near the solidus surface, a zone with a low melt concentration develops, with the melt filling the space between osculating crystals (so-called rigidus). Some rheological properties of this mixture are similar to those of a solid material, but it does not lose its plasticity. As the fraction of crystals in the rigidus zone decreases, it grades into a zone of crystal mush and, further, to a magmatic suspension, which contains less than 25% of the solid phase [Marsh, 1989a]. Some researchers believe that the rheological boundary between the rigidus and crystal mush corresponds to a drastic (by a few orders of magnitude) change in the dynamic viscosity at a concentration of the crystalline material of approximately 50–60 vol % [Bergantz, 1990; Sharapov *et al.*, 1997]. This value is referred to as the critical crystallinity of magma F_{mag} [Marsh, 1989a]. The content of the complementary (or residual) liquid is the fraction of the critical melt (see, for example, [Renner *et al.*, 2000]). Hence, magmas can be regarded as heterogeneous systems containing crystals and/or their aggregates in amounts below the maximum possible crystallinity. The liquid constituent of magma is referred to as magmatic melt.

The determination of the composition of initial and derivative magmatic melts is of paramount importance for genetic interpretations of magmatic rocks. The problem is further complicated by the paucity of direct information on the composition of the liquid constituent of magmatic materials, because of which magmatic liquids are commonly approximated by vitreous or aphyric rock varieties. If the rocks and cumulates are highly crystalline, the composition of the intercumulus melt is calculated from the whole-rock compositions of the samples with the use of various techniques (see Chapter 3).

New possibilities were opened with progress in studying melt inclusions, which yield estimates for the composition and temperature of the silicate liquid entrapped by a host mineral at the front of the growing crystal. It was established that, in certain instances, the chemistry of these inclusions satisfactorily approximates the compositions of the comagmatic quenched glasses and, thus, can be employed as a model of natural magmatic melts (see, for example, [Sobolev, 1996]). At the same time, the development of more accurate and sensitive analytical techniques with a high spatial resolution enables the identification of diverse and often strongly contrasting compositional heterogeneities of melt inclusions contained not in the same samples but also in a single crystal. These observations provide the basis for subdividing microinclusions into provisional groups that represent "integral" and "differential" melts (according to A.V. Sobolev's terminology). Integral melts are believed to be those entraining crystalline products to the surface and producing natural magmatic rocks after crystallization. Differential melts are interpreted as representing the "genuine" diversity of the initial magmatic liquids, with the scatter of their compositions explained by the crystallization of the phenocrysts in discrete portions of the magmatic system. According to this hypothesis, integral melts are the products of mixing of initial liquids in magma-generation zones and magma conduits.

Hence, the compositional variations identified in inclusions (which are a few tens of microns in size) are regarded as providing a "record" of megascopical heterogeneities and large-scale processes of mass transfer in magma chambers. This interpretation implies that drastic changes in the concentrations of some major and trace elements can be considered as specific "geochemical signals" that mark distinct geodynamic environments in the crust and mantle. The researchers were cautioned about using the compositions of natural rocks for devising petrological models if these rocks exhibit no compositional changes of this kind and, thus, are less informative than melt inclusions [Sobolev, 2002]. This approach has received ever widening recognition and seems to be appealing as warranting a decrease in the volume of geological work and the amount of petrological materials employed.

However, the chemical characteristics of microscopical objects could hardly be preserved unchanged during the evolution and cooling of magmatic masses. Because of this, the degrees of modification of the com-

positions of primary inclusions and the role of the boundary layer are assayed with the use of experimental data on phase equilibria and the diffusion of components in the system melt–crystals [Nakamura and Shimakita, 1998; Zhang, 1998; Danyushevsky *et al.*, 2000; Agoshkov, 2002]. Unfortunately, information of this kind is still too scarce (and pertains mostly to systems with *Ol* as the host mineral) to provide a comprehensive picture of the redistributions of main elements during the capture and transformations of melt inclusions.

The problem of the nature of the heterogeneous (sometimes highly contrasting) redistribution of minor elements in these objects remains unsettled as of yet, although it seems to be appealing to relate the drastic compositional changes to the occurrence of compositionally contrasting magmatic liquids supposedly entrapped by growing crystals. Analysis of the systematics of major and trace elements indicates that geochemical deviations (such as "ultradepleted" REE patterns, drastic changes in Sr concentrations, etc.) sometimes reflect reactions between the initial magmas and low-temperature crystallization products in magma conduits [Danyushevsky *et al.*, 2003].

Here we focus on these issues because petrological criteria for distinguishing between "initial melts" and their mixing products are still not developed in detail, while the volume of geochemical data on the composition of inclusions is rapidly increasing. In this situation the researchers are prone to identify the compositions of melt inclusions (as microscopical objects) with the compositions of natural melts (as rock-forming systems). We believe that this identity should be justified in every given instance with the use of specialized approaches (see, for example, [Danyushevsky *et al.*, 2002; Gaetani *et al.*, 2002]).

In the context of materials presented in this publication, it is pertinent to mention that this research was centered mainly on transporting and intercumulus melts, which are represented by natural rocks and magmatic bodies of significant volume. Because of this, in thermodynamic modeling and reproducing the conditions under which basites are produced, we commonly used the bulk compositions of subaphyric and vitreous rocks or the predicted compositions of magmatic liquids, calculated based on the mass balance. In rare situations when the compositions of primitive melt inclusions were consistent with the data of petrological and geochemical observations, these compositions were also utilized in the calculations. Details of the choice are discussed below in the sections devoted to the geochemical thermometry of intrusive basites (Chapter 3) and techniques for interpreting the genesis of volcanic and subvolcanic rocks (Chapters 4 and 5).

1.2. Techniques for Studying Fractional Crystallization

The concept of primitive melt fractionation proposed by Bowen predetermined the main avenues for the development of igneous petrology throughout the whole 20th century. Until now no alternative physicochemical mechanisms had been proposed that could account as consistently as this concept for (1) the direction of the petrochemical trends of magmatic series, (2) the succession of mineral assemblages observed in the rocks, (3) the systematic variations in the chemistry of these minerals, (4) the evolution in the concentrations of trace elements, and (5) the petrogenetically significant variations in the chemistry of melt inclusions. However, modern interpretations of fractional crystallization are remarkably different from the examples quoted by Bowen [1928]. Now the term *Crystallization fractionation* is understood much more broadly, namely, as "the integral result of the fractionation of components in magma that is convectively unstable" [Sharapov and Cherepanov, 1986]. Thus, petrologists are focusing their attention on additional factors of magmatic evolution in convection regimes that determine the possibility for the trends of natural rocks to deviate from the trajectories expected to result from perfect fractional crystallization.

There are numerous lines of evidence demonstrating that the fractionation nature of crystallization processes is caused by the interplay of a diversity of differentiation mechanisms, which involve not only the gravitational sorting of crystals and melt but also the assimilation of the host rocks by the magma, mixing of derivative melts, or crystallization at periodical magma replenishment in the chamber [O'Hara and Mathews, 1981; DePaolo, 1981; Grove *et al.*, 1982; Kelemen, 1990]. Attempts to numerically simulate the process of magma crystallization with regard for these additional factors are limited to simple numerical schemes proceeding from the principle of addition or subtraction of components. Nevertheless, the analysis of these AFC models demonstrates that the integral chemical effect of "combined fractionation" may be only slightly different from the results of perfect fractional crystallization [Nielsen, 1990]. There are two explanations for this phenomenon.

First, the analysis of convection phenomena during magma differentiation leads to the important conclusion that the processes of perfect fractionation occur when vigorous sedimentation convection (in the form of oppositely directed suspension flows [Frenkel *et al.*, 1988, 1989; Trubitsyn and Kharybin, 1997]) dominates over phase convection [Frenkel *et al.*, 1995], which includes the Stokes settling of crystalline individuals or the porous infiltration of the interstitial melt (compositional convection) [Tait and Jaupart, 1992; Jaupart and Tait, 1995]. This implies that most magma chambers and conduits are characterized by low to moderate magma crystallinity, $F_{mag} < 0.5$, active stirring, and the absence of any significant temperature gradients within the reservoir. The second cause of the resistance of crystallization trends to the effects of the accompanying processes is caused by the fact that the chemical

evolution of the magma is controlled by the general topology of the respective phase diagram.

It follows that the presence of a realistic model for phase equilibria in basaltic magmas and for their differentiation is an important element in devising and analyzing physicochemical schemes of magmatic differentiation. This condition gains a decisive role in the modeling of natural fractionation processes, particularly considering that these processes are controlled by multiple factors, the possibility of incomplete separation of the crystals and melt, and the diversity of the thermodynamic regimes of crystallization. Below we will discuss some approaches to the description of fractionating systems and offer algorithms modeling the fractional and equilibrium crystallization of basaltic magmas.

1.2.1. Subtraction diagrams and simple mass-balance calculations

As an example illustrating the plausibility of the fractional crystallization hypothesis, Bowen [1928] presented the results of interpreting the basaltic associations from the Island of Mull, Hebrides [Baily *et al.*, 1924]. These basalts were subdivided into two major types: a "plateau type" (~45 wt % SiO_2 and 8 wt % MgO) and a "central aphyric type" (50 wt % SiO_2 and 5 wt % MgO). Later these types were redefined as olivine and tholeiitic basalts [Kennedy, 1933]. Bowen hypothesized that the parental magma had an olivine basaltic composition, and tholeiitic melts could be derived from it by means of subtracting (i.e., crystallization) of SiO_2-depleted crystalline material. To evaluate the composition of this material, it was proposed to use *subtraction diagrams* (Fig. 1). As was eventually demonstrated, the composition of the "crystallizing components" is identical to that of a mixture of *Pl*, *Ol*, *Cpx*, and *Mt* crystals taken in the approximate proportion of 52 : 27 : 7 : 4. These were the minerals observed in the "plateau" rocks and ascribed, based on petrographic evidence, to early crystallizing phases [Baily *et al.*, 1924]. These data led to the conclusion that the transition between the magmas resulted from the predominant settling of plagioclase and olivine crystals, and the silica enrichment observed in the tholeiitic basalts reflects reaction relations between olivine and magmatic melt.

We quoted this example because, in fact, this was the very first attempt by petrologists to evaluate the results of basaltic magma fractionation using the graphical method of subtracting solid phases from the system. In compliance with the modern terminology, this approach should be ascribed to techniques for solving inverse geochemical problems: Bowen proceeded from the mass-balance method to evaluate the bulk chemical composition of the subtracted (crystalline) component and then recalculated it into the proportions of the observed minerals.

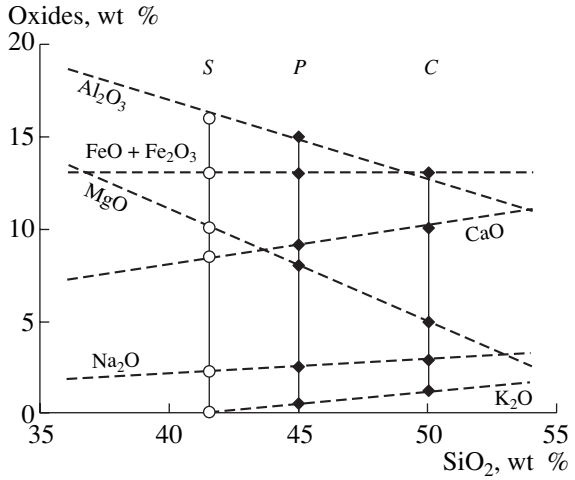

Fig. 1. Subtraction diagrams for magmas of the "plateau type" (*P*) and "central aphyric type" from Mull Island (*C*) [Bowen, 1928]. Composition *S* corresponds to the deduced component, which can be represented as a mixture of *Pl*, *Ol*, *Cpx*, and *Mt* crystals.

Later years witnessed broad recognition of another method for the "inverse modeling" of fractional crystallization with the use of a specified set of mineral phases and their compositions [Wright and Doherty, 1970]. This approach is underlain by the solution of systems of linear mass-balance equations for a selected succession of chemical elements i and crystallizing minerals j ($1 \le j \le m$)

$$C_l^i = \sum_{j=1}^{m} C_j^i f_j + C_d^i f_d, \qquad (1)$$

where C_l^i is the assumed composition of the initial melt (for which a relatively "primitive" rock sample is selected); C_d^i is the assumed composition of the derivative, i.e., a rock or melt that could be produced by the fractionation of the specified source; C_j^i and C_d^i are the concentrations of element i in mineral j and the derivative; and f_j and f_d are the desired proportions of the crystallizing minerals and derivative (wt %).

Indicators of the satisfactory quality of the calculations are positive values of $f_j > 0$, the sum of the phases close to unity ($\sum f_j + f_d \approx 1$), and discrepancies for each element $\sum R_i^2 < 1$, which are determined as the differences between the specified and calculated compositions of the initial melt. The fulfillment of the aforementioned conditions is usually considered to validate the fractionation hypothesis [Wright and Doherty, 1970]. Calculations of this type have been crucial for understanding the fractionation of basaltic magmas and, in a sense, were prototypes of semiempirical fractional crystallization models developed in the 1970s

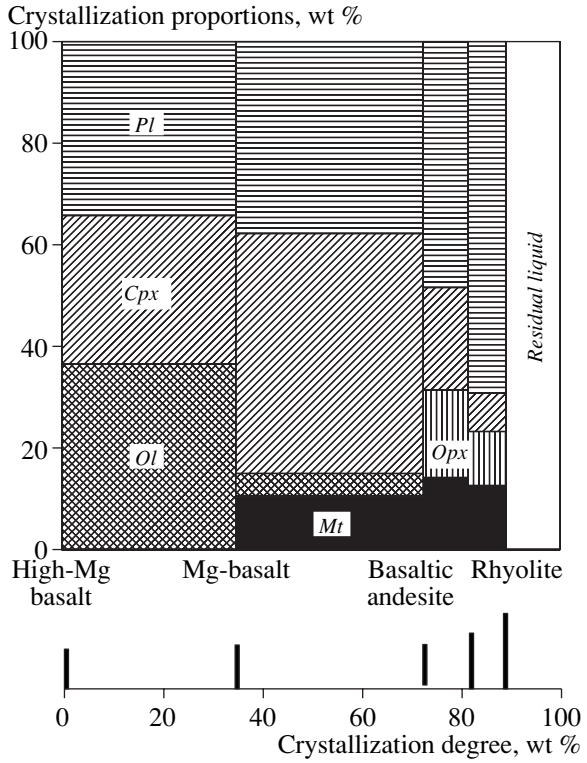

Fig. 2. Proportions of minerals crystallizing over specified intervals of fractionation of the high-Mg magma assumed to be parental to the tholeiitic series in Iceland [Polyakov and Muravieva, 1981].

and early 1980s [Drake, 1976a; Longhi, 1977; Nathan and Vankirk, 1978; French and Cameron, 1981; Ariskin and Frenkel, 1982; Petitpierre and Boivin, 1983].

At the same time, these fractionation models based on least squares techniques exhibit an obvious disadvantage. The solution of systems of mass balance equations is a mathematical procedure that does not ensure a consistency between the compositions calculated with these techniques and experimental data on mineral–melt equilibria. This forces the researcher to assume the constancy of the mineral compositions and crystallization proportions over broad range of fractionation (this approach usually leads to the subdivision of the differentiation succession into four or five stages, Fig. 2). Obviously, making these assumptions, petrologists often cannot decide unambiguously, based only on the discrepancies in the solutions for individual elements, whether the magma fractionation process took place. This disadvantage of simple mass-balance techniques can be illustrated by the end of the story about Bowen's interpretations of genetic relationships in the Mull basaltoids (Fig. 1). The interpretations of olivine and tholeiitic basalts on the basis of a more detailed examination of their geochemistry indicate that the former rocks should have given rise to alkaline, but not tholeiitic, rock series, whose end members are mugearites [Kennedy, 1933; Sheinmann, 1968].

Another disadvantage of this method involves the ambiguity of the interpretations of the nature of genetic relationships in the source–derivative system, even if the values of the overall discrepancies of the inverse-problem solutions are small. In particular, when the least squares technique is applied to problems of phonolite genesis, there is always an alternative of partial melting and fractional crystallization of the same source of alkaline basaltic composition [Hay and Wendlandt, 1995]. This is caused by the fact that the "optimal" proportions of mineral phases linking the parental and derivative compositions can also be formally interpreted as proportions of either the melting or the fractionation of minerals.

It follows that realistic models of the fractional crystallization of basaltic magmas can be developed if the systems of mass-balance Eqs. (1) of the source–derivative type are consistent with data on melt–mineral equilibria, which should uniquely relate the compositions of the silicate liquid and solid phase over any interval of the crystallization process. Approaches to devising corresponding computational schemes will be considered below.

1.2.2. Analytical solutions for perfect fractionation

The processes of melt fractionation are described in the general form by ordinary differential equations for mass balance (see, for example, [Greenland, 1970; Maaloe, 1976]. The main condition of balance for component i in a melt and solid phase during its crystallization has the form

$$x_i^s dW^s + d(x_i^l W^l) = 0, \quad (2)$$

where dW^s is the mass increment of the crystals formed, W^l is the amount of melt, and x_i^s and x_i^l are the concentrations of component i in the solid phase (s) and liquid (l). For the purposes of further description, it is convenient to use the parameter that is referred to as the degree of melt fractionation and characterizes the ratio of the overall mass of the crystallizing matter $W^s = W_0 - W^l$ to the amount of the initial melt W_0 [Kravchenko, 1977]

$$\varphi = (W_0 - W^l)/W_0. \quad (3)$$

Constraints of form (2) and (3) give a system of n differential equations ($1 \le i \le n$)

$$dx_i^l = \frac{x_i^l - x_i^s}{1 - \varphi} d\varphi, \quad (4)$$

that uniquely relate the evolution of the melt composition dx_i^l with the progress of the fractional crystallization process. This system can be solved analytically only in the simplest situations, when there are addi-

tional known dependences between the compositions of the melt and solid phase.

Fractionation of trace elements. It can be assumed that, for example, the following condition is fulfilled during any fractionation stage

$$x_i^s = K_i x_i^l, \quad K_i = \text{const}, \tag{5}$$

where K_i is the weighted mean bulk partition coefficient [Ryabchikov, 1965] of component i between the solid phase and melt

$$K_i = \sum_{j=1}^{m} f_j^s D_i^j, \tag{6}$$

where f_j^s is the weight fraction of phase j in the crystallizing material, and D_i^j is the individual partition coefficient of element i between mineral j and melt. Relations (4), (5) yield the well-known Rayleigh fractionation formula

$$x_i^l = x_i^{l(0)}(1-\varphi)^{K_i - 1}, \tag{7}$$

where $x_i^{l(0)}$ is the concentration of element i in the initial melt.

Equation (7) describes the situation of the so-called perfect fractional crystallization [Maaloe, 1976] and was widely applied to the analysis of the behavior of trace elements in the magmatic processes and evaluations of their effective partition coefficients [McIntire, 1963; Ryabchikov, 1965; Gast, 1968; and others]. Perfect fractionation is characterized by 100% removal of the crystallizing material from the melt under the condition that the amount of the residual melt is complementary with the amount of crystals produced $W^l = W_0 - W^s$ during any stage of the process.

Imperfect or partial fractional crystallization also implies the complete removal of the crystalline material, but in this process it is assumed that part of the liquid can also be removed from the main melt volume in the form of, for example, intercumulus material [Maaloe, 1976]. This results in an effective decrease in the overall amount of the fractioning liquid not only by means of its crystallization but also through the removal of the "melt captured by crystals." The main balance condition (2) therewith acquires the form

$$f^s x_i^s dW^s + d(x_i^l W^l) - (1-f^s)x_i^l dW^l = 0, \tag{8}$$

where $0 \le f^s \le 1$ is the fractionation factor, equal to the fraction of solid phases in the overall amount of material removed from the melt over a given crystallization interval. With regard for this factor, the Rayleigh equation (7) acquires the form

$$x_i^l = x_i^{l(0)}(1-\varphi)^{f^s(K_i - 1)}. \tag{9}$$

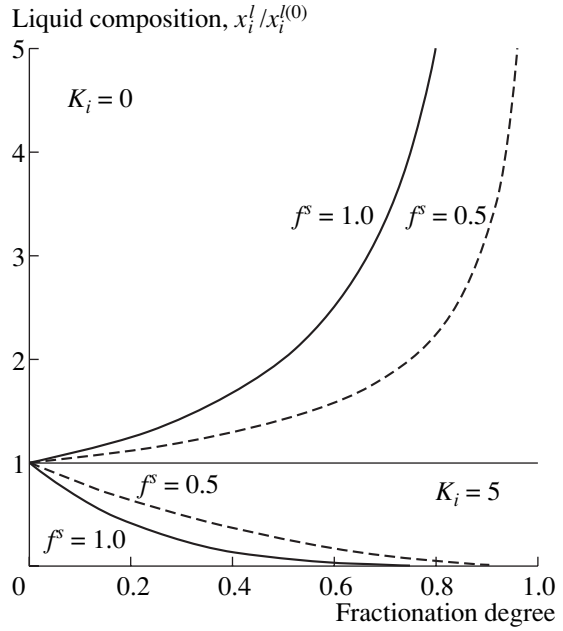

Fig. 3. Evolution of the melt composition at perfect ($f^s = 1.0$) and partial fractional ($f^s = 0.5$) crystallization. The calculations simulate the behavior of elements incompatible ($K_i = 0$) and compatible ($K_i = 5$) with the solid phase. The concentrations are normalized to the initial concentration of the element in the melt $x_i^{l(0)}$.

Figure 3 demonstrates dependences calculated with Eq. (9) for perfect and partial fractional crystallization. In the latter situation, the fractionation factor was 0.5, which meant that solid phases and melt were removed from the fractionating system in the proportion 1 : 1. The calculations were conducted with two values of the bulk partition coefficient: $K_i = 0$ (the model of an incompatible element) and $K_i = 5$ (the model of an element preferably fractionating into the solid phase). These data demonstrate that the rapid enrichment of the liquid in the incompatible element during perfect fractional crystallization starts during the very first fractionation stages. During partial fractional crystallization these processes slow down because the efficiency of the partitioning of elements is buffered by the amount and composition of the entrapped melt. The principal petrological implications of the dependences portrayed in Fig. 3 are as follows.

(1) These lines demonstrate a noteworthy fact that, during perfect fractional crystallization, the amount of residual melt with a high concentration of the incompatible element $x_i^l/x_i^{l(0)} > 5$ is four to five times greater than the amount of the analogous derivative produced when 50% of the liquid was removed. This result is a direct consequence of the progressive diminish in the amount of the fractionating melt, with this effect enhanced with an increase in the fraction of the intercumulus material captured by the crystals. This means

that, depending on the fractionation dynamics, the same initial melt is able to generate different amounts of end-member derivatives of the same composition. Understanding the nature of these relationships calls for caution in the petrological interpretations of mass-balance calculations that are underlain by direct application of the results of physical and numerical experiments on rock melting to natural magmatic objects.

(2) Another point concerns the form of the dependence of the concentration curve on the degree of fractionation. As can be seen from Fig. 3, partial fractional crystallization is characterized by a much more drastic transition to the stage of strong enrichment of the melt in the incompatible element. If such dependences are extrapolated to natural systems with fractionating major components (SiO_2 among others), it is reasonable to expect that, when all other factors are the same, the capture of portions of the crystallizing melt should enhance the bimodal distribution of the basic and acid derivatives, particularly in the vicinity of sharp bends in the petrochemical trends at the appearance of magnetite on the liquidus [Lukanin, 1985].

(3) Although the main relationships arising in the fractionation of elements when crystals are removed and melt is captured were already described in the 1970s [Greenland, 1970; Maaloe, 1976] and modeled in the early 1980s [Frenkel, 1982], it was the concept of perfect fractional crystallization that received predominant recognition among petrologists. Dependences of form (7) were used not only in modeling the direct course of fractional crystallization but also in solving inverse problems related to the evaluation of the effective partition coefficients of trace elements on the basis of geochemical data [Kravchenko, 1977]. The analysis of Eq. (9) indicates that ignoring the fractionation factor f^s in this approach can result in K_i estimates that differ from the actual values by factors of 1.5–2.5. At the same time, in the presence of reliable experimental data on the mineral–melt partition coefficients, relation (9) makes it possible to estimate the average fractionation factor (fraction of cumulus) that is characteristic of the fractionation of mafic magmas [Barmina *et al.*, 1982] in the chamber.

In conclusion, it is pertinent to mention that partial fractional crystallization should not been identified with intermediate fractionation. In natural systems, crystals are sometimes incompletely removed from a fractionating liquid, and part of these crystals remains as a suspension in the main magma volume. Therewith not all crystalline material is excluded from equilibrium with melt, and the fractionation process acquires an intermediate character between fractional and equilibrium crystallization.

Fractionation of solid-solution minerals. Many researchers pointed out that equations like (4)–(7) are of limited applicability to the devising and analysis of models for the fractionation of major elements, first of all, because of broad variations in the values of individual (D_i^j) and weighted mean (K_i) partition coefficients for major oxides. These variations can be monotonous (for example, because of the dependence of D_i^j and K_i on composition and/or temperature). However, the main difficulties are related to jumps in these parameters in response to changes in the phase compositions of the crystallizing assemblages. Another problem is linked to the evolution of the crystallization proportions x_j^s even at an unchanging set of crystallizing phases [see Eq. (6)]. This information is explicitly or implicitly presented in the phase diagrams of silicate systems. Let us first examine the simple binary system *Fa–Fo* [Bowen and Schairer, 1935]. The only mineral crystallizing in this system is olivine, because of which no effects of the crystallization sequence and proportion should be taken into consideration in describing the fractionation of this mineral.

It is convenient to describe the compositional evolution of olivine using the "exchange" coefficient K_D

$$K_D = (x_{Fo}^{Ol}/x_{Fo}^{l})/(x_{Fa}^{Ol}/x_{Fa}^{l}), \quad (10)$$

which relates the compositions of the solid phase (*Ol*) and melt. The solution of Eq. (4) with regard for (10) and the balance conditions $x_{Fa}^{Ol} = 1 - x_{Fo}^{Ol}$ and $x_{Fa}^{l} = 1 - x_{Fo}^{l}$ leads to the expression [Ariskin and Frenkel, 1982]

$$x_{Fo}^{l}/(1 - x_{Fo}^{l})^{K_D} = [x_{Fo}^{l(0)}/(1 - x_{Fo}^{l(0)})^{K_D}](1 - \varphi)^{K_D - 1}, \quad (11)$$

where $x_{Fo}^{l(0)}$ is the initial *Fo* concentration in the melt at $\varphi = 0$. This nonlinear equation can be readily resolved for x_{Fo}^{l} by iterative techniques. The composition of the melt at a given degree of its fractionation φ determines the composition of the crystallizing olivine

$$x_{Fo}^{Ol} = K_D x_{Fo}^{l}/[1 + (K_D - 1)x_{Fo}^{l}]. \quad (12)$$

The calculated dependences of the *Fo* concentration in the melt and olivine on the degree of fractionation in the binary *Fo–Fa* system are demonstrated in Fig. 4. The calculations were conducted with an average value of $K_D = 4.5$, because experimental data on the *Fa–Fo* system [Bowen and Schairer, 1935] indicate that the coefficient varies from 4.1 to 5.2 [Bradley, 1962b].

The characteristic feature of these trajectories is the clearly pronounced dependence of the rate of the compositional change for the melt and olivine $dx_{Fo}^{l/Ol}/d\varphi$ on the initial *Fo* concentration in the silicate liquid. The higher the *Fo* concentration of the initial melt, the lower the rates of the phase compositions change during the initial fractionation stages and the higher these rates change during the final stages. Conversely, melts with intermediate and low initial *Fo* concentrations fractionate more quickly during early crystallization stages.

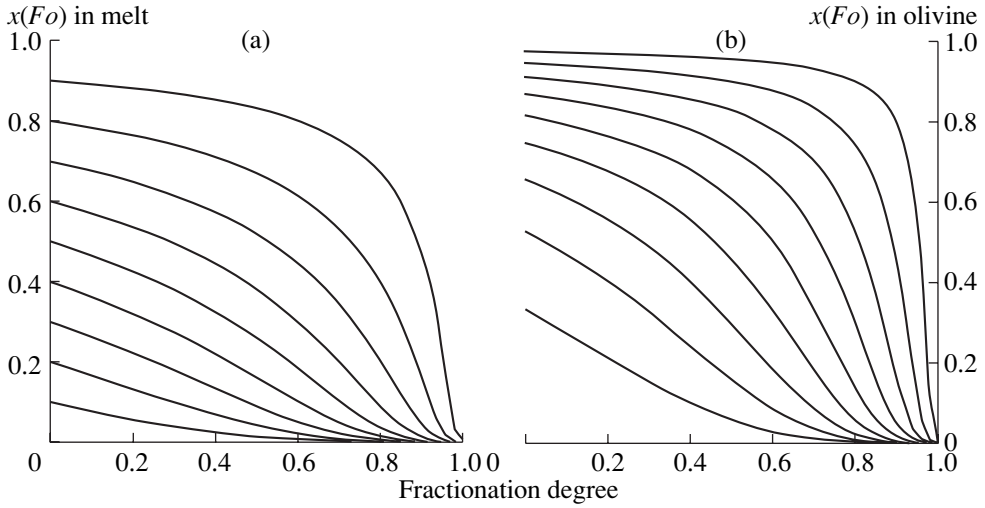

Fig. 4. Evolution of the compositions of melt and olivine in the process of perfect fractionation in the binary *Fa–Fo* system. (a) Melt composition, (b) olivine composition. Numerals near lines indicate the *Fo* content in the initial liquid. The calculations were conducted by Eqs. (11) and (12) for $K_D = 4.5$.

Similar relationships were identified in the *Ab–An* system, in which the rates of the compositional changes of the fractionating melt and plagioclase were proved to depend on the initial concentration of the anorthite component [Maaloe, 1976]. This suggests that dependences of this type are of a general character: the rates of fractionation (changes in the composition) of silicate systems are predetermined by the normative ratios of refractory and low-melting end members in the initial melt.

Extrapolating these dependences to natural multicomponent silicate melts, it can be expected that the decrease in the MGN of the magnesian systems should be slower early in the course of the fractionation of mafic minerals ($0 < \varphi < 20$–40%); moderate during the intermediate stages ($0 < \varphi < 40$–70%); and fast, with a drastic depletion in MgO, up to the origin of pure ferrous end members, during the final stages. When plagioclase or plagioclase-bearing associations crystallize, the fractionation rate of the systems in terms of CaO, Na_2O, Al_2O_3, and SiO_2 should vary depending on the alkalinity.

Valuable information on the fractionation of binary systems can also be obtained by comparing the evolutionary trajectories in Figs. 4a and 4b. Since the solid phase is enriched in the refractory component relative to the melt, a change in the mineral chemistry (Fig. 4b) is not as fast as the change in the composition of the liquid (Fig. 4a). This is why insignificant compositional variations in olivine (on the order of a few mol %) in natural rocks can be coupled with remarkable variations in the major-component composition of the magmatic melt.

Attempts to analytically solve fractionation problems for multicomponent silicate systems are limited to the analysis of ternary diagrams like *Ab–An–Di* [Maaloe, 1976] with the coupled solution of two problems: the necessity of tracing changes in the composition of plagioclase and variations in the proportions of crystallizing *Pl* and *Di*. For this purpose, information on the configurations of the phase fields is used, with these data represented in the form of polynomials approximating relationships between experimental values for x_i^l and x_i^s, which are substituted in equations of form (4). Models of this kind are rather of theoretical interest and can be applied only to systems in which the position of phase boundaries as compositional functions have been fully characterized during a preliminary stage. Note that, within the scope of these approaches, it is difficult to take into account reaction phase relationships, which result in bends in the melt fractionation trajectories because of shifting the compositional data points from peritectic lines into the crystallization field of a newly formed mineral.

1.2.3. Numerical schemes for fractionation of minerals and melts

The essence of numerical techniques for calculating fractional crystallization trajectories is the replacement of infinitesimal increments *d* in Eq. (4) for finite Δ

$$\Delta x_i^l = \frac{x_i^l - x_i^s}{1 - \varphi}\Delta\varphi. \quad (13)$$

After each *k*th crystallization step, this yields

$$\varphi^k = \varphi^{k-1} + \Delta\varphi, \quad (14)$$

and the melt composition

$$x_i^{l(k)} = x_i^{l(k-1)} + [x_i^{l(k-1)} - x_i^{s(k-1)}]\Delta\varphi/(1 - \varphi^{k-1}). \quad (15)$$

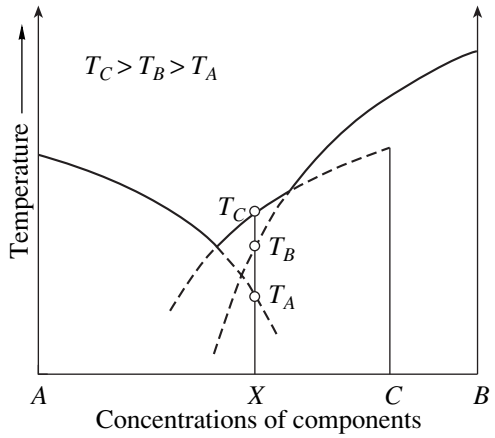

Fig. 5. Schematic diagram for the possible relationships between the liquidus and pseudoliquidus temperatures of minerals in a binary system with one peritectic and one eutectic points.

This finite-difference scheme ensures a high accuracy of the trajectory calculated for fractional crystallization at specified small increments of $\Delta\varphi = 0.1$–0.01% and less. The closeness of the calculated evolutionary trajectories to reality depends on the accuracy with which the dependences between x_i^l and x_i^s were predicted for each fractionation stage. These relationships are determined by (a) the phase composition of the liquidus association, (b) the proportions of the crystallizing minerals, and (c) the compositions of the crystallizing phases. In the 1970s, a number of approaches were worked out to solve these problems [Drake, 1976a; Longhi, 1977; Nathan and Vankirk, 1978]. The most universal and coherent, from the thermodynamic viewpoint, crystallization model was that developed by Nathan and Vankirk [1978], who generalized available materials on phase equilibria in synthetic and natural silicate systems. Noting that experimental petrology had provided merely unsystematic data obtained for limited ranges of temperature and pressure in the multidimensional compositional space of magmatic rocks, these researchers believed that the task can be formulated as a search for a method enabling the achievement of agreement between the results of diverse experiments on the melting of natural rocks and synthetic mixtures and allowing the extrapolation of these results.

Method for estimating the association of crystallizing minerals. To determine the liquidus phases that should crystallize from a melt of a given composition, an algorithm was proposed that was underlain by the common topologic features of phase diagrams for silicate systems. The fundamentals of this methods are schematically illustrated in the diagram of Fig. 5. The diagram presents an example of an *A*–*B* binary system with one eutectic and one peritectic point (such as the system SiO_2–Mg_2SiO_4). In addition to phases *A* and *B*, phase *C* can crystallize in this system, with the latter phase occurring in reaction relationships with phase *B*.

As is seen in the diagram, the temperature of equilibrium between the melt and each of the three phases is described by an equation for the liquidus line $T_j = f(x)$, which is defined throughout the whole compositional space. This means that, at a specified composition *X*, the melt can potentially be in equilibrium with any of the three minerals but only at a certain "pseudoliquidus" temperature, defined for each mineral [Ariskin and Frenkel, 1982]. In fact, a liquidus mineral is that whose liquidus temperature is the highest, i.e., mineral *C* in our situation (Fig. 5). Hence, the calculation of the set of the potentially possible solid phases and the comparison of their preudoliquidus temperatures provides a procedure for the selection of the mineral that should crystallize from a melt of specified composition.

Originally there was no rigorous justification for this method [Nathan and Vankirk, 1978], and the thermodynamic sense of these relations became clear later [Frenkel and Ariskin, 1984]. The point is that there is only one energetically preferable state of three conditional equilibrium states of a heterogeneous system (melt of composition *X* + infinitesimal amount of solid phase *A*, *B*, or *C*; Fig. 5), with this state corresponding to the maximum possible liquidus temperature. In practice, it is important that this statement is also applicable to cotectic associations, whose condition of crystallization in numerical models for fractionation acquires the form

$$|T_j - T_{liq}| \le \varepsilon_T, \quad T_{liq} = \max\{T_j\}, \quad 1 \le j \le m, \quad (16)$$

where T_j is the pseudoliquidus temperature for mineral *j*, T_{liq} is the melt liquidus temperature, and ε_T is the accuracy specified for temperature. In fact, relation (16) determines the intersection point for the liquidus surfaces of different phases (Fig. 5). In this formulation, to determine the phase composition of a crystallizing association, one has to have a system of equations linking the temperatures of equilibria between each mineral and melt with the composition of the melt.

It was proposed to solve problems of this kind using empirical equations of the form

$$T_j = a_0 + \sum_{i=1}^{8} a_i x_i^l + a_9 f(x_j) + a_{10}\sqrt{x_{\mathrm{Al}}^l (x_{\mathrm{Na}}^l + x_{\mathrm{K}}^l)}, \quad (17)$$

where $a_0, \ldots, a_{10}$ are regression coefficients; x_i^l is the melt composition normalized to ten cations (Si, Al, Ti, Fe^{3+}, Fe^{2+}, Mg, Ca, Na, and K); and $f(x_j)$ is a function of the silicate liquid composition, specific for each mineral. The statistical treatment of a significant amount of experimental data on the crystallization temperatures of silicates yielded Eqs. (17) for nine main minerals: olivine, plagioclase, augite, orthopyroxene, magnetite,

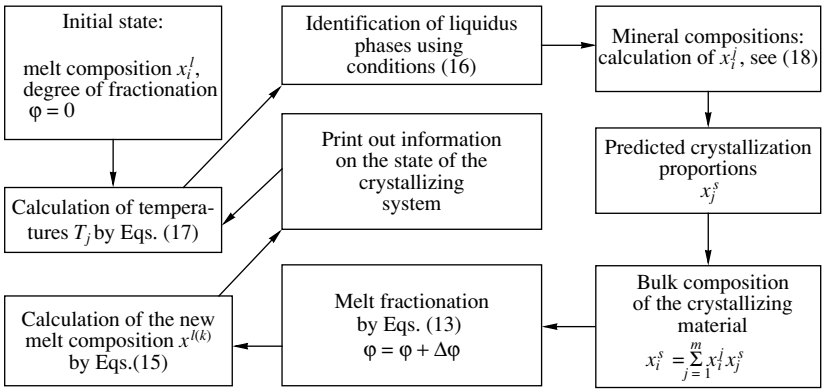

Fig. 6. Flowchart for the numerical simulation of the course of fractional crystallization of basaltic magmas [Nathan and Vankirk, 1978].

orthoclase, nepheline, leucite, and quartz [Nathan and Vankirk, 1978].

Simulation algorithm and calculation of the proportions of crystallizing minerals. If there is a fast and reliable technique for determining liquidus minerals, the calculation of the bulk composition of the crystallizing assemblage is reduced to the evaluation of the compositions of these minerals and their proportions. The former problem can be resolved with the use of exchange coefficients of the form

$$K_{\mathrm{Mg/Fe}}^{Ol-l} = (x_{\mathrm{Mg}}^{Ol}/x_{\mathrm{Fe}}^{Ol})/(x_{\mathrm{Mg}}^{l}/x_{\mathrm{Fe}}^{l}) \qquad (18a)$$

or

$$K_{\mathrm{Ca/Na}}^{Pl-l} = (x_{\mathrm{Ca}}^{Pl}/x_{\mathrm{Na}}^{Pl})/(x_{\mathrm{Ca}}^{l}/x_{\mathrm{Na}}^{l}), \qquad (18b)$$

which were calculated from experimental and petrological data and were temperature-independent [Nathan and Vankirk, 1978]. The calculation of the crystallization proportions is directly related to the algorithm proposed for modeling the fractionation trajectories. The succession is illustrated in the scheme of Fig. 6.

In compliance with this scheme, the initial state of a magmatic system always corresponds to the presence of a specified amount of melt, whose composition is known and which contains no equilibrium solid phase (the degree of fractionation of this melt φ = 0). Constraints (16), (17) make it possible to evaluate the liquidus temperature and to determine the phases that should crystallize from the melt. The composition of these phases was calculated by Eqs. (18). If the liquidus temperature corresponds to the presence of two mineral phases *j*1 and *j*2, fractionation proceeds by means of removal (subtraction) of these minerals, taken in a certain proportion (for example, 2 : 1), from the system. The subtracted amounts of the minerals should thereby meet the condition $n_{j1} + n_{j2} = \Delta\varphi$, where Δφ is the specified increment of the solid-phase amount.

Relation (15) enables the calculation of the composition of the newly formed melt x_i^l, but it is possible that the new (pseudo)liquidus temperatures T_{j1} and T_{j2} (17) cease to be compatible with the conditions of cotectic crystallization (16). This means that the cotectic surface can be attained if an additional amount Δ*n* of a solid phase crystallizes, with this solid phase characterized by the maximum value of $T_{liq} = \max\{T_j\}$. Consequently, the value φ = φ + Δφ + Δ*n* increases, and the composition of the fractionating melt changes. The routine of additional crystallization is conducted alternatively for all cotectic phases until their (pseudo)liquidus temperatures become consistent with conditions (16). The integral proportions of the crystallizing minerals are thereby the desired crystallization proportions. They can be used during the next fractionation step as a more reliable estimate, which facilitates an increase in the calculation speed of this scheme.

It can readily be seen that this algorithm does not require subdividing the fractionation trajectory into the predetermined crystallization intervals of various cotectic assemblages, and there is no need to specify *a priori* the proportions of crystallizing minerals [Drake, 1976a; French and Cameron, 1981; Petitpierre and Boivin, 1983]. These proportions are calculated in the course of simulations and depend exclusively on the form of the liquidus equation for each mineral (Fig. 5). An advantageous feature of the algorithm, proposed by Nathan and Vankirk [1978], is the absence of limitations imposed in this algorithm on the number of components of the silicate liquid, and, thus, this algorithm can be applied to magmatic systems of complex chemical composition. This somewhat modified calculation routine is an important constituent of the computer program developed in later years by our research team [Ariskin and Frenkel, 1982; Frenkel and Ariskin, 1984, 1985] and of some other models [Nielsen and Dungan, 1983; Nielsen, 1990].

Table 1. Parameters of mineral–melt geothermometers used in developing the CFCT model [Ariskin and Frenkel, 1982]

Mineral	Component	No.	Geothermometer parameters	Number of points	Reference
Olivine	MgO	1	$\log K = 3740/T - 1.87$	27	[Roeder and Emslie, 1970]
(*Ol*)	FeO	2	$\log K = 3911/T - 2.50$		
Plagioclase	*An*	3	$\ln K = 12900/T - 1.89$	55	[Drake, 1976b]
(*Pl*)	*Ab*	4	$\ln K = 6100/T - 2.29$		
High-Ca pyroxene (augite–*Px*1)	*En*	5	$\ln K = 6360/T - 3.59$	32	[Nielsen and Drake, 1979]
	Fs	6	$\ln K = 4709/T - 3.90$		
	Wo	7	$\ln K = 4194/T - 2.53$		
	Al	8	$\ln K = 23350/T - 18.54$		
Low-Ca pyroxene	*En*	9	$\ln K = 5351/T - 2.55$	31	[Nielsen and Drake, 1979]
	Fs	10	$\ln K = 4488/T - 3.18$		
(*Pig*/*Opx*–*Px*2)	*Wo*	11	$\ln K = 28240/T - 20.68$		
	Al	12	$\ln K = 29990/T - 23.65$		

1.3. CFCT Model for Calculating Fractional Crystallization Trajectories

The comparison of the a_0, …, a_{10} parameters in Eq. (17) for different mineral phases demonstrates that, at a given configuration of the liquidus surface, the greatest contribution to the estimated crystallization temperature is made by the linear terms of the equations, which is in conflict with the logarithmic nature of the dependence of the chemical potentials on the concentrations in the variable-composition phases. Another disadvantage of the routine proposed by Nathan and Vankirk [1978] is linked to the utilization of invariable values for the exchange coefficients for different minerals, which can be applied, with certain limitations, only to the olivine–melt equilibrium [Roeder and Emslie, 1970]. Moreover, because of the deficit in information on phase equilibria of pyroxenes, magnetite, and alkaline minerals, the reference selection for equation calibrations was compiled not only from direct experimental data but also of estimates of crystallization temperature with various geothermometers. This made it difficult to achieve a high accuracy of the calculations: at an average error of about 20–30°C, some deviations of the calculated temperatures from the experimental values were as great as 100°C. Thus, by the early 1980s it became necessary to develop a more realistic model for the fractionation of silicate melts that would be consistent with the fundamental thermodynamic principles and ensure a better accuracy of the temperature and phase-composition estimates. A principal achievement was the designing of the CFCT computer program [Ariskin and Frenkel, 1982], the first in a series of computer programs subsequently known under the names THOLEMAG and COMAGMAT.

1.3.1. Empirical basis of the CFCT model

In developing this model for the fractionation of silicate melts, we have relied on empirical temperature dependences characterizing an equilibrium partitioning of components between minerals and melt at given temperatures and pressures. These dependences were derived in the 1970s by the statistical treatment of empirical data on the melting of igneous rocks and synthetic mixtures and eventually received the name of mineral–melt geothermometers [Roeder and Emslie, 1970; Drake, 1976b; Nielsen and Drake, 1979]. These geothermometers are simple regression equations of the form

$$\log K_i^j = A_i^j/T + B_i^j \quad (19a)$$

or

$$\ln K_r^j = A_r^j/T + B_r^j, \quad (19b)$$

where K_i^j is the molar partition coefficient of component i between mineral j and the liquid; K_r^j is the equilibrium constant for the crystallization reaction; r is a component of the solid solution of mineral j (such as *An* in *Pl*); and A_i^j, B_i^j, A_r^j, and B_r^j are the regression coefficients (Table 1).

The olivine geothermometers of Roeder and Emslie [1970] have played a prominent role in the development of thermometric techniques in application to igneous rocks and the progress of numerical models for the crystallization and melting of silicate systems. Although they were repeatedly refined and revised on the basis of newly obtained experimental data, the utilization of simple MgO and FeO partition coefficients could ensure stable inaccuracies of the temperature estimates within 20°C [Roeder, 1974], which met the requirements for the solutions of most traditional petrologic and geochemical problems.

The nature of the temperature dependences of the partition coefficients (19a) is well known and related to the temperature dependences of the equilib-

rium constants for the corresponding mineral-forming reactions. For example, olivine crystallization from melt can be described by the reaction

$$2\mathrm{MgO}(l) + \mathrm{SiO_2}(l) = \mathrm{Mg_2SiO_4}(Ol), \quad (20)$$

whose equilibrium constant is

$$K_{eq}^{Fo-l} = a_{Fo}^{Ol}/(a_{\mathrm{MgO}}^{l})^2 a_{\mathrm{SiO_2}}^{l}. \quad (21)$$

Taking into account that, at an ideal mixing of the Mg^{2+} and Fe^{2+} cations at the common octahedral site, $a_{Fo}^{Ol} = (x_{Fo}^{Ol})^2$ [Wood and Fraser, 1981], and the stoichiometric composition $x_{Fo}^{Ol} = x_{\mathrm{MgO}}^{Ol}/0.667$, expression (21) acquires the form

$$K_{eq}^{Fo-l} = (x_{\mathrm{MgO}}^{Ol}/x_{\mathrm{MgO}}^{l})^2 \frac{1}{0.667^2(\gamma_{\mathrm{MgO}}^{l})^2 a_{\mathrm{SiO_2}}^{l}}, \quad (22)$$

where $\gamma_{\mathrm{MgO}}^{l}$ is the MgO activity coefficient in the silicate liquid. The temperature dependence of K_{eq}^{Fo-l} at a constant pressure can be determined using known thermodynamic relationships

$$\ln K_{eq}^{Fo-l} = -\Delta G_{crys}^{Fo}/RT = -\Delta H_{crys}^{Fo}/RT + \Delta S_{crys}^{Fo}/R = \Delta H_{melt}^{Fo}/RT - \Delta S_{melt}^{Fo}/R, \quad (23)$$

where the *crys* and *melt* indices refer to forsterite crystallization and melting, and ΔH and ΔS are the changes in enthalpy and entropy. Substituting (22) into (23) and transforming natural logarithms into decimal ones, we obtain an expression for the molar partition coefficient of MgO between olivine and melt $K_{\mathrm{MgO}}^{Ol} = x_{\mathrm{MgO}}^{Ol}/x_{\mathrm{MgO}}^{l}$

$$\log K_{\mathrm{MgO}}^{Ol} = \Delta H_{melt}^{Fo}/4.6RT - \Delta S_{melt}^{Fo}/4.6R + \log 0.667\gamma_{\mathrm{MgO}}^{l}(a_{\mathrm{SiO_2}}^{l})^{1/2}. \quad (24)$$

Equation (24) clarifies the thermodynamic meaning of empirical geothermometers (19a): the statistical treatment of the pairs of $\log K_{\mathrm{MgO}}^{Ol}$ and $1/T$ values yields regression coefficients of the reciprocal temperature A_i^j that are multiples of the melting enthalpy of pure forsterite. This can be readily demonstrated by multiplying the temperature coefficient of the first geothermometer in Table 1 by the value of $4.6R$: the calculated "effective enthalpy" value of 34 480 cal/mol is only insignificantly different from the *Fo* melting enthalpy of 29.3 kcal/mol, a value calculated by Bradley [1962b] from experimental data for the *Fa–Fo* diagram [Bowen and Schairer, 1935].

Another important conclusion can be drawn from the analysis of relationships (19a) and (24): the *Ol*–melt partition coefficients should depend on the composition of the silicate liquid, with the integral effect of this "recorded" in the parameter $\log 0.667\gamma_{\mathrm{MgO}}^{l}(a_{\mathrm{SiO_2}}^{l})^{1/2}$ and implicitly (but efficiently) taken into account in the regression coefficient B_i^j. The composition factor imposes certain limitations on the use of partition coefficients with thermometric purposes, because of which the accuracy of the temperature estimates cited by the authors can be guaranteed only for compositional ranges for which the corresponding empirical dependences have been calibrated.

Evidently, the utilization of the equilibrium constants of reactions like (20) and (21) should significantly minimize the effect of composition on the calculated regression parameters (19b). This has been convincingly demonstrated by the examples of plagioclase–melt [Drake, 1976b] and pyroxene–melt [Nielsen and Drake, 1979] equilibria. These researchers were the first to establish that the geothermometers readily estimate temperatures accurate up to 10–15°C, even if the corresponding data were obtained by different authors at different laboratories for broad compositional ranges. Issues related to the calibration of empirical dependences for melt–mineral equilibria will be considered in detail in Chapter 2.

1.3.2. Thermodynamic principles of the CFCT model

The crystallization reactions of solid-solution components (20) can be expressed in the general form as the equation

$$\sum_{i=1}^{n} \nu_{i(r)}^{j} L_i = M_r^j, \quad (25)$$

where n is number of melt components of the form L_i (SiO_2, MgO, $NaAlO_2$, etc.), $\nu_{i(r)}^{j}$ is the stoichiometric coefficients of the reaction, and M_r^j represents component r of mineral j (*Fo*, *An*, *En*, and other end members). If dependences (19b) and (21) are known for each possible reaction,

$$\ln K_r^j = \ln x_r^j/\prod_{i=1}^{n} x_i^{\nu_{i(r)}^{j}} = A_r^j/T_r^j + B_r^j, \quad (26)$$

where x_r^j are the concentrations (activities) of solid-solution components and x_i are the concentrations of melt components, then, taking into account the stoichiometry of the minerals,

$$\sum_{r=1}^{R(j)} x_r^j = 1 \quad (27)$$

the condition of equilibrium between mineral j and melt has the form

$$\sum_{r=1}^{R(j)} \prod_{i=1}^{n} x_i^{\nu_{i(r)}^j} \exp(A_r^j/T_j + B_r^j) = 1, \quad (28)$$

where T_j is the desired equilibrium temperature, because the condition $T_r^j = T_j$ is valid for all end members. It follows from Eq. (28) that, to determine the (pseudo)liquidus temperature of any of the minerals at a constant pressure, it is sufficient to know the composition of the melt and the temperature dependences of the equilibrium constants for the crystallization reactions of the corresponding components. When T_j is evaluated, it is possible to calculate the composition of the mineral in terms of each component r

$$x_r^j = \prod_{i=1}^{n} x_i^{\nu_{i(r)}^j} \exp(A_r^j/T_j + B_r^j). \quad (29)$$

The system of Eqs. (26)–(29) is preferable to the purely empirical dependences (17) and (18) [Nathan and Vankirk, 1978], because they relate the compositions of the melt and minerals and the equilibrium temperature in compliance with thermodynamic laws. The practical utilization of these relationships can be illustrated by the example of the *Pl*-melt equilibrium. Using the parameters of plagioclase geothermometers from Table 1, the stoichiometry constraint $x_{An}^{Pl} + x_{Ab}^{Pl} = 1$, and relationships (26) for the crystallization reaction of anorthite and albite [Drake, 1976b]

$$CaO(l1) + 2AlO_{1.5}(l1) + 2SiO_2(l1) = An(Pl), \quad (30a)$$

$$NaAlO_2(l2) + 3SiO_2(l2) = Ab(Pl), \quad (30b)$$

it is possible to obtain an integral equation for the plagioclase liquidus surface

$$x_{CaO}^{l1}(x_{AlO_{1.5}}^{l1})^2(x_{SiO_2}^{l1})^2 \exp(12900/T_{Pl} - 1.89) + x_{NaAlO_2}^{l2}(x_{SiO_2}^{l2})^3 \exp(6100/T_{Pl} - 2.29) = 1, \quad (31)$$

which can be resolved using the technique of successive iterations [Ariskin and Frenkel, 1982]. The equation for the olivine liquidus surface has a simpler form

$$x_{MgO}^{l} 10^{(3740/T_{Ol} - 1.87)} + x_{FeO}^{l} 10^{(3911/T_{Ol} - 2.50)} = 0.667. \quad (32)$$

Note that indices l, $l1$, and $l2$ in Eqs. (31, 32) denote different models for the description of the concentrations and activities of melt components. This results in a certain incoherence in the thermodynamic description of the system, which is, however, not crucial [Ghiorso, 1987], because these equations are applied to the basaltic compositions but not the marginal portions of silicate systems. For us it is important that the technique proposed for the estimation of the (pseudo)liquidus temperatures and compositions of minerals in the range of basaltic magmas allows using different models for the liquid phase: the main criterion is the accuracy of the solutions of the thermometric problems, regardless of how the equilibrium constants were calculated. Nevertheless, in our further research we tried to utilize the same model for the activities of liquid-phase components for the calibration of mineral–melt geothermometers.

1.3.3. Computer simulation of perfect fractionation of basic silicate melts

Using integral *Ol* and *Pl* geothermometers (31) and (32), analogous dependences for high- and low-Ca pyroxenes (Table 1), and corresponding Eqs. (29) for the calculation of the equilibrium mineral compositions, we have designed a calculation routine for the computer simulation of the fractionation of mafic silicate melts, the CFCT program [Ariskin and Frenkel, 1982]. In this model, the melt composition included 8 components (SiO_2, TiO_2, Al_2O_3, FeO, MgO, CaO, Na_2O, and K_2O) with the formal subdivision of iron into ferrous and ferric oxides by means of attributing the oxidized part of FeO to TiO_2 as a presumably "incompatible" component. The main design features of the CFCT program resemble the algorithm in [Nathan and Vankirk, 1978] (Fig. 6) with the only exception being the technique of evaluating the crystallization proportions of minerals. For this purpose, we developed a simple and fast routine.

The essence of this method is the subdivision of the fractionation interval into a great number of small crystallization steps (in our situation, $k = 20\,000$), with only one mineral crystallizing at each of them (regardless of whether the melt is or is not cotectic), and this mineral characterized by the highest (pseudo)liquidus temperature T_j [see Eq. (28)]. If the melt was cotectic with respect to two, three, or four minerals [the temperatures of more than one phase simultaneously fulfilled condition (16)], the settling of minor amounts of one mineral $j1$ caused a change (usually a decrease) in the temperature T_{j1} relative to the T_j of other cotectic phases. Thus, the liquidus phase was alternatively represented by different minerals, which crystallized depending on how much the calculated value of their temperature was greater than the T_j of the other minerals. This routine ensured that the melt composition did not depart from the vicinity of the cotectic surface during certain fractionation intervals $\Delta\varphi = 1\%$ (which included 200 small crystallization steps). The crystallization proportions of the minerals can be calculated as the relative proportions of the solid phases that were formed in the system over a 1% interval of its crystallization.

In fact, this method is a routine of roaming near the cotectic or peritectic surface (later this approach was utilized by L.V. Danyushevsky to develop the PETROLOG program). Such a design of the computational scheme makes it possible to follow the evolution of the crystallization proportions of minerals in the pro-

Table 2. Compositions of the silicate melts used in studying the effects of fractionation of basaltic systems by means of the CFCT model

No.	Concentrations of components, wt %						Liquidus temperatures, °C	
	SiO_2	Al_2O_3	FeO	MgO	CaO	Na_2O	φ = 0	φ = 0.90
1	50	17	10	10	12	1	1204	1076
2	50	17	5	15	12	1	1299	1117
3	50	17	15	5	12	1	1215	1004
4	50	17	10	10	10	3	1205	1107
5	50	17	5	15	10	3	1299	1175
6	50	17	15	5	10	3	1209	1081
7	50	14	10	10	15	1	1207	1087
8	50	14	5	15	15	1	1293	1140
9	50	14	15	5	15	1	1194	1066
10	50	14	10	10	13	3	1205	1120
11	50	17	10	7	15	1	1237	1078
12	50	17	7	10	15	1	1222	1097

cess of fractionation, an issue that had been virtually unexplored by the early 1980s. Using the CFCT program, we simulated numerically the perfect fractional crystallization of twelve silicate melts representing a broad spectrum of "basalts" from magnesian and ferrobasaltic (conditionally "tholeiitic") melts to high-Al compositions with variable CaO/Na_2O ratios (Table 2). In these simulations, the weight percentages of components in the starting compositions were recalculated into molar amounts of oxides in one mole of the initial silicate liquid. Because of this, the total degree of fractionation of the system φ was calculated to be the sum of the mole fractions of oxides crystallizing as minerals. The principal results of these simulations are as follows.

Evolution of liquidus temperatures. Figure 7 demonstrates variations in the liquidus temperatures during the perfect fractionation of ferrobasaltic melt of composition *6* in Table 2. As can be seen, the most sharp temperature decrease is characteristic of the crystallization of an excess mineral (here, it is plagioclase), and, when bi- and tri-mineral cotectics crystallize, the decrease rate of the liquidus temperature $dT_{liq}/d\varphi$ becomes more significant as the degree of fractionation is increased.

Crystallization sequence of minerals. The relatively high CaO and Al_2O_3 concentrations in the starting melts predetermined that plagioclase was the main crystallizing mineral (it accounted for 50–70% of the solid phase). This mineral was the first to appear on the liquidus of the FeO-enriched melts (Table 2, compositions 3, 6, and 9), as well as those high in CaO and Al_2O_3 (Table 2, compositions 11 and 12). Olivine was the first to crystallize in the high-Mg melts (Table 2, compositions 2, 5, and 8). The compositions in question are characterized by the cotectic crystallization of all possible combinations of minerals, except only the *Ol–Px2* pair, a fact pointing to peritectic relations between these phases. However, when *Pl* appeared on the liquidus of high-Fe compositions, *Ol* was noted to crystallize in the presence of low-Ca pyroxene (Fig. 7).

The compositional evolution of the melt and minerals corresponds to the relationships identified when the analytical model for the fractional crystallization of solid-solution minerals was explored (using the example of olivine; Fig. 4). The rate of changes in the com-

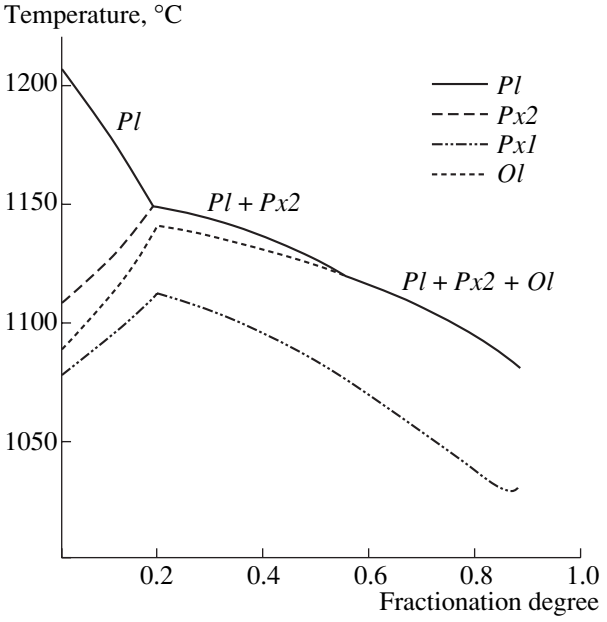

Fig. 7. Dependences of the liquidus and pseudoliquidus temperatures of minerals on the bulk degree of melt fractionation (Table 2, composition *6*).

Table 3. Modal composition of crystallizing mineral assemblages (computer simulation of the fractionation of basaltic melts)

Mineral assemblage	Crystallization proportions, vol %			
	Pl	*Px1*	*Px2*	*Ol*
Pl-Ol	74–78	–	–	22–26
Pl-Px1	46–51	49–54	–	–
Pl-Px2	48–69	–	31–52	–
Pl-Px1-Ol	55–63	23–36	–	8–14
Pl-Px1-Px2	56–60	9–21	19–35	–

position of phases during fractionation was at a maximum for compositions enriched in low-melting components (FeO and Na_2O). Plagioclase has been established to fractionate with a higher rate in melts with elevated initial Na/Ca ratios, with the fractionation rate decreasing as the Al_2O_3 concentration was increased.

Evolution of crystallization proportions. By analyzing calculation results for cotectic assemblages, it was established that the maximum crystallization proportions of minerals are typical of phases characterized by weak dependences of their (pseudo)liquidus temperatures on the degree of fractionation. At a steep slope of the liquidus surface $dT_j/d\varphi$, the fraction of this mineral in the crystallizing material is at a minimum. Changes in the melt composition in the process of fractionation result in changes in the $dT_j/d\varphi$ value for each mineral, and, consequently, the crystallization proportions of the same assemblage can systematically vary. The data of Table 3 provide a general idea of the variations in the model crystallization proportions for the main cotectics. This is the most important of the results obtained with the CFCT program. In spite of certain imperfections of the thermodynamic basis of this model and a simplified character of the compositions examined, these data demonstrate that any approaches to the analysis of fractionation processes with the use of invariable crystallization proportions do not have much chance of success in reproducing the crystallization conditions of natural magmatic melts.

1.4. Calculations of Thermodynamic Equilibria in a Closed Melt–Mineral System

The development of models for the evolution of magmatic systems involves two parts, which are referred to as the thermodynamic and dynamic aspects of physicochemical simulations [Frenkel *et al.*, 1988b]. The thermodynamic aspect is underlain by the necessity of designing a realistic model of phase equilibria in magmas, which can be subsequently utilized to predict changes in the composition of the minerals and magmatic melt in the processes of melting and crystallization. The dynamic aspect accounts for the processes of geological-scale heat and mass transfer and determines the spatiotemporal relations between the chamber boundaries, fronts of crystallization and accumulation of crystals, and, eventually, the crystallization succession and relative proportions of rocks produced as a result of the magmatic evolution.

Here the main difficulty is caused by the coupled character of the effects of thermodynamic and dynamic factors. For example, the model phase diagram for a cooling magmatic system should specify the crystallization sequence of minerals, which can be variably separated from the melt under the effects of dynamic and thermal factors, dissolve or become re-equilibrated with fresh magma portions, etc. The separation of minerals and melt, as well as variations in the phase and bulk chemical compositions of the magma result in that the evolution of the equilibrium phase compositions becomes dependent on the dynamic regime of fractionation or melting. The consequences of this dependence can be readily seen if it is borne in mind that both minerals and silicate liquid are solutions: the model phase diagram becomes "floating," with the configurations of the phase boundaries determined by the shifts of the composition data points for each local equilibrium. Hence, it is necessary first to formulate the principles of solving equilibrium problems in closed systems.

The calculation of thermodynamic equilibrium in a multiphase system involves determining the proportions of the phases and their chemical compositions for the mineral assemblage stable at a given pressure and temperature. Within the scope of chemical thermodynamics, this problem is reduced to the search for a minimum of the free energy G for the system

$$G = \sum_{\phi = 1}^{\Phi} G_\phi \qquad (33)$$

at the fulfillment of mass balance constraints, where $1 \le \phi \le \Phi$ are phases of the system. The algorithms proposed for minimizing the free energy can be subdivided into two major groups [Borisov and Shvarov, 1992]: (i) programs of the first type are designed as routines for the direct minimization of the G function at the polyhedron of limitations, and (ii) the programs of the second type implement numerical schemes for solving systems of nonlinear algebraic equations underlain by the mass action law.

Algorithms for the direct minimization of the G function are characterized by the necessity of describing the chemical potentials of components in phases of variable composition, which, in turn, requires an estimation of the activities of these components as functions of the composition of the solid solutions. The activities of components are also necessary to calculate equilibrium relations by the programs of the second group, which make use of the "equilibrium" constants. This is responsible for the common character of the routines used to calculate phase equilibria: both methods are expected to yield similar or identical results

when using the same thermodynamic database with uniform compositional functions of the activities of components included.

The direct minimization of the thermodynamic potential is preferable due to several reasons: it utilizes information on the thermodynamic properties of substances that is organized more systematically, allows the application of the well-developed theory of nonlinear mathematical programming, and ensures the most universal design of the computer programs in terms of their applicability to the diversity of chemical systems and the means of specifying the external conditions and their ranges. This group of algorithms includes most computer programs developed for the thermodynamic simulation of atmospheric, hydrothermal, metasomatic, and metamorphic processes [White, 1967; Karpov *et al.*, 1976; Shvarov, 1976; Karpov, 1981; Harvie *et al.*, 1987; Borisov and Shvarov, 1992; Powell *et al.*, 1997].

Algorithms of this type have found wide geochemical application to systems for which there are reliable theoretical methods for the calculation of the chemical potentials of components as compositional functions. These are gases of not very high densities and strong electrolyte solutions that are subject to the Debye–Hückel theory, etc. In igneous petrology, this way was chosen by the authors of the MELTS computer program [Ghiorso, 1985, 1994; Ghiorso and Carmichael, 1985], who have twice recalibrated the thermodynamic parameters describing the mixing properties of silicate melts on the basis of the regular-solution model [Ghiorso *et al.*, 1983; Ghiorso and Sack, 1995]. In Russia, attempts were made to calculate phase equilibria in magmas using the algorithms designed by I.K. Karpov [Feoktistov, 1983, 1987].

The method of solving systems of equilibrium equations is underlain by the use of equilibrium constants and stoichiometric coefficients for crystallization reactions (25) occurring in the system. The equations for the mass action law serve as a formal criterion of equilibrium and are solved together with mass balance equations. The procedures designed to solve these equations are based on a variety of iteration techniques (the method of Newton–Raphson, reaction shift estimation, etc.). Algorithms making use of constants become widely applied in igneous petrology [Langmuir and Hanson, 1981; Ariskin and Frenkel, 1990; Weaver and Langmuir, 1990; Ryabchikov, 1994; Camur and Kilinc, 1995; Ariskin *et al.*, 1997a; Ariskin, 1999]. This was mostly because there is still no reliable methods for predicting the activities of components of a silicate melt as the main solution phase, and this makes it difficult to accurately construct the free energy surface for the system melt–crystals.

1.4.1. Characteristic features of models including silicate melts

This situation can be partly resolved by using empirical models for component activities in minerals and liquid that determine the calculation of the effective mineral–melt equilibrium constants [Ariskin and Frenkel, 1982; Nielsen and Dungan, 1983; Weaver and Langmuir, 1990; see Eq. (26)]. The substitution of activities for concentrations in mineral–melt geothermometers (like those listed in Table 1) is counterbalanced by the fact that the relations between temperature and the composition of phases in the liquidus assemblage involved in these thermometers are "read" directly from experimental data and do not involve any additional recalculations with the utilization of data on the thermodynamics of the end members of the silicate systems, such as forsterite Mg_2SiO_4, anorthite $CaAl_2Si_2O_8$, chromite $FeCr_2O_4$, and others.

The point is that the describing of the free energy of mineral phases in the classic formulation of the minimization of the G function requires additional independent data on pure end members, including the standard enthalpies of their formation, temperature functions of the heat capacities, etc. In this sense, models for the solution of the equilibrium problem with algorithms of the first type should be made consistent with available databases of the thermodynamic properties of pure substances. For example, the aforementioned models of Ghiorso are internally consistent with the database in [Berman, 1988]. In the absence of a general theory for the structure of silicate melts, any attempts to achieve consistence lead to certain negative consequences, because the selected experimental data on phase equilibria with multicomponent silicate liquids are processed together with "external" information on marginal systems [Ghiorso *et al.*, 1983; Ghiorso and Sack, 1995]. Evidently, it is easier to achieve consistence in data on phase equilibria when the experimental information is analyzed directly than when additional limitations (even justified thermodynamically) are imposed. This is an advantage of the method using the solution of systems of equations for the mass action law. In contrast to the direct minimization of the thermodynamic potential, this approach does not require detailed information on the compositional functions of the chemical potentials of components in minerals and melt, although some researchers consider this approach excessively empirical [Borisov and Shvarov, 1992] or even oversimplified [Ghiorso, 1987].

It is pertinent to mention that igneous petrologists repeatedly compared and tested crystallization algorithms based on "thermodynamic" (MELTS [Ghiorso and Sack, 1995]), semiempirical (COMAGMAT [Ariskin *et al.*, 1993; Ariskin, 1999]), and empirical models. The results of this comparative testing were often unfavorable for programs making use of the direct minimization of the thermodynamic potential [Yang *et al.*, 1996].

Table 4. Characteristics of computer models designed for simulating equilibrium crystallization (only algorithms for which a thermodynamic background is available)

Program builders	Criteria of equilibrium	Activities of components		Note
		minerals	melt	
[Frenkel and Ariskin, 1984, 1985; Ariskin *et al.,* 1993]	Mass action law coupled with phase proportions corresponding to the minimum of G at the specified bulk degree of system crystallization	Single-site model of ideal mixing. Minerals: *Ol*, *Pl*, *Aug*, *Pig*, *Opx*, *Mt*, *Ilm*	Two-lattice mixing models for components: SiO_2, TiO_2, $AlO_{1.5}$, FeO, $FeO_{1.5}$, MnO, MgO, CaO, $NaAlO_2$, $KAlO_2$, $PO_{2.5}$	**COMAGMAT model**: deviations from ideality in the melt are accounted for by using empirical coefficients of structural–chemical parameters in the equilibrium equations
[Ghiorso, 1985, 1994; Ghiorso and Sack, 1995]	Minimum free energy at a given temperature	Regular solution models. Components: SiO_2, TiO_2, Al_2O_3, Fe_2O_3, $MgCr_2O_4$, Fe_2SiO_4, Mg_2SiO_4, $CaSiO_3$, Na_2SiO_3, $KAlSiO_4$, $Ca_3(PO_4)_2$, H_2O. Minerals: *Ol*, *Pl*, *Aug*, *Opx*, *Sp*, *Ilm*, *Qtz*, *Lc*, *Ap*, corundum, and whitlockite		**MELTS program**: deviations from ideality in the melt and minerals are accounted for by using the mixing parameters of regular solutions W_{ij}
[Langmuir and Hanson, 1981; Weaver and Langmuir, 1990]	Saturation index [Reed, 1982] and mass balance constraints	Single-site ideal-mixing models. Melt components: $CaSiO_3$, $NaAlO_2$, $CaAl_2O_4$, TiO_2, FeO, MgO. Minerals: *Ol*, *Pl*, *Aug*		Deviations from ideality in the melt are ignored. New versions of this model were published in [Langmuir *et al.*, 1992; Reynolds, 1995]
[Camur and Kilinc, 1995]	Formulated unclearly. The algorithm relies on the solution of systems of equilibrium and mass-balance equations (G minimization is implied)	Single- and two-site ideal-mixing models. Minerals: *Ol*, *Pl*, *Aug*, *Opx*, *Ne*, *Lc*	Single-site mixing model. Melt components according to the model [Ghiorso *et al.*, 1983]	Deviations from ideality in the melt are accounted for by introducing excess free energy for each reaction in the form of a functional of the melt composition, temperature, and oxygen fugacity

The distinctive features of some crystallization models are summarized in Table 4. It should be explained why the table includes no information on programs designed by R. Nielsen, which were quite popular among petrologists [Nielsen and Dungan, 1983; Nielsen, 1990]. Although these models are allegedly able to construct equilibrium lines of descent, they, in fact, contain no block for solving the equilibrium problems, and equilibrium crystallization is calculated by a slightly modified fractionation algorithm, analogous to that discussed in Section 1.2.

Our procedure proposed to solve problems of equilibria in basaltic systems is of a hybrid nature with respect to the two aforementioned types of computer programs: being in essence an algorithm for the solution of systems of equilibrium equations, our model retains certain features of the routine for minimizing the free energy, with the phases of the equilibrium assemblage selected automatically [Frenkel and Ariskin, 1984, 1985]. The fundamental principle of this algorithm can be easily explained using the example of the achievement of equilibrium by an assumed melt–mineral association.

1.4.2. Principles of melt equilibration with crystals

The problem is formulated as follows. Let a silicate system of known bulk composition N_i (for simplicity, let $\sum_{i=1}^{n} N_i = 1$ mol) be arbitrarily subdivided into a certain number of minerals (j) and melt, so that the silicate liquid composition meets mass-balance conditions for each component

$$N_i^l = N_i - \sum_{j=1}^{m} \sum_{r=1}^{R(j)} \nu_{i(r)}^j N_r^j, \quad (34)$$

where $1 \le r \le R(j)$ are the marginal components (end members) of solid solutions, $\nu_{i(r)}^j$ are the stoichiometric coefficients of reactions (25) producing the end members, and N_r^j are the number of individual end members in the mixture.

The free energy of the mixture of crystals and melt can be calculated from the molecular amounts and chemical potentials of components of the liquid and solid phases

$$G = \sum_{i=1}^{n} N_i^l \mu_i^l + \sum_{j=1}^{m} \sum_{r=1}^{R(j)} N_r^j \mu_r^{j\cdot} \quad (35)$$

Condition (34), postulating the constancy of the bulk composition, makes it possible to transform Eq. (35) to a form involving the differences in the energies for each mineral-forming reaction

$$G = \sum_{i=1}^{n} N_i \mu_i^l + \sum_{j=1}^{m} \sum_{r=1}^{R(j)} N_r^j \left(\mu_r^j - \sum_{i=1}^{n} \nu_{i(r)}^j \mu_i^l \right), \quad (36)$$

which can be further used to assay the effects of the reactions forming each of the end members on the change in the free energy of the predicted melt–mineral association

$$\partial G / \partial N_r^j = \mu_r^j - \sum_{i=1}^{n} \nu_{i(r)}^j \mu_i^l. \quad (37)$$

For simplicity, let the minerals and melt be ideal solid solutions, and, then, the chemical potentials of given end members in the solid phase and the components of the liquid in the initial unequilibrated melt–crystal mixture is, at any arbitrarily chosen temperature T,

$$\mu_r^j = \mu_r^{j(0)} + RT \ln x_r^j, \quad \mu_i^l = \mu_i^{l(0)} + RT \ln x_i^l, \quad (38)$$

where the values of $\mu_r^{j(0)}$ and $\mu_i^{l(0)}$ correspond to the standard states of pure components, and x_i^l and x_r^j are the compositions of the initial melt and mineral j. Correspondingly, the subtrahend of Eq. (37) can be written in the form

$$\sum_{i=1}^{n} \nu_{i(r)}^j \mu_i^l = \sum_{i=1}^{n} \nu_{i(r)}^j \mu_i^{l(0)} + RT \ln \prod_{i=1}^{n} (x_i^l)^{\nu_{i(r)}^j}. \quad (39)$$

It follows from Eqs. (37)–(39) that

$$\partial G / \partial N_r^j = \left[\mu_r^{j(0)} - \sum_{i=1}^{n} \nu_{i(r)}^j \mu_i^{l(0)} \right] + RT \ln x_r^j - RT \ln \prod_{i=1}^{n} (x_i^l)^{\nu_{i(r)}^j}. \quad (40)$$

The difference of the chemical potentials in the standard state corresponds to the change in the free energy, which is related to the equilibrium constant of the crystallization reaction (25) for pure end member by the known formula

$$\mu_r^{j(0)} - \sum_{i=1}^{n} \nu_{i(r)}^j \mu_i^{l(0)} = -RT \ln K_r^{j(0)}. \quad (41)$$

The two last right-hand terms of Eq. (40) represent the concentration constant K_r^j, calculated based on the predicted composition of the silicate liquid and mineral j

$$RT \ln x_r^j / \prod_{i=1}^{n} (x_i^l)^{\nu_{i(r)}^j} = RT \ln K_r^j. \quad (42)$$

Thus, expression (40) assumes the form

$$\partial G / \partial N_r^j = -RT \ln K_r^{j(0)} + RT \ln K_r^j, \quad (43)$$

which resembles the Van't Hoff reaction isotherm that is usually utilized in the analysis of conditions under which spontaneous processes can occur in a homogeneous system (see, for example, [Nikolaev, 1979]).

Relation (43) indicates that, depending on the selected initial state that determines the activities of components and the K_r^j value during the initial stage, the decrease in the free energy of the melt–mineral system can occur via crystallization reactions ($dN_r^j > 0$) or through the dissolution of the solid phase ($dN_r^j < 0$). This feature of Eq. (43) enables its use as the basis for designing various algorithms for free-energy minimization with the utilization of equilibrium constants.

For example, taking into account the expression for the temperature dependence of the equilibrium constant for (26), Eq. (43) can be written in the form

$$\partial G / \partial N_r^j = -RT(A_r^j / T + B_r^j) + RT(A_r^j / T_r^j + B_r^j), \quad (44)$$

or

$$\partial G / \partial N_r^j = RA_r^j (T / T_r^j - 1), \quad (45)$$

where T is the temperature of the equilibrium, and T_r^j is the temperature of the metastable (predicted) equilibrium with melt for a given end member. Equation (45) makes it possible to proceed from the terms of chemical potentials (37) and equilibrium constants (43) to the temperature relations determining the conditions of free energy minimization. Recall that R is the gas constant, and the values of A_r^j are divisible into the melting enthalpy of the pure component and are always positive [see Eqs. (19)–(24)].

In the situation when the searched equilibrium temperature T is known beforehand, Eq. (45) enables the prediction that end member r of mineral j should be formed from the melt at $T < T_r^j$, and, conversely, this end member should be transferred into the melt at $T > T_r^j$ (if the amount of this component in the mixture is nonzero), to decrease the free energy of the system $dG < 0$. Hence, the calculation of the temperatures of metastable equilibria between each end member and melt is an important element of the routine for minimizing the free energy of the system of melt and crystals.

If the minerals were ideal solutions of components, this problem could be resolved separately for each end member by calculating the values of, for example, T_{Fo}^{Ol} and T_{Fa}^{Ol} and the molar amounts N_{Fo}^{Ol} and N_{Fa}^{Ol}. In practice, deviations from ideality were detected for all min-

eral phases, and the use of empirical geothermometers (26), which were calibrated for phases of variable composition (Table 1), implies that a common temperature value should be utilized for all components of a given mineral $T_j = T_r^j$.

The method proposed in this publication to evaluate the temperatures of metastable mineral–melt equilibria T_j resembles the technique of calculating pseudoliquidus temperatures (28) but differs from it by taking into account the occurrence of specified amounts of minerals (along with the melt) in the system. An important feature of this algorithm is its adaptation to the solution of equilibrium problems not at a specified temperature but at a given bulk degree of system crystallization, when the overall number of moles of melt components does not vary in the course of crystallization and dissolution of minerals $\sum_{i=1}^{n} N_i^l = \text{const}$ [Frenkel and Ariskin, 1984, 1985]. This somewhat complicates the minimization routine of the G function but enables developing computer programs for a constant increment of crystallization [Ariskin *et al.*, 1993] or melting [Ariskin *et al.*, 1997a] in the system. The significance of this possibility can be appreciated by those interested in calculating equilibrium, fractional, and critical melting of mantle rocks, if the solidus temperature of the system is not known beforehand.

1.4.3. Calculating the temperatures of metastable equilibria

Let us now return to the initial predicted state: the silicate system includes N_l moles of melt of composition x_i^l and a certain number of minerals N_j of composition x_r^j:

$$N_l = \sum_{i=1}^{n} N_i^l, \quad x_i^l = N_i^l / N_l \tag{46a}$$

and

$$N_j = \sum_{j=1}^{R(j)} N_r^j, \quad x_r^j = N_r^j / N_j, \tag{46b}$$

which are interrelated only through mass-balance constraints (34), so that the bulk degree of system crystallization (in the fractions of oxide components) is

$$\varphi_{cr} = \sum_{j=1}^{m} \sum_{r=1}^{R(j)} \nu_{i(r)}^j N_r^j = 1 - N_l. \tag{47}$$

In order to calculate the equilibrium phase composition of the system by relations (45), the system should first be transferred into the state of metastable equilibrium, i.e., the compositions of the mineral and melt should be changed to satisfy the mass action law (29) at a temperature T_j specified for each mineral. At constant phase proportions, this "partial equilibration" can be implemented by means of exchange reactions with the transfer of components from crystals to melt and *vice versa* until the composition of the mineral and melt meet the conditions of Eq. (29).

This is a well known problem of physical chemistry that can be solved by finding the shift in the chemical reaction for each mineral. In the general form, it is reduced to the solution of systems of equilibrium equations (29), whose right- and left-hand parts contain the values of the chemical composition shifts,

$$x_r^j + \Delta x_r^j = \sum_{i=1}^{n} [x_i^l + \Delta x_{i(r)}^j]^{\nu_{i(r)}^j} \exp(A_r^j / T_j + B_r^j), \tag{48}$$

which have different signs and are interrelated through the stoichiometry of the corresponding reactions $\Delta x_{i(r)}^j = -f(\Delta x_r^j)$, see Eq. (25).

The system of equations (48) becomes solvable for temperature if additional conditions are introduced for the stoichiometry of a given mineral phase (27). In this situation, the shifted equilibrium equation for one of the end members (48) should be replaced by the obvious condition of material balance in the solid phase

$$\sum_{r=1}^{R(j)} \Delta x_r^j = 0 \quad \text{or} \quad \sum_{r=1}^{R(j)} \Delta N_r^j = 0, \tag{49}$$

which ensures the constancy of the amount of the mineral in the mixture $N_j = \text{const}$ and, correspondingly, $\varphi_{cr} = \text{const}$.

The solution of such a problem can be illustrated by the system of equilibrium and mass balance equations utilized to equilibrate a given amount of plagioclase $N_{Pl} = N_{Ab}^{Pl} + N_{An}^{Pl}$ and a complementary melt N_l in one of the earlier versions of COMAGMAT (1985)

$$\begin{gathered}
K_{Ab}^{Pl-l} = 6100/T_{Pl} - 2.29, \\
K_{An}^{Pl-l} = 12\,900/T_{Pl} - 1.89, \\
NF = N_{SiO_2}^l + N_{Al_2O_3}^l + N_{Na_2O}^l + N_{K_2O}^l, \\
NM = N_l + N_{Al_2O_3}^l + N_{Na_2O}^l + N_{K_2O}^l, \\
(N_{Ab}^{Pl} - \Delta_{Ab}^{Pl})/N_{Pl} = K_{Ab}^{Pl-l}(2N_{Na_2O}^l + \Delta_{Ab}^{Pl}) \\
\times (N_{SiO_2}^l + \Delta_{Ab}^{Pl})^3/(NF + \Delta_{Ab}^{Pl})^4, \\
x_{Ab}^{Pl} = (N_{Ab}^{Pl} - \Delta_{Ab}^{Pl})/N_{Pl}, \\
x_{An}^{Pl} = K_{An}^{Pl-l}(N_{CaO}^l + \Delta_{An}^{Pl})(2N_{Al_2O_3}^l + \Delta_{An}^{Pl})^2 \\
\times (N_{SiO_2}^l + \Delta_{Ab}^{Pl})^2/(NM)^5, \\
x_{Ab}^{Pl} + x_{An}^{Pl} = 1, \quad \Delta_{Ab}^{Pl} + \Delta_{An}^{Pl} = 0.
\end{gathered} \tag{50}$$

In determining this system, we used the parameters of *Pl*–melt geothermometers and the two-lattice model proposed for silicate liquids [Drake, 1976b]. Later, these parameters were revised, but the principle underlying the search for the numerical characteristics of the reaction shifts remained unchanged. The solution of the system of equations (50) gives the change in the compositions of plagioclase ($\Delta x_{Ab}^{Pl} = \Delta_{Ab}^{Pl}/N_{Pl}$, $\Delta x_{An}^{Pl} = \Delta_{An}^{Pl}/N_{Pl}$) and melt that makes it possible to calculate the newly formed phase compositions corresponding to the mass action law at the metastable equilibrium temperature T_{Pl}. Obviously, when the predicted state includes a two-phase association of plagioclase and melt, these compositions and temperature correspond to the true equilibrium state. Systems of equations of this type were also proposed for olivine and pyroxenes and are an important element of our models.

For the partial (selective) equilibration of multiphase predicted assemblages, exchange reactions can be conducted sequentially for all minerals, with the changes in the melt composition controlled during each *k*th iteration. Therewith the solution of the metastable equilibrium problem corresponds to the condition

$$\sum_{j=1}^{m}\sum_{r=1}^{R(j)} \Delta x_{i(r)}^{j} \le \varepsilon_i^l, \qquad (51)$$

which indicates that the overall shift in the liquid phase composition after one equilibration cycle for all minerals does not extend beyond a certain preset accuracy ε_i^l (mol %). This means that the compositions of the predicted mineral phases have achieved equilibrium with the composition of the same liquid at a temperature T_j specified for each mineral.

1.4.4. Search for equilibrium phase proportions

The presence of a set of T_j values for all phases of the "partly equilibrated" melt–mineral association allows one to use relation (45) in searches for the equilibrium proportions of crystals and melt. The condition of phase composition equilibration at a given degree of crystallization complicates the situation inasmuch as the temperature of the target equilibrium is unknown. It is known, however, that this temperature should range from the maximum of all possible pseudoliquidus temperatures $T_j^{\max}$ to the minimum $T_j^{\min}$ for minerals that are contained in the mixture in nonzero amounts. Because of this, the minimization of *G* is, in fact, equivalent to the minimization of the difference $T_j^{\max} - T_{j(N_j>0)}^{\min}$, a procedure that is convenient to carry out by means of the sequential crystallization (subtraction from the melt) and melting (addition to the melt) of mineral components [Frenkel *et al.*, 1988b]. This problem could be resolved if the condition $T_j^{\max} - T_{j(N_j>0)}^{\min} < \varepsilon_T$ is fulfilled, where ε_T is the specified accuracy of the calculated equilibrium temperature. This, however, presents certain additional difficulties.

The point is that, although each step of the crystallization or melting of minerals of constant composition (48) brings the system closer to the equilibrium phase proportions, this inevitably violates constraints (29). The violation is manifested in the fact that any change in the mineral proportions is not coupled with changes in their composition, although the liquid phase composition does change (imagine *Ol* crystallization and complementary *Pl* dissolution). The disequilibration of the compositions makes it necessary to return to the search for the metastable equilibrium temperatures and new mineral compositions. Thus, the main algorithm of free energy minimization for the partly molten system (45) comprises two major iteration loops (Fig. 8): (i) **the cycle of the thermometry of melt–mineral equilibria** brings the system into a metastable state, in which the composition of each solid phase is linked to the composition of the liquid by the mass action law, and (ii) **the cycle calculating the phase proportions** minimizes the differences between the equilibrium temperatures of individual minerals by means of their crystallization or melting. As a result of the alternating action of these calculation routines, the model system tends to a state in which the equilibrium temperatures of each mineral phase differ from one another by a value no greater than ε_T, and the melt composition is in equilibrium with the compositions of minerals accurate to no worse than $\pm\varepsilon_i^l$. One of the major advantages of this scheme is the possibility of direct control over the calculation accuracy.

It should be mentioned that this algorithm for minimizing the Gibbs free energy is implicitly universal and can be applied to the solution of the thermodynamic equilibrium problems not only for igneous but also other heterogeneous systems for which there are reliable data on the temperature dependences of the equilibrium constants of chemical reactions.

1.4.5. Algorithm for simulating equilibrium crystallization

Practical calculations in application to magmatic equilibria demonstrate that the scheme in Fig. 8 ensures the convergence of the iteration cycles at predicted N_i^l and N_r^j values that do not differ too much from the equilibrium values. This has largely predetermined the designing of the equilibrium crystallization algorithm as a technique for the sequential solution of the equilibrium problem with regard for an increase of crystallizing material in the system. Figure 9 presents a flowchart of the CECT computer program (Calculation of Equi-

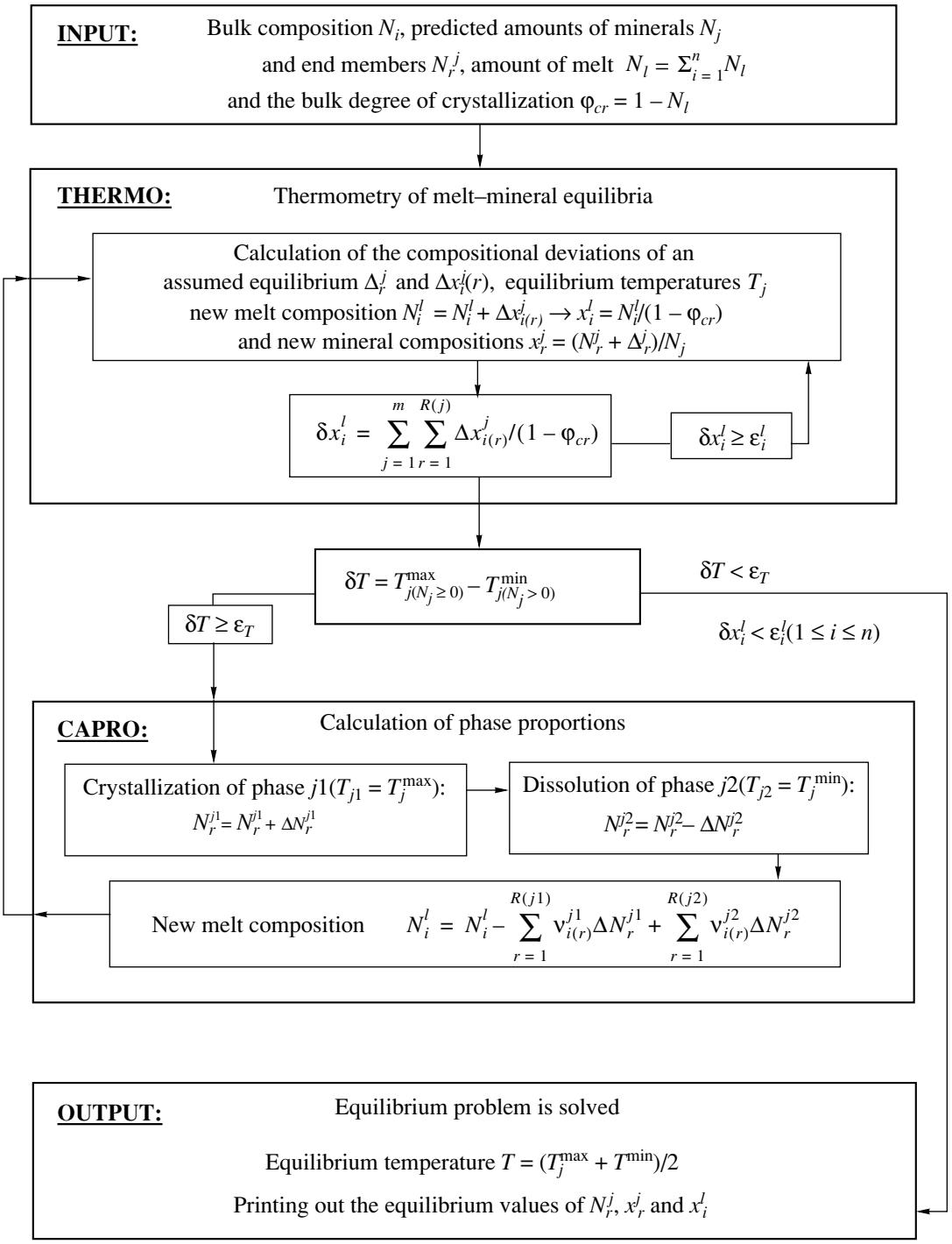

Fig. 8. General flowchart of the algorithm designed to solve the equilibrium problem for multiphase assemblages of melt and minerals of variable composition at a specified degree of system crystallization.

librium Crystallization Trajectories; the abbreviation in Russian is RTKR), which was the precursor of the COMAGMAT crystallization models. This scheme has not experienced any significant transformations from the time of its designing, and crystallization models were further developed mostly via the universalization of the algorithm, improvement of the calculation accuracy, and the extension of the models to a wider range of compositions and conditions.

The initial state of the system in the CECT program corresponds to the occurrence of melt free of solid phases ($\varphi_{cr} = 0$, $N_i^l = N_i$), so that the melt amount equals the sum of the mole amounts of oxides in the system

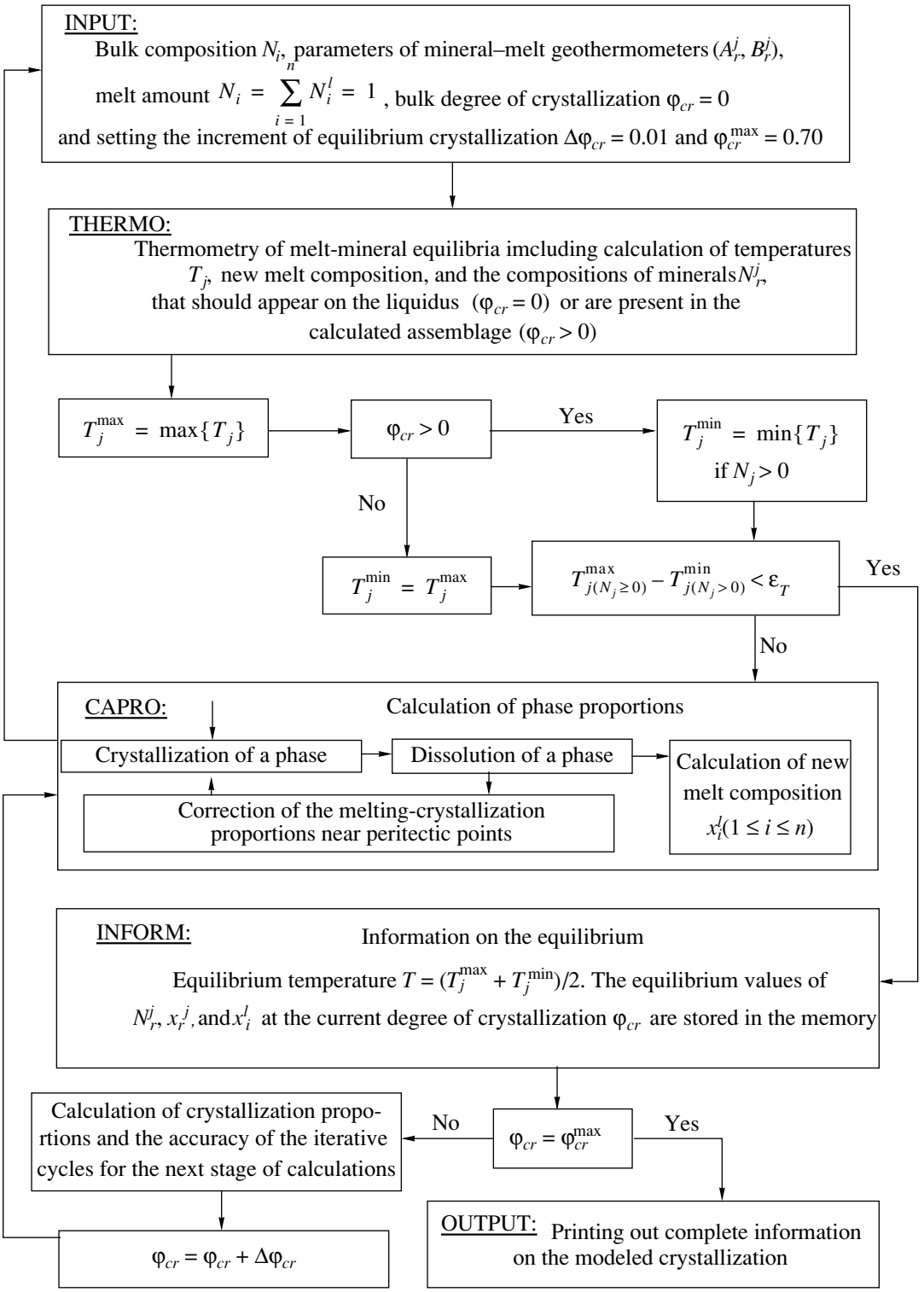

Fig. 9. Flowchart for the CECT (initially RTRK) program developed for the computer simulating the equilibrium crystallization of basic melts [Frenkel and Ariskin, 1984, 1985].

$N_i = \sum_{i=1}^{n} N_i$ (1 mol). To construct the equilibrium liquid line of descent, it is necessary to specify the shift in the degree of crystallization $\Delta\varphi_{cr}$, which determines the periodicity of the solutions of the equilibrium problem. In practice, $\Delta\varphi_{cr}$ is usually equal to 0.01–0.02. Furthermore, it is helpful to evaluate the φ_{cr}^{max} (usually 0.6–0.8), which determines the maximum degree of crystal-

lization to which the calculations will be conducted. This limitation is related to the fact that programs of the COMAGMAT series were originally adapted for simulating fractional type crystallization processes, which have little chance of proceeding to $\varphi \approx 1$ in nature. Because of this, at first we did not explore the situation corresponding to the presence of a minor amount of melt in equilibrium with a great amount of the solid phase, as well as the calculation problems that arise when these equilibria are modeled. These problems were solved later, when the METEOMOD model was developed [Ariskin *et al.*, 1997a].

INPUT in the CECT program is intended to initialize the A_r^j and B_r^j parameters of mineral–melt geothermometers [see Eq. (26)]. They can be set constant or determined in the process of calculations, as will be demonstrated below using polybaric fractionation models (see Chapter 4). At a known initial melt composition and specified A_r^j and B_r^j values, the pseudoliquidus equilibrium temperatures T_j for all minerals and the corresponding mineral compositions x_r^j are calculated in the THERMO block by Eqs. (28) and (29). After this, the program finds mineral phase $j1$ corresponding to the liquidus temperature $T_j^{\max} = \max\{T_j\}$ and considers, in compliance with the initial condition $T_{j(N_j \geq 0)}^{\max} - T_{j(N_j > 0)}^{\min} = 0$, the equilibrium problem to be solved at $\varphi_{cr} = 0$ (Fig. 9). The exit from the INFORM block at $\varphi_{cr} < \varphi_{cr}^{\max}$ switches the program execution to the block for calculating the crystallization proportions and the accuracy of the iteration loops during the next calculation stage.

The crystallization proportions during the initial formation of excess mineral $j1$ are assumed to be equal to unity ($x_{j1}^s = 1$); for other phases, $x_j^s = 0$. In further calculations, they are calculated by a formula that allows for changes in the relative amount of each mineral phase over a preceding crystallization interval from φ_{cr} to $\varphi_{cr} + \Delta\varphi_{cr}$:

$$x_j^s = (N_j^{\varphi_{cr}+\Delta\varphi_{cr}} - N_j^{\varphi_{cr}}) / \sum_{j=1}^{m} (N_j^{\varphi_{cr}+\Delta\varphi_{cr}} - N_j^{\varphi_{cr}}), \quad (52)$$

where the values of x_j^s are obtained in mole fractions. Similar expressions can be written for the weight or volumetric crystallization proportions. The crystallization proportions of phases that crystallize from the melt in cotectic proportions are always positive $x_j^s > 0$, whereas minerals occurring in peritectic relationships with the melts have $x_j^s < 0$. Regardless of the nature of the cotectic or peritectic association, the condition $\sum_{j=1}^{m} x_j^s = 1$ is valid for the phase proportions over any crystallization interval.

Upon exit from the block for the calculation of crystallization proportions and redetermination of the accuracy of the iteration loops (see below), the CECT program sets the degree of crystallization to be equal to $\varphi_{cr} + \Delta\varphi_{cr}$, and the current information is fed into the CAPRO block, in which the "numerical crystallization" of the system is conducted. After this, the newly formed phase assemblage is equilibrated following the scheme THERMO $\Leftrightarrow$ CAPRO. Information on the new equilibrium state of the crystallizing system is stored in the INFORM block, and the whole calculation cycle is repeated.

An important comment should be made as to how peritectic reactions are considered. As can be seen from Fig. 9, the CAPRO block involves a specialized routine referred to as *Correction of the Melting–Crystallization Proportions in the Vicinity of Peritectic Points.* It was necessary to include this subroutine in the block because of the possibility that one of the liquidus phases can completely dissolve in the course of crystallization. In the latest versions of COMAGMAT, this problem is solved in the general form and does not depend on the type of the solid phase dissolving in the melt.

The accuracy of the calculated temperatures and compositions should be redetermined during each calculation stage, because these parameters control the convergence of the iteration loops. This mathematical accuracy of the "core" of the calculation scheme (Fig. 8) should not be mistaken for the accuracy of the solution of the equilibrium problem, which is determined by specifying the integral external parameters ε_T and ε_i^l (Fig. 9). At a crystallization step of $\Delta\varphi_{cr}$ = 1–2 mol %, the optimum values are ε_T = 0.2–0.5°C; and for the accurate calculation of the liquid phase composition, we usually assume ε_i^l = 0.1–0.2 mol %. Of course, these characteristics do not correspond to the actual accuracies of the calculated phase equilibria, which involve the inaccuracies of the input data, primarily, the parameters A_r^j and B_r^j of mineral–melt geothermometers (26).

The plausibility of the modeled liquid lines of descent is assayed by comparing with experimental data (see Chapter 2). We believe that the inaccuracies in the liquid lines of descent constructed with the COMAGMAT program meet the requirements of most petrological and geochemical problems that can be solved with the use of this model. Twenty years of our experience in the practical utilization of this algorithm have convinced us that the computation scheme is universal and fast. It allows the convenient introduction of other mineral phases and enables the user to take into

account the effects of pressure, oxygen fugacity, and water occurrence in the melt. This routine is modernized mostly through recalibrating the basic equilibrium equations and improving their accuracy on the basis of extensive data provided by experimental petrology.

CHAPTER 2. DEVELOPMENT OF THE COMAGMAT CRYSTALLIZATION MODEL

The algorithm proposed above for simulating the crystallization of multiphase system is the thermodynamic basis for developing realistic models of petrogenetic processes. In constructing such models, we proceeded from the analysis of simplified silicate systems (CFCT and CECT programs) and the use of the simplest mineral–melt geothermometers [Roeder and Emslie, 1970; Longhi *et al.*, 1978; Drake, 1976b; Nielsen and Drake, 1979] to more complicated models that include the effects of melt nonideality, pressure, and water on the phase equilibria and the crystallization of Fe-Ti oxides depending on the redox conditions. Years of calculations with the use of these programs, their analysis and testing led us to the conclusion that it was necessary to calibrate the equilibrium mineral–melt equations for compositional ranges close to those of natural rocks supposed to be examined with these programs. This deliberate limitation of the selection of experimental data utilized in the model calibration allowed us to achieve the maximum accuracy of the calculations and, eventually, improve the reliability of our genetic interpretations of the igneous rocks.

This ideology is principally different from the approach to the modeling of magmatic equilibria explored by, for example, Ghiorso and his colleagues, who had already declared in the mid-1980s that they had developed a MELTS "supersystem" able to cope with the maximally broad composition ranges and crystallization conditions of magmatic melts [Ghiorso *et al.*, 1983; Ghiorso, 1985]. Now these authors admit that the problems of thermodynamic treatment and the quality of some of the experimental data leave little hope that any accurate enough "supersystem for magma modeling" can be developed in the years immediately ahead [Ghiorso, 1997]. Below we will consider empirical equations and dependences making up the basis of the COMAGMAT model, which was designed for solving genetic problems concerning the differentiation of tholeiitic and calc–alkaline magmas [Ariskin *et al.*, 1993; Ariskin, 1999].

2.1. Experimental Database of Phase Equilibria in Igneous Rocks (INFOREX System)

Progress in the application of experimental techniques to studying phase equilibria in igneous rocks resulted in the accumulation of a vast amount of data on the conditions of melting experiments and the compositions of their products. According to our estimates, these data comprise the results of tens of thousands of experimental runs conducted with synthetic and natural silicate systems. The transition from the accumulation of these materials to their active utilization requires from the researcher not only good knowledge of the extensive literature but also his ability to assay how reliable the information is and the knowledge of methodical problems arising when experiments are carried out under different conditions. These problems become even more acute considering progress in the computer simulation of magmatic equilibria with the use of calibrations on the basis of hundreds and thousands of experiments. The wide application of phase diagrams, geothermobarometers, various concentration correlations, etc. to petrologic reconstructions also requires the use of experimental data to evaluate the accuracies of models proposed by different authors and their empirical dependences and extrapolations.

In practice, the solutions of these problems imply the ability to access available information and "filter" the data on the basis of petrochemical criteria (magma composition) and the conditions of the experiments, including their duration, temperature, pressure, oxygen fugacity, and the presence of volatiles. Obviously, the solution of these problems calls for the development of a computer system able to accumulate the flow of experimental information on phase equilibria in igneous rocks and providing a fast expert appraisal of the data obtained. Works centered on the designing of such a system were launched in the 1990s [Ariskin *et al.*, 1992] and resulted in the construction of the INFOREX-4.0 experimental database [Ariskin *et al.*, 1996, 1997b; Meshalkin and Ariskin, 1996; Meshalkin *et al.*, 1996], which was adopted to IBM-PC compatibles and serves as a useful tool for calibrating and testing the COMAGMAT model.

2.1.1. Structure of the INFOREX-4.0 database

In this section, we will refer to the INFOREX system bearing in mind that it includes not only a database but also a related block for processing the information obtained from the database according to certain queries. In fact, this is the first, inevitable step to the designing of an expert petrological system that makes it possible not only to find and process experimental data but also to use these results in the numerical simulation of phase equilibria and testing a diversity of computerized models. The first brief paper devoted to the INFOREX database described the program that included information on 2446 experiments published in 78 papers [Ariskin *et al.*, 1992]. Later, the archive of the database was significantly extended, and the working interface included a series of specialized functions for the search for specified information, its processing, and analysis [Ariskin *et al.*, 1979b].

Statistics of the experimental data. During the preparation of this manuscript, the INFOREX database included information compiled from 310 papers,

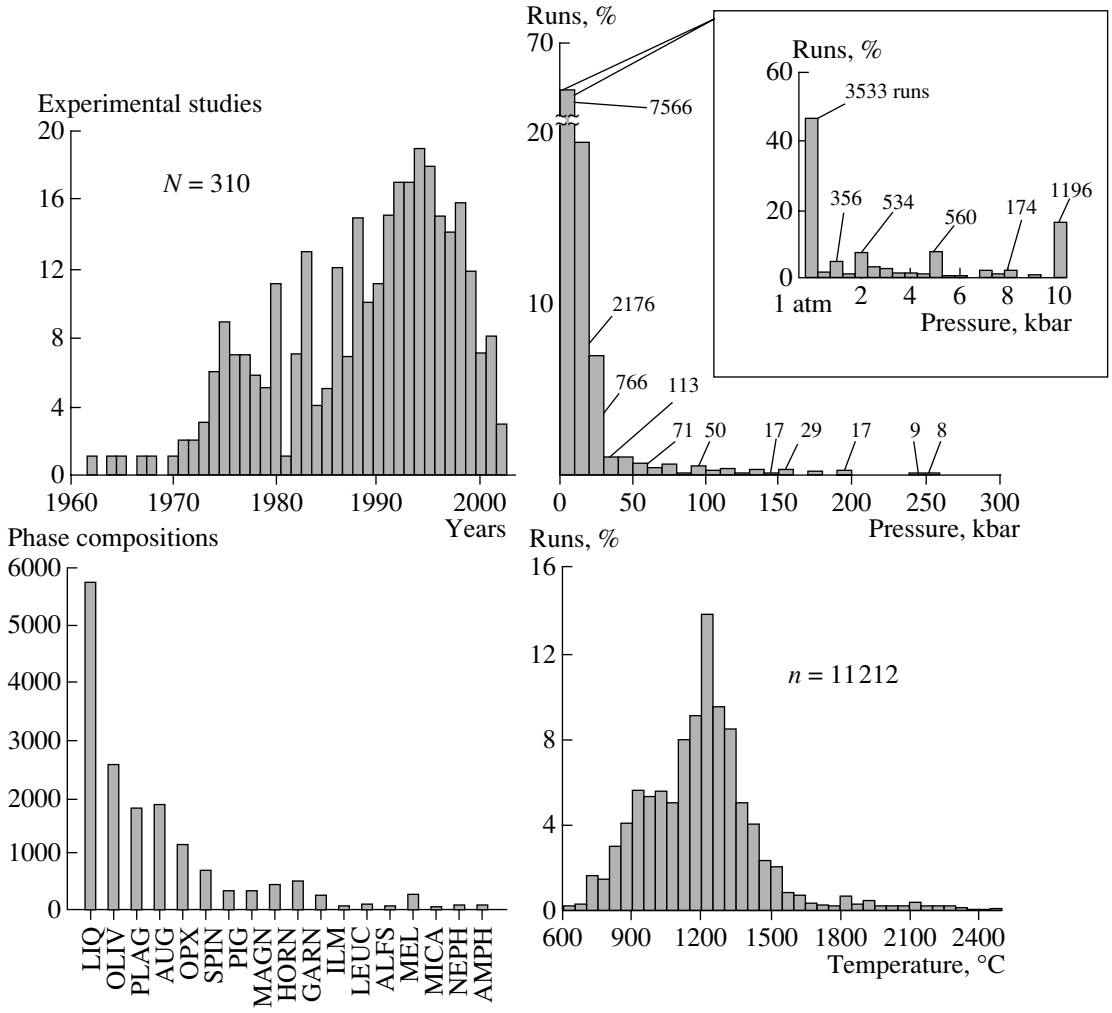

Fig. 10. Statistics of melting-experiment information available in the INFOREX system (as of the publication time).

monographs, and dissertations published from 1962 to 2002 and from some unpublished materials available to the authors (Fig. 10). This data selection represents 11 212 experiments, 78% of which pertained to natural rocks, 6317 experiments conducted under anhydrous conditions, and the rest carried out in the presence of $H_2O \pm CO_2$. The experiments at $P = 1$ atm account for ~32%, and, hence, the bulk of the information pertains to experiments under elevated and high pressures. Figure 10 illustrates the distribution of the experimental runs according to pressure and temperature. The overall number of microprobe analyses of experimentally synthesized phases was 16 210, with the most representative data characterizing quench glasses (n = 5727), *Ol* (2520), *Pl* (1802), and high-Ca pyroxene 1924 (see bottom left-hand plot in Fig. 10). A special data block in the INFOREX system includes 442 glass compositions with known Fe^{3+}/Fe^{2+} ratios.

File structure and hierarchy. The basis of the INFOREX database is made up of text files (tables of the compositions of experimentally synthesized phases, starting materials, and volatile components): the hierarchically topmost files include the conditions of the experiments and respective literature references (Fig. 11). These data are stored in the form of ASCII files with constant record lengths and with references in the BIBL.TXT file having an arbitrary order of the bibliographic information record. The files are interrelated through the consecutive numbers of the references, numbers of experiments within a given reference, and file names for phases obtained in the experiments.

The main file with the experimental conditions CONDIT.EXP (Fig. 11) is subdivided into tabulated fields that contain the number of the reference, number of the experiment, rock name, address of the starting material composition, indication of the presence or absence of volatile components in the system, pressure, temperature, oxygen fugacity, experiment duration, and the container capacity. The farther fields are allotted for the phase assemblage identification (glass, olivine, garnet, etc.) with indications of the availability of microprobe analyses.

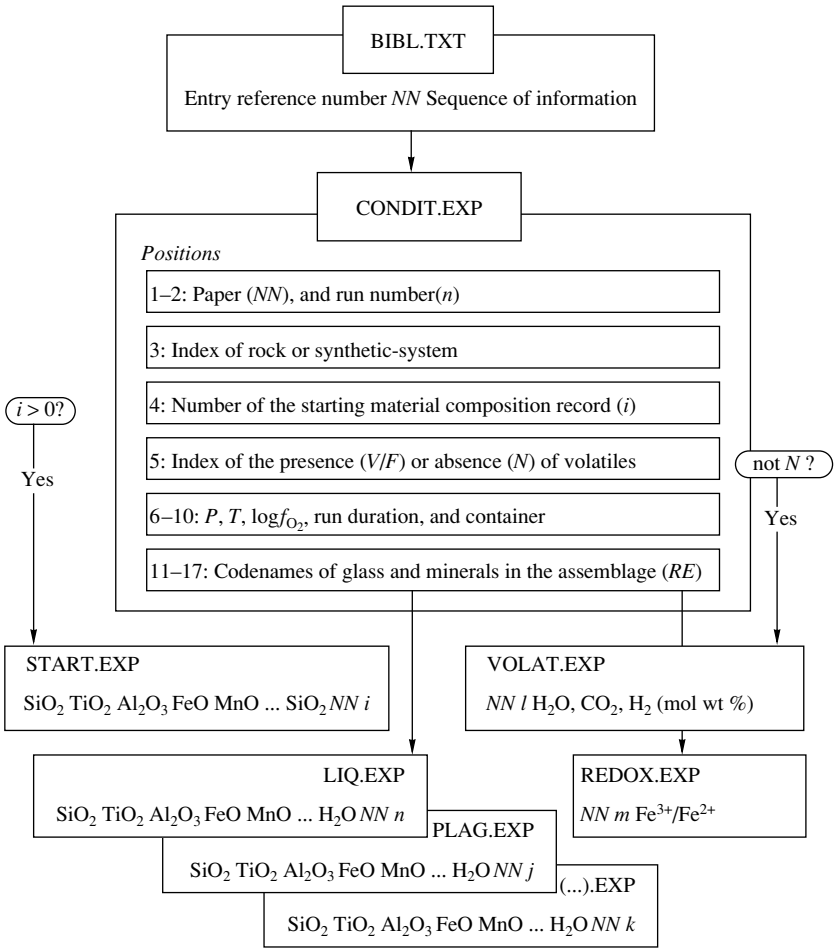

Fig. 11. Structure of the INFOREX-4.0 database (1997). Characters *n*, *j*, *k*, *l*, and *m* denote different run numbers.

Except certain situations (sulfide, carbonate, and metal), the composition files have uniform structures and include concentrations of 12 major oxides in the following order: SiO_2, TiO_2, Al_2O_3, FeO (total), MnO, MgO, CaO, Na_2O, K_2O, P_2O_5, Cr_2O_3, and H_2O. A separate file VOLAT.EXP stores information on experiments under water-saturated (index *F*) or water-undersaturated (index *V*) conditions: the file contains data on the bulk H_2O, CO_2, and H_2 concentrations in the system and/or vapor phase (in weight or molar percent). An important file of nonstandard format is REDOX.EXP, which can be addressed to by the user for retrieving information on the Fe^{3+}/Fe^{2+} ratio of the quench glass.

The system proposed for the accumulation and storage of information in the INFOREX database encompasses various physical parameters and conditions that are cited in most experimental papers and contains components arranged in the succession most customarily used when major-component analyses are published.

Another no less important issue is the compatibility between the formats of data on phase and starting-material compositions and the formats used in the files of initial data for computerized programs of the COMAGMAT series. This significantly facilitates the calibration and testing of the models developed for phase equilibria (see below).

2.1.2. Description of the system management

In developing the system for database management, we adhered to the following principles. First and foremost, the system should be oriented to the solution of petrological problems that are attacked with the use of experimental information on phase equilibria. This implies the designing of easily perceptible and convenient interfaces with the utilization of conventional symbolism and a comprehensive help system accessible from any part of the program. Another requirement is that the system should offer the possibility of correcting and exchanging easily data files that have been created by different researchers and are represented in different formats. This constraint is satisfied by the ASCII structure proposed for INFOREX data files (which allows corrections to be introduced and new files to be created) and the routine of file exchange either via stan-

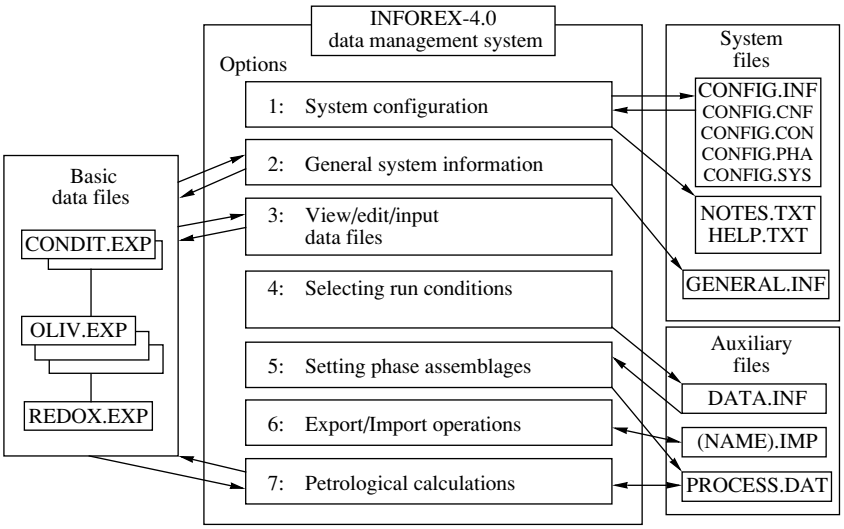

Fig. 12. Main options of the INFOREX-4.0 data management system and the linkage of basic data files.

dard editing programs or, in an interactive regime, directly form the INFOREX system.

Of course, information representation in the form of ASCII files of constant length that is convenient for editing manually results in these files having greater sizes than they could have if stored in a machine representation. Moreover, this makes the information search slightly slower. These disadvantages are, however, apparently compensated by the speed of modern computers. Let us now consider more closely the main options in the management of the INFOREX-4.0 database, which can be arbitrarily subdivided into informational (1, 2, 3, and 6), searching (4 and 5), and applied (7) (Fig. 12).

Configuring the system. This option is intended for specifying the working directories, mineral phase assemblages, and types of rocks and containers in which the experiments were conducted. For this purpose, a specialized interface was proposed, whose structure was described in [Ariskin and Barmina, 2000] and in the manual available at the Internet address http://www.geokhi.ru/~dynamics/ (use the INFOREX option). This documentation also includes descriptions of other interfaces considered below.

General information about the INFOREX system. This command allows the user to retrieve information about the current state of the database, including the total number of papers and experiments, references, contents of the composition files, number of experiments conducted under atmospheric or elevated pressures, and the distribution of the experiments between anhydrous and hydrous systems. The information window can be written to the file GENERAL.INF. The content of any file can also be browsed using the database management system with a keyword-based search for information specified according to a pattern in the files.

Browsing, editing, and appending the database. This regime is convenient for dealing with the results of certain experiments and creating data files including only part of the information, for example, only the temperatures and compositions of the melts published in the paper. The possibility of editing enables corrections of mistakes in the preexisting information.

The DATA INPUT option was developed for relatively small papers, whose data can be input during a single work session with the data management system. Here certain lines in the files of the mineral compositions can be reserved. This routine is carried out after filling the file of conditions and input of information on phase assemblages. The lines are numbered automatically, which precludes mistakes and confusion of the numbers of the experiments.

Selecting experimental conditions. During this stage, the INFOREX-4.0 program browses the file CONDIT.EXP and selects experiments meeting the search criteria, such as (1) affiliation of the systems with global sets like *Terrestrial*, *Lunar*, *Meteoritic*, or *Synthetic*; (2) correspondence to rock indexes, such as *KOM* for komatiites, *PIC* for picrites, or *BAS* for basalts; (3) the absence and/or presence of volatile components; (4) indices of the containers, such as *PTC* for Pt wire-loop containers; (5) ranges of pressure, temperature, and oxygen fugacity and the duration of the experiment; (6) limitations imposed onto the composition of the experimental glasses in terms of water content and FeO/MgO and Mg/(Mg + Fe) (mol) ratios.

Option (4) is also appended with the possibility of selecting experiments conducted in water-saturated and/or undersaturated conditions, with the data on specified water concentrations in the melts assigned to a separate file. An analogous search can be carried out for experiments with known Fe^{3+}/Fe^{2+} ratios in the quench glasses. Moreover, recently an option was

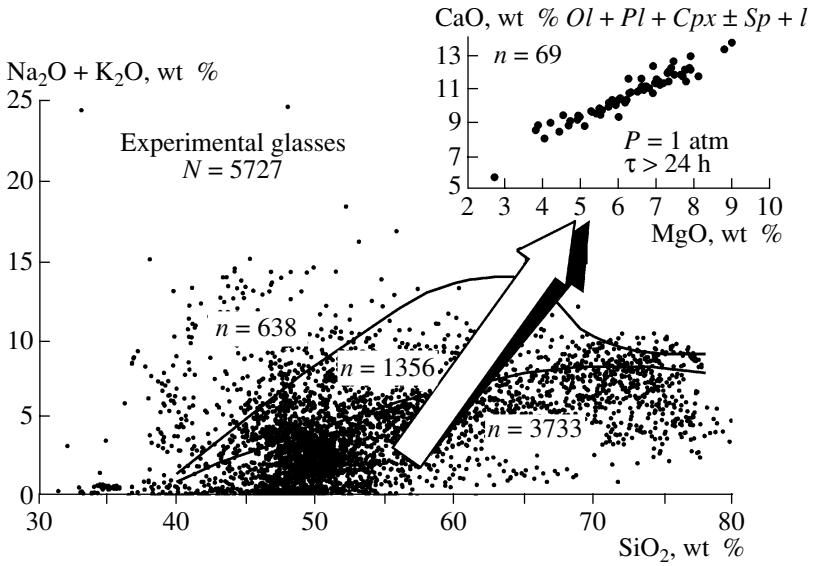

Fig. 13. Subdivision of the composition of experimental glasses into the "tholeiitic", "subalkaline," and "alkaline" series [*Classification and Nomenclature*…, 1981]. The insert shows an additional selection of "tholeiitic" glasses produced in anhydrous experiments lasting for $\tau > 24$ h under 1 atm pressure and with *Ol*, *Pl*, and *Aug* (±*Sp*) on the liquidus.

designed that allows data subdivision based on affiliation with certain petrochemical series (tholeiitic, subalkaline, and alkaline) with the use of the $Na_2O + K_2O$–SiO_2 diagram [*Classification and Nomenclature*…, 1981] (Fig. 13).

Selecting phase assemblage. The temporary file created after the execution of the SELECTING EXPERIMENTAL CONDITIONS routine is identical in format with the file CONDIT.EXP and contains information on the sets of phase assemblages and melt–mineral equilibria at the specified ranges of parameters. When the option SELECTING PHASE ASSEMBLAGE is executed, this file is addressed to, and data on the liquidus phases are browsed. This allows the user to select phase compositions for certain associations of melt and minerals, for example, *Ol*–*Pl*–melt or *Ol*–*Pl*–*Aug*. This problem often arises in petrological practice when it is desirable to systematize the compositions of liquids derived by the partial melting of peridotites and occurring in equilibrium with three or four minerals. Other applications of this option pertain to the analysis of data on mineral–melt and mineral–mineral equilibria when geothermometers and geobarometers are developed.

Exchanging data files. The extension of the circle of INFOREX users puts forth the problem of the simple and convenient exchange of data files. This task is fulfilled with the option EXCHANGING DATA FILES, which can be used to write information related to the selected paper (export routines) or to append the database with data on experiments conducted by other researchers (import routine).

2.1.3. Petrological applications and significance of the INFOREX system

The INFOREX system is centered mainly on data preparing for the construction of mineral–melt geothermometers with the further including of these dependences in the COMAGMAT petrological complex [Ariskin *et al.*, 1993]. At the same time, in solving this particular problem, the user often faces a series of utilitarian petrological problems linked with the determination of the Fe^{3+}/Fe^{2+} ratio in experimental glasses, evaluation of the oxygen fugacity and water concentration in the melt, and various petrochemical calculations (such as projecting glass compositions into pseudoternary diagrams and the construction of concentration plots). The necessity of additional programming to automate these operations led us to design a specialized block of the iNFOREX database that is referred to as PETROLOGICAL CALCULATIONS and includes the following options (Fig. 14):

(1) calculating regression coefficients describing mineral–melt equilibria for olivine, plagioclase, augite, pigeonite, orthopyroxene, spinels, and ilmenite (32 geothermometers);

(2) calculating the Fe^{3+}/Fe^{2+} ratio in experimental glasses in compliance with nine different models [Sack *et al.*, 1980; Kilinc *et al.*, 1983; Kress and Carmichael, 1988; Borisov and Shapkin, 1990; Kress and Carmichael, 1991; Mysen, 1991; Nikolaev *et al.*, 1996 (three variants)];

(3) calculating the H_2O solubility in melts for water-saturated experiments in compliance with three models [Burnham, 1994; Dixon *et al.*, 1996; Al'meev and Ariskin, 1996];

(4) auxiliary calculations, including the normalization of glass compositions to 100% (for anhydrous and hydrous systems) and their projecting into ternary plots, such as OLIV–PLAG–QTZ or QTZ–AN–AB.

The sequence of these operations is unified for all types of the calculations: (i) the user selects (on the monitor) a file of initial data (like PROCESS.DAT, see Fig. 12), which has been preliminarily composed with the aid of search routines; and (ii) the user selects the type of calculations, for which parameters are specified if necessary in compliance with a certain model. Then the control is transferred to the computer program that creates an output file with the calculation results. Below we will consider examples of the practical utilization of these petrological options for constructing geothermometers of mineral–melt equilibria, evaluating the Fe^{3+}/Fe^{2+} ratio in the melt, and calculating water concentrations in quench glasses.

The INFOREX-4.0 database and related subroutines for processing experimental information offer a new efficient tool for petrologic research. With the appearance of this system, the problem of searches for and analysis of subliquidus experiments can be solved within a few seconds, and maximally accurate mineral–melt geothermometers can be constructed by a user with certain skills in a matter of only a few hours. The petrologists acquires access to the results of thousands of experiments on the melting of synthetic and natural samples, and the thermometers and various empirical dependences can be tested therewith against approximately 15000 analyses of experimental phases.

We think that the system can right now become a petrological tool as necessary as a microscope or microprobe for each qualified petrologist. Having INFOREX at hand, petrologists can test and estimate the applicability of melt–mineral and two-mineral geothermometers abounding in the literature and, what is particularly appealing, design them personally for any desirable ranges of compositions and conditions.

Now INFOREX is actively introduced into the practice of petrological research in spite of the traditional interest of specialists in computerized models of fractionation, melting, and other algorithms oriented to the solution of petrological problems *per se*. Many researchers realize that problems of the accuracy and applicability of certain computer programs cannot be addressed exclusively to the program builders. The direct application of computerized models to natural objects seems to be possible only if these programs are preliminarily tested with the use of experimental data encompassing the range of magma compositions of interest for the pertologist or geochemist. The INFOREX-4.0 system offers here a wealth of possibilities.

2.2. Calibration of the COMAGMAT Crystallization Model

2.2.1. Fe^{3+}/Fe^{2+} equilibrium in magmatic melts

FeO and Fe_2O_3 are among the most important components of any silicate melt, and their proportions control the physical properties of magmatic liquids [Dingwell, 1991; Kress and Carmichael, 1989; Toplis *et al.*, 1994b], the composition of mafic silicates crystallizing from them, the conditions under which iron ore minerals appear on the liquidus [Hill and Roeder, 1974; Nielsen *et al.*, 1994; Toplis and Carroll, 1995; Ariskin and Nikolaev, 1996], and, eventually, the direction of basaltic magma fractionation [Osborn, 1959; Presnall, 1966; Babansky *et al.*, 1983; Ghiorso and Carmichael, 1985; Kadik *et al.*, 1986, 1900; Ariskin *et al.*, 1988a, 1988b; Toplis and Carroll, 1996].

From the thermodynamic viewpoint, there are two conventionally recognized regimes of FeO and Fe_2O_3 behaviors in the crystallization process. In a closed system, variations in the proportions of these components are controlled by the composition of mafic silicates and the proportions and compositions of crystallizing Fe-bearing oxides (magnetite and ilmenite). Olivine and pyroxene crystallization results in the partial removal of FeO from the silicate melt, the relative enrichment of Fe_2O_3, and an increase in the bulk degree of Fe oxidation in the melt $Fe_{ox} = Fe^{3+}/(Fe^{3+} + Fe^{2+})$. Magnetite crystallization exerts the opposite effect, because the removal of Fe_2O_3 and FeO in the approximate proportion of 1 : 1 causes a rapid decrease in the "degree of oxidation" of the silicate liquid [Ghiorso and Carmichael, 1985; Ariskin *et al.*, 1988b; Toplis and Carroll, 1996].

When the crystallizing system is open or buffered with respect to oxygen pressure, the Fe^{3+}/Fe^{2+} ratio in the melt is controlled by the redox reactions

$$FeO(l) + 1/4O_2 = 1/2Fe_2O_3(l) \quad (53a)$$

or

$$FeO(l) + 1/4O_2 = FeO_{1.5}(l) \quad (53b)$$

depending on the chosen melt components. Reaction (53b) is more convenient in the sense that its thermodynamic analysis makes it possible to identify the nature of the dependence of the Fe^{3+}/Fe^{2+} ratio in the melt on intensive parameters. The equilibrium constant of this reaction is

$$K_{eq}^{ox} = a^l_{FeO_{1.5}}/(f^{1/4}_{O_2} a^l_{FeO}), \quad (54)$$

where $a^l_{FeO_{1.5}}$ and a^l_{FeO} are the $FeO_{1.5}$ and FeO activities in the melt. Taking into account the concentration dependences of the activities ($a^l_{FeO_{1.5}} = \gamma^l_{FeO_{1.5}} x^l_{FeO_{1.5}}$ and $a^l_{FeO} = \gamma^l_{FeO} x^l_{FeO}$), expression (54) can be transformed into the equation

$$\ln(x^l_{FeO_{1.5}}/x^l_{FeO}) = \ln K^{ox}_{eq} + 0.25\ln f_{O_2} - \ln(\gamma^l_{FeO_{1.5}}/\gamma^l_{FeO}). \quad (55)$$

In the general case, the value of K^{ox}_{eq} depends on the changes in enthalpy and entropy of reaction (53b)

$$\ln K^{ox}_{eq} = -(\Delta H^{ox}_{eq} - T\Delta S^{ox}_{eq})/RT, \quad (56)$$

and, theoretically, the Fe^{3+}/Fe^{2+} ratio (55) can be calculated from the thermodynamic properties of Fe_2O_3 and FeO in melt and a specified oxygen fugacity. In practice, the values of the FeO and Fe_2O_3 (or $FeO_{1.5}$) activity coefficients in melt are unknown, because of which the proportions of *Fe(III)* and *Fe(II)* can be evaluated by empirical dependences in the form

$$\ln[Fe(III)/Fe(II)] = a\ln f_{O_2} + b/T + c + \sum_{i=1}^{n} d_i x^l_i, \quad (57)$$

where a, b, and d_i ($1 \le i \le n$) are the regression coefficients, and $Fe(III)/Fe(II) = x^l_{Fe_2O_3}/x^l_{FeO}$ [Sack *et al.*, 1980; Kilinik *et al.*, 1983; Kress and Carmichael, 1989, 1991; Borisov and Shapkin, 1990; Moore *et al.*, 1995; Baker and Rutherford, 1996; Righter and Carmichael, 1996] or $x^l_{FeO_{1.5}}/x^l_{FeO}$ [Mysen, 1991; Nikolaev *et al.*, 1996].

Equation (57) is calibrated based on the results of redox experiments in which the starting materials are held at temperatures above the liquidus and a specified oxygen fugacity, and the quench glasses are analyzed for the actual FeO concentration. This enables estimating the Fe_2O_3 concentration in the melt as $Fe_2O_3 = 1.1113 \times (FeO_{total}–FeO)$. Comparing (53)–(57) indicates that, in the ideal case, the coefficient a is equal to 0.25, b is commensurable with the reaction enthalpy ΔH^{ox}_{eq}, and the sum $c + \sum_{i=1}^{n} d_i x^l_i$ takes into account the effect of the entropy change ΔS^{ox}_{eq} and that of composition.

Sack *et al.* [1980] conducted a series of 57 anhydrous experiments with the aim of exploring the degree of Fe oxidation in natural melts and processed the results using Eq. (57) together with data on 86 redox experiments conducted by other researchers at atmo-

Table 5. Regression coefficients obtained for Eq. (57) by different researchers over the time span of 1980–1996

Equation parameter	[Sack *et al.*, 1980] (n = 143)	[Kilink *et al.*, 1983] (n = 186)	[Kress and Carmichael, 1991] (n = 228)	[Nikolaev *et al.*, 1996]: (tholeiitic series, n = 56)
	$\ln(x^l_{Fe_2O_3}/x^*_{FeO})$			$\log(x^*_{FeO_{1.5}}/x^*_{FeO})$
$a(\ln f_{O_2})$	0.2181	0.2185	0.196	0.1395*
$b(1/T)$	13185	12670	11492	3282.2
c	–4.4993	–7.54	–6.675	–
d_{SiO_2}	–2.1504	–	–	–1.4238
d_{TiO_2}	–	–	–	–4.3585
$d_{Al_2O_3}$	–8.3516	–2.24	–2.243	–9.4488
$d_{FeO(tot)}$	–4.4951	1.55	–1.828	–0.7550
d_{MgO}	–5.4364	–	–	–2.2326
d_{CaO}	0.0731	2.96	3.201	0.3404
d_{Na_2O}	3.5415	8.42	5.854	2.4766
d_{K_2O}	4.1869	9.59	6.215	4.4534
$d_{P_2O_5}$	–	~(–6)**	–	–
d_{OH^-}	–	~(+8.8)***	–	–
Pressure	–	–	taken into account****	–

*The equations in [Nikolaev *et al.*, 1996] used decimal logarithms $\log f_{O_2}$;

** the effect of phosphorus was evaluated using the results in [Toplis *et al.*, 1994b];

*** the effect of water was evaluated based on data from [Baker and Rutherford, 1996] for systems of rhyolite composition;

****the pressure factor was calibrated based on data on the compressibility and heat capacity of iron oxides in melt.

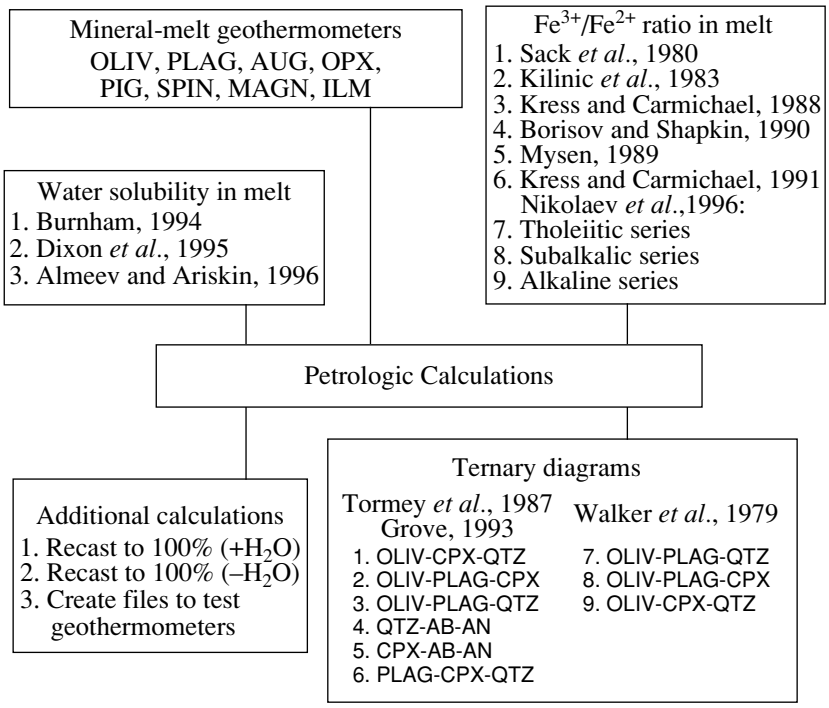

Fig. 14. Main options of the PETROLOGICAL CALCULATIONS routine.

spheric pressure [Kennedy, 1948; Fudali, 1965; Shibata, 1967; Thornbern, 1980]. As a result, an empirical dependence was derived, whose parameters are listed in Table 5. A few years later, the basic selection for the calibration was appended with the results of other experiments conducted in air [Kilink *et al.*, 1983]. The Kilink equation (see Table 5 for parameters) is the most popular among specialists in the computer simulation of phase equilibria and is commonly employed as an accuracy criterion in the analysis of newly obtained results of redox experiments [Moore *et al.*, 1995; Baker and Rutherford, 1996; Righter and Carmichael, 1996]. Later attempts to revise the form of Eq. (57) and incorporate newly obtained experimental data have not improved its accuracy: the accuracies in the estimates of the concentrations of iron oxides persistently varied about 0.2 wt % for FeO and 0.3–0.4 wt % for Fe_2O_3 [Kress and Carmichael, 1989, 1991].

Analyzing data on redox equilibria in melts, Borisov [1988] noted that the empirical coefficients *b* of the reciprocal temperature in (57) are not constant and vary within broad limits, roughly from 2000 to 10000 for different compositions. This cast some suspicion on the possibility of adequate describing the Fe_2O_3/FeO or Fe^{3+}/Fe^{2+} ratios in all classes of igneous rocks by equations that make use of constant coefficients *b*. To take this factor into account, another equation was proposed, whose *a* and *b* parameters were compositional functions [Borisov and Shapkin, 1990]. The parameters of this equation were calibrated on the basis of data from [Kilink *et al.*, 1983], and a comparison of the results with the model of Kilink has testified to a slight but systematic improvement of the accuracy when the B&S equation was used to solve inverse problems.

Another way to attack this problem was proposed by Mysen [1991], who published an empirical equation with six chemical parameters (Al/Al + Si, Fe^{3+}/Fe^{3+} + Si, and others) as independent variables, which were based on the author's understanding of the structural state of a silicate liquid. The use of this equation is complicated by the necessity of constructing an iteration loop that takes into account that the FeO and Fe_2O_3 concentrations are simultaneously contained in the right- and left-hand parts of the equation. Testing of Mysen's [1991] equation demonstrates that, in spite of the optimistic declarations, it does not lead to any improvements of the calculation accuracy as compared with other models [Nikolaev *et al.*, 1996].

A more pragmatic approach to the improvement of the accuracy of the redox calculations required imposing additional limitations on the calibration conditions in terms of the compositions of the quench glasses and the oxygen fugacity. To solve this problem, we used information from the INFOREX-3.0 database [Ariskin *et al.*, 1996]. Of the 298 redox experiments contained there, we rejected the results obtained in simple synthetic systems and under the most oxidizing conditions $\log f_{O_2} > \mathrm{NNO} + 1$. The selection of compositions thus obtained (170 analyses) was subdivided into four series: arbitrarily "tholeiitic" (n = 56), "subalkaline" (n = 50), "alkaline" (n = 50), and "andesite–rhyolitic"

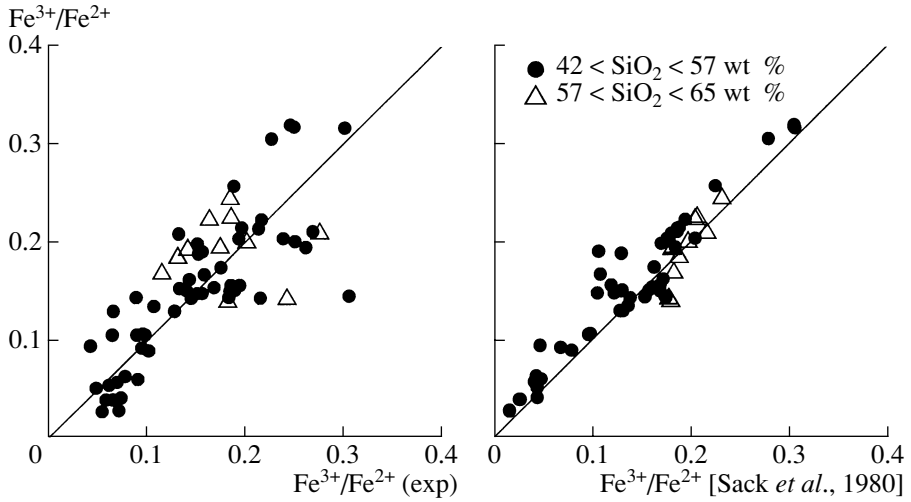

Fig. 15. Comparison of experimental and calculated Fe^{3+}/Fe^{2+} ratios in "tholeiitic" and andesitic melts at oxygen fugacities below NNO + 1. Data on redox equilibria from the INFOREX-4.0 system [Ariskin *et al.*, 1997b]: tholeiitic basalts—55, andesites—11. The left-hand plot demonstrates how experimental values are reproduced when the B&S equation is used [Borisov and Shapkin, 1990]; the right-hand plot compares the results of calculations by the B&S [Borisov and Shapkin, 1990] and Sack *et al.* [1980] models.

($n = 14$), which were processed separately according to linear model (57).

The parameters of the corresponding empirical dependence for melts of the tholeiitic series are listed in Table 5. The accuracy with which the inverse problem was solved in terms of the Fe^{3+}/Fe^{2+} ratio with the use of these coefficients was ±0.029 on average, which is virtually undistinguishable from the B&S model (±0.032) and is slightly better than the average accuracy of equations in [Sack *et al.*, 1980; Kilink *et al.*, 1983; Kress and Carmichael, 1989, 1991; Mysen 1991], which is about ±0.035.

Thus it has to be acknowledged that there is still no approach enabling a principal improvement in the accuracy of redox calculations in determining the Fe^{3+}/Fe^{2+} ratios of melts. The average inaccuracies of $(Fe^{3+}/Fe^{2+})_{exp}$–$(Fe^{3+}/Fe^{2+})_{calc}$ are likely to be on the order of ±0.03, and this is the best that can be achieved if data from different laboratories are made consistent [Nikolaev *et al.*, 1996]. This situation is illustrated in Fig. 15, in which experimental data on the Fe^{3+}/Fe^{2+} ratio in tholeiitic and andesitic melts are compared with calculation results by the models of Borisov and Shapkin [1990] and Sack *et al.* [1980].

Effects of other parameters. The results in [Toplis *et al.*, 1994] demonstrate that an increase in the P_2O_5 concentration leads to the partial reduction of Fe_2O_3, and the scale of this phenomenon is comparable with the effect of alkaline components and is enhanced with the transition to more reduced conditions (Table 5). The effect of water was examined in [Moore *et al.*, 1995; Baker and Rutherford, 1996]. A somewhat unexpected conclusion was that water does not significantly affect redox equilibria involving iron: most of the experiments show a good agreement between the values of melt oxidation determined experimentally and calculated by the equation from [Kilink *et al.*, 1983]. The high coefficient of the hydroxyl component (Table 5) pertains only to systems of rhyolitic composition [Baker and Rutherford, 1996]. The influence of pressure was quantified based on data on the FeO and Fe_2O_3 compressibility and heat capacity in melt [Kress and Carmichael, 1991]. These authors note that the volume difference of oxidation reaction (53) remains positive up to pressures of about 30 kbar, and the Fe^{3+}/Fe^{2+} ratio at a constant temperature and oxygen fugacity slightly decreases with increasing pressure. In practical calculations, this effect is negligibly small.

Most programs of the COMAGMAT series use Eq. (57) with the parameters proposed by Sack (Table 5). The newest version of the METEOMOD model [Ariskin *et al.*, 1997a] allows the user to vary the regression coefficients and to use the equations from [Kilink *et al.*, 1983; Borisov and Shapkin, 1990; Kress and Carmichael, 1991]. Later calculations have demonstrated that the insignificant differences in the accuracy of these equations practically do not affect the temperatures and compositions of the crystallizing silicates. In simulating the crystallization of Fe-bearing oxides, the errors in the estimates of the FeO and Fe_2O_3 concentrations are always significant, which calls for the application of specialized calibrations techniques for ilmenite and magnetite (see below).

Also, it seems to be important that the method proposed in Chapter 1 for the minimization of the thermodynamic potential allows for the openness of the system with respect to oxygen and the simultaneous solution of the equilibrium equations for oxidation reactions (53) and for the crystallization of minerals. This required a principal transformation of the algorithms presented in Figs. 8 and 9. When closed systems are simulated, Eq. (57) is transformed into a depen-

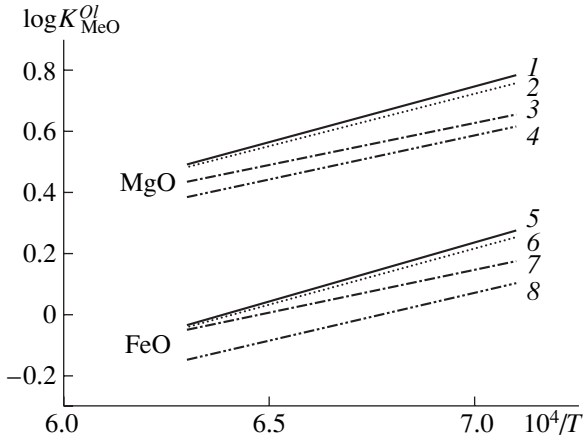

Fig. 16. Temperature dependence of the MgO and FeO partition coefficients for olivine and melt. Data: (*1*, *5*) [Roeder and Emslie, 1970]; (*2*, *6*) [Roeder, 1974]; (*3*, *7*) [Longhi *et al.*, 1978], low-Ti lunar basalts; (*4*, *8*) [Longhi *et al.*, 1978], high-Ti lunar basalts.

dence of $\log f_{O_2}$ on temperature and the degree of melt oxidation, with $\log f_{O_2}$ calculated accurate to 0.5–0.7 logarithmic units.

2.2.2. Principles of construction of mineral–melt geothermometers

Roeder and Emslie [1970] were the first to start systematically experimentally studying the distribution of major elements between minerals and basaltic melt. These researchers conducted 27 melting experiments on alkaline basalts from Hawaii and demonstrated that the dependence of the molar partition coefficients for MgO and FeO between olivine and melt on reciprocal temperature is linear at temperatures within the range of 1150–1300°C and an oxygen fugacity of $-12 < \log f_{O_2} < -0.7$ (Table 1, Fig. 16). The correlation coefficients between $\log K^{Ol}_{MeO}$ and $1/T$ appeared to be quite high, $r = 0.965$ for MgO and $r = 0.880$ for FeO, which suggested that these empirical relations can be utilized for the thermometry of olivine-bearing igneous rocks. The later testing of these equations with the use of independent experimental data has demonstrated that they yield estimates accurate to approximately 20°C at known olivine and melt compositions.

Later 19 additional experiments with basalts from other areas were conducted at lower oxygen fugacities $\log f_{O_2} < -12$ [Roeder, 1974]. The processing of these results together with those from [Roeder and Emslie, 1970] confirmed the dependences identified previously (Fig. 16), but the experimental points were significantly scattered relative to the calculated regression lines.

These studies coincided in time with the beginning of the intense investigations of lunar rocks, including the experimental studies of phase equilibria in lunar basalts. The experiments with low- and high-Ti mare basalts in strongly reduced environments also resulted in establishing linear dependences between $\log K^{Ol}_{MeO}$ and $1/T$ [Longhi *et al.*, 1978], although the regression lines deviated from the trends presented in [Roeder and Emslie, 1970; Roeder, 1974] (Fig. 16).

The thermodynamic consideration of this problem pointed to a strong dependence of the *Ol*–melt partition coefficient on the SiO_2 activity in the liquid [Longhi *et al.*, 1978], see Eqs. (20)–(24). Longhi examined several versions of geothermometers and arrived at the conclusion that the introduction of concentration (X^l_{Si}) or structural–chemical [2Si/O, Si/(Si + Al). etc.] parameters in Eqs. (22), (24) enables one to calculate the complex partition coefficients $K^{Ol(*)}_{MeO} = K^{Ol}_{MeO}/a^l_{SiO_2}$, which provide a better correlation of $\log K^{Ol(*)}_{MeO}$ and $1/T$. The improvements were achieved for both terrestrial [Roeder, 1974] and lunar [Longhi *et al.*, 1978] olivine geothermometers, and the space between the regression lines for the same component in diagrams like Fig. 16 somewhat decreased (although was still significant).

This fact can be explained by certain compositional features of lunar basalts, which are systematically enriched in FeO and depleted in alkalis compared with terrestrial basalts. This conclusion was compatible with the results obtained for simple synthetic systems: the coherent description of the olivine liquidus surface in various diagrams requires the assumption that the *Fo* and *Fa* activities strongly depend on the normative *Ab* and *Ne* concentrations [Perchuk and Vaganov, 1978]. The problem of the effect of silicity and alkalinity on partition coefficients was further explored by Drake [1976b], who examined the *Pl*–melt equilibrium both experimentally and theoretically.

Drake conducted 55 experiments with synthetic compositions ranging from "basalts" to "rhyolites" under atmospheric pressure and temperatures of 1095–1400°C. The oxygen fugacity was not controlled, and the melting experiments lasted for no less than one week, which allowed the author to obtain crystals of relatively homogeneous composition (±3 mol % *An*). During the first stage of the thermodynamic treatment of these experimental data, simple weight partition coefficients D^{Pl}_i (i = Na, Ca, Al, Si) were calculated and a dependence of $\ln D^{Pl}_i$ on $1/T$ was derived. The correlation between these parameters appeared to be insignificant to recommend them as geothermometers for natural magmatic equilibria.

In order to create a reliable plagioclase geothermometer, Drake proposed not to consider the partition coefficients but instead to analyze the temperature dependences for equilibrium constants of the crystalli-

zation reactions of plagioclase components, see Eqs. (30a) and (30b)

$$K_{An}^{Pl} = x_{An}^{Pl}/a_{\mathrm{CaO}}^{l1}(a_{\mathrm{AlO}_{1.5}}^{l1})^2(a_{\mathrm{SiO}_2}^{l1})^2, \quad (58a)$$

$$K_{Ab}^{Pl} = x_{Ab}^{Pl}/a_{\mathrm{NaAlO}_2}^{l2}(a_{\mathrm{SiO}_2}^{l2})^3. \quad (58b)$$

The activities of components in plagioclase were taken equal to the anorthite and albite mole fractions (which implies the ideal mixing model of plagioclase components). In this approach, the main contribution to the integral effect of nonideal mixing is attributed to interactions between melt components.

The choice of these components for the formal thermodynamic description is arbitrary: the problem was formulated as a search for such a set of components of the liquid phase that the substitution of their activities for concentrations in Eqs. (58a) and (58b) would make it possible to effectively take into account interaction reactions in the melt and to obtain maximally linear dependences of $\ln K_{An}^{Pl}$ and $\ln K_{Ab}^{Pl}$ on $1/T$. To develop this subideal model, Drake inspected two variants of the activities of melt components: $l1$ was the model of ideal mixing of single-cation oxides, and $l2$ was a modified variant of the model in [Bottinga and Weill, 1972].

In the former model, the melt components were assumed to be molecules like SiO_2, $AlO_{1.5}$, FeO, $NaO_{0.5}$, and others. The other model considered the liquid to be an ideal mixture of unassociated (MgO, FeO, and SiO_2) and associated oxides. The approaches of Drake [1976b] and Bottinga and Weill [1972] differed in that, upon subdividing cations into two groups: network-modifying (TiO_2, MgO, FeO, and CaO_{ex}) and network-forming (SiO_2, $KAlO_2$, $NaAlO_2$, and $CaAl_2O_4$), the former author postulated that components of only one type could mix ideally. Formally, this meant that the activity of, for example, silica was calculated as the ratio of the number of SiO_2 moles to the sum of the molar numbers of network-forming components, which implied the absence of their interaction (mixing) with network-modifying components. These models were eventually referred to as two-lattice models.

An analysis of the temperature functions of the equilibrium constants calculated for each component in compliance with the two models demonstrated that the best linear correlation between $\ln K_{Ab}^{Pl}$ and $1/T$ can be yielded by the dependence in which K_{Ab}^{Pl} was calculated by the two-lattice model (Fig. 17). This dependence was proposed as a plagioclase thermometer, which ensured an accuracy of ~20°C, according to the results of independent testing [Ariskin and Barmina, 1990].

This result demonstrated that the two-lattice model proposed by Drake can adequately describe the mixing properties of components in silicate liquids, such as the absence of "free" cations of alkaline metals and their association with Al–O tetrahedra. Paradoxically, the

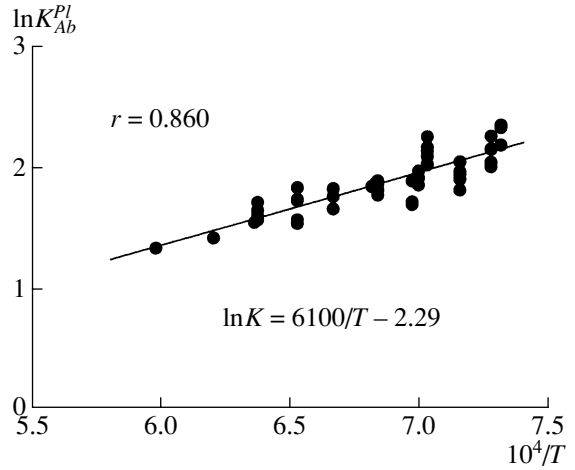

Fig. 17. Temperature dependence for the equilibrium constant of the crystallization reaction of the albite component in plagioclase. Data [Drake, 1976b]: the K_{Ab}^{Pl} was calculated based on the two-lattice model including network formers and network modifiers.

crystallization of anorthite was, conversely, described more adequately by the single-cation model of oxides $l1$ (see parameters in Table 1). This phenomenon was explained by certain mixing properties of CaO in silicate melts [Drake, 1976b]. This assumption has received support from later research conducted by Nielsen and colleagues [Nielsen and Drake, 1979; Nielsen and Dungan, 1983].

Nielsen and Drake [1979] conducted the thermodynamic analysis of the results of experiments describing the *Px*–melt equilibrium. Although practically no systematic data on the distribution of major elements between pyroxenes and silicate melts had been published in the literature by that time, the researchers managed to compile a selection of compositions representing a number of presumably equilibrium experiments. The experiments were conducted at temperatures of 1108–1320°C and f_{O_2} ranging from 10^{-8} to 10^{-14} atm. The compositions of the starting mixtures ranged from low-Fe basalts with significantly varying concentrations of alkalis and alumina to high-Fe, low-alkaline lunar basalts. Nielsen and Drake [1979] subdivided all available data into two groups: one of them included 32 pairs of the compositions of coexisting high-Ca pyroxene (*Aug*) and melts, and the other consisted of 31 compositional pairs of low-Ca pyroxene (*Opx* and *Pig*) and melts. The thermodynamic treatment of the data was carried out separately for each of the groups, without assigning Fe in the melt to FeO and Fe_2O_3. The authors focused on crystallization reactions like

$$\mathrm{MeO}(NM) + \mathrm{SiO}_2(NF) = \mathrm{MeSiO}_3(Px), \quad (59)$$

where Me is Mg, Fe^{2+}, and Ca (*NM* are network modifiers and *NF* are network formers); and reactions

$$\begin{aligned} &MgO(NM) + FeSiO_3(Px) \\ &= MgSiO_3(Px) + FeO(NM). \end{aligned} \quad (60)$$

They considered more than 30 ways of calculating the *Px*–melt equilibrium constants, using the two-lattice model for the silicate liquid in 18 cases and the single-cation model in the rest. The solid phase was considered to be characterized by the ideal mixing of the fictitious solid-solution components ($MgSiO_3$, $FeSiO_3$, and $CaSiO_3$; 24 equations were examined) and to be described by two-site models, including the calculation of the enstatite, ferrosilite, hedenbergite, and diopside activities with regard for the distributions of cations between the M1 and M2 sites (8 equations). The results of these considerations led to two conclusions: (i) the best fits can be obtained with the two-lattice mixing model for the liquid phase, and (ii) the differences between the mixing models for solid-solution components are insignificant from the viewpoint of the accuracy of the geothermometers [Nielsen and Drake, 1979].

Another important outcome of this research was the introduction of a small but significant modification into the preexisting two-lattice model of silicate liquid [Drake, 1976b]: CaO was completely attributed to network modifiers, and the network-forming component $CaAl_2O_4$ was excluded from consideration. The excess Al relative to alkalis was also attributed to network modifiers. The maximally accurate geothermometers *Aug*–melt (1σ = 18.8°C) and low-Ca *Px*–melt (1σ = 22.4°C) were obtained with this new modified variant of the model [Bottinga and Weill, 1972]. We utilized some of these pyroxene geothermometers when developing the first models for basaltic magmas [Ariskin and Frenkel, 1982] (Table 1). In conclusion, it is pertinent to mention that the two-lattice model of melts was most systematically used in [Nielsen and Dungan, 1983].

Thus, the concepts that melt molecules are associated, as followed from physical properties of the melts [Bottinga and Weill, 1972], have been transformed into the empirical model of a two-lattice structure of silicate liquids, which was underlain by data on mineral–melt equilibria. This model provides the basis of most equilibrium equations that serve as the empirical background of the COMAGMAT model.

2.2.3. Thermodynamic and structural interpretation of the two-lattice model

The activities of components in a silicate liquid are calculated by the model [Nielsen and Drake, 1979; Nielsen and Dungan, 1983] in the following succession:

$$\begin{aligned} N^l_{NaAlO_2} &= 2N^l_{Na_2O}, \quad N^l_{KAlO_2} = 2N^l_{K_2O} \\ NF &= N^l_{SiO_2} + N^l_{NaAlO_2} + N^l_{KAlO_2}, \\ N^l_{AlO_{1.5}} &= 2N^l_{Al_2O_3} - N^l_{NaAlO_2} - N^l_{KAlO_2}, \\ N^l_{CrO_{1.5}} &= 2N^l_{Cr_2O_3}, \quad N^l_{PO_{2.5}} = 2N^l_{P_2O_5}, \\ NM &= N^l_{FeO} + N^l_{MnO} + N^l_{MgO} + N^l_{CaO} + N^l_{FeO_{1.5}} \\ &\quad + N^l_{TiO_2} + N^l_{AlO_{1.5}} + N^l_{CrO_{1.5}} + N^l_{PO_{2.5}}, \\ a^l_{SiO_2} &= N^l_{SiO_2}/NF, \quad a^l_{NaAlO_2} = N^l_{NaAlO_2}/NF, \\ a^l_{KAlO_2} &= N^l_{KAlO_2}/NF, \\ a^l_{FeO} &= N^l_{FeO}/NM, \ldots \quad a^l_{FeO_{1.5}} = N^l_{FeO_{1.5}}/NF, \ldots \\ a^l_{PO_{2.5}} &= N^l_{PO_{2.5}}/NM. \end{aligned} \quad (61)$$

This algorithm implies that the sum of alkalis $Na_2O + K_2O$ does not exceed the bulk Al_2O_3 content in the melt, and Eqs. (61) are applicable to systems of low and moderate alkalinity.

In spite of the fact that the two-lattice model of silicate liquids proved efficient in describing the *Pl*–melt and *Px*–melt equilibria, it was repeatedly criticized for its thermodynamic inconsistency. In particular, it was noted that the equations from [Nielsen and Drake, 1979] "lead to absurd results when applied to compositions with broad variations in the ratios of network-forming and network-modifying elements" [Ryabchikov, 1987a]. No less bitter criticism was expressed in Ghiorso [1987], who attracted attention to the fact that the equilibrium constants obtained by Nielsen and Dungan [1983] are inconsistent with available data on the thermodynamic properties of solid phases and melt in the standard state. Nevertheless, it is hard to cast doubt on the fact that the application of the seemingly absurd two-lattice model makes it possible to principally improve the accuracy of mineral–melt geothermometers and achieve consistency between the data of hundreds of experiments conducted at tens of different laboratories. To illustrate this, we use data on the *Ol*–melt equilibrium that were processed with and without the two-lattice model for the silicate melt structure (Fig. 18).

Figure 18 demonstrates the results of thermodynamic treatment of the data of 213 experiments on the *Ol*–melt equilibrium in dry tholeiitic systems ($48 < SiO_2 < 65\%$) under atmospheric pressure. These data were retrieved using the INFOREX-4.0 system and were published in 20 different papers. The duration of all experiments was no less than 48 h, which suggests an equilibrium Mg^{2+} and Fe^{2+} distribution between olivine and melt. The parameters of the regression lines

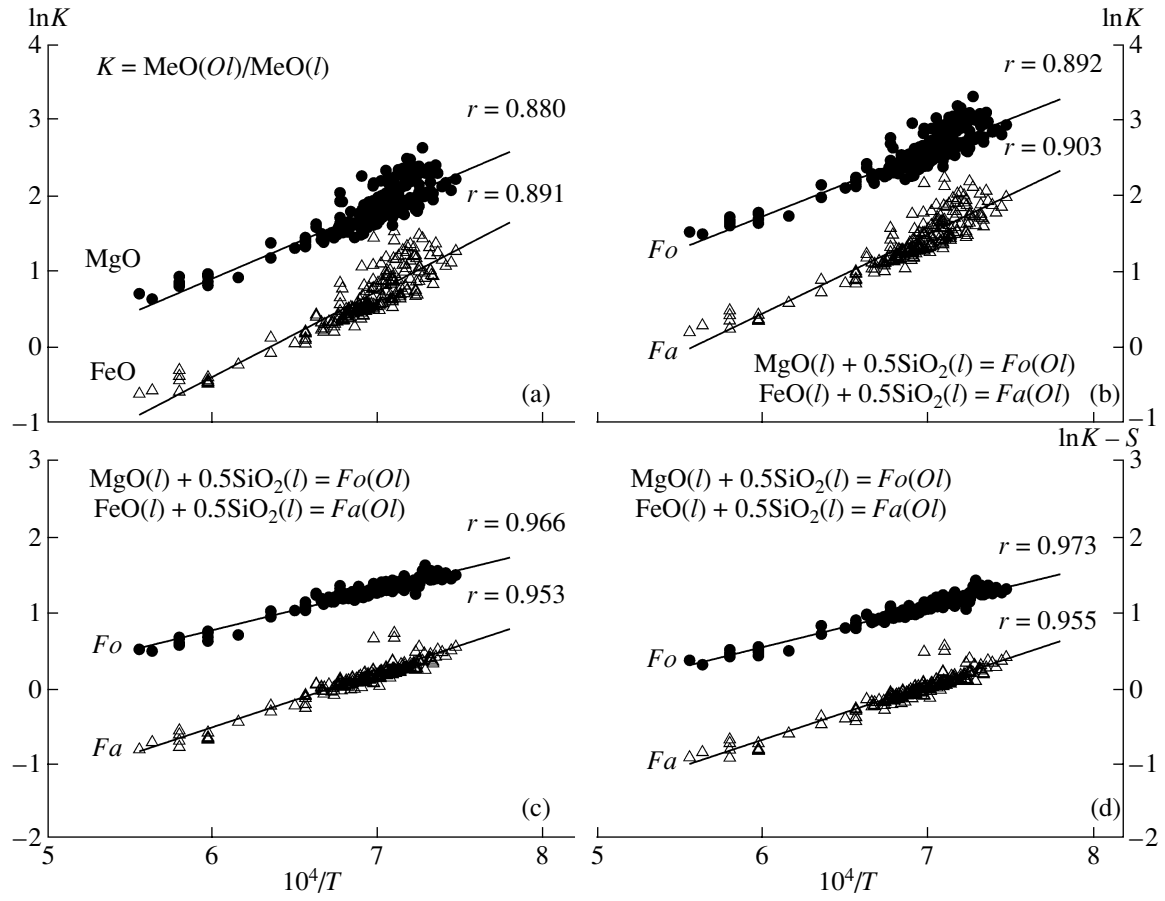

Fig. 18. Temperature dependences of the partition coefficients and equilibrium constants of the crystallization reactions for olivine components. (a, b) Model of the ideal mixing of single-cation oxides; (c, d) two-lattice model of melt components [Nielsen and Drake, 1979]. In (d), an additional correction for the liquid nonideality was introduced $S = \beta \ln[\mathrm{Si}/(\mathrm{Si} + \mathrm{Al})]^l$, where $\beta_{Fo} = -0.826$ and $\beta_{Fa} = -0.608$.

shown in Fig. 18 were utilized to solve the inverse problem: to calculate the equilibrium temperature from the composition of coexisting phases. The results demonstrate that the accuracy of the geothermometers increases by factors of 2.5–3 with transition to the two-lattice liquid model and achieves approximately ±10°C.

The thermodynamic interpretation of this fact explains why the silica activity [see system of equations (61)] can only insignificantly differ from 0.90–0.95 over a broad interval of SiO_2 concentrations, although tholeiitic magmas are characterized by low alkali concentrations. This also implies an answer to the question as to why the activities of *Fo*, *Fa*, *En*, and other mafic components in melt are virtually independent of the silica activity when the two-lattice model is used, with these activities controlled by the concentrations of the respective cations among the network modifiers. To solve this problem, we can use concepts of the structural state of silicate liquids and the species that should control the activities of components in crystallization reactions.

Most researchers consider silicate melts to be ion–polymer systems, whose "ionic constituent" is made up mostly of bivalent cations (Mg^{2+}, Mn^{2+}, Fe^{2+}, and Ca^{2+}), which maintain the charge balance of the variably polymerized Si–O groups (see the reviews [Hess, 1995; Mysen, 1995]). The presence of tetrahedrally coordinated ions of Al^{3+} facilitates the additional polymerization of the silicate liquid, with the local electroneutrality maintained mostly by alkali-metal cations. Raman spectroscopic evidence suggests that part of the Al^{3+} ions are definitely coordinated octahedrally by oxygens, which implies the simultaneous presence of the $Al\,O_2^-$ species [Mysen, 1995].

The fundamentals of the thermodynamic description of ionized systems have been formulated by Korzhinsky [1959], but the forecasting potential of his hypothesis of acid–base interactions suggests that this concept cannot be completely consistent with data on the actual structure of polymerized silicate melts. In the context of the problem of the two-lattice melt model, it is expedient to address to papers by Bradley [1962a, 1962b, 1964].

Table 6. Parameters of mineral–melt geothermometers used in the calibration of the COMAGMAT model

Mineral	Component	Parameters of geothermometers	Number of points	Reference
Olivine	*Fo* (1)	$\ln K = 5543/T - 2.32 + 0.210 \ln(\mathrm{Al/Si})$	67	[Ariskin *et al.,* 1993]
	Fa (2)	$\ln K = 6457/T - 4.22 + 0.084 \ln(\mathrm{Al/Si})$		
Plagioclase	*An* (3)	$\ln K = 10641/T - 1.32 + 0.369 \ln R$	58	[Ariskin and Barmina, 1990]
	Ab (4)	$\ln K = 11683/T - 6.16 + 0.119 \ln R$		
Augite	*En* (5)	$\ln K = 8521/T - 5.16$	25	[Ariskin *et al.,* 1987]
	Fs (6)	$\ln K = 13535/T - 9.87$		
	Wo (7)	$\ln K = 2408/T - 1.24$		
	$AlO_{1.5}$	$D = 0.20$		
Pigeonite	*En* (8)	$\ln K = 8502/T - 4.74$	18	[Ariskin *et al.,* 1987]
	Fs (9)	$\ln K = 5865/T - 4.04$		
	Wo (10)	$\ln K = 4371/T - 4.02$		
	$AlO_{1.5}$	$D = 0.10$		
Orthopyroxene	*En* (11)	$\ln K = 7208/T - 3.71$	39	[Bolikhovskaya *et al.,* 1996]
	Fs (12)	$\ln K = 6386/T - 4.39$		
	Wo (13)	$\ln K = 11950/T - 10.40$		
	$AlO_{1.5}$	$D = 0.10$		

Note: $R = \ln[(\mathrm{Na} + \mathrm{K})\mathrm{Al/Si}^2]$; numbers in parentheses after components corresponds to the equation numbers.

This author proposed to describe reactions with the participation of free cations and polymerized anion groups by equations taking into account the degree of polymerization [Bradley, 1964]. In this approach, the usual crystallization reaction of, for example, the enstatite component of pyroxene

$$Mg^{2+}(l) + SiO_3^{2-}(l) = MgSiO_3(Px), \quad (62)$$

is written as

$$Mg^{2+}(l) + \frac{1}{\alpha}(SiO_3)_\alpha^{2\alpha-}(l) = MgSiO_3(Px), \quad (63)$$

where α is the statistical average number of SiO_3^{2-} particles in the polymerized chain. The equilibrium constant of reaction (63) includes the activities of the metasilicate anion in the polymerized form

$$K_{En}^{Px-l} = a_{En}^{Px}/a_{Mg^{2+}}^{l}[a_{(SiO_3)_\alpha^{2\alpha-}}^{l}]^{1/\alpha}, \quad (64)$$

which makes Eq. (64) principally different from expressions like (21) or (58). The latter operates with a single, equal for all reactions activity of SiO_2 in the liquid.

The analysis of (64) leads to the conclusion that, as the degree of polymerization increases, $\alpha \longrightarrow \infty$, and $1/\alpha \longrightarrow 0$, because of which the term responsible for the silica activity tends to one. An increase in the degree of polymerization is coupled with a drastic decrease in the overall number of charged particles, so that the value of $a_{Mg^{2+}}^{l} \longrightarrow N_{Mg^{2+}}^{l}/NM$, where *NM* is the total number of cations. Hence, the ionic–polymeric interpretation of melt–mineral equilibria yields the same activity–composition relations as those following from the analysis of the purely heuristic two-lattice model for the silicate liquid.

We believe that this coincidence is not simply due to chance, and Bradley's method deserves closer consideration by specialists in the thermodynamics of melt–mineral equilibria. This approach can also be made consistent with experimental data on the distributions of Si– and Al–O groups in melts and enables a critical analysis of some petrological models that include, for example, the concept of the integral silica activity or chemical affinity of minerals for SiO_2 in silicate liquids [Ghiorso and Carmichael, 1987].

2.2.4. Geothermometers for silicate minerals

Raman spectroscopic data indicate that the main building blocks of silicate melts are silicon–oxygen radicals, such as SiO_4^{4-}, $Si_2O_7^{6-}$, SiO_3^{2-}, $Si_2O_5^{2-}$, and SiO_2 [Hess, 1995; Mysen, 1995]. This means that crystallization reactions of components of olivine, pyroxenes, and plagioclase written as Eqs. (63) should be participated in by different silica species. Their common feature is the weak dependence of the equilibrium constants on the bulk SiO_2 concentration in the melt, caused by the polymerization [see Eq. (64)]. In this sense, it becomes clear why the two-lattice melt model was able to realistically describe melt–mineral equilib-

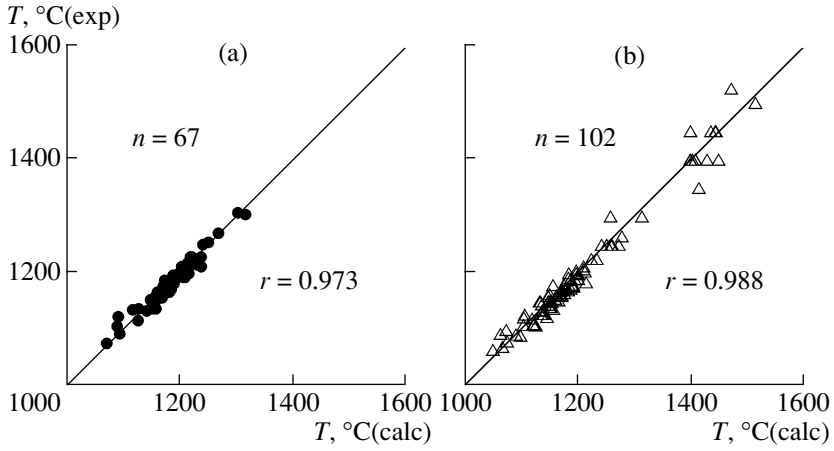

Fig. 19. Experimental and calculated temperatures of the *Ol*–melt equilibrium for moderately alkaline systems under atmospheric pressure. The equilibrium temperatures were calculated by the *Fo* and *Fa* geothermometers from Table 6; (a) results obtained while calibrating the basic version of the COMAGMAT model (in 1974–1988); (b) independent data obtained in 1989–1996.

ria within broad compositional ranges, from basalts to dacites (Figs. 18c, 18d).

However, the degree of polymerization of a silicate liquid is known to strongly depend on the integral Si/O ratio and temperature and decreases with a shift to higher-temperature and olivine-enriched compositions (see, for example, [Hess, 1980]). This imposes certain constraints on the use of geothermometers designed in compliance with Nielsen's method. We usually conducted calibrations within the compositional range of $45 < SiO_2 < 65\%$ and at temperatures of ≤1300°C. The mineral–melt geothermometers utilized in the basic version of the COMAGMAT model are listed in Table 6.

Olivine. In 1986–1990 we completely recalibrated the thermodynamic basis of the CECT (RTRK) and THOLEMAG models [Ariskin *et al.*, 1987] by processing the results of experiments on the melting of terrestrial mafic and intermediate rocks with the utilization of the approach presented in [Nielsen and Dungan, 1983]. These experiments were accomplished from 1974–1988, and their starting materials were subalkaline basalts, abyssal tholeiites, calc–alkaline lavas, and pyroxene–phyric basalts from mid-oceanic ridges. To thermodynamically process the data on the *Ol*–melt equilibrium, we selected glass compositions with 45–60 wt % SiO_2 and $Na_2O + K_2O \le 4$ wt %. The experiments covered the temperature range of 1070–1300°C and oxygen fugacities of $-14 \le \log f_{O_2} \le -8$, and lasted for no less than 48 h.

During the initial stage of data processing with the equation from [Sack *et al.*, 1980], we subdivided Fe contained in the melts into Fe^{3+} and Fe^{2+} and then calculated the exchange coefficients K_D^{Fe-Mg}. Pairs of compositions outside the range of $0.30 \le K_D^{Fe-Mg} \le 0.36$ were rejected from further consideration, and we eventually selected 67 olivine–melt compositional pairs. By processing these data with the linear model (19b), we derived two geothermometers, which were characterized by high correlation coefficients between $\ln K$ and $1/T$

$$\begin{aligned} \ln K_{Fo}^{Ol-l} &= 4915/T - 2.14 \ (r = 0.944), \\ \ln K_{Fa}^{Ol-l} &= 6207/T - 4.14 \ (r = 0.968). \end{aligned} \quad (65)$$

However, it has been found out that, in spite of the strong correlation, this treatment procedure leads to the plotting of $\ln K_{Fo/Fa}^{Ol-l}$ values mostly above the correlation lines for more aluminous compositions and below these lines for less aluminous compositions [Ariskin *et al.*, 1987].

In order to reduce the effect of composition on the calculated temperature dependences, the logarithm of the Al/Si ratio in the melt was included as an additional parameter in the calibration equation

$$\ln K_{Fo/Fa}^{Ol-l} = A/T + B + C\ln(\mathrm{Al/Si}). \quad (66)$$

The values of the regression coefficients for the *Fo* and *Fa* geothermometers are listed in Table 6 [Eqs. (1) and (2)].

When these equations are used together, the integral *Ol*–melt geothermometer reproduces 70% of the experimental temperature for 67 starting glasses accurate to ±10°C (Fig. 19a). The differences between the calculated and experimental olivine compositions do not exceed 2 mol % for *Fo* and average 0.5–0.7 mol % for *Fo*.

In preparing the manuscript of our monograph [Ariskin and Barmina, 2000], we additionally tested the basic olivine geothermometers of the COMAGMAT model with the use of an independent selection of experimental data published after 1988. This selection was composed with the INFOREX-4.0 program and met the same search criteria as those utilized previously

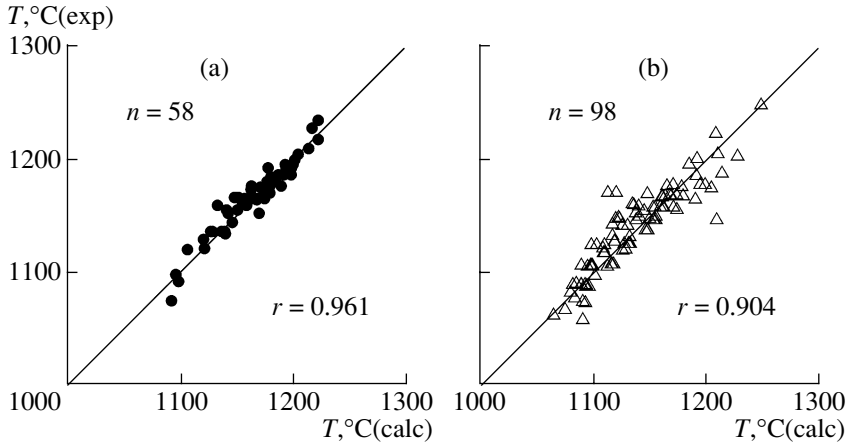

Fig. 20. Experimental and calculated temperatures of the *Pl*–melt equilibrium for moderately alkaline systems under atmospheric pressure. The equilibrium temperatures were calculated by the *An* and *Ab* geothermometers from Table 6; (a) results obtained while calibrating the basic version of the COMAGMAT model (in 1982–1987); (b) independent data obtained in 1988–1996.

for the main calibrations. The results of this comparison of the experimental and calculated temperatures are demonstrated in Fig. 19b. These data show that the model yields realistic temperatures of the *Ol*–melt equilibrium within the temperature range of 1050°C < T < 1300°C. At temperatures above 1400°C, some deviations can be as large as 40–50°C. Our experience suggests that these inaccuracies can be minimized by utilizing other compositional parameters or their combinations in the calibrations (Fig. 18d).

Plagioclase. Later we used the method of compositional corrections to construct maximally accurate mineral–melt geothermometers for a broad range of compositions. The thermodynamic sense of the additional terms in the equilibrium equations is quite obvious: these corrections present effective means to take into account component mixing within the scope of the two-lattice melt model. They can be somewhat arbitrarily interpreted as the product of unknown component activities expressed in the form of an empirical dependence on the liquid composition. This approach to the calibration of equilibrium equations proved efficient in designing new geothermometers.

When using Drake's plagioclase thermometers (Table 1) in our simulations of tholeiitic magma crystallization, we arrived at the conclusion that these thermometers provide reliable temperature evaluations within a narrow compositional range of approximately 49–55 wt % SiO_2 [Ariskin *et al.*, 1987, 1988a, 1988b]. When the SiO_2 concentration was lower than 49 wt %, the calculated *Pl* crystallization temperatures appeared to be underestimated by 20–30°C compared with the experimental values, and these discrepancies were found to be positive and equal to 20–50°C for the range of 55 < SiO_2 < 65%. It was also established that there is a tendency toward underestimating the model *An* concentration in *Pl* by 5–7 mol % for high-temperature *Ol–Pl* cotectics (at $T \geq 1220$°C). This called for a revision of the input data utilized to calibrate the plagioclase geothermometers and a more careful exploration of the problem of the optimal selection of the silicate liquid model. For this purpose, we systematized data obtained on the *Pl*–melt equilibrium in experiments with natural compositions [Grove and Bryan, 1983; Mahood and Baker, 1986; Sack *et al.*, 1987; Tormey *et al.*, 1987]. The data set included information on 158 quench experiments conducted at temperatures of 1026–1235°C on basalts and andesites of the tholeiitic, calc–alkaline, and alkali-basalt series. In the thermodynamic analysis of these data, we limited ourselves to considering a selection of the 58 "most equilibrated" experiments whose durations were no less than 96 h (4 days), and whose melt compositions did not extend beyond the system of moderate alkalinity $Na_2O + K_2O \leq 4$ wt % [Ariskin and Barmina, 1990]. The processing of these data following the method from [Nielsen and Dungan, 1983] yielded two equations

$$\ln K_{An}^{Pl-l} = -1635/T + 4.91,$$
$$\ln K_{Ab}^{Pl-l} = 18440/T - 11.21. \quad (67)$$

The relationships derived for the albite end member offer a good geothermometer, which ensures an accuracy of about 10°C. However, the regression parameters for anorthite suggest the virtual absence of a dependence of $\ln K_{An}^{Pl-l}$ on $1/T$, which led us to revise and modify the two-lattice melt model. We inspected a few other variants of Al partition between network modifiers and network formers and have discovered that, when $AlO_{1.5}$ is included in the list of network formers $NF = N^l_{SiO_2} + N^l_{NaAlO_2} + N^l_{KAlO_2} + N^l_{AlO_{1.5}}$, the dependence of $\ln K_{An}^{Pl-l}$ on $1/T$ acquires a positive slope comparable with the temperature dependence for albite [Ariskin and Barmina, 1990]. The maximum accuracy

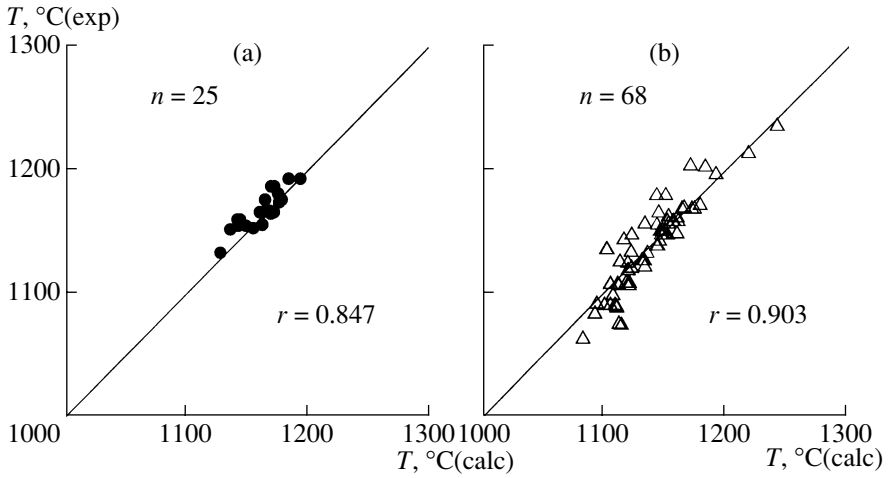

Fig. 21. Experimental and calculated temperatures of the *Aug*–melt equilibrium for moderately alkaline systems under atmospheric pressure. The equilibrium temperatures were calculated by pyroxene geothermometers (5)–(7) in Table 6; (a) results obtained while calibrating the basic version of the COMAGMAT model (in 1979–1983); (b) independent data obtained in 1987–1996.

of the geothermometers was achieved by including an additional compositional factor $\ln[(Na + K)Al/Si^2]$ in the regression equation. Thus, the simultaneous application of the equations for *An* and *Ab* (Table 6) to the basic selection of 58 experiments allowed a 70% reproduction of the experimental temperatures accurate to at least 10°C (Fig. 20a). The average discrepancy between the experimental and calculated *Pl* compositions was 2.8 mol % *An*.

Figure 20b demonstrates the results of the testing of these plagioclase geothermometers with the use of independent experimental data published after 1987. When selecting data for comparison with the aid of the INFOREX-4.0 system, we introduced a less rigorous criterion for the duration of the experiments $\tau \geq 72$ h and somewhat widened the alkalinity interval for the quench glasses $Na_2O + K_2O \leq 5$ wt %. Nevertheless, the integral *Pl* geothermometer reproduces well the results of 98 experiments borrowed from 14 different experimental studies.

The equation for the *Pl*–melt equilibrium that is utilized in the COMAGMAT model has not been recalibrated after 1990 (Table 6). The use of these thermometers indicates that they work best at temperatures of 1120–1200°C: the temperatures calculated for basaltic andesite and andesite compositions are 10–15°C underestimated at $T < 1120$°C (and the model plagioclase composition can be excessively enriched in *Ab*), while the temperatures calculated for high-Al magmas at $T >$ 1200°C are systematically higher than the experimental values. In practical calculations, this problem is handled by introducing small temperature corrections, which are determined during the initial stages of work with the COMAGMAT program through a specialized interface (see below).

Augite. The inclusion of high-Ca pyroxene–melt geothermometers [Nielsen and Drake, 1979] in the algorithm for modeling liquid lines of descent made it possible to accurately predict the general order of augite appearance on the liquidus, but the crystallization temperatures of this pyroxene were underestimated by 15–20°C [Frenkel and Ariskin, 1985]. Experimental data obtained from 1979–1983 provided the basis for refining and revising the pyroxene geothermometers [Walker *et al.*, 1979; Grove *et al.*, 1982; Grove and Bryan, 1983]. These papers present 33 analyses of augite and coexisting quench glasses. In this context, it is pertinent to mention the papers by Grove *et al.* [1982] and Grove and Bryan [1983], in which the duration of the melting experiments for low-temperature multiphase assemblages was 100–600 h.

Nevertheless, eight pairs of *Aug*–melt compositions with K_D^{Fe-Mg} values outside the permitted range were rejected from the thermodynamic processing of this information. The remaining 25 pairs of analyses characterized temperatures of 1133–1193°C at an average $K_D^{Fe-Mg} = 0.29$ ($1\sigma = 0.03$) and were processed using the model of Nielsen and Drake [1979], see reaction equation (59). The temperature dependences thus derived for the equilibrium constants of the *En*, *Fs*, and *Wo* crystallization reactions are listed in Table 6 [see Eqs. (5)–(7)]. The distribution of Al between augite and melt was characterized using the average distribution coefficient $D_{Al}^{Aug-l} = x_{AlO_{1.5}}^{Aug} / x_{AlO_{1.5}}^{l(MN)} = 0.20$ ($1\sigma = 0.09$).

The parameters of the *Aug*–melt equilibrium presented in Table 6 were incorporated into the COMAGMAT program and employed for calculating the saturation temperatures of 25 initial melts. As a result, the experimental values were reproduced for 72% of the calculations accurate to no worse than 10°C (Fig. 21a), with average discrepancies between the calculated and experimental temperatures of 7.2°C. The testing results of these

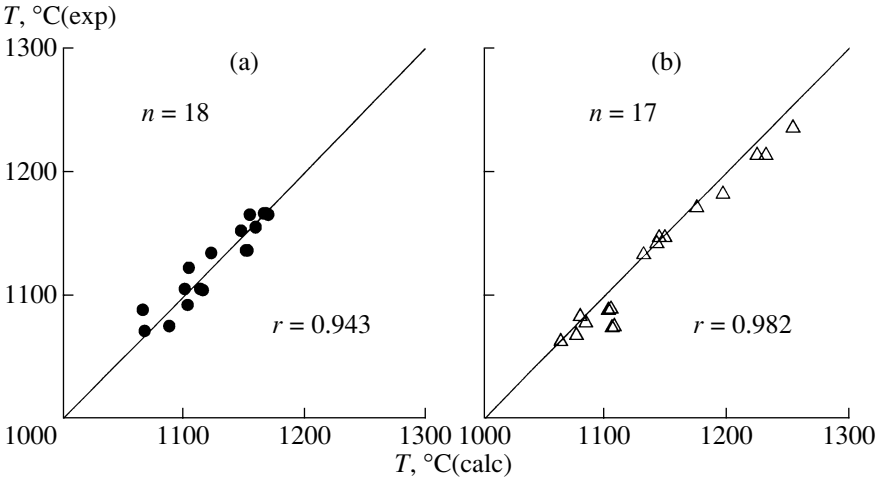

Fig. 22. Experimental and calculated temperatures of the *Pig*–melt equilibrium for moderately alkaline systems under atmospheric pressure. The equilibrium temperatures were calculated by pyroxene geothermometers (8)–(10) in Table 6; (a) results obtained while calibrating the basic version of the COMAGMAT model (in 1982–1983); (b) independent data obtained in 1987–1996.

pyroxene geothermometers with the use of independent experimental data are shown in Fig. 21b.

Pigeonite and orthopyroxene. As was mentioned above, the equations proposed previously to describe the equilibrium between low-Ca pyroxene and melt are based on selected data on the compositions of pigeonite and orthopyroxene (Table 1). These equations were employed to describe the crystallization of a single low-Ca pyroxene [Ariskin and Frenkel, 1982; Frenkel and Ariskin, 1985]. However, in modeling the crystallization of natural magmatic melts, we arrived at the conclusion that, in a situation when *Opx* is among the first crystallizing phases, calculations by the geothermometers from [Nielsen and Drake, 1979] yield significantly underestimated temperatures, at which model low-Ca *Px* appears on the liquidus. This required the subdivision of the experimental data into the "pigeonite" and "hypersthene" series and the use of at least two varieties of low-Ca pyroxenes in the calculations.

Grove *et al.* [1982] and Grove and Bryan [1983] published the compositions of 18 pairs of coexisting pigeonite and glass pairs, which characterized the distributions of elements at temperatures of 1059–1167°C. The average value of $K_D^{\mathrm{Fe-Mg}}$ calculated from these data was equal to 0.30 ($1\sigma = 0.04$). This information was processed, as in the case with augite, in compliance with the two-lattice model. The parameters of the derived *Pig*–melt geothermometers are listed in Table 6 [Eqs. (8)–(10)]. The partition of Al between pigeonite and melt was characterized by the average distribution coefficient $D_{\mathrm{Al}}^{Pig-l} = 0.10$ ($1\sigma = 0.05$).

Figure 22a compares the equilibrium temperatures of 18 initial melts with pigeonite evaluated experimentally and calculated by Eqs. (8)–(10) (Table 6). As is demonstrated by these results, the experimental temperature values are reproduced accurate to no worse than 10°C in 69% of the calculations, and the average discrepancies between the experimental and calculated temperature values are 7.9°C. The testing of these pigeonite geothermometers against independent experimental data also points to a good accuracy of the equations (Fig. 22b). This is particularly important in simulating tholeiitic systems, in which pigeonite is one of the main phases during the final crystallization stages of the magmatic melts.

The first versions of the COMAGMAT program (for example, THOLEMAG) included *Opx*–melt geothermometers for *En*, *Fs*, and *Wo*, which were calibrated based on the data of 13 experiments with samples of lunar basalts, terrestrial andesites, and some synthetic compositions. These equations enabled the calculation of *Opx* crystallization temperatures accurate to approximately 10–15°C, but the CaO concentrations in the model orthopyroxenes appeared to be overestimated nearly twofold. The *Opx* geothermometers were recalibrated with the use of a more representative set of data, which included the data of 39 experiments with samples of terrestrial basalts and andesites [Bolikhovskaya *et al.*, 1996]. These experiments covered the temperature interval of 1076–1339°C at oxygen fugacities of $-12.2 \le \log f_{\mathrm{O_2}} \le -6.1$ and lasted for no less than 48 h. The parameters of the orthopyroxene geothermometers thus derived are presented in Table 6 [Eqs. (11)–(13)]. The results of testing of these dependences point to an accuracy of approximately 10°C at the *Opx* compositions evaluated accurate to 1–2 mol %.

2.2.5. Geothermometers for Fe–Ti oxides

In spite of their relatively rare occurrence, magnetite and ilmenite are important phases of basaltic systems that control the behaviors of FeO, Fe_2O_3, TiO_2, and some trace elements (Cr and V) in the crystallization

process. Data published in the literature over the past 10 years include the results of hundreds of experiments on the melting of silicate systems with the crystallization of these minerals. This provides the basis for the development of a model of phase equilibria with regard for the crystallization of iron and titanium oxides. The situation was less optimistic when we started to develop the COMAGMAT model: data on *Mt* and *Ilm* were scarce and fragmentary, and it was very difficult to process them and make consistent. Nevertheless, a series of attempts to describe the conditions of basaltic magma saturation in Fe–Ti oxides were made in the 1980s with the aim of incorporating these equations into a variety of crystallization models [Nielsen and Dungan, 1983; Ghiorso, 1985; Ghiorso and Carmichael, 1985; Ariskin *et al.*, 1988b].

During the initial stages of developing the model for the *Mt*–melt equilibrium, we utilized the experimental data from [Hill and Roeder, 1974; Sack, 1982; Lapin *et al.*, 1985] and proposed a system of empirical equations able to describe the conditions of saturation of basaltic melts in titanomagnetite of variable composition (Fe_3O_4–Fe_2TiO_4) as a function of the melt composition and f_{O_2}. This system of equations was incorporated into the THOLEMAG [Ariskin *et al.*, 1988b] and COMAGMAT-3.0 [Ariskin *et al.*, 1993] models and remained in use until 1997. These model calculations realistically reproduced the sequence of magnetite formation during the crystallization of samples 12017 [Lapin *et al.*, 1985] and GL-RHB [Hill and Roeder, 1974], as well as the general expansion of the spinel crystallization field with the transition to more oxidized conditions.

Later, it was the simulation of magnetite crystallization that caused criticism from some specialists and users of the COMAGMAT-3.0 program (for example, [Yang *et al.*, 1996]). The liquid lines of descent calculated for basaltic magmas at the QFM and NNO buffers exhibited systematic 20–40°C overestimates for the temperatures when *Mt* started to crystallize. The causes of these discrepancies became clear when the experimental data used in the calibrations were compared with the results of later investigations (Fig. 23). The shaded field in this figure comprises approximately 100 experimental data points of titanomagnetite stability, which were compiled from papers published from 1987–1996 [Ariskin, 1998].

These data suggest that there is a local minimum of titanomagnetite crystallization temperatures between the WM and NNO buffers. At the same time, the calibration of the "magnetite" model with the use of data from [Hill and Roeder, 1974; Lapin *et al.*, 1985] yielded a monotonous and insignificant (~8–10°C/$\log f_{O_2}$) change in the *Mt* temperature with variations in f_{O_2} (Fig. 23). In 1998, we completely recalibrated the magnetite–melt equilibrium [Ariskin and

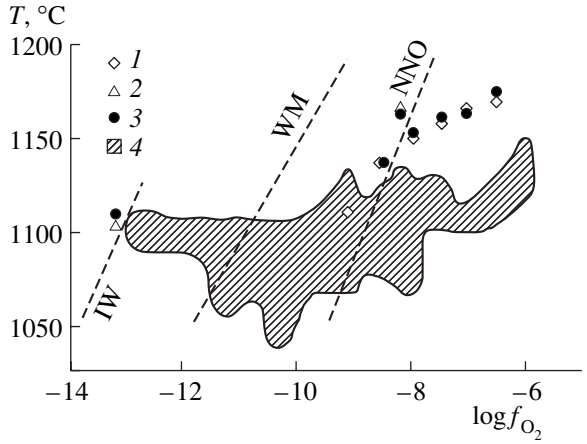

Fig. 23. Experimental and calculated temperatures of titanomagnetite crystallization in ferrobasaltic systems under different redox conditions. (*1*, *2*) Data used in calibrating the "magnetite" equations of the THOLEMAG and COMAGMAT-3.0 models: (*1*) [Hill and Roeder, 1974], (*2*) [Lapin *et al.*, 1985]; (*3*) calculations with the COMAGMAT-3.0 program [Ariskin *et al.*, 1993]; (*4*) summary of experimental data (1987–1996) on the *Mt*–melt equilibrium (see Fig. 24).

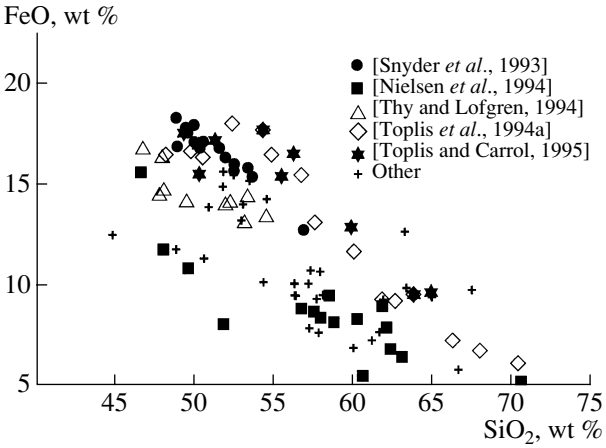

Fig. 24. Composition of the main selection of experimental glasses corresponding to the *Mt*–melt equilibrium.

Barmina, 1999]. The new equations were incorporated into the programs of COMAGMAT-3.5 and higher.

Experimental information. Using the INFOREX-4.0 database, we searched for experiments on the melting of terrestrial igneous rocks and synthetic basaltic mixtures whose quench products included Fe- and Ti-enriched spinel. As a result, we have selected 213 experiments reported in 22 papers, with approximately half of them describing experiments with alkaline basalts and nephelinites. For our further analysis, we chose only experiments conducted in systems of low and moderate alkalinity and placed additional restrictions on the quench glass compositions ($Na_2O + K_2O < 7$ wt %) and the durations of the melting experiments (no less than 48 h). In the INFOREX database,

we identified 99 experiments meeting these requirements and representing 13 independent investigations.

Most of these experiments characterized systems of basaltic and ferrobasaltic composition (10–18 wt % FeO, Fig. 24) at variations in the TiO_2 concentrations in the residual melts of 1–5 wt %. The range of the titanomagnetite crystallization temperatures was 1040–1160°C. All experiments were carried out using the Pt-loop technique at a controlled oxygen fugacity of $10^{-13} \le f_{O_2} \le 10^{-6}$ bar, which corresponded to the interval between IW and NNO + 2 buffers. The phase assemblages produced in these experiments usually consisted of four or five minerals plus quench glass, and the fourth or fifth crystallizing phase in all of the experiments (except a few instances) was magnetite. Plagioclase was present on the liquidus in all of the 99 compositions. The mafic minerals were *Ol*, *Aug*, *Pig*, and *Opx* in variable proportions. The products of 49 experiments included ilmenite: the appearance of this phase was observed in experiments conducted at $\log f_{O_2} < -10$.

The most representative investigations were published in five papers [Snyder *et al.*, 1993; Nielsen *et al.*, 1994; Thy and Lofgren, 1994; Toplis *et al.*, 1994; Toplis and Carroll, 1995], and their results were considered in detail in a review [Ariskin, 1998]. Here we will discuss only the data from [Toplis and Carroll, 1995], who presented the most exhaustive analysis of phase relations in melt–mineral equilibria during the crystallization of tholeiitic magmas with the presence of magnetite and ilmenite.

First, according to the results of calculations with the use of the compositions and proportions of the experimental products, the fraction of titanomagnetite in assemblages crystallizing in systems open with respect to oxygen can be as high as 15–22 wt %, and, obviously, this is the main factor predetermining the enrichment of the residual melts in SiO_2 during the crystallization of *Mt*-bearing assemblages. Second, the slope of the *Mt* liquidus temperature as a function of f_{O_2} between the QFM – 2 and QFM + 1 buffer equilibria is approximately $30°C/\log f_{O_2}$. Third, it was established that, for melts becoming saturated in magnetite, there is a negative correlation between $1/T$ and the Fe_2O_3 concentration in the melt, which implies that high crystallization temperatures of magnetite correspond to elevated degrees of iron oxidation in melts.

Problem of calculating the Fe^{3+}/Fe^{2+} ratio of melts. We mentioned above that the COMAGMAT-3.0 program [Ariskin *et al.*, 1993] overestimated the model temperatures of *Mt* crystallization by 20–40°C at oxygen fugacities close to QFM, and this required the introduction of special temperature corrections. An uncomfortable situation was encountered when the MELTS program was tested: calculations at variable f_{O_2} suggested a decrease in the *Mt* model temperature with increasing ΔQFM and the degree of melt oxidation [Toplis and Carroll, 1996]. These discrepancies likely stemmed mainly from problems in evaluating the Fe^{3+}/Fe^{2+} ratio in the silicate liquid and the use of this parameter for low-temperature *Mt*-bearing assemblages. This problem included the following three aspects:

(1) The analysis of experimental information on redox equilibria stored in the INFOREX database (372 experiments) indicates that, when the compositional and temperature dependences of the Fe^{3+}/Fe^{2+} ratios in melts were calibrated, approximately 40% of the data pertained to strongly oxidized liquids at $f_{O_2} > 10^{-3}$ bar, and only six of the experimental glasses were produced at $f_{O_2} < 10^{-9}$ bar [Fudali, 1965; Shibata, 1967; Sack *et al.*, 1980; Thornber *et al.*, 1980; Kilinc *et al.*, 1983; Kress and Carmichael, 1988, 1991], see Section 2.2.1. Hence, much of the input data pertained to f_{O_2} conditions that extend far outside the range characteristic of the crystallization of tholeiitic magmas [Carmichael and Ghiorso, 1986, 1991] and only insignificantly overlap the magnetite stability field (as it was determined in [Ariskin, 1998]). This issue is related to another problem: the comparison of the accuracies of the equations for calculating the degrees of Fe oxidation in magmatic melts indicates that the relative error of the Fe^{3+}/Fe^{2+} estimates at $\log f_{O_2} < -10$ may sometimes be as high as 50% at an absolute accuracy of ±0.03 [Nikolaev *et al.*, 1996].

(2) Kinetic experiments demonstrate that the Fe^{3+}/Fe^{2+} ratio of melts is equilibrated with the gas phase within 48 h [Fudali, 1965; Thornber *et al.*, 1980]. If the duration–temperature relationships are compared for experiments aimed at studying redox equilibria (n = 289) and magnetite stability (n = 99), one can note that the former group included only a few melting runs with durations of >48 h, and none of the compositions for which the Fe^{3+}/Fe^{2+} ratio was determined experimentally fell into the temperature range characteristic of magnetite crystallization (1040–1160°C, Fig. 25). This problem becomes even more acute due to the fact that the experimental melts were saturated with magnetite not only at low temperatures but also at high bulk degrees of crystallization (no less than 20–40%), which required an additional increase in run duration to achieve equilibrium.

(3) Mössbauer spectroscopic data on silicate glasses indicate that, at $Fe^{3+}/\Sigma Fe < 0.5$, the Fe^{3+} ion occurs at two sites: tetrahedrally and octahedrally coordinated by oxygen [Mysen *et al.*, 1985]. This means that any attempts to calculate the activities of magnetite or Fe_2O_3 in a melt on the basis of its bulk Fe^{3+}/Fe^{2+} ratio should lead to erroneous results unless the partitioning of Fe^{3+} between the sites is taken into account.

We have to admit that information now available on the composition and structural state of silicate liquids is

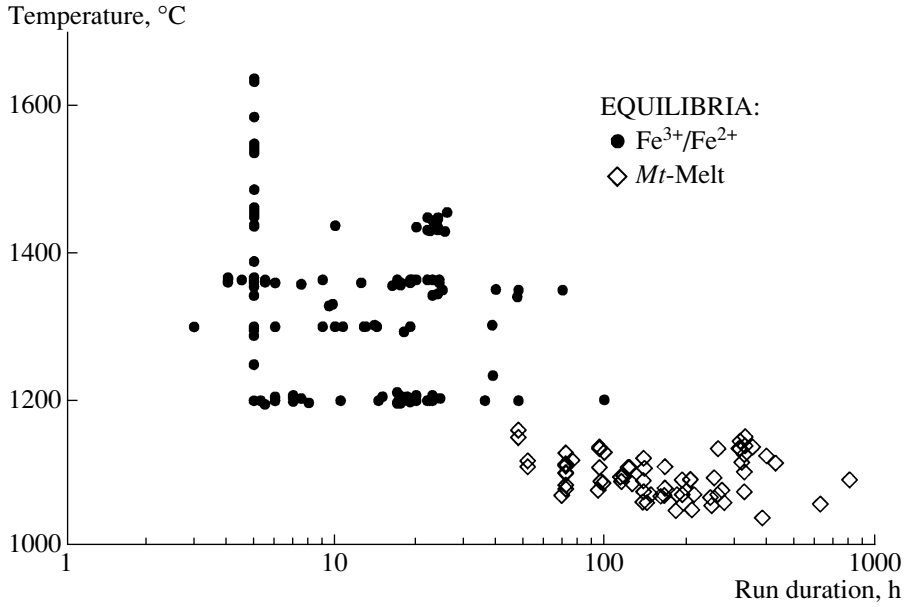

Fig. 25. Relations between the temperature and run duration during the experimental studying of the Fe^{3+}/Fe^{2+} equilibria in liquid (n = 289) and the *Mt*–melt equilibrium (n = 99).

still insufficient for developing an adequate thermodynamic model for the *Mt*–melt equilibrium, even if there is a realistic model for the activities of components of the magnetite solid solution [Sack and Ghiorso, 1991; Ghiorso and Sack, 1995]. This leads to the necessity of utilizing empirical approaches to the description of equilibria with the participation of Fe–Ti oxides.

Equation of the magnetite liquidus. The aforementioned selection of 99 experimentally produced glass compositions corresponding to the *Mt*–melt equilibrium was processed in compliance with the linear model

$$10^4/T = (b_0 + b_1 x^l_{SiO_2} + b_2 x^l_{TiO_2} + b_3 x^l_{FeO}) \log f_{O_2} + c + d_1 x^l_{SiO_2} + d_2 x^l_{TiO_2} + d_3 x^l_{FeO} + d_4 x^l_{P_2O_5}, \quad (68)$$

where T is the temperature (K), x^l_i are the mole fractions of components in the melt, and b, c, and d_i are the regression coefficients [Ariskin, 1998]. In conducting these calculations, we deliberately did not regard Fe_2O_3 as an independent component and operated only with the bulk FeO concentration. This was done with the aim to minimize the inaccuracies of the FeO/Fe_2O_3 estimates for the melts. Another reason was the fact that the equations proposed for calculating the FeO/Fe_2O_3 ratio did not take into account the effect of phosphorus, which can be fairly significant, judging from the recent data in [Toplis *et al.*, 1994a, 1994b]. An important difference of this calibration is that we explored the possibility of changing the integral parameter at the oxygen fugacity controlled by the liquid phase composition. The regression coefficients are listed in Table 7.

Comparing the experimental temperatures and the values calculated by Eq. (68), it can be seen that the differences $\Delta T = T_{exp} - T_{calcd}$ are occasionally as great as 40–50°C but most of them (approximately 90%) are within ±15°C, and the average absolute value of ΔT is 9.3°C [Ariskin, 1998]. This led us to propose that the form of the empirical dependence (68) does reflect the redox and structural–chemical equilibria in the liquid phase with the participation of the Fe^{3+} and Fe^{2+} ions that control the stability conditions on the titanomagnetite liquidus.

Using Eq. (68), it is easy to estimate the dependence of the *Mt* crystallization temperature on f_{O_2} for basaltic systems of different compositions. According to the parameters in Table 7, the effect of redox conditions is expectedly at a maximum for ferrobasaltic composi-

Table 7. Regression coefficients for magnetite liquidus equation (68)

Parameter	Coefficient	1σ deviation
b_0	−0.6232	0.0205
b_1	0.6826	0.0359
b_2	4.0438	0.9327
b_3	0.8251	0.2567
c	0.0159	0.0686
d_1	8.3626	0.2804
d_2	35.9674	8.0819
d_3	10.7347	2.1842
d_4	12.4418	2.3521

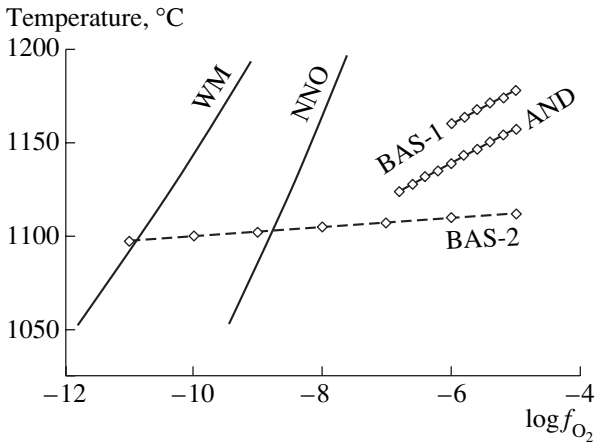

Fig. 26. Dependences of the magnetite crystallization temperature on the oxygen fugacity calculated by Eq. (68) for two model ferrobasalts and one ferroandesite (Table 8).

tions with low and moderate concentrations of TiO_2 and FeO. For melts enriched in TiO_2 and FeO (like the Galapagos tholeiites), this dependence can be fairly weak. This conclusion can be illustrated by the results shown in Fig. 26, in which the titanomagnetite liquidus temperatures were calculated for three model compositions (Table 8) as functions of $\log f_{O_2}$.

These compositions correspond to low-Ti ferrobasalt (BAS-1), ferroandesite (AND), and high-Ti ferrobasalt (BAS-2). Their liquidus temperatures were calculated by the COMAGMAT program and corresponded to the *Ol–Pl* cotectics for the basalts (~1165 and ~1135°C) and to a system somewhat oversaturated in *Pl* at $T \sim 1125$°C for the andesite. Using Eq. (68), we calculated the temperatures of magnetite stability above the silicate liquidus for the BAS-1 and AND compositions. These data indicate that the slopes of the *Mt* liquidus for both melts are approximately 20°C/$\log f_{O_2}$ (Fig. 26). This value is about 1.5 times lower than the estimate in [Toplis and Carroll, 1995]. However, it should be taken into account that our evaluations were obtained for a constant melt composition. Considering the change in the liquid composition with the transition from ferrobasalt BAS-1 to ferroandesite (for example, in the process of fractionation), the decrease in $\log f_{O_2}$ from –6 to –7 is equivalent to a decrease in the magnetite liquidus by roughly 35°C (Fig. 26).

Table 8. Modeled melts

Component	BAS-1	AND	BAS-2
SiO_2	50.0	60.0	48.0
TiO_2	2.0	0.5	4.0
Al_2O_3	15.0	16.0	13.5
FeO	15.0	10.0	17.5
MnO	–	–	–
MgO	6.0	3.0	5.0
CaO	9.0	5.5	9.0
Na_2O	2.5	3.5	2.5
K_2O	0.5	1.5	0.5
P_2O_5	–	–	–
T_{Pl}, °C	1164	1126	1142
T_{Ol}, °C	1164	1094	1133

For the high-Ti ferrobasalt BAS-2, the system was not saturated in titanomagnetite within a broad range of oxygen fugacity values, because the calculated temperatures varied around 1100°C, i.e., 25–30°C below the olivine and plagioclase liquidi. Evidently, the temperature at which *Mt* first appeared during the crystallization in this system was buffered by the composition and should have not notably differed from 1100°C if the melt did not become significantly enriched in SiO_2 or depleted in TiO_2.

New *Mt*–melt geothermometers. Although the empirical liquidus equation (68) is useful in the general analysis of the effects of composition and f_{O_2} on the position of the titanomagnetite liquidus, there are reasons that make it impossible to utilize this equation in developing crystallization models. First, this equation ignores the composition of natural magnetites, which usually contain, along with Fe_2O_3, FeO, and TiO_2, also appreciable amounts of MgO and Al_2O_3; and, second, after treatment with the least-squares technique, the integral effect of composition turned out to be greater than the dependence on f_{O_2}. The latter consideration is particularly important: all of our attempts to incorporate Eq. (68) into COMAGMAT-3.0 failed, because they resulted in the excessive depletion of the melt in FeO and its complementary enrichment in SiO_2. This, in turn, called for the development of a more coherent model based on the calibrations of individual *Mt*–melt geothermometers for the main components of the magnetite solid solutions [Ariskin and Barmina, 1999].

In order to fulfill this task, we used the basic set of 99 compositions (Fig. 25), from which 74 experiments were selected that provided information on the composition of magnetite. In the latter data set, we imposed additional constraints on the compositions of Ti-*Mt* (<3 wt % Cr_2O_3) and melt (46 < SiO_2 < 70 wt %, P_2O_5 < 1.5 wt %), which were met by the data of 62 experiments. Their results were then utilized to calibrate five geothermometers that described the partition of the Fe^{3+}, Fe^{2+}, Ti^{4+}, Al^{3+} and Mg^{2+} ions between magnetite and a silicate liquid as functions of the melt composi-

tion and oxygen fugacity. The processing of these data was carried out according to the linear model

$$\ln D_i^{Mt-l} = a/T + b\log f_{O_2} + c + d_1 x_{Na} + d_2 x_K + d_3 x_P, \quad (69)$$

where D_i^{Mt-l} are the molar distribution coefficients for the aforementioned ions between Fe–Ti spinel and melt, x_{Na}, x_K, and x_P are the molar fractions of Na, K, and P in the liquid recalculated to the single-cation basis; and a, b, c, d_1, d_2, and d_3 are the regression coefficients. Note that the Fe^{3+} and Fe^{2+} "distribution coefficients" were calculated with respect to the total iron in the melt, i.e., without estimating the concentrations of these ions in the liquid. From the viewpoint of thermodynamics, this approach is inconsequent. It is, however, advantageous because it does not introduce additional inaccuracies related to the uncertainties in the Fe^{3+}/Fe^{2+} estimates and the structural state of Fe^{3+} in the melt.

The geothermometers were calibrated in two stages. First, the whole data set of 62 composition pairs of magnetite and melt was processed.

The regression coefficients thus obtained were used to solve the inverse problem: to calculate the temperature of the *Mt*–melt equilibrium for the same data set with known compositions and f_{O_2}. If the discrepancies between the model and experimental temperatures were more than three times greater that the average deviations for the data set, these compositions were considered unequilibrated and were rejected. As a rule, for each component there were 10–12 experimental points with temperature deviations of 60–150°C. The remaining compositions were reprocessed with the least-squares technique, and the coefficients thus corrected were tabulated for the purposes of further simulations. Our experience in developing mineral–melt equilibrium equations testifies that this approach is fairly efficient at improving the accuracy of the thermometers and the adequacy of the crystallization models. The optimum parameters of the magnetite geothermometers for each component were published in [Ariskin and Barmina, 1999]. These dependences were used to develop a model of the *Mt*–melt equilibrium.

The new magnetite model is an autonomous computer program that enables the user to calculate not only the liquidus temperature but also the composition of Ti-*Mt* if the melt composition and f_{O_2} are known. The program is based on the solution of a nonlinear system of equations including five geothermometers (69) and the equation of magnetite stoichiometry

$$x_{Fe^{3+}}^{Mt} + x_{Fe^{2+}}^{Mt} + x_{Ti^{4+}}^{Mt} + x_{Al^{3+}}^{Mt} + x_{Mg^{2+}}^{Mt} = 1. \quad (70)$$

The algorithm used to solve this system is based on the method of successive iterations and the principles incorporated into the SPINMELT program [Ariskin and Nikolaev, 1996]. The new magnetite model was

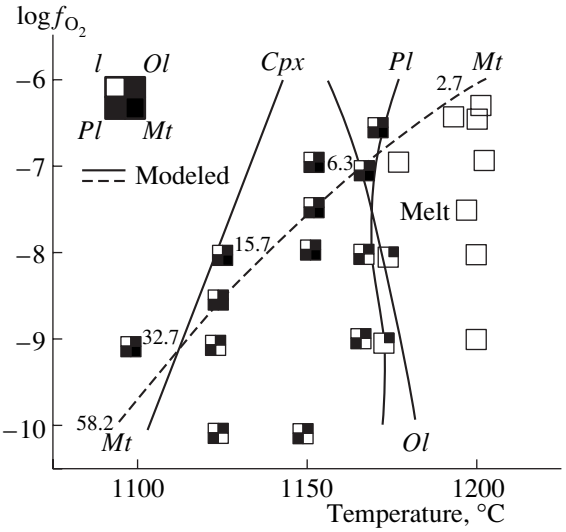

Fig. 27. Experimental and calculated mineral assemblages corresponding to the equilibrium crystallization of ferrobasalt GL-RHB [Hill and Roeder, 1974]. The simulations were conducted by the COMAGMAT-3.5 program with minor corrections of the calculated *Ol* and *Pl* crystallization temperatures [Ariskin and Barmina, 2000]. Numerals near the line of magnetite appearance are X_{Ulv} in *Mt*, calculated by the method [Stormer, 1983].

tested against the compositions of 32 experimental glasses produced in experiments that lasted for more than 100 h [Grove and Juster, 1989; Snyder *et al.*, 1993; Toplis *et al.*, 1994a; Toplis and Carroll, 1995]. The results of these calculations reproduced fairly well the experimental data. For instance, the model compositions of magnetite reproduced experimental data with an average accuracy of ±2.3 mol % for Fe^{3+} and Fe^{2+}, ±0.5% for Al^{3+}, ±0.4% for Mg^{2+}, and ±1.3% for Ti^{4+}, and the overall errors in the calculated Fe contents of *Mt* ($Fe^{2+} + Fe^{3+}$) are approximately 1 mol %. The experimental temperatures were reproduced accurate to 10°C [Ariskin and Barmina, 1999].

The newly developed model of the *Mt*–melt equilibrium was incorporated into the COMAGMAT program and is now an important constituent of the COMAGMAT-3.5 and higher versions [Ariskin, 1999]. The realism of the results obtained by calculating phase equilibria with this program can be illustrated by comparing the results obtained by simulating equilibrium crystallization of basalt GL-RHB and experimental data on this composition [Hill and Roeder, 1974]. Figure 27 exhibits a good agreement between the calculations and experiments. Magnetite is the first to crystallize at $f_{O_2} = 10^{-6}$ bar and is the fourth phase in the crystallization sequence at $f_{O_2} = 10^{-9}$ bar. The model temperatures of *Mt* stability differ from the experimental values by no more than 10–15°C, which corresponds to the accuracy of the computer model. It is interesting that the calculated dependence of the magnetite liqui-

dus on f_{O_2} changes under different redox conditions: it is 30–35°C/$\log f_{O_2}$ at $-7 < \log f_{O_2} < -6$ and does not exceed 15°C/$\log f_{O_2}$ at $\log f_{O_2} < -10$. Our later experience with the COMAGMAT-3.5 program has demonstrated that it worked best within the range of WM < f_{O_2} < NNO. Under more oxidized conditions, the calculation results can overestimate the magnetite liquidus temperature by 15–30°C. With regard to this factor, the COMAGMAT-3.5 program enables the automated correction of the calculated temperature of magnetite crystallization.

***Ilm*–melt geothermometers.** The model for the *Ilm*–melt equilibrium utilized in the COMAGMAT-3.0 program was based on the geothermometers from [Nielsen and Dungan, 1983] and empirical relations that involve the composition of hypothetically existing magnetite [Ariskin *et al.*, 1988b]. The use of this model led to *Ilm* crystallization temperatures underestimated by 20–30°C. Consequently, ilmenite crystallized at anomalously high TiO_2 concentrations in the melt (6.5–7 wt %). This also led us to recalibrate the "ilmenite" model, which now allows one to calculate the temperature of the *Ilm*–melt equilibrium accurate to approximately 10°C [Ariskin and Barmina, 1999].

In developing the new *Ilm* model, we applied the same method as that for magnetite (see above). First, a global search in the INFOREX-4.0 database let us to retrieve 85 compositional pairs of coexisting ilmenite and quenched glasses [Juster and Grove, 1989; Snyder *et al.*, 1993; Auwera and Longhi, 1994; Toplis *et al.*, 1994a; Toplis and Carroll, 1995], from which we rejected 10 experiments that presented no reliable evaluations of the oxygen fugacity. The remaining selection of 75 experiments was employed for further calibrations. All of these experiments lasted for more than 48 h and were conducted at controlled oxygen fugacities of $10^{-13} < f_{O_2} < 10^{-8}$ and temperatures of 1050–1150°C. Most glasses varied in composition from ferrobasalt to ferroandesite at ($Na_2O + K_2O$) < 7 wt %. The mathematical processing of the data was carried out in two stages as a linear regression (69) for five cations: Fe^{3+}, Fe^{2+}, Ti^{4+}, Al^{3+}, and Mg^{2+}. The optimum values of the regression coefficients were published in [Ariskin and Barmina, 1999].

In order to assay the accuracy of the ilmenite model, 64 experiments were chosen from a basic selection of compositions that lasted for more than 100 h and were conducted at $-12.6 < \log f_{O_2} < -9$. The solutions of the inverse problem for this selection are shown in Fig. 28 and demonstrate the high accuracy of the calculated ilmenite crystallization temperatures (±7.2°C on average). The model and experimental *Ilm* compositions differ by approximately 1 wt % for Fe^{3+} and Fe^{2+} and no more than ±0.07% for Al^{3+}, ±0.48% for Mg^{2+}, and ±0.52% for Ti^{4+}.

The ilmenite crystallization model was also integrated into the COMAGMAT-3.5 program, which now enables simulating complex effects of the crystallization of Fe–Ti oxides within the petrologically important range of oxygen fugacities, approximately between the IW and NNO buffers. Note that the new version of the COMAGMAT program outputs the compositions of ilmenite and magnetite in the form of cation fractions (of Fe^{3+}, Fe^{2+}, Al^{3+}, Mg^{2+}, and Ti^{4+}) and as the X_{Ulv} and X_{Il} parameters, corresponding to the *Ulv* and *Ilm* activities calculated by the equations from [Stormer, 1983].

Figure 29 compares the phase diagrams for synthetic ferrobasalt SC1, which were constructed proceeding from the experimental results in [Toplis and Carroll, 1995, 1996] and from simulations with the COMAGMAT-3.5 program. The phase diagram in Fig. 29b is based on 17 liquid lines of descent simulated for f_{O_2} conditions parallel to the QFM buffer for ΔQFM from –2.5 to +1.5 with a step of 0.25 logarithmic units. This diagram is interesting in its ability to realistically reproduce the observed relationships between ilmenite and magnetite near the QFM buffer (*Mt* predominance under more oxidized conditions and early *Ilm* crystallization under reduced conditions). The inaccuracies in the simulated magnetite and ilmenite stability fields are on the order of 10–12°C.

The results of these simulations provide valuable information on the crystallization proportions of the oxides: near the point of magnetite appearance on the liquidus, it is 35–40%, which is in good agreement with the evaluations in [Hill and Roeder, 1974; Toplis and Carroll, 1996]. However, for the main crystallization range of the *Ol* + *Pl* ± *Aug* + *Mt* assemblage, it ranges from 16 to 22%. The model proportion of ilmenite does not vary as significantly (from 8 to 14%).

2.2.6. Accounting for total pressure

The simplest way to account for the effect of pressure on phase equilibria is to introduce empirical coefficients allowing for the different slopes of the liquidus $\beta_j = dT/dP$ for different minerals. The addition of the $\Delta T_j = \beta_j \Delta P$ increments to the T_j values calculated at atmospheric pressure does not require any modifications of the proposed calculation algorithm (Fig. 8) and makes it possible to assay the overall shift of the crystallization fields of minerals as a function of pressure. In constructing high-pressure versions of the COMAGMAT model, we utilized a modification of this method that took into account the thermodynamic nature of the dependences of phase equilibria on pressure [Ariskin *et al.*, 1990, 1992].

The effect of pressure on the equilibrium constant of reaction (25) at a constant temperature *T* can be written in the form

$$(\partial \ln K_r^j / \partial P)_T = -\Delta V_{crys}^r / RT, \qquad (71)$$

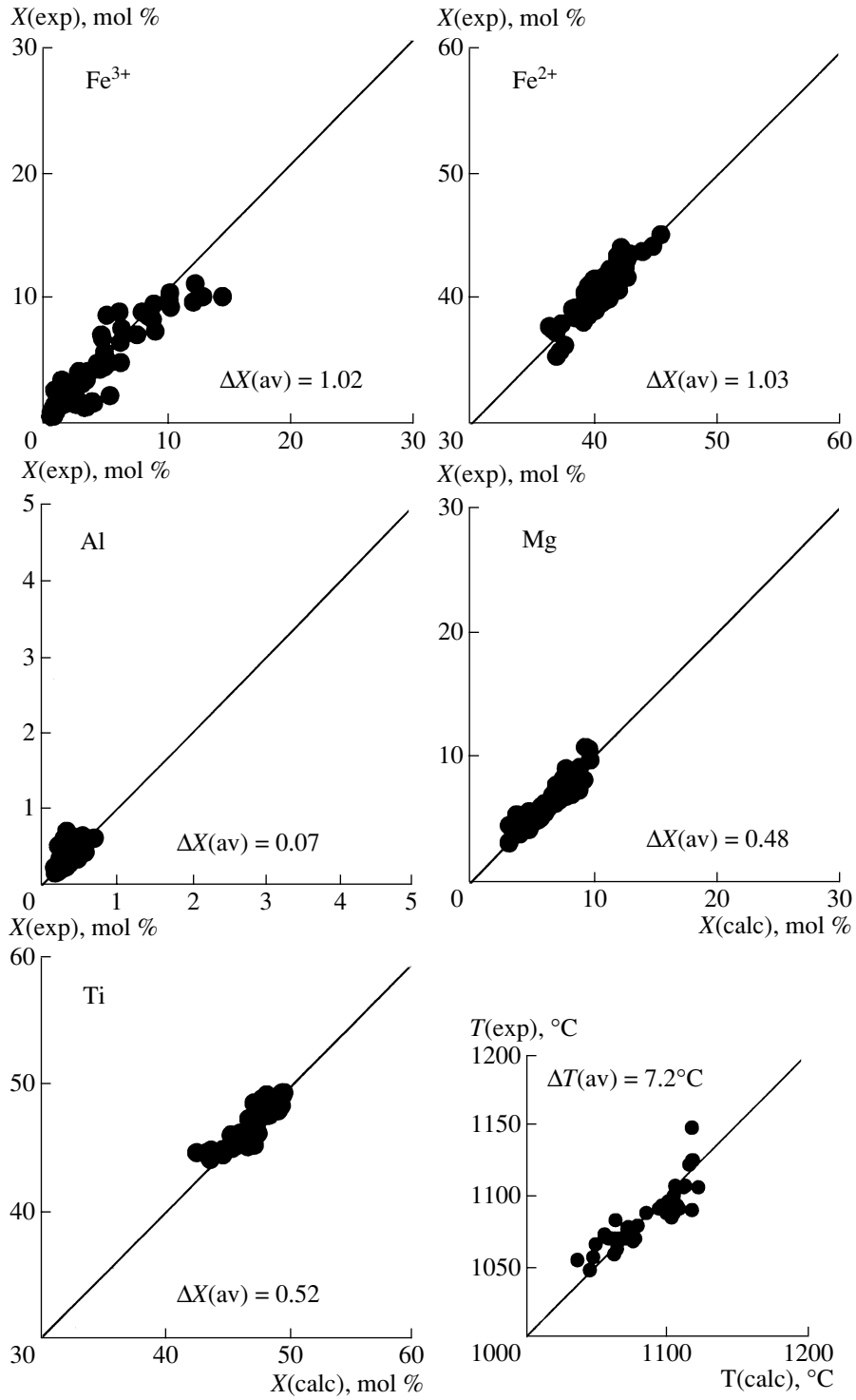

Fig. 28. Experimental parameters of the *Ilm*–melt equilibrium in comparison with the compositions and temperatures calculated by the new ilmenite model. ΔX(av) and ΔT(av) are the average deviations of the calculated parameters from experimental values.

where ΔV^r_{crys} is the volume change in this reaction. From this it follows that the increment in the $\Delta \ln K^j_r$ with pressure increasing from P_0 to P is

$$\Delta \ln K^j_r = -\Delta V^r_{crys} \Delta P / RT, \quad (72)$$

where $\Delta P = P - P_0$. In this situation, the integral effect of temperature and pressure on the equilibrium constant can be presented as

$$\ln K^j_r = (\Delta H^r_{melt} + \Delta V^r_{melt} \Delta P)/RT - \Delta S^r_{melt}/R, \quad (73)$$

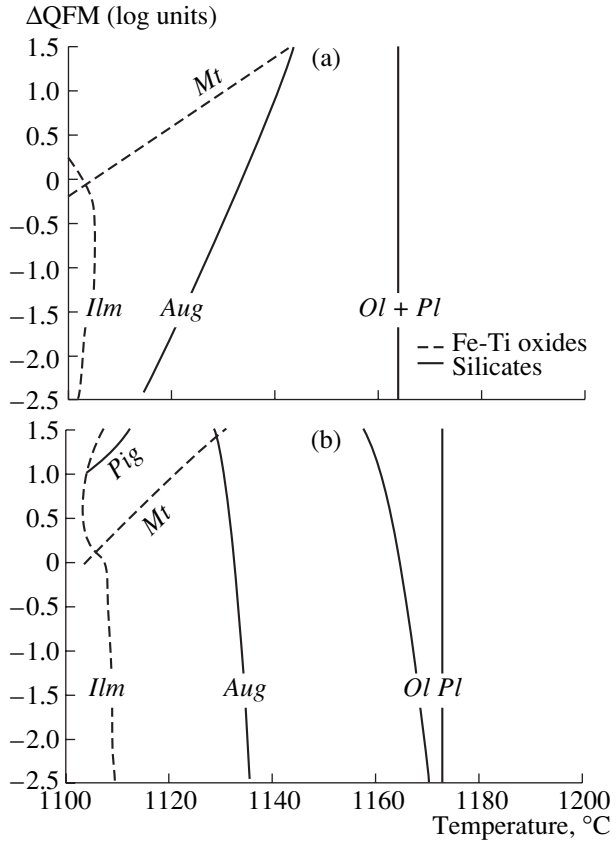

Fig. 29. Phase diagram for synthetic ferrobasalt SC1. (a) results of experiments, after [Toplis and Carroll, 1995, 1996], (b) simulations with the COMAGMAT-3.5 program.

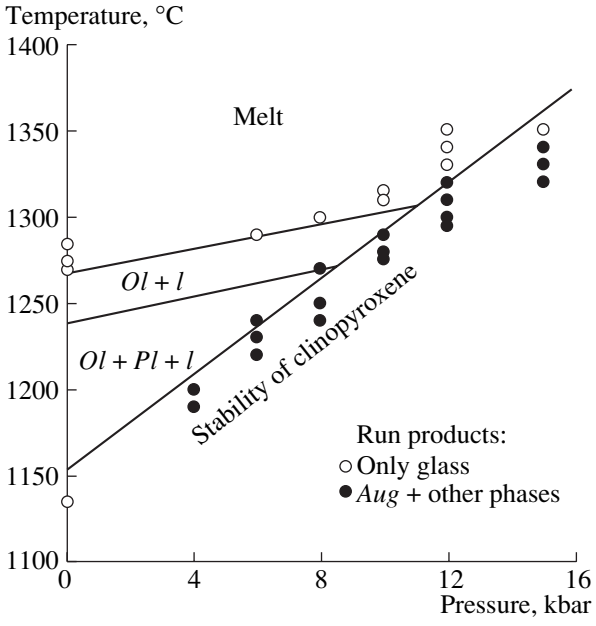

Fig. 30. *P–T* diagram for phase relations in magnesian tholeiite constructed based on experimental results [Bender *et al.*, 1978].

where $\Delta V^r_{melt} = -\Delta V^r_{crys}$. By analogy with Eq. (73), empirical geothermometers (19b) that characterize melt–mineral equilibria at $P_0 = 1$ atm can be modified into the form

$$\ln K^j_r = (A^j_r + \beta^j_r P)/T + B^j_r, \qquad (74)$$

in which the empirical coefficients β^j_r should be divisible into the volume change during the melting of the mineral $\Delta V^r_{melt}/R$, and $P \approx \Delta P = P - P_0$. Thus, the problem is reduced to determining the β^j_r values for each component of a given mineral.

Since our attempts to utilize tabulated data on the volume effects of the melting reactions for *Fo*, *Fa*, *En*, *Fs*, *Wo*, *An*, and *Ab* failed, we decided to rely only upon direct experimental data on the melting of rocks under high pressures. For this purpose, we compiled the results of experiments with high-Mg tholeiites (>10 wt % MgO) conducted under pressures from 1 atm to 15 kbar [Bender *et al.*, 1978; Green *et al.*, 1979; Fujii and Bougault, 1983]. These data include nearly 100 high-pressure experiments that were carried out at temperatures of 1200–1360°C in the highly reduced environments of graphite capsules. The main outcome of these studies was the establishment of a strong dependence of clinopyroxene crystallization temperature on pressure: although olivine was observed to be the first liquidus phase of all compositions at $P < 10$ kbar, augitic clinopyroxene is the first to crystallize at 10–12 kbar (Fig. 30). The slope of the *Aug* liquidus here is approximately 15 °C/kbar. The position of the *Ol* and *Pl* liquidi suggested that these minerals were characterized by weak and similar dependences of their liquidus temperatures on pressure (~5 °C/kbar). These values were utilized as provisional parameters for the choice of optimum coefficients β^j_r for a variety of end members.

The β^j_r could be evaluated by the coupled processing (by the least squares method) of the results obtained at 1 atm and in high-pressure experiments [see Eq. (74)]. The problem here is that the quality of data obtained at high pressures is commonly poorer than that in 1 atm experiments. To eliminate the effect of this factor on the equilibrium parameters, we accomplished the search for the baric coefficients at constant low-pressure values of A^j_r and B^j_r (Table 6) and then adopted β^j_r values that best fit the liquidus temperatures in terms of pressure. To accomplish this goal, we used the most complete dataset [Bender *et al.*, 1978] (Fig. 30), with the results from [Green *et al.*, 1979; Fujii and Bougault, 1983] used for additional corrections and control over the calculation quality.

In selecting the optimum baric coefficients, we assumed the same volume changes ΔV_{melt} for *Fo* and *Fa*

in *Ol* (supposing a weak dependence of the K_D^{Fe-Mg} on pressure [Ford *et al.*, 1983]) and utilized the ratio $\Delta V_{melt}^{Ab}/\Delta V_{melt}^{An} = 2:1$, which is consistent with the results of the thermodynamic analysis of data on the *Pl*–melt equilibrium [Loomis, 1979]. For augite, we also assumed equal melting volume differences for *En*, *Fs*, and *Wo* but introduced an empirical correction into the values of the Al partition coefficient (Table 6) that allowed us to take into account the enrichment of clinopyroxene in Al_2O_3 by 0.5–0.7 wt % with a pressure increase of 1 kbar [Ariskin *et al.*, 1992].

Starting in 1992, the COMAGMAT models of version 3.0 and higher use the following baric coefficients: $\beta_{Fo}^{Ol} = \beta_{Fa}^{Ol} = 1.2$, $\beta_{An}^{Pl} = 1.0$, $\beta_{Ab}^{Pl} = 2.0$, and $\beta_{En}^{Aug} = \beta_{Fs}^{Aug} = \beta_{Wo}^{Aug} = 1.4$ [Ariskin *et al.*, 1993]. Since we failed to determine reliably enough the analogous parameters for pigeonite and orthopyroxene, in further simulations these coefficients were varied within the range of 1.4–1.8. No such calibrations were conducted for Fe–Ti oxides. Nevertheless, this simple approach allowed us to simulate all principal features of the polybaric fractionation of tholeiitic systems attributed to changes in the augite stability field (see Section 4.3).

The last comment concerns the application of the COMAGMAT program to calculations at $P > 20$ kbar. Evidently, the empirical basis presented above becomes insufficient for the high-pressure model to be extended on such a broad pressure range. This is caused by the fact that the pressure effect is accounted for by the crystallization temperatures but not by the composition of silicate phases. Thus, any simulations with the COMAGMAT model and attempts to test it pertologically outside the plagioclase and spinel depth facies are senseless (for example, Putirka [1999] simulated clinopyroxene compositions up to pressures of 100 kbar). For the purposes of practical simulations, we recommend the user conducts them for pressures below 10–12 kbar. In certain instances we specify the possibility of calculations for P = 15–20 kbar and quote the uncertainties (see Chapter 4).

2.2.7. Effect of water on the crystallization temperatures of minerals

The occurrence of dissolved water depresses the liquidus temperature [Yoder and Tilley, 1962; Baker and Eggler, 1983] and results in changes in phase boundaries with respect to those at dry conditions. From the standpoint of thermodynamics, these effects are caused by the influence of water on the activities of mineral-forming components, with this phenomenon expressed in the form of different dependences of mineral crystallization temperatures on the H_2O concentration in the melt (Fig. 31). To account for this factor, a simple empirical approach was proposed to be utilized in the COMAGMAT model. This approach still does not consider all complexities of interactions between water and silicate melts and does not imply any specific mechanism of water dissolution [Al'meev and Ariskin, 1996]. It involves an empirical equation for water solubility in basic to acid melts, estimation of the H_2O solubility in water-saturated experimental glasses, and the calculation (on this basis) of correction coefficients for evaluating the liquidus temperatures of rock-forming minerals at a specified H_2O concentration. The substitution of these coefficients into the algorithm for calculating the equilibrium crystallization temperatures of minerals (see Chapter 1) makes it possible to provisionally evaluate the effect of H_2O on phase equilibria.

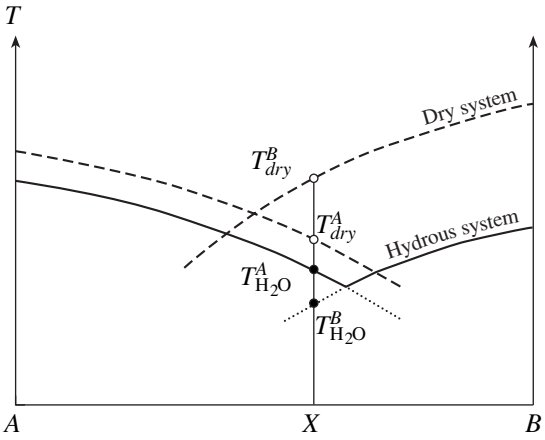

Fig. 31. Schematic plot for liquidus relations in a binary system for dry and hydrous conditions. The diagram demonstrates the possibility of changing the liquidus phases of the same melt *X* with the appearance of water in the system.

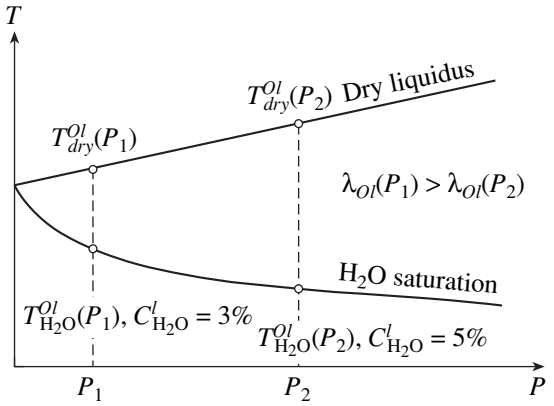

Fig. 32. Schematic plot for liquidus relations in basaltic melt at anhydrous and hydrous conditions. The diagram elucidates the meaning of the proportionality coefficient λ_j (76) using the example of olivine.

A decrease in the liquidus temperatures of different minerals can be expressed in the form

$$T^j_{H_2O} = T^j_{dry} - \lambda_j C_{H_2O}, \quad (75)$$

where $T^j_{H_2O}$ and T^j_{dry} are the temperatures at which mineral j starts to crystallize on the liquidus of the hydrous and dry systems, respectively; C_{H_2O} is the water concentration in the melt; and λ_j (°C/wt % of H_2O) is the proportionality coefficient that corresponds to a decrease in the liquidus temperature for mineral j at a change in the H_2O concentration in the melt by 1 wt %. The values of the coefficient λ_j for olivine, plagioclase, augite, and low-Ca pyroxene (mostly *Opx*) can be calculated from experimental data on phase equilibria in hydrous silicate systems (Fig. 32)

$$\lambda_j = (T^j_{H_2O} - T^j_{dry})/C_{H_2O}, \quad (76)$$

where $T^j_{H_2O}$ is the experimental temperature, T^j_{dry} is the crystallization temperature of mineral j calculated by mineral–melt geothermometers at dry conditions (Table 6), and C_{H_2O} is the experimentally determined or calculated H_2O concentration (wt %) in the quenched glass. Processing in such a manner data on melts equilibrated with a given mineral, it is possible to calculate the average values of λ_j for different pressures [Al'meev and Ariskin, 1996].

In attacking this problem, we used information retrieved from the INFOREX-4.0 system (version of 1997). By this time, the archive of the database included more than 2000 water-saturated experiments. These experiments were carried out with natural rocks (basalts, andesites, dacites, and rhyolites) and synthetic mixtures in the excess of H_2O at temperatures of $675 < T < 1300$°C and pressures of 100 bar $< P <$ 30 kbar; the duration of these experiments ranged from 1 to 800 h. Approximately 500 experimental results included data on the composition of the quenched glasses, and some results also provided information on the composition of coexisting minerals. The utilization of this information for quantifying the effect of water on the crystallization temperatures (76) is complicated by the unknown H_2O concentrations in the water-saturated melts in most of the experiments. In this situation, a decisive role belonged to searching for a functional dependence that would enable predicting the water solubility in a silicate liquid.

Estimating water solubility in melt. This problem was solved by building an empirical equation based on the results of processing direct data on water solubility in silicate melts [Al'meev and Ariskin, 1996]

$$\ln C_{H_2O} = 4.39 + [38483(Si/O)^l - 14710]/T + 0.59\ln P - 21.45(Si/O)^l + 3.89(Al/Si)^l, \quad (77)$$

where the temperature is expressed in Kelvins, pressure is in bars, and melt parameters are in atomic units.

Equation (77) was calibrated against the data of 79 experiments characterizing melt–vapor equilibrium under pressures from 200 bar to 9 kbar and temperatures of 800–1200°C [Hamilton *et al.*, 1964; Kadik *et al.*, 1971; Sisson and Grove, 1993; Dixon *et al.*, 1996]. The comparison of the calculated and experimental data on the H_2O solubility in melts indicates that Eq. (77) reproduces experimental values accurate to about 0.3 wt % and can be applied to calculating H_2O solubilities up to pressures of 10 kbar.

Calculating correction coefficients λ_j. Using search routines of the INFOREX-4.0 systems, we selected those "hydrous" experiments that were conducted with lherzolites, basalts, and andesites under pressures of up to 10 kbar. The quenched glass compositions reported in these experiments were grouped according to the presence of a given mineral in the assemblage in equilibrium with the melt (for example, for olivine: $Ol + l$, $Ol + Pl + l$, $Ol + Aug + Pl + l$, and so on). Thus we created four datasets: *Ol*–melt (69 experiments), *Pl*–melt ($n = 81$), *Aug*–melt ($n = 56$), and *Opx*–melt ($n = 19$).

For the compositions of the quenched glasses of each of the four datasets, we calculated (with the COMAGMAT program) the crystallization tempera-

Table 9. Values of correction coefficients λ_j for various pressures

P, kbar	*Ol*	*Aug*	*Opx*	*Pl*
1	17.9 ± 6.0 (14)	34.3 ± 7.1 (12)	22.4 ± 3.4 (2)	59.6 ± 7.8 (23)
2	18.7 ± 2.9 (21)	24.8 ± 2.2 (19)	22.3 ± 1.2 (4)	49.9 ± 4.2 (18)
2.5		23.7 ± 3.9 (3)		47.6 ± 1.0 (3)
3			18.3 (1)	43.1 ± 1.5 (23)
4				38.3 ± 1.6 (3)
5	10.2 ± 5.5 (3)	15.5 ± 3.3 (8)		38.1 ± 3.1 (6)
6.9				37.8 ± 0.6 (5)
7.5	5.1 ± 3.7 (3)	14.5 ± 1.6 (4)	12.5 ± 2.2 (4)	
10	1.3 ± 0.7 (2)	10.5 ± 1.1 (5)	9.3 ± 1.0 (4)	

Note: Numerals in parentheses indicate the numbers of points.

tures under dry conditions T^j_{dry} and specified pressures. These values turned out to be 100–300°C higher than the experimental temperatures $T^j_{H_2O}$. Then, the difference $T^j_{dry} - T^j_{H_2O}$ for each experiment was normalized to the H_2O concentration in the melt, which was calculated by Eq. (77). The average values of the crystallization temperature decrease λ_j calculated in this manner for olivine, plagioclase, augite, and orthopyroxene as functions of pressure $P = P_{H_2O}$ are listed in Table 9. When developing the first "hydrous" version of the COMAGMAT model, we used the following average values of λ_j (which were independent of pressure): 42.2 for *Pl*, 17.5 for *Ol*, 27.4 for *Aug*, and 22.4°C/% H_2O for *Opx* [Ariskin *et al.*, 1995].

2.2.8. Partitioning of trace elements

The behavior of trace elements in magmatic systems can be simulated independent of solving the problem of major-element equilibria. This makes it possible to conduct trace-element calculations after estimating the proportions of solid phases and melt. The traditional approach makes use of weighted partition coefficients

$$D^j_i = C^j_i / C^l_i, \quad (78)$$

where the concentrations of element *i* in mineral *j* and melt are in wt % or ppm. This empirical parameter can be calculated from the compositions of experimentally synthesized crystals and quenched glasses [Irving, 1978; Jones, 1995] or from the data of natural observations characterizing the systems phenocryst–matrix and host mineral–melt inclusion [Sobolev *et al.*, 1996]. There are also indirect methods for calculating the values of D^j_i on the basis of models describing the behavior of trace elements during the differentiation of basaltic magmas (see, for example [Kravchenko, 1977; Barmina *et al.*, 1982]).

In practice, the choice of an empirical background for developing models of trace-element partitioning is not as obvious. The bulk of the experimental data was obtained for systems doped with a certain trace element. This puts forth the problem as to whether thermodynamic simulations can be based on partition coefficients measured at concentrations much higher than the content of a given element in nature. Fortunately, as has been demonstrated by a specialized research of the validity of Henry's law, dependence (78) holds true within broad limits and includes the natural concentration ranges of most trace elements (see the review [Frenkel *et al.*, 1988b]).

The fulfillment of Henry's law for partition coefficients (78) suggests that the behavior of trace elements in the solid phase–melt system is subject to thermodynamic laws and can be described in terms of the dependence of the free energy of formation of minor components in the mineral on temperature, pressure, and the composition of the system [see, for example, Eqs. (20)–(24), in which MgO can be substituted for Ni, Mn, or Co]. Although such attempts were repeatedly made (in this context, it is worth noting papers by Nielsen *et al.*), no uniform and systematic approach to the description of trace-element partition have been developed as yet. This was largely caused by the necessity to accurately describe the activities of trace elements in a melt and minerals, a problem still awaiting resolution.

Table 10. Temperature dependences of the partition coefficients of trace elements used in the COMAGMAT model

Element	$\ln D^j_i = A/T + B + C\log f_{O_2}$			References
	A	*B*	*C*	
Plagioclase				
Sr	9050	–5.24	–	[Drake and Weill, 1975]
Ba	11800	–8.85	–	
Eu	3989	–5.47	–0.256	[Barmina *et al.*, 1992]
Olivine				
Mn	10219	–6.73	–	[Frenkel *et al.*, 1988b]
Ni	11703	–5.21	–	
Co	16527	–10.03	–	
Augite				
Mn	19495	–13.24	–	[Frenkel *et al.*, 1988b]
Eu	15053	–10.62	0.086	[Barmina *et al.*, 1992]

Thus, models of the COMAGMAT series make use of constant values or temperature–composition dependences of weight partition coefficients, most of which were calculated from the results of experiments on phase equilibria in synthetic and natural silicate systems. The COMAGMAT program enables simulating the evolution of the concentrations of 20 trace elements, which can be provisionally subdivided into two groups. Group I includes Mn, Ni, Co, Cr, Sc, V, Sr, Ba, Rb, and Cu. Data on the partition of these elements were systematized and processed in the late 1980s [Frenkel *et al.*, 1988b], and the temperature dependences for some of them are presented in Table 10.

Group II comprises REE (La, Ce, Nd, Sm, Eu, Gd, Dy, Er, Lu, and Yb). The temperature–composition and baric functions of the REE partition coefficients were derived from the values of more than 200 experimentally determined D^j_{REE}, which were obtained in 1974–1988 (see the review [Barmina *et al.*, 1992]). Based on this information, empirical equations were calculated for *Ol*, *Pl*, *Aug*, *Opx*, and *Ilm* in the form

$$\ln D^j_{\mathrm{REE}} = A/T + B + C(P-1)/T + D\ln C^l_{\mathrm{SiO_2}} + E\ln N_{\mathrm{REE}}, \quad (79)$$

where T is temperature (K), P is pressure (bar), $C^l_{\mathrm{SiO_2}}$ is the concentration of SiO_2 in the melt (wt %), $1 \le N_{\mathrm{REE}} \le 15$ is the consecutive number of the rare-earth element from La to Lu, and A, B, C, D, and E are regression coefficients. Each mineral is characterized by two dependences: one for LREE and the other for HREE (the "boundary" element was Gd). This permits us to make allowance for the maximum of D^j_{REE} values for Dy and Gd in augite and simulate the evolution of the complete REE patterns. The regression parameters were published in [Barmina *et al.*, 1992; Ariskin *et al.*, 1993]. The Eu partition coefficients between *Aug*, *Pl*, and melt were determined using additional data on the dependences on oxygen fugacity, which were calculated from data in [Sun *et al.*, 1974; Drake and Weil, 1975] (Table 10). In modeling phase equilibria with pigeonite and magnetite, it was postulated that $D^{Pig}_{\mathrm{REE}} = D^{Opx}_{\mathrm{REE}}$ and $D^{Mt}_{\mathrm{REE}} = D^{Ilm}_{\mathrm{REE}}$.

The partition of trace elements between phases in the COMAGMAT model is calculated in the INFORM block after determining the equilibrium amounts of minerals N_j at a specified amount of melt N_l (Fig. 9). The molar amounts of minerals and melt are recalculated to their weight amounts F_j and F_l, and the trace-element concentrations in the melt are calculated by mass-balance equations

$$C^l_i = C^0_i \Big/ \left(F_l + \sum_{j=1}^{m} D^j_i F_j \right) \quad \text{and} \quad C^j_i = D^j_i C^l_i, \quad (80)$$

where C^0_i is the overall concentration of element i in the system.

2.3. Calculation Procedures, Tuning and Verification of the COMAGMAT Model

The algorithm presented above for simulating the crystallization of silicate melts, experimental database of phase equilibria, and routines for calibrating equilibrium equations compose a computerized system for the simulation of crystallizing magmas. An important element of this system is search options of the INFOREX program, which are combined within a single interface with routines for calculating the regression coefficients of mineral–melt geothermometers. These coefficients are written in the output file, whose format allows the user to prompt COMAGMAT to calculate liquid lines of descent during fractional or equilibrium crystallization. This organization of work makes it possible to calibrate models for a specified magma composition range and different P–T–$f_{\mathrm{O_2}}$ conditions.

In order to verify the model, the INFOREX program offers the possibility of creating mineral–melt files (*Ol–l*, *Pig–l*, *Mt–l*, and others) that include data on the temperature and composition of glasses quenched in the presence of a given mineral, even if there are no data on the composition of this mineral. This information, which is independent of calibrations, can be used for additional testing and correcting integral mineral–melt geothermometers. Another important way of tuning and testing models for phase equilibria utilizes data on the bulk compositions of experimental materials. Using these compositions as starting for simulations, the user can readily calculate the equilibrium lines of descent for certain experimental conditions and compare them with the observations. If there is a systematic temperature difference for the appearance of one of the phases on the liquidus, models of the COMAGMAT series allow the user to introduce an additional temperature correction, which is usually no greater than 10°C and lies within the accuracy of the geothermometers developed previously.

These methods of calculations of phase equilibria in the automated mode were first implemented in the METEOMOD program, which was developed for simulating the partial melting of ordinary chondrites [Ariskin *et al.*, 1997b]. The same principles underlie the basic version of the COMAGMAT-3.0 model and its later modifications. The main possibilities and characteristics of work with this multifunctional package of petrological programs will be considered in the following section.

2.3.1. Main versions and functions of the COMAGMAT computer program

The COMAGMAT model is designed for calculating phase equilibria and simulating the crystallization differentiation of magmas within a wide range of compositions, including magnesian and high-alumina basalts, various tholeiites, and basaltic andesites. The first version of the program (COMAGMAT-1.*n*) was designed in 1989 for use on EC series computers (EC is Russian abbreviation for United System), which were built in Eastern European countries. The DOS-based versions were developed in the early 1990s for IBM compatible personal computers (COMAGMAT-2.*n*). Their final form was implemented in the COMAGMAT-3.0 system, which was issued in 1993 [Ariskin *et al.*, 1993] and received wide recognition from petrologists. The currently used versions of COMAGMAT-3.5 and higher include more realistic models for the crystallization of Fe–Ti oxides [Ariskin and Barmina, 1999; Ariskin *et al.*, 1999]. A specialized modification of this program (COMAGMAT-3.65) presented in the late 2000 simplifies the calculations in systems closed with respect to oxygen and allows the user to utilize direct data on the FeO and Fe_2O_3 concentrations in the rocks [Ariskin *et al.*, 2002].

The core of the COMAGMAT system is an algorithm for solving the problems of equilibria in crystallizing magmas (Fig. 9), which is utilized in the "shell" of various calculation modes and conditions of crystallization simulations. These modes and conditions can be specified from a user-friendly interface (see Appendix in [Ariskin *et al.*, 1993]), whose structure is maximally preserved in the WINDOWS-based version of the modern model. Now consider the main calculation modes.

1. Thermometry of Mineral–Melt Equilibria. This mode allows the user to calculate the temperatures of magmatic melt saturation with respect to mineral phases at specified external conditions (P–T–$\log f_{O_2}$ and the composition of the melt, including the H_2O concentration). The mode is recommended for evaluating the crystallization temperatures of natural glasses (melt inclusions) and the testing of COMAGMAT-incorporated geothermometers with the use of mineral–melt files created in the INFOREX database.

2. Simulating Equilibrium Crystallization. This mode enables the user to calculate the compositional evolution trajectories for the melt and minerals and changes in the phase proportions during crystallization in a closed system. This mode can also be used to additionally tune and correct the COMAGMAT model by comparing the calculated mineral crystallization sequences with those obtained in experiments. The calculation of liquid lines of descent for natural samples is the basis of the method of geochemical thermometry (which will be discussed in Chapter 3).

3. Simulating Fractional Crystallization. This option enables the user to calculate the evolutionary trajectories of the liquid and solid phases during perfect fractionation, when the crystallizing minerals are completely separated from the fractionating melt. This option is designed to test the fractionation hypothesis for a certain source (primary or parental magma). In some situations, the comparison of the calculated liquid lines of descent and the geochemical trends observed in rocks enables the user to estimate the conditions of the crystallization process, for instance, the total pressure and oxygen fugacity (see Chapter 4).

4. Simulating Layered Intrusion Formation. This part of COMAGMAT involves an algorithm for simulating the dynamics of heat–mass transfer and chemical differentiation in magma chambers. The reader can find examples of applications of the INTRUSION subroutine in [Frenkel *et al.*, 1988b, 1989; Chalokwu *et al.*, 1996; Ariskin *et al.*, 1999]. Note that this program allows the user to model partial or intermediate magma fractionation (see Section 1.2).

Calculation conditions. External conditions are specified by defining the baric and redox regimes. In the former situation, the user has to select one of the following modes: (a) regime of isobaric crystallization P = const (*Isobaric crystallization* option), (b) regime of increasing pressure for conducting a series of isobaric calculations at $P = P + \Delta P$ (*Increasing pressure routine*), or (c) regime of decompression crystallization (*Decompression crystallization*), which simulates liquid lines of descent when the pressure is decreased in the course of crystallization of the initial melt $P(\varphi) = P(\varphi) - \Delta P$.

If the redox conditions are specified, the user can choose between the following two options: (a) the system is closed with respect to oxygen (*Closed system* (Fe^{2+}/FeO) *ratios*) and (b) the oxygen pressure is buffered (*Open system*). In the former situation, the user has to specify the total degree of Fe reduction in the melt $Fe(II) = Fe^{2+}/(Fe^{3+} + Fe^{2+})$, which usually falls within the range $0.80 \le Fe(II) \le 0.95$. In situation (b), the user selects one of the twelve oxygen buffers traditionally used in petrological interpretations (such as QFM, WM, or NNO) or specify a constant oxygen pressure $\log f_{O_2}$ = const.

Activating dynamic calculations. Combinations of the main modes and thermodynamic conditions predetermine the multifunctional character of COMAGMAT programs and their applicability to a diversity of geological situations. Another important feature of this system is its ability to combine the solution of the equilibrium problem with dynamic calculations, which allow for the separation of the crystallizing minerals and a part of the fractionating liquid from the main magma body. This algorithm, referred to as the INTRUSION routine, was designed to simulate the convective–cumulative mechanism, which is responsible for the formation of large-scale and cryptic layering of igneous rocks [Frenkel *et al.*, 1988b, 1989]. This program makes it possible to calculate the proportions of cumulus minerals in the rock succession of an intrusion, the compositional evolution of the phases, and the distribution of major and trace elements as functions of the thermal-physical properties of the host rocks and the dynamic parameters controlling the differentiation process in the chamber. The principal scheme of relations between the thermodynamic and dynamic calculations is shown in Fig. 33.

Modern versions of the COMAGMAT program. The wide recognition of the COMAGMAT-3.0 program by petrologists, revision of the local DOS-based versions, and the wide spread of modern communication technologies put forth the problem of designing a network version of the program available via the Internet. For this purpose, we separated the calculational core of the local version of the COMAGMAT-3.0 model, which receives a data flow from the interface program, processes these data, and sends the result to the user in HTML format. This allows the user to calculate phase equilibria for different magmatic systems working in remote access mode. The network version of the COMAGMAT-3.3 model is now available at the server of the Division of Geology of Moscow State University (designers P.Yu. Plechov and K.A. Bychkov). At present we are in a final stage of developing WINDOWS-applications of COMAGMAT, see site

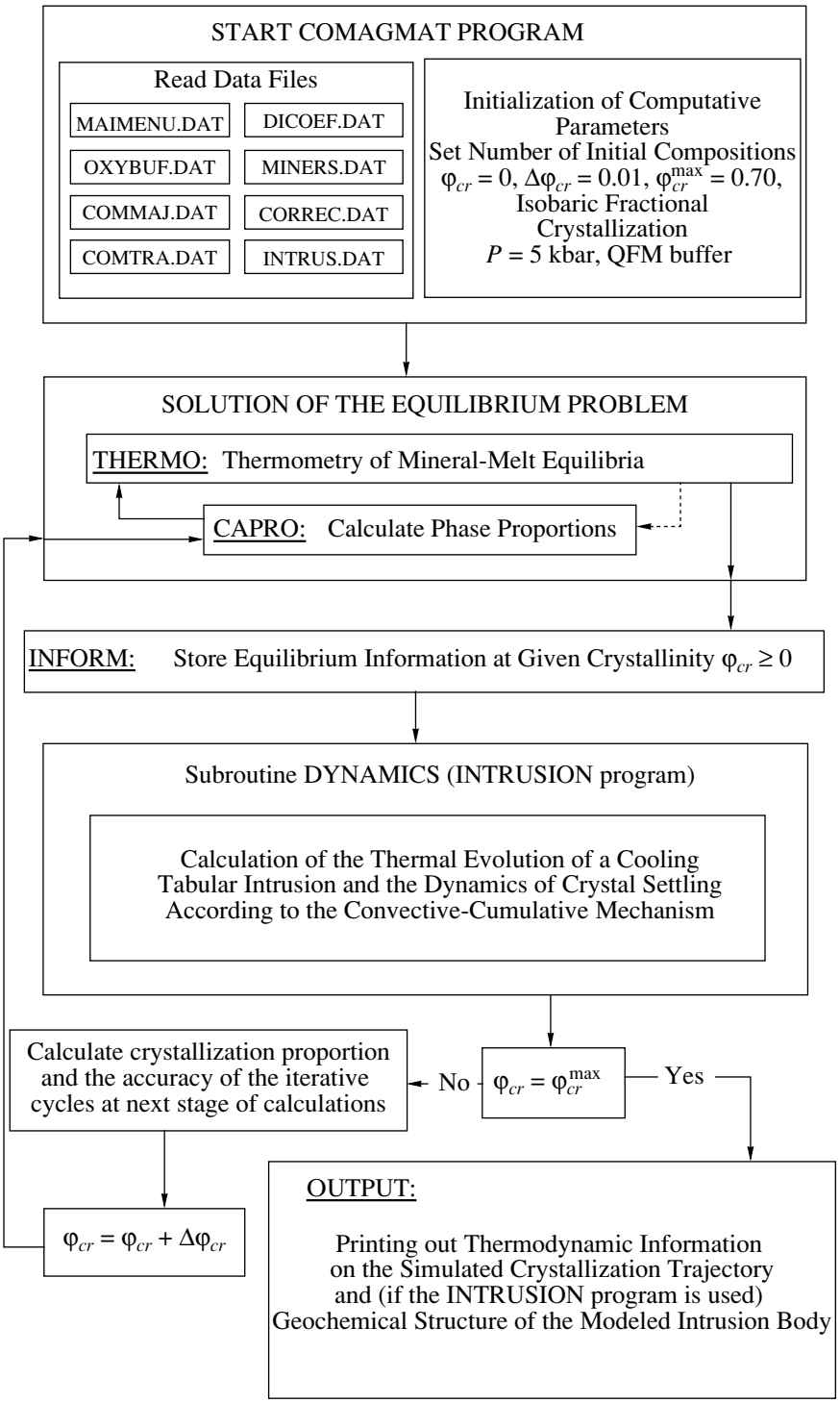

Fig. 33. General structure of the COMAGMAT model [Ariskin *et al.*, 1993]. See Figs. 8 and 9 for details of the thermodynamic blocks. The purpose of the INTRUSION subroutine is described in [Ariskin *et al.*, 1999; Ariskin and Barmina, 2000]. The reader can find descriptions of the data files in the manual in our website at http://www.geokhi.ru/~dynamics (see the COMAGMAT option).

http://www.geokhi.ru/~dynamics/ for the most recent information. The user can also find a manual for the COMAGMAT program there and download pdf files with papers describing examples of its petrological applications.

2.3.2. Calculation of equilibrium crystallization at 1 atm

The efficiency of the COMAGMAT complex and the accuracy of the numerical simulations of phase

equilibria can be assayed by comparing the calculated liquid lines of descent with those determined experimentally. For this purpose, one can use the data of melting experiments with rocks of known composition, when the samples were held at subliquidus temperatures. It should be born in mind that the bulk composition of the system virtually never remains unchanged in the course of experiments.

Most experiments under atmospheric pressure were carried out using the Pt-wire loop technique in a gas mixture flow, which controlled the oxygen fugacity. At high temperatures, this method results in the loss of volatile elements (Na, K, and P), which can reach tens of relative percent at a melting duration of hundreds of hours (see, for example, [Grove *et al.*, 1982]). This phenomenon is significant because maintaining a mass balance is of crucial importance for the COMAGMAT program, in which it determines the crystallization temperatures and the proportions and compositions of minerals with increasing degree of crystallization in the system.

Hence, when experimental and calculation results are compared, it is necessary to focus on the early and middle crystallization stages, with much attention paid to the appearance sequence of minerals on the liquidus. The first results of this comparative analysis were published by Ariskin *et al.* [1987], who considered experimental and model crystallization sequences for nine melts, most of which were of tholeiitic composition. The calculations were carried out by the program that was later used as the basis for the main version of COMAGMAT-1.*n* (see above). In this section, we present the results of our calculations with one of the latest versions of COMAGMAT-3.51 that included improved versions of the *Mt*–melt and *Ilm*–melt geothermometers and some additional modifications [Ariskin and Barmina, 1999].

Input data and calculation conditions. The liquid lines of descent were simulated for ten selected compositions from ten experimental works carried out from 1979–1996 (Tables 11, 12). Data from [Walker *et al.*, 1979; Grove *et al.*, 1982; Grove and Bryan, 1983; Tormey *et al.*, 1987] were utilized earlier, when the COMAGMAT-3.0 model was calibrated, and the other publications represented independent experiments. Six of these starting compositions characterized various tholeiitic basalts (Table 11), and four were high-Al and subalkaline basaltoids (Table 12).

The equilibrium crystallization trajectories were calculated using the *Simulating Equilibrium Crystallization* routine under conditions maximally close to those in the experiments: 1 atm pressure and an oxygen fugacity corresponding to the QFM buffer equilibrium. The crystallization increment $\Delta\varphi$ was 1 mol % as the maximum degree of crystallization varied from 70 to 80%. The calculated and experimental crystallization sequences are demonstrated in Figs. 34 and 35. The plots were constructed for temperatures of 1050–1300°C, which corresponded to the calibration conditions of the basic mineral–melt geothermometers.

Table 11. Composition of experimentally studied tholeiitic basalts used to test the COMAGMAT-3.51 program

Oxide	*1*	*2*	*3*	*4*	*5*	*6*
SiO_2	48.73	49.60	48.80	50.00	47.40	48.80
TiO_2	1.21	0.67	0.96	1.66	2.27	0.62
Al_2O_3	16.19	16.00	17.50	15.70	14.20	15.40
FeO	9.29	9.57	9.58	10.20	14.34	8.91
MnO	0.18	0.16	0.14	0.14	0.20	0.16
MgO	8.05	10.40	9.62	7.78	6.13	10.70
CaO	12.43	11.90	10.20	11.00	9.04	13.50
Na_2O	2.24	1.74	2.71	3.07	2.97	1.55
K_2O	0.35	0.10	0.11	0.13	0.70	0.01
P_2O_5	–	–	–	0.16	0.22	0.03

Note: (*1–6*) Starting compositions (see Fig. 34, *1–6*): (*1*) tholeiitic basalt V30RD8-P12 [Walker *et al.*, 1979], (*2*) magnesian tholeiite ALV-528-1-1 [Grove and Bryan, 1983], (*3*) magnesian tholeiite AII78-3-102 [Tormey *et al.*, 1987], (*4*) tholeiitic basalt ALV-1690-20 [Grove *et al.*, 1990], (*5*) ferrobasalt 4-3 [Snyder *et al.*, 1993], (*6*) low-Na tholeiite RE-46 [Yang *et al.*, 1996].

Table 12. Compositions of high-Al and subalkaline basaltoids used to test the COMAGMAT-3.51 program

Oxide	*1*	*2*	*3*	*4*
SiO_2	47.50	53.82	48.14	48.17
TiO_2	0.56	0.93	0.89	4.51
Al_2O_3	18.00	17.28	13.50	13.07
FeO	11.10	7.49	10.70	14.86
MnO	0.14	0.16	0.24	0.21
MgO	9.81	5.68	7.28	4.81
CaO	11.40	8.58	12.76	9.38
Na_2O	1.67	3.66	2.55	3.20
K_2O	0.09	0.97	2.35	0.89
P_2O_5	–	0.22	0.37	0.60

Note: (*1–4*) Starting compositions (see Fig. 35, 1–4): (*1*) high-Al basalt 79-35g [Grove *et al.*, 1982]; (*2*) basaltic andesite 79-38b [Grove and Juster, 1989]; (*3*) alkaline basalt 78LH1 [Kennedy *et al.*, 1990]; (*4*) subalkaline Fe–Ti basalt 9005 [Thy and Lofgren, 1994].

Comparing crystallization sequences. Data in Fig. 34 demonstrate that the COMAGMAT model reproduces accurately enough the crystallization sequences of minerals in tholeiitic systems: $Ol \pm Pl \longrightarrow Aug \longrightarrow Pig \longrightarrow$ oxides ($Mt \pm Ilm$). The calculated temperatures at which minerals start to crystallize deviate from the experimental values usually by no more than 10–15°C. This result reflects the fact that the basic model was calibrated mostly on tholeiitic-system compositions. The data in Fig. 34, *5* deserve closer exami-

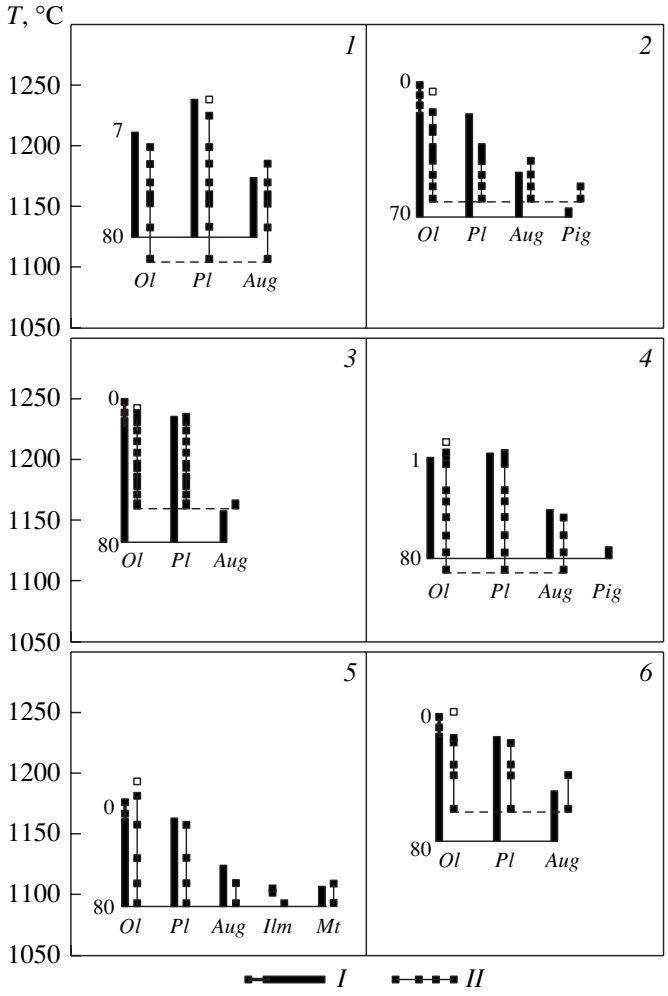

Fig. 34. Experimental and calculated crystallization temperatures of minerals during the equilibrium solidification of tholeiite basaltic melts. (*I*) Simulations by the COMAGMAT-3.5 program for QFM conditions; (*II*) experimental results. (*1–6*) Correspond to the numbers of compositions in Table 11: (*1*) [Walker *et al.*, 1979], (*2*) [Grove and Bryan, 1983], (*3*) [Tormey *et al.*, 1987], (*4*) [Grove *et al.*, 1990], (*5*) [Snyder *et al.*, 1993], (*6*) [Yang *et al.*, 1996].

nation. This plot shows that the program adequately reacts to the saturation of the residual melt with Fe–Ti oxides. The data on high-Al and subalkaline basalts are more diverse (Fig. 35). In three of them, *Pl* is a liquidus phase, and the crystallization fields of oxides are wider. The model crystallization temperatures of *Aug* and *Ilm* are slightly overestimated, but the calculated crystallization sequences and liquidus phase assemblages are in general agreement with the experimental results.

In the context of the plausibility of the COMAGMAT model, it is important to emphasize that the accuracy of the calculated liquid lines of descent is determined not so much by the absolute temperatures as by the relative crystallization temperatures of minerals. In this sense, the data of experiments and calculations in Fig. 34, *2* are practically identical and can yield highly consistent model and experimental trends in variation diagrams (Figs. 36, 37).

Crystallization proportions of minerals. In analyzing the calculation results obtained with the CFCT program, it was noted that the directions of the petrochemical and geochemical trends were controlled by the proportions of the crystallizing minerals, and the errors in the mineral compositions were less significant (see Section 1.4). These crystallization proportions were calculated based on the difference between the amounts of specified solid phases in the previous and current states of the partly crystallized system [see Eq. (52)]. Because of this, it is so important to track variations in the modal proportions of minerals as the bulk degree of crystallization is increased. The empirical basis for such a comparison was limited when the early versions of the COMAGMAT model were developed: we managed to find only one publication [Bender *et al.*, 1978], in which the changes in the *Ol* and *Pl* amounts in the experimental products were assayed by microscopical observations. A comparison of these

Table 13. Average crystallization proportions during the equilibrium solidification of natural silicate melts (results of computer simulations with the COMAGMAT-3.51 model)

Starting composition	Crystallization proportions (wt %) for different assemblages			
	Ol–Pl	*Ol–Pl–Aug*	*Ol–Pl–Aug–Pig*	*Ol–Pl–Aug–Mt*
In Table 11				
1	29.0–71.0	6.6–44.3–49.1	–	–
2	31.7–68.3	7.7–41.8–50.5	(–2.5)–40.7–51.8–10.0	–
3	29.1–70.9	9.1–43.9–47.0	–	–
4	26.4–73.6	5.5–46.2–48.3	(–13.3)–43.3–53.3–16.7	–
5	26.4–73.6	7.8–43.2–49.0	–	(–12.9)–35.4–58.0–19.5
6	32.1–67.9	7.4–41.6–51.0	–	–
In Table 12				
1	33.4–66.6	13.5–41.2–45.3	(–11.7)–37.3–50.0–24.4	–
2	21.8–78.2	2.5–54.0–43.5	(–23.2)–45.3–46.2–31.7	–
3	–	7.6–51.1–41.3	–	(–8.7)–37.5–51.3–19.9
4	25.5–74.5	–	–	(–0.3)–42.7–48.1–9.5*

* The value of 9.5 wt % refers to ilmenite. The modeled crystallization proportions for the *Ol–Pl–Ilm* assemblage are 17.6 : 68.6 : 13.8. Negative values for *Ol* point to a peritectic reaction.

experimental data and the calculated phase proportions convinced us that our models can predict accurately enough the crystallization proportions of *Ol* and *Pl* (approximately 3 : 7 [Frenkel and Ariskin, 1985]).

Extensive experimental information obtained in the 1980s and 1990s made it possible to calculate the modal mineral proportions using the mass balance technique. For example, Yang *et al.* [1996] systematized experimental data on tholeiitic systems at atmospheric pressure and compared them with simulations by the MELTS and COMAGMAT-3.0 programs and with some empirical models. The COMAGMAT program was found to reproduce most accurately the results of melting experiments, if the modal amounts of *Ol*, *Pl*, and *Aug* were recalculated into the crystallization proportions of these minerals. This issue is considered in much detail in [Ariskin and Barmina, 2000].

Table 13 summarizes data on the average crystallization proportions for different mineral assemblages displayed in Figs. 34 and 35. These data led us to the following two conclusions. First, the modeled crystallization sequences of *Ol*, *Pl*, and *Aug* fall within the range of experimentally established values, which provides further arguments for the plausibility of the COMAGMAT model. Second, these values for the same cotectics slightly vary, and it is difficult to differentiate between the effects of melt composition and the instability of the mathematical solutions [Ariskin and Barmina, 2000]. In the course of practical calculations, we learned that the accuracy of the convergence of the iteration loops recommended in the COMAGMAT model (~1°C) guarantees the stability of the integral simulation result but sometimes cannot ensure stable solutions over small crystallization intervals. Because of this, during the initial stages of calculations with the COMAGMAT program, it is recommended to set the temperature accuracy at approximately 0.25–0.5°C (with a corresponding change in the accuracy of the calculated compositions).

Evolution of melt composition. The realistic character of the crystallization proportions of minerals provide promise that the temperature dependence of the composition of the residual melt can be calculated fairly precisely during the accurate simulation of the crystallization sequence of minerals. This finds support in the comparison of model and experimental compositional trajectories of melts in Fig. 36. For the purpose of testing, we selected the results of experiments with two samples of tholeiitic basalt (Figs. 34, *2*, *3*). For both of them, the calculation results reproduced the compositions of the experimental glasses well, and all bends on the evolutionary trajectories could be explained by certain changes in the modal composition of the crystallizing assemblages and the chemical compositions of the minerals. The calculation of such temperature–composition dependences for the liquid phase forms the basis for the method of geochemical thermometry, which will be considered in Chapter 3.

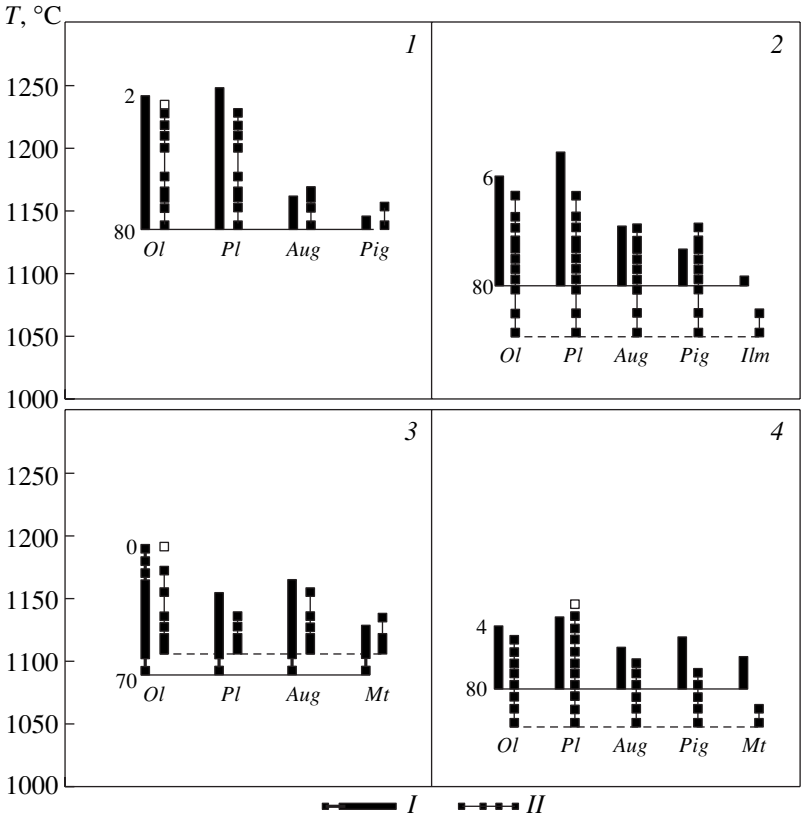

Fig. 35. Experimental and calculated crystallization temperatures of minerals during the equilibrium solidification of high-Al and subalkaline basalts. (*I*) Simulations by the COMAGMAT-3.5 program for QFM conditions; (*II*) experimental results. (*1–4*) Correspond to the numbers of compositions in Table 12: (*1*) [Grove *et al.*, 1982], (*2*) [Grove and Juster, 1989], (*3*) [Kennedy *et al.*, 1990], (*4*) [Thy and Lofgren, 1994].

Another representation of the evolutionary trajectories is variation diagrams. Figure 37 demonstrates the same results of calculations and experiments, but the compositions of the liquid phase are shown as functions of the MgO content in the melt. The structure of the model trends did not principally change (see Fig. 36, MgO vs. *T* plots). These data indicate that the COMAGMAT program can also be used for solving traditional petrological problems, including estimating the conditions under which petrochemical trends could have developed in the course of crystallization processes (see Chapter 4).

2.3.3. Phase equilibria under elevated pressures

The comparative analysis of experimental data and calculation results indicates that the COMAGMAT-3.5 model is able to realistically predict phase equilibria at atmospheric pressure for various combinations of rock-forming minerals. It is more problematic to simulate high-pressure crystallization. As an illustrative example, consider a model *P–T* diagram for the phase relation in magnesian tholeiite (Fig. 38). For these simulations, we selected a starting composition representing MORB from the Mid-Atlantic Ridge with ~10 wt % MgO. Previously this magnesian tholeiite was utilized in a series of experiments at pressures from 1 atm to 15 kbar [Bender *et al.*, 1978], which served as the basis for calibrating the high-pressure version of the COMAGMAT program (Fig. 30).

Simulation conditions. The equilibrium liquid lines of descent were calculated by the *Simulating Equilibrium Crystallization* routine in the mode of pressure sequentially increased in a series of isobaric calculations (the *Increasing Pressure* routine). The redox conditions were identical to those in the experiments (WM buffer), and the crystallization increment $\Delta\varphi$ was 1 mol %. The calculations were terminated as soon as the degree of melt crystallization attained 60%. The polybaric calculations were carried out with a pressure increment of $\Delta P = 2$ kbar within the pressure range of 1 atm to 10 kbar, with the calculation grid narrowed to 0.5 kbar at pressures above 10 kbar in order to more precisely identify the anticipated change in the crystallization sequence of *Ol* and *Aug* on the liquidus. This technique allowed us to construct a *P–T* diagram that realistically reproduced the general changes in the phase assemblages with varying pressure.

Uncertainties of polybaric models. First of all, note the differences between the experimental and cal-

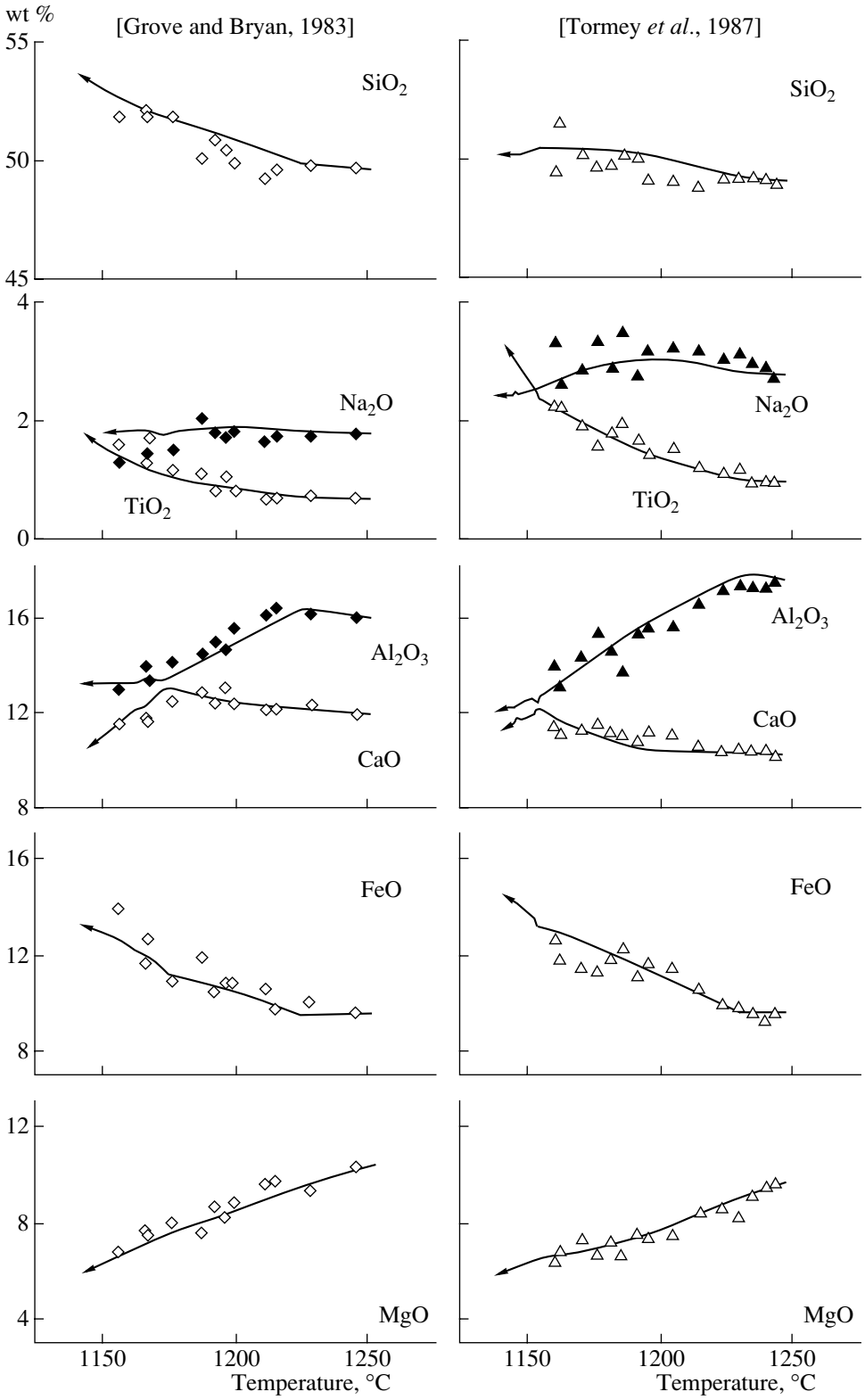

Fig. 36. Experimental and modeled evolution of the compositions of the residual melts during the equilibrium crystallization of tholeiitic basalts depending on temperature. Symbols show experimental data, lines correspond to calculations by the COMAGMAT-3.5 program; see Table 11 for starting compositions; see Fig. 34 for the crystallization sequence.

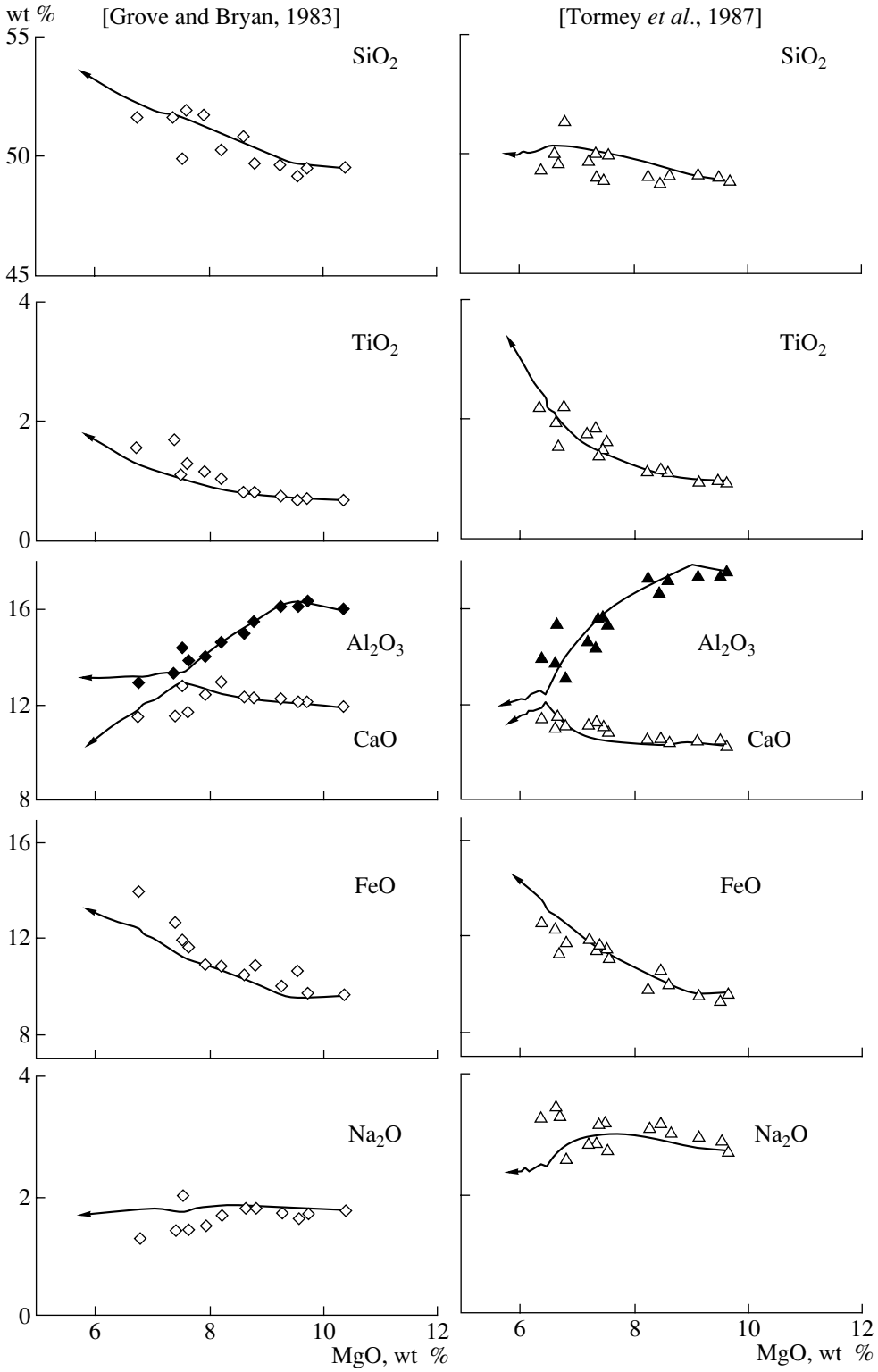

Fig. 37. Experimental and modeled evolution of compositions of the residual melts during the equilibrium crystallization of tholeiitic basalts as a function of the MgO content in the melt. See Fig. 36 for symbol explanations.

culated crystallization temperatures of *Aug* at P = 1 atm. These differences are approximately 30°C (Fig. 38) and notably exceed the errors of the COMAGMAT model for tholeiites (Fig. 34). We believe that this suggests that the 1-atm crystallization of clinopyroxene in the experiments [Bender *et al.*, 1978] was underestimated, perhaps due to the insufficient duration of the experiments. With these considerations, the model diagram in Fig. 38 seems to be quite realistic, at least for the pressure range from 1 atm to 7–8 kbar, for which the crystallization sequence *Ol* ⟶ *Pl* ⟶ *Aug* is predicted correctly. This is also confirmed by the calculation results of the crystallization of another tholeiitic basalt. These calculations were carried out by the COMAGMAT program for a pressure of 4 kbar [Yang *et al.*, 1996]. This agreement is important in the context of the application of the model for high-pressure phase equilibria responsible for the barometry of magmatic melts represented by MORB glasses (see Section 4.2). Under pressures higher than 10–12 kbar, the shift of model phase fields relative to experimental data can be as significant as 3–4 kbar (Fig. 38). This fact should be taken into account in interpreting the results of high-pressure simulations, for example those pertaining to the decompression fractionation of high-Mg island-arc magmas (see Section 4.3).

The main problems encountered in the application of the high-pressure version of the COMAGMAT program are related to the estimation of orthopyroxene stability. At the current state of our model, the appearance of this mineral and its peritectic relations with olivine cannot be predicted very reliably even at 1 atm pressure. In high-pressure simulations conducted with magnesian basalts, these uncertainties are increased by discrepancies between the estimates of the *Opx* stability field at 10–12 kbar [Bender *et al.*, 1978; Green *et al.*, 1979; Fujii and Bougault, 1983; Draper and Johnson, 1992]. Because of this, in conducting high-pressure simulations for natural rocks we will limit ourselves to the consideration of systems in which *Opx* fractionation does not play any significant role.

Attempts to recalibrate the COMAGMAT program and process the results of high-pressure experiments led us to conclude that the quality of experimental data obtained under high pressures is notably lower than that of 1-atm experiments. This pertains to the attainment of equilibrium between the experimental products, the accuracy of the pressure and equilibrium temperature estimates, and the uncertainty of the f_{O_2} values. These data seem to be insufficient for developing polybaric models with accuracies better than 20–30°C. Other designers of models for phase equilibria also expressed certain skepticism about this possibility [Ghiorso and Sack, 1995; Ghiorso, 1997].

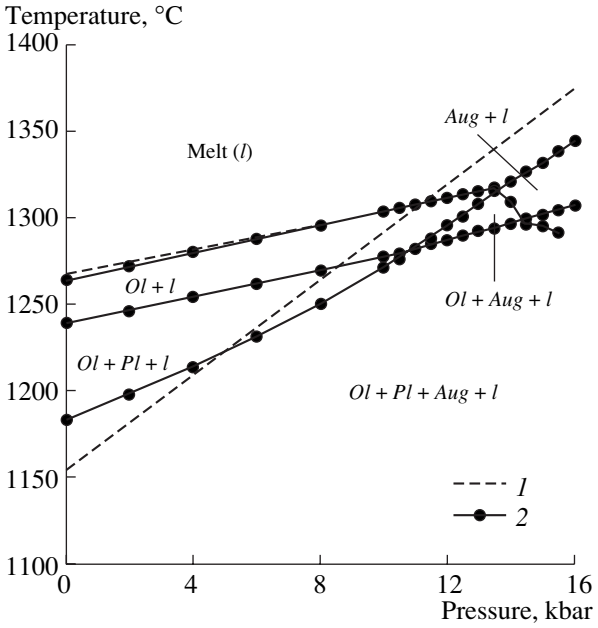

Fig. 38. *P–T* diagram for phase relations in magnesian tholeiite. (*1*) Experiment (see Fig. 30); (*2*) calculations by the high-pressure version of the COMAGMAT-3.5 model.

2.3.4. Modeling crystallization in hydrous systems

In modeling phase equilibria in hydrous systems, we consider water to be an analogue of an incompatible component completely dissolved in the melt. Simulations in hydrous systems are conducted in such a manner that H_2O acts as a fictive component whose concentration is not incorporated into the calculations of the equilibrium constants and does not affect the activities of mineral-forming components. This approach implies that water monotonously enriches the liquid in the process of crystallization, with silicate constituent of this liquid evolving according to dry-system relationships. Water enrichment in the melt is supposed to continue up to a critical concentration corresponding to the solubility limit under a given pressure. Thus, the effect of H_2O on phase equilibria is accounted for indirectly, through changes in the relative crystallization temperatures of minerals [see Eq. (75) and Fig. 32].

Algorithm and simulation results. The water content in the starting melt is specified by the main interface of the COMAGMAT model. Hydrous system crystallization is simulated starting with the calculation of the temperatures predicted for equilibrium between minerals and the "dry" melt, and these values are then corrected (decreased) proportionally to the coefficients listed in Table 9 and the model H_2O concentration [Eq. (75)]. In these simulations, the calculated water concentration in the liquid phase after each crystallization step is compared with the limiting solubility, evaluated by Eq. (77). If the model H_2O concentration is higher than the H_2O solubility, the calculations can be terminated or continued under the assumption that the

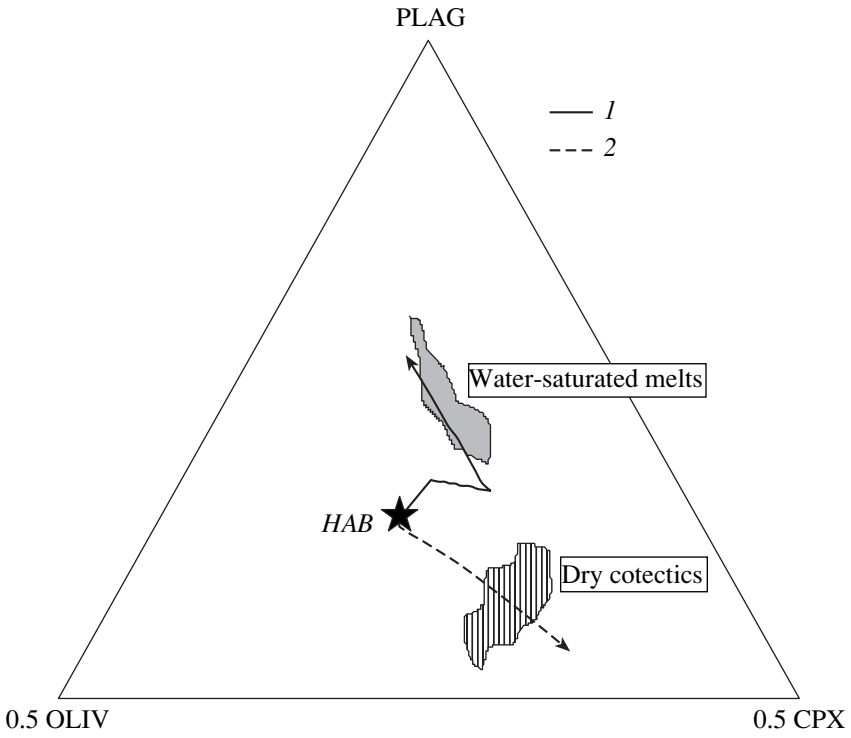

Fig. 39. Compositions of the experimental and modeled cotectic melts for anhydrous and water–saturated conditions. (*1*, *2*) COMAGMAT-3.5 simulations at P = 2 kbar: (*1*) 2 wt % H_2O in the melt, (*2*) anhydrous system; HAB is the initial high-Al basalt (sample 79-35g) [Sisson and Grove, 1993]). The experimental melts correspond to $Ol + Pl + Aug \pm Mt \pm Pig + l$ assemblages. The projection method is after [Tormey *et al.*, 1987] modified by [Grove, 1993].

excess water (3–5% H_2O at each step) is progressively separated from the melt. The latter situation accounts for the degassing of a water-saturated magmatic melt and the evolution of the phase composition of the system under the pressure of the vapor phase. This simplified approach to the calculation of melt–mineral equilibria in the presence of water should be regarded as a tentative approximation, which, however, satisfactorily reproduces the known systematic shifts in the phase boundaries in hydrous systems [Al'meev and Ariskin, 1996].

Figure 39 shows the computer simulation results on phase equilibria during the crystallization of a high-Al basaltic (HAB) melt at dry and hydrous conditions. The starting composition corresponded to sample 79-35g, which was used in a series of water-saturated experiments at 2 kbar [Sisson and Grove, 1993]. The conditions of melt saturation with H_2O were simulated as follows: specified water amounts (1.0, 1.5, 2.0 wt % or others) were added to the starting HAB composition, and the trajectory of equilibrium crystallization was calculated for each system with an increment of $\Delta\varphi$ = 1% (P = 2 kbar, QFM buffer). As a result, the parameters of the equilibrium between the melt, minerals, and vapor phase were determined for compositions with different initial water contents. These parameters included the degree of melt crystallization φ_{cr}, equilibrium temperature T_j, mineral proportions on the liquidus, and the liquid composition.

It was determined that the simulated liquid lines of descent realistically reproduce the experimental temperatures (1020–1070°C) and H_2O concentrations (5.5–6.0 wt %) in water-saturated melts at starting H_2O concentrations of 2–2.5 wt % [Al'meev and Ariskin, 1996]. The overall decrease in the liquidus temperature is coupled with a remarkable expansion of the fields of mafic minerals and the contraction of the crystallization field of plagioclase as compared to those in dry systems. Thus, resultant evolutionary trajectories of the composition of the high-Al basaltic melt are consistent with the concept that plagioclase crystallization in the presence of water is suppressed and results in an Al_2O_3 enrichment in the residual liquid.

CHAPTER 3. GEOCHEMICAL THERMOMETRY FOR INTRUSIVE BASIC ROCKS

Difficulties in the genetic interpretation of magmas as heterogeneous systems are caused by the partial disequilibrium of these melt–mineral assemblages, a phenomenon manifested in that each of the minerals entrained by the melt is characterized by a certain compositional range. These solid phases can be phenocrysts captured by the magma during its motions, or the crystallization products of a more primitive parental melt,

which bear "record" of the previous evolution of the common source. Hence, the typical state of a magmatic suspension is visualized as a mixture of melt and solids, whose average compositions do not necessarily correspond to the temperature and composition of the liquid but are more probably shifted toward more refractory (high-temperature) components. The degree of these deviations from equilibrium can vary and should be examined separately in every instance. Nevertheless, progress in igneous petrology in the 20th century was stimulated by the idea that both volcanic and intrusive assemblages are "subequilibrial," and, thus, thermobarometric techniques can be used to evaluate the conditions of their origin.

This assumption is most plausible for intrusive magmas, if the crystals suspended in them had enough time to reach equilibrium with the melt before the magmatic material arrived at the magma chamber. This situation offers the possibility of accurately estimating the parameters of the parental magmas, including the composition of the initial melt and intratelluric phases, the original modal proportions of these crystals and liquid, and, eventually, the overall crystallinity of the initial magma [Ariskin and Barmina, 2000]. There are experimental and calculation techniques for estimating the composition of the liquid part of natural magmas.

In the experimental approach, rocks are partially melted and held at temperatures above the solidus, and, then, the composition of glasses filling in the space between crystals (presumably primary) is analyzed. A study of this type was described, for example, in [McBirney and Nakamura, 1973; McBirney and Naslund, 1990], who presented a series of experiments with gabbroids from the main zones of the Layered Series in the Skaergaard intrusion. The results of similar experiments with contact gabbros from the Marginal Border Series are given in [Hoover, 1989b]. The main disadvantages of this method are related to the fact that the researchers did not know beforehand the equilibrium temperature of the primary crystals and liquid and, hence, in interpreting the experimental results, could mistakenly use a compositional range notably deviating from the initial characteristics. The probability of such mistakes is particularly high when multiphase assemblages are examined that contain less than 50% intercumulus melt.

In the mid-1980s, we proposed the *method of geochemical thermometry* of intrusive basites, which combines and expands the application possibilities of geothermometers based on the laws of equilibrium partition of components between minerals and melt [Frenkel *et al.*, 1988a, 1988b]. The method is underlain by equilibrium crystallization models of the COMAGMAT series and involves simulations conducted for intrusive rocks that were produced during close differentiation stages of a parental magma but have contrastingly different compositions. Of course, the method of geochemical thermometry cannot replace experimental research and has its own applicability limitations. However, in certain situations, it allows the researcher to eliminate uncertainties in the estimated magma temperature, which, in turn, makes it possible to significantly constrain the range of the possible compositions of the intercumulus liquid [Ariskin and Barmina, 2000].

Our earlier publications presented the results of such reconstruction, including the temperature–compositional and phase characteristics of magmas parental to differentiated sills in the Siberian Platform and eastern Kamchatka [Frenkel *et al.*, 1988b; Barmina *et al.*, 1989a, 1989b], as well as several layered intrusions and large plutons [Chalokwu *et al.*, 1993; Krivolutskaya *et al.*, 2001; Ariskin, 1999, 2002; Barmina and Ariskin, 2002; Ariskin *et al.*, 2003]. Below, we will discuss the methodical basis of such thermometric calculations and summarize the main results of genetic reconstructions for basic and ultrabasic rocks.

3.1. Method of Geochemical Thermometry

3.1.1. Parameters of formation of igneous rocks

The process producing magmatic rocks can be subdivided into a number of stages, whose initial states include mechanical mixtures of crystals of different composition j and melt l

$$\sum_{j=1}^{m} F_j^0 + F_l^0 = 1, \tag{81}$$

where F_j^0 and F_l^0 are the initial proportions of mineral grains and silicate liquid. Obviously, a system of this type can be exemplified by diverse cumulates, in which the development of a network of cumulus grains (in intrusive basites) or fast cooling (in cumulative basalts) prevent the relative motions of solid phases and liquid. Let us refer to this initial state as the *moment of rock formation* in the geochemical sense, meaning that the bulk chemical composition of the rock is produced during this stage and, if the system is closed, does not change during further cooling and recrystallization.

The bulk composition of such a system can be calculated from the relative proportions of solid phases in the melt and the melt itself, the composition of the liquid phase $C_i^{l(0)}$, and the weighted mean concentration of a major or trace element in phenocrysts or cumulative grains of a given mineral species $\overline{C}_i^{j(0)}$

$$C_i^{rock} = F_l^0 C_i^{l(0)} + \sum_{j=1}^{m} F_j^0 \overline{C}_i^{j(0)}. \tag{82}$$

The parameters of this equation provide the complete description of the initial state of the magmatic mixture that later crystallizes into a certain rock. This makes it possible to determine the values of F_j^0 and F_l^0

as the *original modal proportions* and $\bar{C}_i^{j(0)}$ and $C_i^{l(0)}$ as the *original compositions* of the minerals and melt. The initial melt is characterized by a certain liquidus temperature, which can be naturally determined as the *temperature of rock formation.* This definition pertains only to the initial conditions of the existence of the melt–mineral assemblage and is the temperature of the transporting magma for volcanic rocks and the temperature of the intercumulus melt for intrusive varieties.

The aforementioned characteristics of the rock-forming process should be distinguished from the modal proportions and mineral compositions that can be directly observed by petrologists, because the cooling of the magmatic mixture and the continuing crystallization of the interstitial liquid change not only the composition of the melt but also the compositions of the minerals [Barnes, 1986], as well as, perhaps, the morphology of the aggregates shaping the texture of the crystallizing rock. These comments also pertain to the temperature estimates, which are calculated under the assumption of "frozen mineral equilibria" that characterize not initial but later low-temperature stages of system solidification. Hence, the "memory" of the initial state is "recorded" in the bulk chemical composition of a magmatic rock, so that the problem of reconstructing the conditions under which a given rock was produced can be formulated as the utilization of this information with the purpose of evaluating the original modal proportions and initial compositions.

Calculations based on the mass balance method. To evaluate the composition of a magmatic liquid, Eq. (82) can be rearranged to the form

$$C_i^{l(0)} = \left(C_i^{rock} - \sum_{j=1}^{m} F_j^0 \bar{C}_i^{j(0)} \right) / F_l^0, \qquad (83)$$

whose solving requires independent information on the original modal proportions and the compositions of the minerals. Data on the mineral compositions can be provided by microprobe analyses, but even if, supposedly, they represent the initial but not modified characteristics of the primary phases, the original modal proportions remain uncertain. In principle, they can be calculated from the results of modal analysis, but this approach always involves subjective interpretations of rock textures. While it is reasonable to assume that the initial mineral assemblage of volcanic rocks is that of phenocrysts, it is much more difficult to make an analogous choice for subvolcanic and intrusive rocks. This situation can sometimes be resolved with the aid of linear programming techniques, which are based on relation (82) for an overdetermined set of major or trace elements [Wright and Doherty, 1970]. However, this leaves uncertain how to evaluate the initial mineral compositions based on microprobe data, if estimates of this kind may be incorrect for olivine and pyroxenes, which are extensively re-equilibrated during rock cooling (see below).

A useful assumption, which makes it possible not to utilize microprobe analyses but instead proceeds from hypothetical relations between the initial compositions of the melt and minerals, is as follows:

$$\bar{C}_i^{j(0)} = D_i^j C_i^{l(0)}, \qquad (84)$$

where D_i^j is the distribution coefficient of element i between mineral j and the silicate liquid. Using experimentally determined D_i^j values, relation (84) can be substituted into Eq. (82) for various elements, and these systems of equations can be then solved for the melt composition and modal proportions. This approach is widespread in extraterrestrial petrology, for example, in the context of interpreting the REE patterns of cumulates representing various types of basaltic achondrites (see, for example [Treiman and Sutton, 1992; Wadhwa *et al.*, 1994]).

In spite of the attractiveness and simplicity of this approach (now we put aside the problem of the justification of the equilibrium approximation), it still has two disadvantages. First, the mass-balance equation ignores the dependence of D_i^j on the composition and temperature. There is another related problem: the search for the original modal proportions cannot be accomplished with the utilization of complete information on the concentrations of major and trace elements. The proposed method of geochemical thermometry involves a complex solution of these problems.

3.1.2. Main postulates and the basis of the method

The main assumption is that, at a certain initial moment of time, the compositions of the minerals and melt were interrelated through thermodynamic equilibrium constraints (26), which included the temperature of rock formation (see the definition above) as one of the parameters. This temperature corresponded to the existence conditions of the mineral–melt assemblage and affected, as a factor of thermodynamic equilibrium, the partitioning of major and trace elements in the liquid and solid phases.

The other principal assumption is that the diversity of rocks composing a magmatic body may include samples whose compositional variations are exclusively due to the differences in the original modal proportions F_j^0 and F_l^0 [Frenkel *et al.*, 1988a, 1988b]. Such varieties make up rock groups produced at the same temperature from a common melt and minerals of the same composition. There are many physical reasons for such diversity: the random character of filling the rock space with cumulus minerals, the uneven distributions of crystalline phases suspended in the magma, the postcumulus sorting of mineral grains, flow differentiation, and others.

The constancy of the composition of the transporting or entrapped magmatic liquid implies two means of

the genetic and geological interpretations of these rocks. First, they could result from a local (on the scale of several centimeters or meters, perhaps, tens of meters for large intrusions) heterogeneity of the body, which can be manifested, as the limiting case, in the form of magmatic layering. Second, very limited (if any) magma fractionation, which suggests similar conditions under which the rocks were produced on the scale of the whole magmatic body or its marginal portions. As will be clear from further considerations, the numerical simulation of phase equilibria permits one not only to identify these groups of genetically related rocks but also to give their complete phase interpretation, including the melt composition and temperature at the moment of rock formation.

Implementation. Following the assumption presented above, it can be stated that the simulation of the equilibrium crystallization of melts corresponding to rocks of chemically contrasting compositions (but composed of the same equilibrium mineral assemblages) yields liquid lines of descent that should intersect in composition–temperature space. The temperature at the intersection point should be interpreted as the common formation temperature for all of the rocks, whereas the average liquid composition calculated at this temperature should be regarded as the parental melt composition. Correspondingly, the compositions of minerals calculated for the intersection point should represent the original contents of end members and trace elements, and the proportions of the minerals should correspond to the original modal proportions of primarily accumulated crystals.

Thus, the proposed method of geochemical thermometry involves the numerical simulation of liquid lines of descent for the melts of selected rocks and the subsequent search for the intersections of the evolutionary trajectories in composition–temperature space. If the number of the calculated liquid lines of descent (rock samples) is relatively small, the intersection region can be identified by the visual analysis of a series of *T–X* diagrams for major and trace elements. Most of the examples presented below will make use of this technique. If the selections of rock compositions are large, it is necessary to employ specialized algorithms for the search for the most compact and numerous clusters of compositions, which could represent series of isothermal sections in the five- to ten-dimensional space of the contents of major components.

3.1.3. Analysis of intersections of liquid lines of descent

The informativeness of the intersections depends on the dimension of the model crystallization trajectories. The COMAGMAT program presents them in the form of evolutionary trajectories in $(K + 1)$-dimensional composition–temperature space, where K is the number of melt components. In practice, it is necessary to keep in mind that liquid lines of petrogenetic importance are

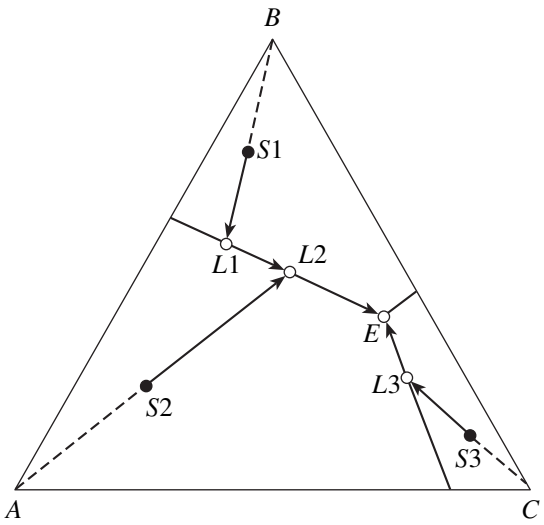

Fig. 40. Intersections of crystallization trajectories in the *A–B–C* eutectic system with phases of constant composition (analogue of the *Fo–An–Di* system). *S*1, *S*2, and *S*3 are the assumed initial (bulk "rock") compositions, *L*1, *L*2, and *L*3 are the compositions of the partial melts of the original mixtures when they appear on the cotectics.

located in a space of lesser dimension ω, which is equal to the variance of the corresponding multiphase equilibrium [Frenkel *et al.*, 1988a]. The value of ω for simple systems is determined by the Gibbs phase rule, according to which, at a constant pressure,

$$\omega = K_\phi - \Phi + 1, \qquad (85)$$

where ω is the number of degrees of freedom, Φ is the number of phases in the equilibrium assemblage, and $K_\Phi \le K$ is the number of phase-forming components.

The importance of this factor becomes clear from the analysis of crystallization–melting trajectories in a simple three-component system with only one eutectic point, such as *Fo–An –Di*. Figure 40 demonstrates that the crystallization trajectories of any compositions converge at eutectic point E ($\Phi = 4$, $\omega = 0$), and the liquid lines of descent of these compositions always form a compact cluster in composition–temperature space corresponding to the parameters of the eutectic mixture. Such an intersection of the evolutionary lines at an invariant point does not provide information on the initial compositions. It is less probable that the crystallization trajectories accidentally coincide with the $A + B + l$, $A + C + l$, or $B + C + l$ cotectics ($\Phi = 3$, $\omega = 1$). However, even in this case, the intersection is not informative, because it is caused by a thermodynamic factor: the one-dimensionality of the space of the cotectic lines. The situation becomes principally different when a fourth component D is added to the system. Even if this component is not phase-forming, cotectic lines become surfaces, and the point of the four-phase eutectic equilibrium is transformed into a line, which con-

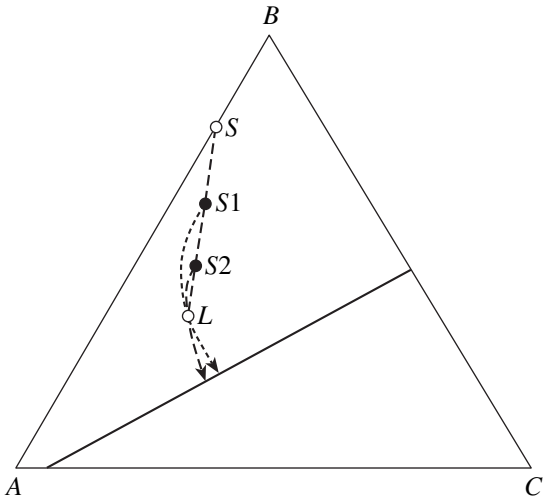

Fig. 41. Intersections of crystallization trajectories in the *A–B–C* eutectic systems with phases of variable (*A–B*) and constant (*C*) composition (analogue of the *Ab–An–Di* system). *S* is the composition of the solid solution in the liquidus assemblage, *S*1 and *S*2 are the assumed bulk "rock" compositions on the same tie-line *S–L*, *L* is the composition of the melt common for "rocks" *S*1 and *S*2.

nects the temperature and the concentration of component *D* in the melt.

This means that an occasional intersection of the trajectories in some cotectic surface (for instance, $A + B + l$) becomes hardly probable and can occur only if two or more of the initial compositions were mixtures of arbitrary amounts of crystals *A* and *B* and a melt of the same composition (x_A, x_B, x_C, and x_D). This leads to the conclusion that the genetic meaning of the convergence of liquid lines of descent is the condition of at least binary equilibrium, when the number of components of the liquid is greater than the number of the phases in the melt–mineral assemblage at the intersection point $K \geq \Phi + 1$.

The simplest binary equilibrium in systems with solid solutions is demonstrated in Fig. 41 and offers an example of the intersection of evolutionary trajectories having a genetic sense. This diagram illustrates the following statement: at the point of a binary liquidus equilibrium *L*, trajectories of equilibrium (closed) crystallization intersect only for melts whose compositions can be obtained by combining arbitrary proportions of melt *L* and mineral *S* in equilibrium with it. This statement can be proved by *reductio ad absurdum*: if a trajectory could not intersect at point *L*, this would mean that the mixture contained a mineral not in equilibrium with melt *L*. This statement could be obviously extended on multicomponent systems with more than one solid-solution mineral [Frenkel *et al.*, 1988a].

It follows from this analysis that the occasional occurrence of more than Φ compositions in the space of one tie-line assemblage is impossible, and this makes intersections at $\omega \geq 2$ (or $K \geq \Phi + 1$) genetically informative. The fulfillment of these conditions is obligatory in conducting magmatic-rock thermometry. Considering that the overall number of phases in liquidus assemblages commonly varies from two ($Ol + l$, $Pl + l$) to seven ($Ol + Pl + Aug + Pig + Mt + Ilm + l$), the calculation results should involve the analysis of the concentrations of three to eight components in the melt, and from two to seven evolutionary trajectories should be considered. It also should be noted that intersections of liquid lines of descent in systems with solid solutions occur in the form of a characteristic two-fan structure: bundles of lines that can be easily identified visually (see below).

Calculation errors. It should be mentioned that thermodynamic conclusions are valid only as an ideal approximation. In practical calculations, the analytical inaccuracies and uncertainties related to the use of phase equilibria models result in that the intersection point of the calculated liquid lines of descent is determined with some errors in terms of composition and temperature and occurs as an area of thickening of the intersection clusters in a *T–X* diagram (see below). In applying the COMAGMAT program to tholeiitic systems, the accuracies of temperature calculations correspond to the accuracies of the geothermometers utilized (10–15°C, Chapter 2), and the major-component liquid compositions are estimated accurate to 0.5–1 wt % (Figs. 36, 37).

The main problem in the applicability of the thermometric calculations is related to the assumption of the equilibrium character of the primary phase assemblages. These techniques seem to be applied most successfully to the interpretation of intrusive basites, dolerites in differentiated sills, and other holocrystalline rocks that crystallized over relatively long time spans when the magmatic masses cooled. Indirect evidence of the subequilibrium character of the original magmas of these rocks is provided by insignificant variations in the composition of phenocrysts in the inner contact rocks (see, for example, [Hoover, 1989a, 1989b]).

The use of this method for the thermometry of volcanic rocks is more problematic. Microprobe analyses of minerals from basalts often reveal compositions of the phenocrysts that are notably scattered, and some of them can be interpreted as xenocrysts. This suggests that the original liquidus assemblage was not completely equilibrated but does not mean at all that calculations by the geochemical thermometry method become senseless. In fact, mass-balance constraints (81) and (82) are valid for any igneous rocks, and the researcher analyzing liquid lines of descent should simply make sure that the difference between the calculated equilibrium compositions of minerals and the weighted mean compositions of the phenocrysts and xenocrysts $\Delta C_i^j = C_i^j(\text{calculated}) - \overline{C}_i^j(\text{observed})$ is insignificant (no more than a few mol %). In this sense, the method of geochemical thermometry is advantageous over other traditional approaches that make use

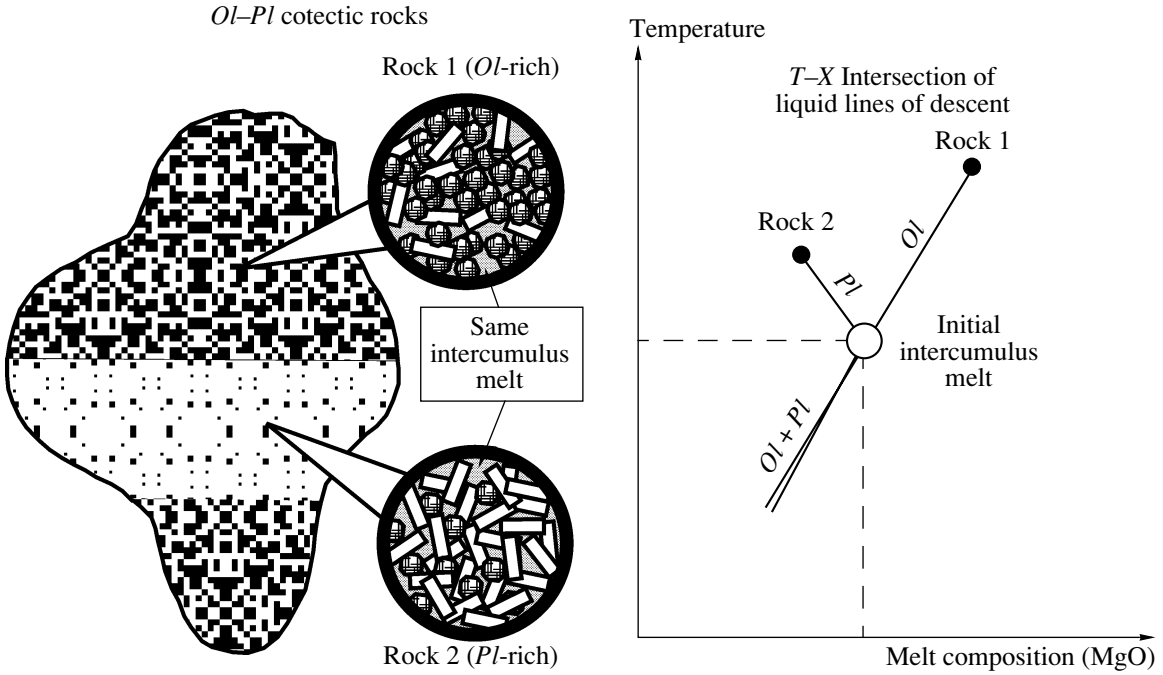

Fig. 42. Scheme of geochemical thermometry for two genetically related rocks that have contrastingly different chemical and modal compositions.

of experimental data and presume the ideally equilibrium character of the mineral assemblages.

3.2. Geochemical Thermometry for Marginal Rock Facies and the Most Primitive Cumulates

The main outcome of calculations by the method of geochemical thermometry is the evaluation of the temperatures and compositions of melts representing the original suspensions (cumulates) from which the intrusive rocks crystallized (see scheme in Fig. 42). This problem has more than one variant of solution depending on which stage of differentiation in the chamber is examined [Ariskin and Barmina, 2000]. The first estimates for the initial stages of solidification of intrusive bodies were obtained for plagioclase-enriched diabases from the Kamenistyi sill in eastern Kamchatka [Barmina *et al.*, 1989a]. This approach was further developed in application to the genetic problems of the Partridge River [Chalokwu *et al.*, 1993], Skaergaard [Ariskin, 1999], and Talnakh [Krivolutskaya *et al.*, 2001] intrusions, and, more recently to the Kiglapait [Barmina and Ariskin, 2002] and Ioko-Dovyren [Ariskin *et al.*, 2003] plutons.

This approach makes use of the bulk chemical compositions of rocks that were produced during the earliest crystallization stages of the intrusive magma. They are usually restricted to the contact zones of marginal series or the lower portions of layered intrusions. The least evolved character of these rocks is manifested in the chemistry of their cumulus minerals, which are maximally enriched in refractory components. Another characteristic feature of these rocks is that they contain certain amounts of liquid that was captured at the crystallization front or entrapped in the interstices of cumulus minerals or primocrysts. It is natural to assume that the composition of this trapped liquid should be close to the composition of the magmatic melt during its emplacement into the chamber. This implies that the system is considered to be completely closed after crystal settling, and there were no phenomena like the migration or re-equilibration of the pore liquid. Strictly speaking, this should be proved for each rock sample. This constraint is, however, not very important for marginal rocks, which commonly crystallize at rapid cooling and are made up of orthocumulates.

Thus, there are good grounds to believe that the bulk composition of marginal rocks "records" adequately the proportions and chemistry not only of the high-temperature cumulus minerals but also of the liquid constituent of the parental magma [Ariskin and Barmina, 2000]. In this situation, the problem of the search for the chemical characteristics of this parent is reduced to the selection of samples able to represent the earliest crystallization stages of the intrusion and the calculation of the corresponding trajectories of equilibrium crystallization in temperature–composition coordinates. The processing of these data yields the compositions of the initial melt and original intratelluric minerals, with the calculated equilibrium temperature taken as the "magma emplacement temperature."

Another application of the geochemical thermometry to intrusive basites is the estimation of the composi-

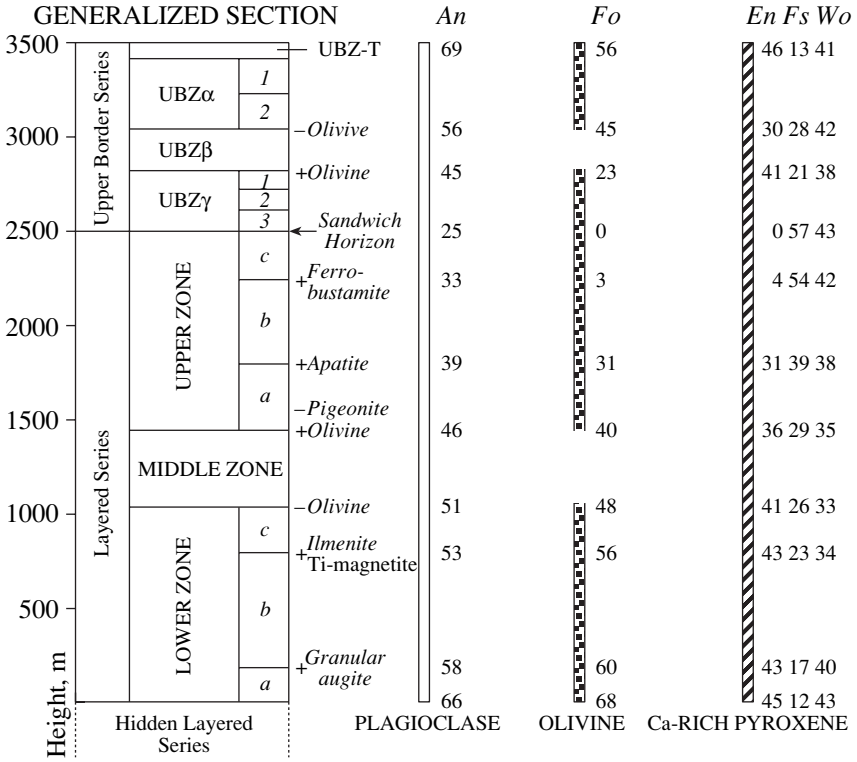

Fig. 43. Main units of the Layered Series and the Upper Border Series [McBirney, 1996]. The LS zones are defined by the appearance or disappearance of primary phases, or, in the case of LZ*b*, by the transition from poikilitic to granular Ca-pyroxene. The Upper Border Series is divided into three subzones (α, β, and γ) equivalent to the LZ, MZ, and UZ. The compositions given for *Ol*, *Pl*, and *Aug* at zone boundaries are approximate and may vary laterally.

tion and temperature of the residual melts generated as the successive derivatives of a parental magma. This approach has certain features in common with mass-balance calculations [Wager, 1960; Wager and Brown, 1967] but differs from them in taking into account the occurrence of a crystalline phase in the residual suspensions and the porosity of the cumulates. The method of thermometry of magmatic derivatives was first utilized for the "inverse" simulation of the inner structures of dolerite sills in the Siberian Platform [Frenkel *et al.*, 1988a, 1988b; Barmina *et al.*, 1989a]. Later, this approach was used to reconstruct the conditions under which the main zones of the Layered Series in the Skaergaard intrusion were produced [Ariskin, 2002, 2003]. These petrological materials will be discussed beginning with the most obvious results of geochemical thermometry for contact rocks.

3.2.1. Skaergaard intrusion, East Greenland

The Skaergaard intrusion in the eastern shore of Greenland is a layered massif of basic rocks approximately 6 × 11 km in map view. The massif has the morphology of a cube-shaped funnel inclined southward and having a thickness of approximately 3.5 km at the modern erosion level. The part of the intrusion inaccessible to direct observation is referred to as the *Hidden Layered Series*, whose volume was estimated [McBirney, 1989] at no more than 10–15% of the massif. The main subdivisions of the Skaergaard intrusion are the *Layered Series* (LS) and the overlying *Upper Border Series* (UBS), whose relative proportion is approximately 2 : 1 [Wager and Deer, 1939]. An important mappable structural unit is the *Marginal Border Series* (MBS), which encircles the intrusion along its contacts with the country rocks.

The Layered Series is a rock succession that developed from the magma chamber bottom upward. Structurally and lithologically, it differs from MBS and UBS, which were produced at magma crystallization starting from the walls and roof of the intrusion. The upper boundary of the Layered Series is drawn along its contact with the Upper Border Series, along the unit know as the *Sandwich Horizon* (SH) [Wager and Deer, 1939]. The latter can usually be easily mapped in field because of the contrast between the mesocratic ferrodiorites of LS and feldspar-richer rocks of UBS [McBirney, 1989]. Based on the nomenclature proposed in [Wager and Brown, 1967], the Layered Series was subdivided into zones with different cumulus mineral assemblages (they are shown in Fig. 43 after [McBirney, 1996]).

The rocks of the Marginal Border Series account for no more than 5% of the exposed portion of the intrusion, and the crystallization sequence of their minerals

Table 14. Composition of cumulus rocks from the Marginal Border Series and the chilled gabbro EG4507 that were used to estimate the composition of the Skaergaard original melt

Component	Primitive cumulates of the Marginal Border series [Hoover, 1989b]					Chilled gabbro [Wager and Brown, 1967]
	UT-04, d = 2.5	UT-08, d = 8.5	EC-10, d = 1.0	MEO-10, d = 3.0	KT-47, d = 6.0	EG4507, n.d.
SiO_2	44.65	48.38	46.92	47.45	48.19	48.08
TiO_2	0.69	0.60	0.63	0.40	0.81	1.17
Al_2O_3	4.88	20.91	9.36	18.32	11.37	17.22
FeO	14.16	7.19	12.84	9.49	11.04	9.63
MnO	0.24	0.10	0.10	0.15	0.19	0.16
MgO	23.61	7.06	17.22	9.83	14.53	8.62
CaO	9.15	11.79	11.14	10.40	11.60	11.38
Na_2O	0.81	2.61	1.22	2.36	1.78	2.37
K_2O	0.03	0.17	0.04	0.06	0.13	0.25
P_2O_5	0.00	0.03	0.02	0.00	0.08	0.10
Total	98.22	98.84	99.49	98.46	99.72	98.98
Mg/(Mg + Fe)	0.748	0.636	0.705	0.648	0.701	0.614

Note: The Mg/(Mg + Fe) molar ratio was calculated based on the total FeO content; d is the distance from the contact with the host rocks (m); n.d. means no data.

and the chemistry of these minerals systematically change away from the contact. Directed crystallization produced here a rock series (including various cumulates) whose mineralogy reproduces the succession of rocks in the Layered Series [Hoover, 1989a, 1989b]. In both cases, the determined crystallization sequence was $Ol + Pl \longrightarrow Ol + Pl + Aug \longrightarrow Ol + Pl + Aug + Pig \longrightarrow Pl + Aug + Pig + Ilm \longrightarrow Pl + Aug + Pig + Ilm + Mt$, which is manifested in changes of cumulus minerals. These mineralogical relations are independent of the spatial position of the rocks in the Marginal Border Series, which suggests that these rocks and the rocks of the Layered Series had a common composition of their parental magma.

The least fractionated rocks of the Skaergaard intrusion occur in the Marginal Border Series and can usually be identified according to their fine-grained (quenched) textures, the absence of traces of cumulus (liquidus) clinopyroxene, and the most primitive composition of *Ol* (~$Fo_{75–80}$) and *Pl* (~$An_{65–70}$) phenocrysts. These rocks, which are referred to as *Chilled gabbro* [Wager and Brown, 1967] occur within 1 m from the outer contact and were thought to be one of the main candidates for representing the primary Skaergaard magma [Hoover, 1989b]. As will be demonstrated below, some compositions of the chilled gabbro are indeed close to the composition of the captured original melt, as was calculated by means of geochemical thermometry of the primitive cumulates of the Marginal Border Series.

Results of geochemical thermometry. For the calculations we selected five original compositions representing the primitive cumulates of the Marginal Border Series [Hoover, 1989b] and one sample of chilled gabbro (sample EG4507), whose composition was proposed in [Wager and Brown, 1967] as the original composition of the Skaergaard magma (Table 14). The cumulates were sampled within the representative series of weakly altered rocks at distances no greater than 8.5 m from the outer contact of the intrusion. The fulfillment of this conditions provides grounds to believe that the rocks are the least fractionated crystallization products, for which the original composition of the captured melt still had not been modified significantly. The group comprised the most contrasting compositions, including high-Mg (olivine-rich UT-04, EC-10, and KT-47) and high-Al (plagioclase-rich UT-08 and MEO-10) rocks. This was done deliberately, because the method of geochemical thermometry allows one to obtain clear intersections of evolutionary lines only if the compositions significantly differ [Ariskin and Barmina, 2000]. The composition of sample EG4507 appeared to be intermediate in terms of MgO and Al_2O_3 contents.

Calculation conditions and crystallization sequence. Using the compositions of the rocks as the original one, we calculated (by the COMAGMAT-3.51 program) the liquid lines of descent for the range of 0–80% solidification [Ariskin, 1999]. The calculations were carried out with an increment of $\Delta\varphi_{cr}$ = 1 mol % under a pressure of 1 atm, at dry conditions, and an oxygen fugacity corresponding to the QFM buffer. This ensured a moderate degree of oxidation of the melt and

the presence of *Mt* and *Ilm* among the liquidus phases at the early and middle stages of the process.

The calculated crystallization sequence of minerals is in good agreement with the initial rock compositions and demonstrates a wide field of *Ol* crystallization for the high-Mg samples and early *Pl* crystallization for the high-Al compositions:

UT-04: *Ol* (1443°C) ⟶ *Aug* (1233°C) ⟶ *Pl* (1174°C),

UT-08: *Pl* (1332°C) ⟶ *Ol* (1231°C) ⟶ *Aug* (1164°C),

EC-10: *Ol* (1385°C) ⟶ *Aug* (1199°C) ⟶ *Pl* (1187°C),

MEO-10: *Pl* + *Ol* (1248°C) ⟶ *Aug* (1161°C),

KT-47: *Ol* (1346°C) ⟶ *Pl* (1191°C) ⟶ *Aug* (1189°C),

EG4509: *Pl* (1242°C) ⟶ *Ol* (1225°C) ⟶ *Aug* (1163°C).

Two samples, MEO-10 and EG4507, show subcotectic relationships (*Pl* + *Ol*) within the temperature range of 1225–1248°C. It is important to note that augite was the third crystallizing phase in four samples, and its crystallization temperature was no lower than 1161°C. This estimate gives the lower temperature limit for the original melt that was trapped in the intercumulus of the contact rocks, because petrological data on the Layered Series indicate that high-Ca clinopyroxene started to crystallize after a small amount of the *Ol–Pl* cotectic was produced [McBirney, 1989] (Fig. 43).

Compositional evolution of the model melts. The calculated liquid lines of descent are shown in Fig. 44. In a composition–temperature diagram, they define a characteristic bundle of lines that converge toward temperatures below 1180°C. This fact can be interpreted as confirming that all six rocks in Table 14 were mixtures of some amount of a common parental melt and a crystalline assemblage that included olivine and plagioclase (± minor amounts of *Aug)*. Proceeding from the modeled concentrations of Al_2O_3, FeO, MgO, CaO, and Na_2O and from the accuracy of the geothermometers, it

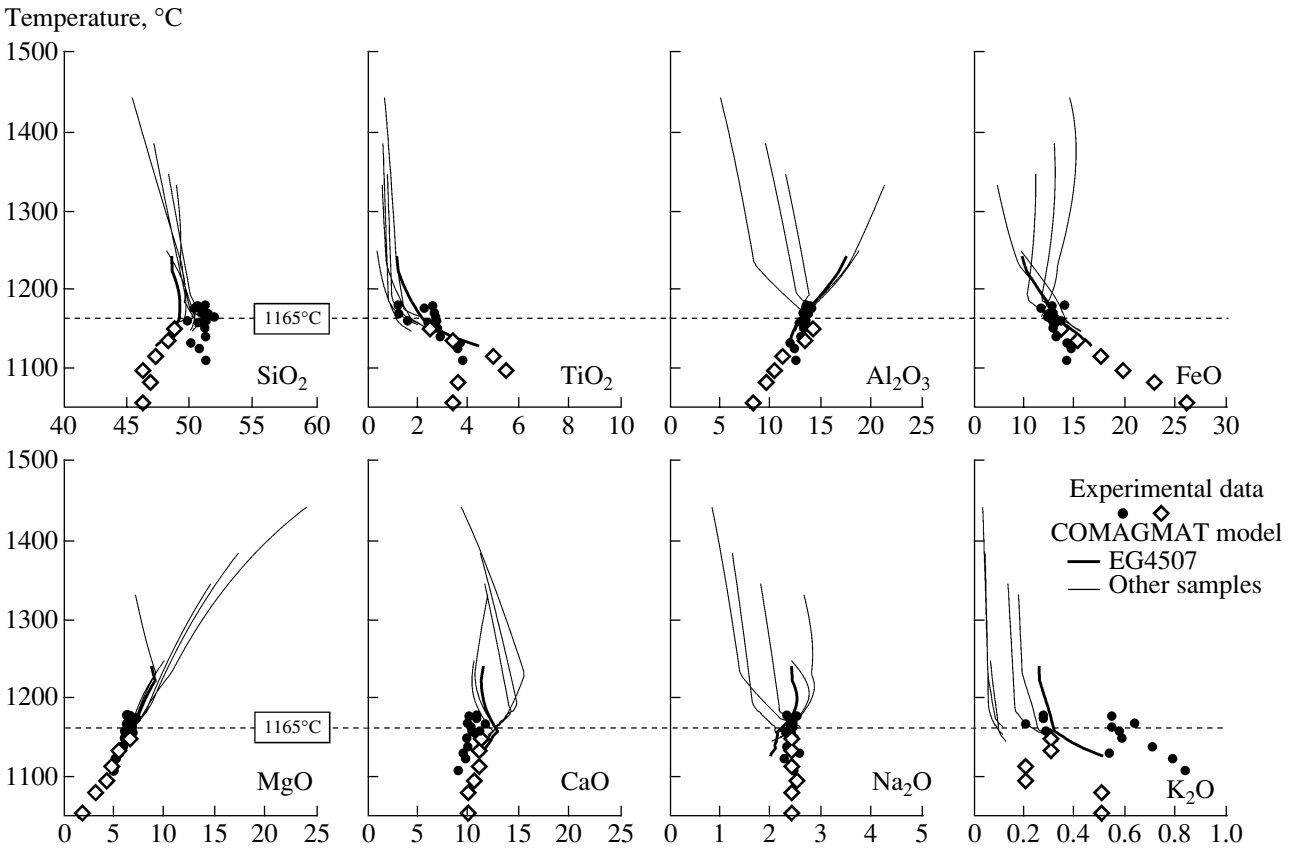

Fig. 44. Example of geochemical thermometry for the Skaergaard MBS rocks. Liquid lines of descent correspond to the equilibrium crystallization trajectories calculated at 1 atm and QFM conditions for six contact gabbros; the temperature of 1165 ± 10°C is assumed to indicate the initial temperature for the trapped liquid [Ariskin, 1999]. Experimental data: circles are residual liquids for the Marginal Border Series pristine rocks [Hoover, 1989b]; diamonds are those obtained for the Lower and Middle Layered Series rocks [McBirney and Nakamura, 1973; McBirney and Naslund, 1990].

can be assumed that the most compact cluster of intersections of these evolutionary lines is restricted to a temperature of 1165 ± 10°C.

This value of the initial crystallization temperature of the Skaergaard rocks was chosen visually with allowance for the aforementioned constraint $T >$ 1161°C. The average composition of the liquid phase calculated for the six model trajectories at a temperature of 1165°C is supposed to represent the model composition of the original magmatic melt and is listed in Table 15 (composition TM). The table also presents the composition of the experimental melt obtained at a temperature of 1160°C by the melting of one of the cumulates of the Marginal Border Series (EC-22 [Hoover, 1989b]). Note that both compositions are close, although the calculated melt composition is characterized by somewhat higher contents of CaO and MgO. The plausibility of these estimates follows from a comparison of the model crystallization trajectories and the melting products of the contact cumulate EC-22 in Fig. 44 (circles). It can be readily seen that the geochemical thermometry technique yielded a result consistent with the experimental data.

It is also interesting to compare the compositions of the parental melt entrapped in the cumulus with the chilled gabbro KT-39, which was proposed as a model for the Skaergaard magma (Table 15). This rock, sampled at a distance of 0.5 m from the outer contact, was selected by means of a detail screening of geochemical and textural data from a set of more than 80 samples of contact rocks of the Skaergaard intrusion [Hoover, 1989b]. In spite of the general similarity, it can be seen that this composition differs slightly more significantly from the model one (TM) and from the experimental liquid than the estimated compositions of the intercumulus liquid differ from one another.

The same pertains to the behavior of incompatible components (TiO_2, K_2O, and P_2O_5), whose concentrations in the chilled gabbro are 1.5–2 times higher than in the intercumulus melts. These deviations are so significant that they cannot be explained by the experimental and analytical uncertainties alone [Ariskin, 1999]. If this problem is considered in the context of thermodynamic calculations, relatively significant enrichment in incompatible components can be obtained at lower temperatures of ~1140–1150°C (i.e., at a more intense accumulation of crystals, see Fig. 44). The parental melt composition should therewith pass into the clinopyroxene field, and this is consistent with the relatively low CaO concentration in the chilled gabbro (Table 15).

This assumption is also favored by data on the melting of rocks from the Layered Series. McBirney and Nakamura [1973] experimentally evaluated the composition of the melt captured in the intercumulus of rocks from the three main zones of the Layered Series in the Skaergaard intrusion. For this purpose, they conducted experiments on the melting of natural rocks and obtained glass compositions for the temperature interval of 1150–1002°C [McBirney and Naslund, 1990]. Figure 44 demonstrates some of these data that represent the intercumulus melts for a sample from the Lower Zone at 1090–1150°C (open diamonds). The data define a monotonous trend of FeO enrichment and SiO_2 depletion. This trend extends to the immiscibility field of the silicate melt with its exsolution into iron- and silica-enriched liquids [McBirney and Nakamura, 1973]. These relatively low-temperature compositions can be regarded as an analogue of the residual melts representing higher degrees of crystallinity of the system.

The highest temperature composition of these experimental glasses (at 1150°C) is close to the experimental data on the melting of contact cumulates at 1160°C [Hoover, 1989b] and our calculated composition of the parental melt TM (Table 15, Fig. 44). This confirms the genetic closeness of the model and the experimental liquids and does not contradict the hypothesis that the intruded magma could have been saturated with respect to *Ol* and *Pl* (±*Cpx*). However, this also leads us to admit that the canonical scheme of the cumulate sequence is not absolutely accurate (Fig. 43), and liquidus augite could be present early in the process of Skaergaard magma crystallization.

Table 15. Composition of the parental melt of the Skaergaard intrusion estimated using the method of geochemical thermometry and inferred from melting experiments and geological observations

Component	Parental melt		Chilled gabbro KT-39 [Hoover, 1989b], $d = 0.5$ m
	TM calculated at 1165°C	experiment at 1160°C	
SiO_2	50.01 (0.42)	51.30	49.69
TiO_2	1.68 (0.33)	1.61	2.66
Al_2O_3	12.95 (0.07)	12.99	13.21
FeO	13.24 (0.51)	13.55	12.76
MnO	0.19 (0.05)	0.26	0.22
MgO	6.90 (0.11)	6.13	6.61
CaO	12.40 (0.20)	11.15	10.18
Na_2O	2.37 (0.15)	2.37	2.37
K_2O	0.26* (0.03)	0.28	0.56
P_2O_5	0.15* (0.05)	0.09	0.22
Total	100.15	99.73	98.48
Mg/(Mg + Fe)	0.481	0.446	0.480

Note: The calculated initial composition is an average of six modeled compositions corresponding to the intersection of liquid lines of descent at 1165°C (Fig. 44). The K_2O and P_2O_5 concentrations in this melt were calculated as an average of three modeled compositions (EG-4507, UT-08, and KT-47, Table 14) with higher initial contents of these components. The experimental composition corresponds to the glass obtained by the melting of cumulate EC-22 under QFM buffer conditions [Hoover, 1989b].

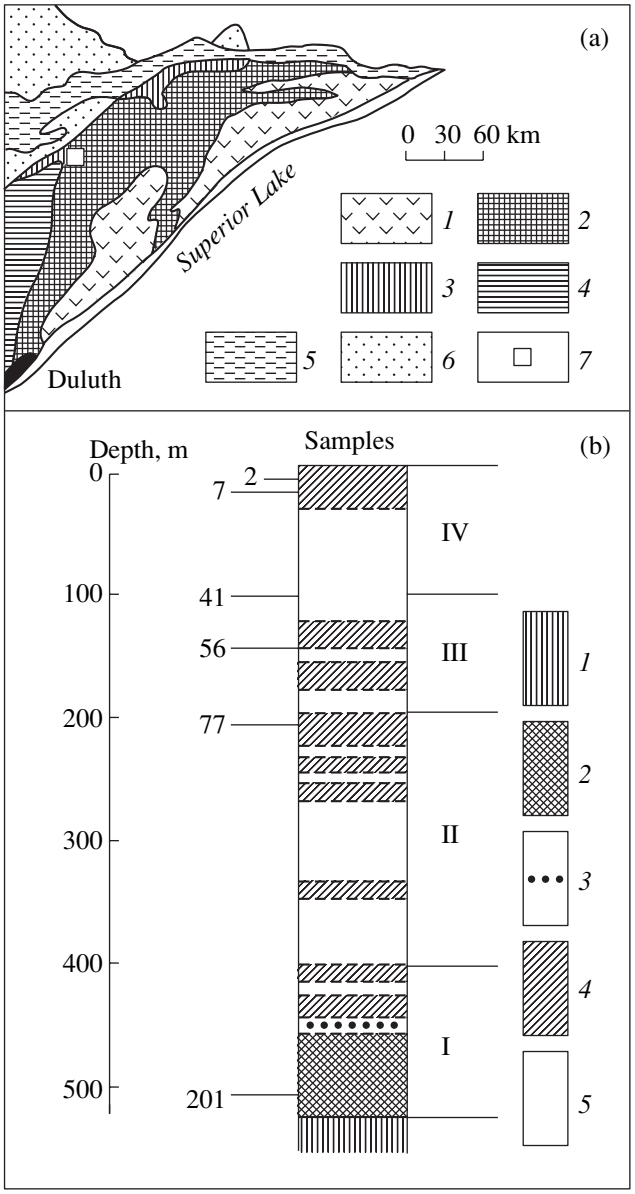

Fig. 45. (a) Geologic setting of the Duluth Complex and (b) inner structure of the Partridge River intrusion. (a) [Miller and Ripley, 1996]: (*1*) Keweenawan basalts; (*2–6*) Duluth Complex: (*2*) troctolite–anorthosite bodies, (*3*) Virginia Formation, (*4*) Bivabik Formation, (*5*) metamorphosed sedimentary and volcanic rocks, (*6*) quartz monzonite and tonalite; (*7*) Hole DDH-221 in the Partridge River intrusion. (b) [Chalokwu and Grant, 1990]: (I–IV) main zones of the intrusion (according to structural–petrologic data); (*1*) underlying rocks of the Virginia Formation; (*2*) oxide-rich gabbro of the basal zone; (*3*) xenoliths of underlying rocks; (*4*) olivine gabbro; (*5*) troctolite. Sampling sites are shown to the left of the column.

Also, it cannot be ruled out that the differences between the concentrations of incompatible elements are related to the more general problem of the lack of mass balance for TiO_2, K_2O, and P_2O_5 between the residual melts of the early crystallization stages and the weighted mean composition of the Skaergaard intrusion [Ariskin, 2003]. In any event, these data testify that it is necessary to examine a range of the probable magma compositions. This is the main reason why we will analyze the fractionation conditions of the Skaergaard magma using two proposed parents: the calculated TM composition and the chilled gabbro KT-39 (see Chapter 4).

3.2.2. Partridge River intrusion, Duluth Complex, Minnesota

This section was prepared based on the results of our research conducted in 1991–1992 in cooperation with Prof. C.I. Chalokwu at Auburn University, Alabama, as well as on the authors' data obtained in the past years with the use of a modernized version of the COMAGMAT model. Our cooperation was initiated by two publications in which the postcumulus re-equilibration of olivine was discussed with reference to rocks of the Partridge River intrusion in Minnesota [Chalokwu and Grant, 1987] and dolerites of the Vel'minskii sill in the Eastern Siberian traps [Barmina *et al.*, 1989b]. In these papers, attempts were made to use various methods to evaluate the composition of primary olivine crystals before they were re-equilibrated with the intercumulus melt. Chalokwu and Grant [1987] attacked this problem using simple mass-balance calculations, including an estimation of the Fe/Mg ratio of the intercumulus liquid and the porosity of the cumulates, while we utilized geochemical thermometry. The application of this approach to rocks of the Partridge River intrusion led us to obtain information on the initial crystallization conditions of the parental magma [Chalorwu *et al.*, 1993, 1996]. This was the first experience of applying geochemical thermometry to magmatic bodies more than 500 m thick.

However, some of our data turned out to be contradictory and could hardly be explained from the viewpoint of physics. In particular, this pertained to the conclusions that magnetite was present in the primary liquidus assemblage (*Ol* + *Pl* + *Mt*) and the parental magma crystallinity was very high (~68%), as followed from the results of geochemical thermometry. Since the first simulations were conducted with the COMAGMAT-3.0 model, which overestimated the temperature of magnetite crystallization by 20–40°C (see Section 2.2.5), we repeated these simulations for the same initial compositions but now using the COMAGMAT-3.52 program. A comparative analysis of the results of these simulations is presented below.

Geologic setting and inner structure. The Partridge River intrusion is part of the Duluth Complex of igneous rocks near Lake Superior in Minnesota (Fig. 45). The complex is a wedge-shaped body up to 15 km thick, which comprises a series of anorthosite, troctolite, gabbroid, granodiorite, and granite intrusions exposed over an area of 1500 km^2 [Miller and Ripley, 1996]. Isotopic–geochemical evidence indicates that

these bodies were emplaced at 1.15–1.40 Ga within a large mid-continental rift system. The complex is underlain by metasedimentary rocks dated at 1.6–1.7 Ga and is overlain by tholeiitic basalts of the Keweenawan Volcanic Group, which was reportedly produced during the same cycle of volcano-plutonic activity. It is commonly thought that anorthosite intrusions predated troctolites and gabbroids.

The Partridge River intrusion is a basite body dominated by troctolites, which are restricted to the northwestern contact of the Duluth Complex (Fig. 45). The complex was actively studied for about 40 years because of the Cu–Ni mineralization, which can be economic and is hosted by the basaltic portions of troctolite intrusions (see, for example, [Tyson and Chang, 1984; Lee and Ripley, 1995]). The same rocks contain PGE mineralization [Mogessie *et al.*, 1991]. Detailed drilling exploration and extensive data on the petrology, geochemistry, and mineralogy of this pluton make it one of the most exhaustively examined bodies of the Duluth Complex. Its inner structure is given based on the results obtained for the core of Hole DDH-221 [Chalokwu and Grant, 1990; Grant and Chalokwu, 1992].

Proceeding from the structural–genetic interpretation of thin sections of more than 60 rock samples from the Partridge River intrusion, it was interpreted as a three-component mixture of cumulus plagioclase, olivine, and intercumulus melt. The intercumulus consists of plagioclase, olivine, clino- and orthopyroxene, Fe–Ti oxides, and trace amounts of biotite and apatite. The inner contacts of the intrusion are drawn according to drastic changes in the proportions of cumulus minerals and the grain size of the rocks, which made it possible to formally distinguish four zones (Fig. 45). Zones II, III, and IV are made up of alternating varieties of troctolites and olivine gabbro, and zone I consists of magnetite-rich fine-grained gabbro (with cumulus *Ol* and *Pl* present in strongly subordinate amounts). The latter zone hosts sulfide ore concentrations.

The main petrological problem of the Partridge River intrusion is, in the regional aspect, the composition of the parental magma. It was hypothesized that the parental melts could be high- or low-Al tholeiites, which are present among the Keweenawan basalts. These possible parents of the Duluth intrusive magmas could be, in turn, derived from a more primitive tholeiite via its fractional crystallization. The solution of this problem is related to the problems of a genetic interpretation of the inner structure of the Partridge River intrusion.

The insignificant variations in the composition of the cores of *Ol* ($Fo_{69\pm3}$) and *Pl* ($An_{66\pm3}$) crystals (Fig. 46), the constancy of the CaO/Al_2O_3 and FeO/MgO ratios throughout almost the whole rock succession (Fig. 47), and the absence of structural–chemical signatures of clinopyroxene appearance in the cumulus suggest that there was no extensive fractionation in the magma chamber of the Partridge River

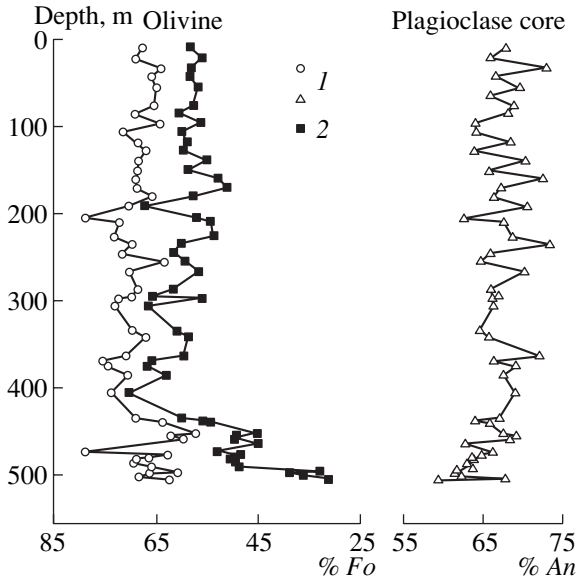

Fig. 46. Observed compositions of *Ol* and *Pl* in comparison with the original *Ol* composition estimated for rocks of the Partridge River intrusion. (*1*) Measured olivine compositions (average of eight spot analyses for each sample; (*2*) calculations [Chalokwu and Grant, 1987].

intrusion. In this situation, the variations in the major-element concentrations can be explained as resulting from the sorting of *Ol* and *Pl* crystals at the variable porosity of the original cumulates [Chalokwu *et al.*, 1993].

This mechanism is consistent with geochemical data pointing that the basal zone of the intrusion is unusually strongly enriched in Ti, P, Zr, Ba, Y, and REE, whose contents are four-, five-, and even nine-fold those in the overlying rocks (Fig. 47). Mass-balance calculations for these highly incompatible elements indicate that their bulk-rock concentrations are strongly dependent on the fraction of the intercumulus melt [Grant and Chalokwu, 1992]. Thus, the variations in the contents of major and trace elements observed in the rocks of the Partridge River intrusion could be controlled by the mechanical redistribution of *Ol* and *Pl* crystals and the melt in the absence of evidence of their chemical fractionation. The rocks produced under these conditions are suitable for geochemical thermometry.

The application of this method to the rocks is facilitated by the existence of preliminary estimates of the thermodynamic conditions under which the pluton was formed. Judging from the mineral assemblages observed in the underlying metasedimentary rocks, the pressure during the intrusion of the magma was estimated at 2–3 kbar [Simmons *et al.*, 1974]. Redoximetric results on the magnetite–ilmenite equilibrium for the rocks of the basal zone indicate that these rocks crystallized at an oxygen fugacity between the QFM and WM buffers [Pasteris, 1985].

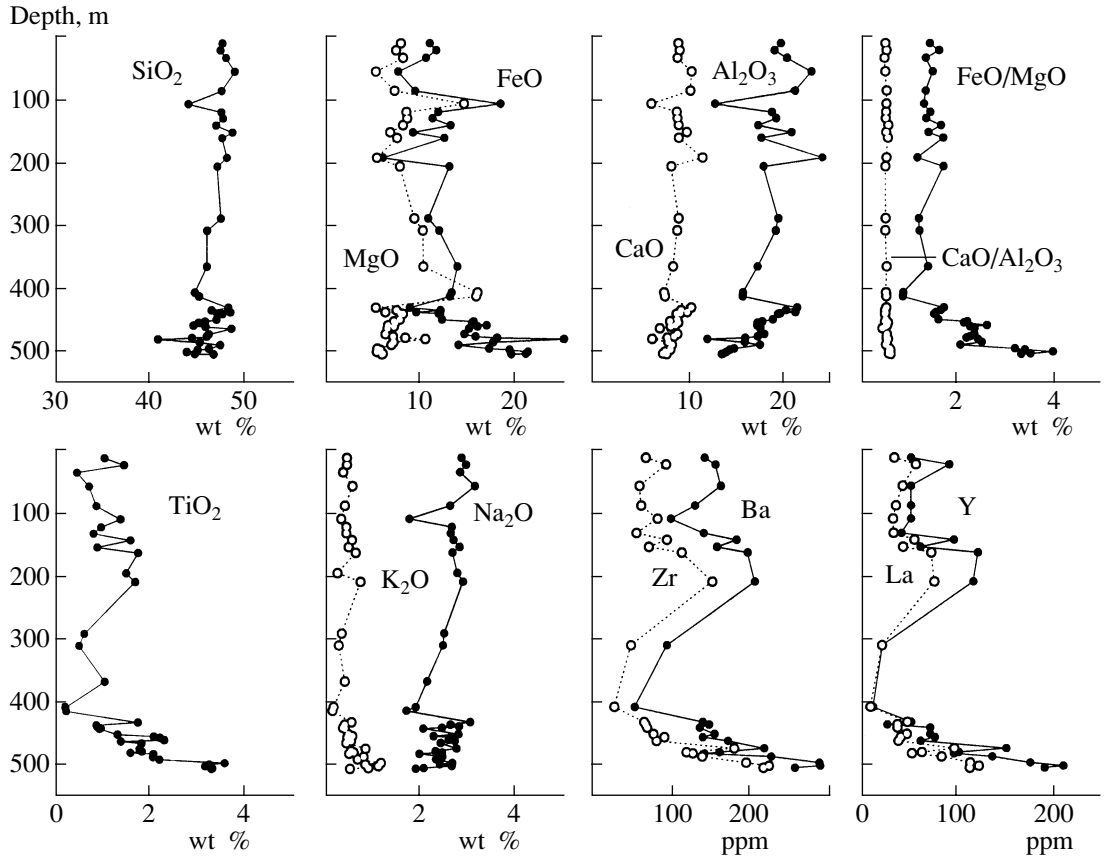

Fig. 47. Variations in the concentrations of major components and incompatible trace elements and selected major-element ratios along Hole DDH-221.

Geochemical thermometry. For geochemical thermometry, we selected the five most contrasting compositions from the upper third of the intrusion (zones III and IV, Fig. 45), fine-grained gabbro from the lower zone I (sample 201), and the weighted mean composition of the intrusion (Table 16). This composition, referred to as PRIM, can be regarded as an approximation of the Partridge River parental magma. Strictly speaking, this approximation should be valid for ideal stratiform bodies, but the assumption that there was no magma fractionation on the scale of the intrusive chamber justifies the utilization of this weighted mean evaluation, which should account for the average proportion of *Ol* and *Pl* crystals and melt in the parental magma [see Eqs. (81) and (82)].

Simulation conditions and crystallization sequence. First, we simulated the liquid lines of descent with the COMAGMAT-3.0 program for a pressure of 2 kbar, redox conditions 0.5 log units above the WM buffer, and a crystallization increment of $\Delta\varphi_{cr} = 1$ mol %. The maximum degree of crystallinity (80%) was calculated for the temperature range of 1080–1130°C. The modeled crystallization sequences of minerals are demonstrated in Fig. 48. As follows from these data, four of the original compositions (samples 2, 7, and 77 and PRIM) are characterized by the *Ol* + *Pl* subcotectic assemblage at temperatures of 1200–1240°C. A wide field of olivine crystallization was identified for the most magnesian sample 41, and *Pl* was the first to crystallize (at approximately 1300°C) for the aluminous troctolite (sample 56).

The most conspicuous feature of these sequences is titanomagnetite crystallization that was identified in all compositions starting from ~1150–1180°C. The maximum *Mt* temperature was determined for a rock from the lower contact zone (sample 201), which represented the *Ol* + *Mt* ± *Pl* low-temperature subcotectic assemblage starting from approximately 1180°C. This result led us to suggest that titanomagnetite was one of the early cotectic phases composing the early mineral assemblage of the parental magma. This conclusion seemed unexpected from the standpoint of textural and petrographic observations of the olivine gabbro and troctolites but was in agreement with magnetite enrichment of rocks of the lower zone I [Chalokwu and Grant, 1990].

The melt composition evolution for the calculated crystallization trajectories is shown in Fig. 49. A visual analysis of these trajectories demonstrates that some of them converge at temperatures slightly above 1200°C, but all lines intersect in the vicinity of 1150°C. As follows from the close consideration of these plots, this

Table 16. Compositions of cumulus rocks, average trapped melt, and the parental magma of the Partridge River intrusion

Component	2 (h = 10)	7 (h = 22)	41 (h = 107)	56 (h = 152)	77 (h = 207)	201 (h = 503)	TM-1993 (1150°C)	PRIM
SiO_2	47.60	47.39	44.00	48.66	47.05	44.73	48.26	46.81
TiO_2	1.05	1.46	1.39	0.90	1.70	3.32	2.94	1.15
Al_2O_3	19.83	19.16	12.82	20.95	18.00	13.74	15.01	18.79
FeO	11.05	11.73	18.58	9.27	13.16	21.28	15.84	12.31
MnO	0.12	0.13	0.23	0.11	0.15	0.20	0.20	0.14
MgO	7.98	7.45	14.70	6.83	7.87	6.08	5.19	8.85
CaO	8.91	9.06	6.05	9.83	8.18	7.32	8.21	8.80
Na_2O	2.89	2.99	1.78	2.85	2.92	2.09	2.63	2.57
K_2O	0.45	0.45	0.33	0.49	0.74	0.91	1.32	0.46
P_2O_5	0.10	0.19	0.11	0.11	0.23	0.34	0.40	0.12
FeO/MgO	1.38	1.58	1.26	1.36	1.67	3.50	3.06	1.39
CaO/Al_2O_3	0.45	0.47	0.47	0.47	0.46	0.53	0.55	0.47

Note: Sample numbers correspond to those in Fig. 45; h is the depth, m; the compositions are normalized to anhydrous basis, wt %. PRIM is the weighted mean composition calculated for 40 rocks with regard for the thicknesses of their layers. TM-1993 is the average composition of the melt trapped in the intercumulus of the rocks at 1150°C, according to geochemical thermometry calculations [Chalokwu *et al.*, 1993].

intersection seems to be unambiguous owing to the model trajectory of the composition of sample 201. In contrast to other compositions, these lines demonstrates a systematic decrease in the contents of TiO_2 and FeO in the liquid, which reflects the high initial abundance of titanomagnetite in sample 201 (Fig. 48).

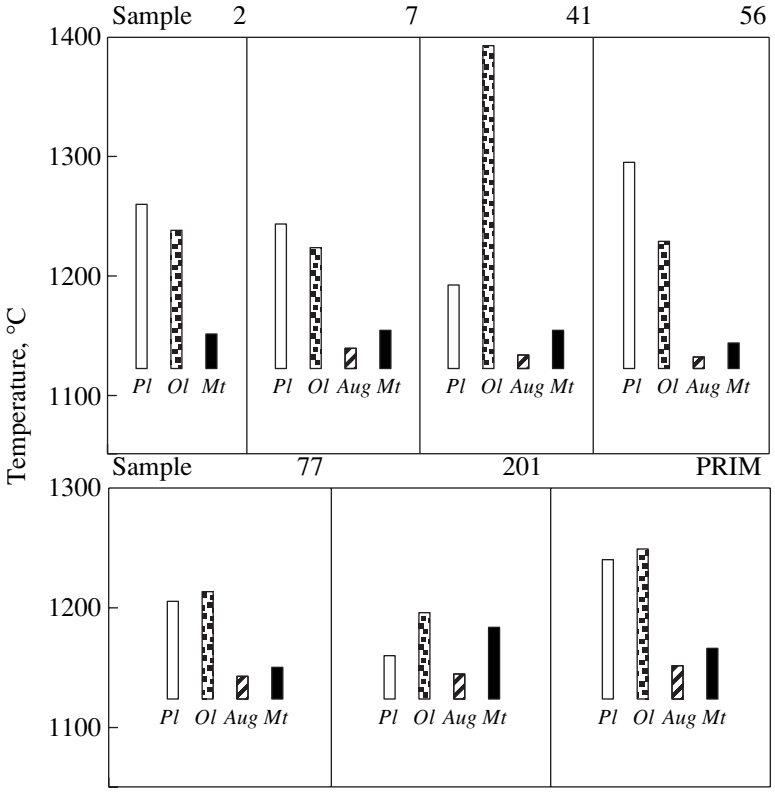

Fig. 48. Sequence of equilibrium crystallization of minerals from the melts of the rocks and the assumed parental magma of the Partridge River intrusion. Calculations were conducted with the COMAGMAT-3.0 program for P = 2 kbar and WM + 0.5 redox conditions [Chalokwu *et al.*, 1993]. See Table 16 for the compositions of the samples.

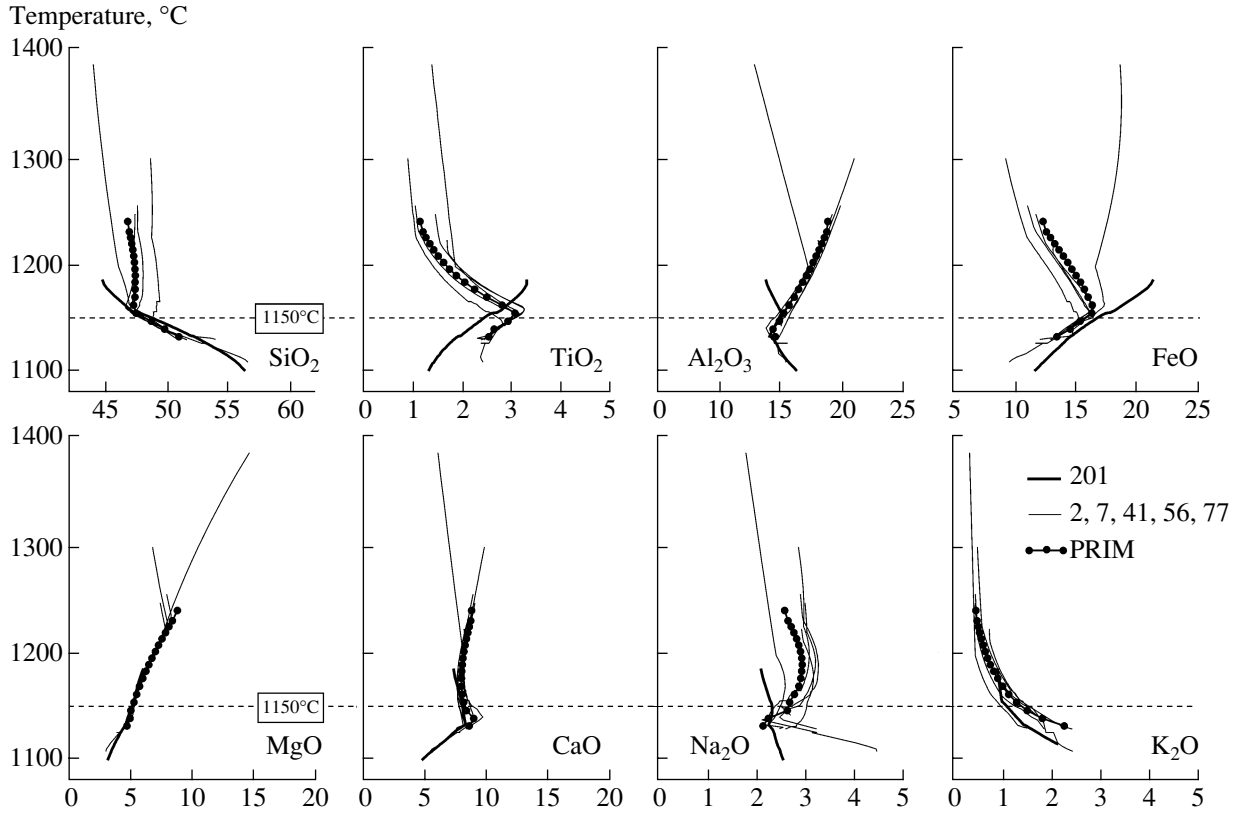

Fig. 49. Liquid lines of descent for the equilibrium crystallization of the melts of the rocks and the parental magma of the Partridge River intrusion. Calculations of the crystallization sequences are presented in Fig. 48.

The model melt compositions of the rocks at 1150°C appeared to be closely similar, because of which the average composition of these liquids was assumed as the estimate of the "melt captured in the intercumulus" (see composition TM-1993 in Table 16). Correspondingly, $T = 1150 \pm 10$°C was considered to be an approximation of the initial temperature of rock formation at which the suspended cotectic crystals were redistributed on the scale of the intrusive chamber [Chalokwu *et al.*, 1993].

The calculated average compositions of initial olivine and plagioclase crystals (which were in equilibrium with this liquid) were $Fo_{66.7 \pm 1.0}$ and $An_{64.2 \pm 2.5}$. These estimates are close to the average composition of olivine ($Fo_{69 \pm 3}$, calculated using data on the porosity of the cumulates [Chalokwu and Grant, 1987]) and the measured composition of *Pl* cores ($An_{66.3 \pm 3}$, microprobe data) (Fig. 46). The differences between the calculated and observed ($Fo_{55 \pm 8}$ [Chalokwu and Grant, 1990]) olivine compositions can be explained as resulting from the postcumulus re-equilibration of the original crystals with the intercumulus liquid. This effect is pronounced most conspicuously in the contact rocks, for example, chilled gabbro. The average observed *Ol* composition in sample 201 is Fo_{31}, whereas the calculations for 1150°C for this sample give approximately Fo_{65}.

Phase composition of cumulates. The method of geochemical thermometry is underlain by the conditions of the closure of the system and a mass balance maintained in it [Eqs. (81) and (82)], and, therefore, the results of the thermometric calculations include (along with the initial compositions) the estimations of the original proportions of minerals and melt for each sample. Thereby it should be taken into account that errors in the temperature estimates of the order of 10°C result in uncertainties in the calculated original phase proportions from 3 to 6 wt % [Ariskin and Barmina, 2000]. The variations in the model proportions of *Ol*, *Pl*, and melt in rocks of the Partridge Ridge intrusions were considered in [Chalokwu *et al.*, 1993].

For instance, it was established for MgO-enriched sample 41 that the amount of *Ol* in the original mixture amounted to approximately 40 wt %, whereas the liquidus assemblage of the high-Al composition of sample 56 was strongly dominated by *Pl* (>50 wt %). The amount of the melt trapped in rocks of the upper part of the intrusion varied from ~25 to 40 wt %. The maximum liquid portion was obtained for sample 201 (~80 wt %), which was previously proposed as the chilled gabbro of the Partridge River intrusion [Chalokwu and Grant, 1990]. The latter result confirms the conclusion that the main cause of the strong enrichment of incompatible elements in the lower contact zone was

a downward increase in the amount of the intercumulus liquid, whose content increased four- to fivefold with the transition from the overlying adcumulates to lower contact rocks. In this situation, the term *trapped liquid* becomes senseless in application to some of the rocks, because their melt fraction exceeded the amount of crystals. This conclusion receives support from the results of direct computer simulations of the redistribution dynamics of the cumulus minerals and the variations in the contents of incompatible elements in the lower portion of the Partridge River intrusion [Chalokwu *et al.*, 1996].

Phase composition of the parental magma. The method of geochemical thermometry is attractive because the reliable estimation of the weighted mean composition of an intrusive body opens up the possibility of calculating the phase composition of the parental magma, i.e., the modal proportions of intratelluric crystals and the initial coexisting liquid at the moment of time when the magma filled the chamber [Ariskin and Barmina, 2000]. This approach rests on the following three postulates:

(i) by analogy with cumulative rocks, the bulk chemical composition of the parental magma can be expressed with Eqs. (81) and (82) if the values of F_j^0 and F_l^0 are assumed to represent the proportions of crystals and melt in the magma, and $\overline{C}_i^{j(0)}$ and $C_i^{l(0)}$ are the initial compositions of these phases;

(ii) the average composition of the crystals and melt in the initial magmatic mixture were identical to the average composition of the cumulus minerals and coexisting intercumulus liquid of the contact rocks;

(iii) the temperature of the magma corresponded to the temperature of the primitive intercumulus liquid.

In order to test the fulfillment of these conditions, it is sufficient to compare the data of geochemical thermometry of the rocks and the simulation results for the weighted mean composition of the intrusion at the calculated temperature. If the values for the model composition of the crystals and the liquid are identical (or close enough), information on the degree of the parental magma crystallization can be derived from the modeling results for the equilibrium crystallization of the weighted mean composition of the intrusion.

A comparison of the thermometric data and calculation results (by the COMAGMAT-3.0 program) for PRIM at 1150°C demonstrates the remarkable closeness, almost perfect similarity of the estimates of the liquid compositions (Tables 16, 17). The average compositions of *Ol* and *Pl* obtained with thermometric techniques ($Fo_{66.7 \pm 1.0}$ and $An_{64.2 \pm 2.5}$) are virtually the same as the "model" compositions in the parental magma ($Fo_{66.7}$ and $An_{63.9}$). This consistence provided grounds to assume the proportions of minerals and liquid calculated for PRIM at 1150°C as the primary modal proportions, characterizing the phase composition of the magma parental for the Partridge River intrusion. These proportions are 32 wt % melt and 68% crystals, including 44.2% *Pl*, 22.5% *Ol*, and 1.3% *Mt* [Chalokwu *et al.*, 1993].

Table 17. Chemical and phase characteristics of the parental magma of the Partridge River intrusion calculated with different versions of the COMAGMAT model

Component	Calculations for the weighted mean PRIM composition (see Table 16)	
	1150°C, COMAGMAT-3.0 model [Chalokwu *et al.*, 1993]	1167°C, COMAGMAT-3.52 model [this study]
Initial melt composition, wt %		
SiO_2	48.16	47.28
TiO_2	3.02	2.69
Al_2O_3	15.01	15.80
FeO	15.72	16.24
MnO	0.20	0.20
MgO	5.19	5.67
CaO	8.29	8.02
Na_2O	2.64	2.86
K_2O	1.41	0.97
P_2O_5	0.37	0.28
Original mineral compositions, mole %		
An	63.9	66.2
Fo	66.7	68.2
Modal phase proportions for the parental magma, wt %		
Melt	32.0	42.8
Pl	44.2	38.3
Ol	22.5	18.9
Mt	1.3	–

Newly conducted calculations. It should be admitted that this result was unexpected, because it was thought that magma can flow and be intruded at a crystallinity of no more than approximately 50–60% (see Section 1.1). Believing that this inconsistency is caused by the underestimated crystallization temperature of the parental magma owing to the overestimation of the magnetite crystallization temperature, we conducted a new series of calculations for the same conditions and compositions (Table 16) using the COMAGMAT-3.52 program.

Our simulation results demonstrate that the modernized version of the COMAGMAT model yields magnetite crystallization temperatures 20–30°C lower than those in [Chalokwu *et al.*, 1993]. Magnetite appears on the liquidus nearly simultaneously with augite and ilmenite within the temperature range of 1120–1130°C. To illustrate these differences, Fig. 50 compares the crystallization sequences for the weighted mean composition of the Partridge River intrusion (PRIM).

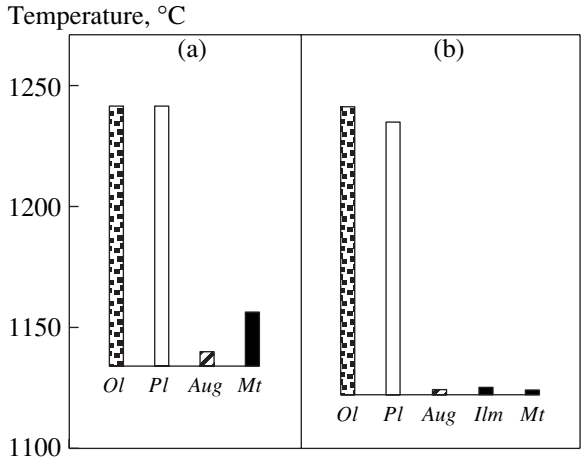

Fig. 50. Chemical and phase characteristics of the parental magma of the Partridge River intrusion calculated with different versions of the COMAGMAT model. (a) COMAGMAT-3.0 [Chalokwu *et al.*, 1993]; (b) COMAGMAT-3.52 (this study).

As a result of the differences in the onset of Fe-Ti oxide crystallization, the intersection point of the model trajectory for sample 201 (which is maximally enriched in FeO and TiO_2, Table 16) with other evolutionary lines is shifted toward temperatures below 1125°C (Fig. 49). The uncertainty interval of the geochemical thermometry expands to 1125–1200°C. The situation seems to be discouraging if the reconstructions of the original characteristics rely on the compositions of the model liquids alone. This problem can be settled if the observed mineral compositions are used, first of all, the composition of plagioclase. The composition of *Pl* cores in the rocks of the intrusion varies very little ($An_{66\pm3}$) and shows practically no traces of postcumulus re-equilibration.

The right column in Table 17 characterizes the temperature, liquid composition, and phase proportions of the parental magma with the proviso that the average composition of plagioclase crystals entrained by the magma corresponded to 66.2 mol % *An*. Evidently, this condition yields a higher temperature melt (1167 instead of 1150°C), which is undersaturated with respect to Fe–Ti oxides and is in equilibrium with *Ol* of composition $Fo_{68.2}$. The latter estimate is close to the average composition of olivine cores ($Fo_{69\pm3}$) calculated using data on the porosity of the cumulates [Chalokwu and Grant, 1987].

The phase composition of this assemblage corresponds to a mixture of 42.8 wt % melt, 38.3% *Pl*, and 18.9% *Ol* (Table 17). The bulk degree of crystallization of this system (57.2 wt %) is notably lower than the estimate of 68% assumed on the basis of earlier simulations [Chalokwu *et al.*, 1993] and does not extend outside the range of the natural magma fluidity. We believe, as before, that it was the high content of the crystalline material in the Partridge River parental magma that precluded the large-scale separation of solid phases and efficient fractionation in the relatively large chamber. This conclusion is in agreement with the estimated high crystallinity (up to 50–60%) of the "parental anorthosite magmas" of the Duluth Complex [Miller and Weiblen, 1990], as well as some subvolcanic bodies in the field of the Keweenawan basalts [Jones, 1984].

Below we will present a few additional examples of the applications of geochemical thermometry to other intrusive bodies. In practice, clear-cut and unambiguous intersections of liquid lines of descent are quite rare (Fig. 44), and, hence, the results of phase equilibrium calculations should always be interpreted with regard for the composition of model minerals, which should be close to the most primitive compositions of crystals in the natural rocks. This makes the results somewhat uncertain, particularly considering that *Ol* could have been re-equilibrated with the intercumulus melt [Barnes, 1986]. Nevertheless, the effects of these deviations on the final results are much less significant than those caused by the approximation of the parental melts by either the rock compositions or the weighted mean composition of the intrusion.

3.2.3. Kiglapait intrusion, Labrador

Petrological interest in the Kiglapait intrusion was whetted by its huge size (the overall rock volume is approximately 3500 km^3) and strong differentiation, which caused the significant enrichment of the late crystallization products in FeO and TiO_2, with the chemistry of the olivine and pyroxenes evolving up to purely ferrous varieties [Morse, 1979a, 1979b]. This highlights a certain analogy between this massif and the Skaergaard intrusion, because of which both of them are often addressed to as typical examples of tholeiite magma differentiation coupled with strong Fe enrichment [Morse, 1990; Snyder *et al.*, 1993]. It is also worth mentioning that the methods for estimating the compositions of differentiated melts, which were first tested on the Layered series of the Skaergaard intrusion [Wager, 1960], were further developed in application to the Kiglapait intrusion [Morse, 1981].

In contrast to Wager, Morse [1981] did not use the graphical mass-balance approach but, instead, constructed evolutionary trajectories for the residual magmas utilizing the method of the numeric summation of rock compositions corresponding to the final crystallization stages of the intrusion. Later, the realism of these calculations was questioned, because they turned out to be inconsistent with the available data on the *Pl*–melt [Blundy and Wood, 1991, 1992] and *Ol*–melt equilibria and with the computer simulations of the fractional crystallization of the Kiglapait parental magma [Toplis and Carroll, 1996]. We believe that the geochemical thermometry of the most primitive rocks are useful for a reconstruction of the differentiation trends during the

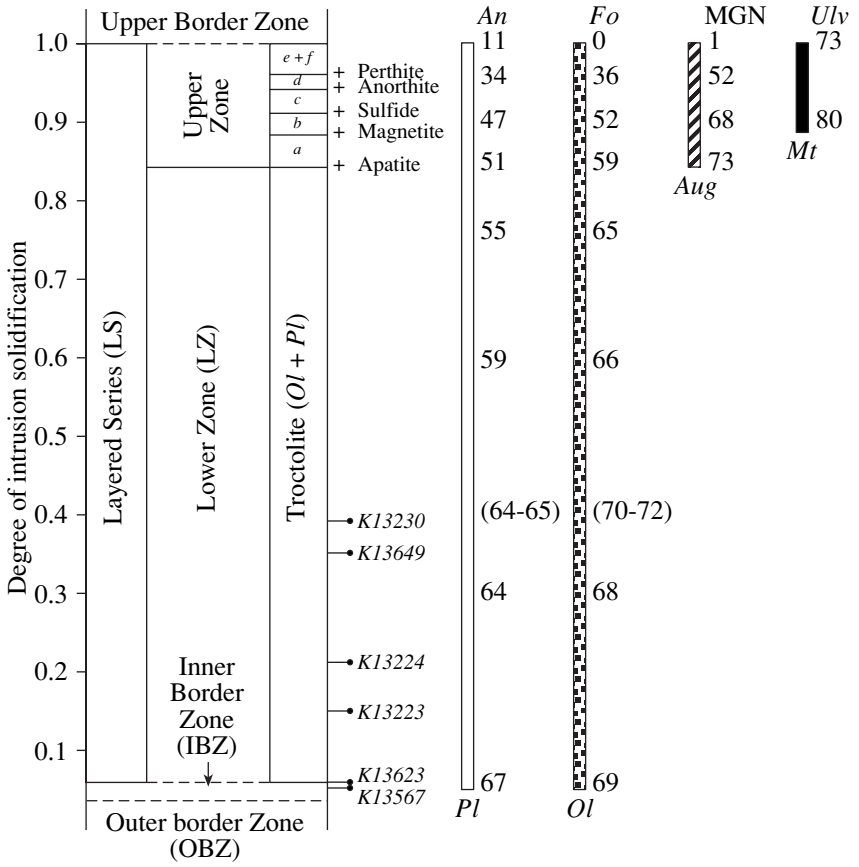

Fig. 51. Main structural units and the percentage of solidification of the Kiglapait intrusion. The Lower (LZ) and Upper (UZ) zones of the Layered Series are subdivided in accordance with the appearance of cumulus pyroxene in the rocks. The evolution of mineral compositions is given according to the generalized trends established in a number of cross sections of the intrusion [Morse, 1979a]. Sampling sites in the vertical section are shown for the six samples used for geochemical thermometry.

development of the inner structure of the Kiglapait intrusion [Barmina and Ariskin, 2002].

Geologic setting and inner structure. The Kiglapait intrusion in the northern shore of Labrador is a funnel-shaped body consisting of troctolites, gabbroids, and ferrosyenites and having a thickness of approximately 9 km in its central part. The massif is slightly elongated northwestward and is ~20 × 30 km in map view. Its structural setting is controlled by the late members of the Nain anorthosite complex of Late Riphean age. The age of the Kiglapait intrusion was assumed to be Late Proterozoic, at the boundary between the Early and Late Riphean [Morse, 1979a].

The main units of the intrusion are the Inner Border Zone (IBZ), Layered Series (LS), and the Upper Border Zone (UBZ) (Fig. 51). The Inner Border Zone rests on the Outer Border Zone of comparable thickness, whose affiliation with this intrusion is debatable. The Inner Border Zone accounts for approximately 2% of the rock succession and is made up of *Ol–Pl* cumulates with ~70% modal plagioclase, 11–12% olivine and augite, 3% Fe–Ti oxides, and minor amounts of hypersthene, apatite, biotite, and brown hornblende. Upward, they give way to the rocks of the Lower Zone (LZ) of the Layered Series, which account for ~80% of the vertical section and consist of troctolite cumulates. Thus, the Kiglapait intrusion is a massif with abundant troctolites and an average modal composition characterized by the predominance of *Pl* (67 wt %) and *Ol* (23%) [Morse, 1979b].

Augite is a quantitatively subordinate mineral, whose appearance among cumulus minerals marks the transition from troctolites to gabbroids of the *Upper Zone* (UZ). Although this zone makes up about 20% of the layered Series, it is characterized by a sharp change in the composition of rocks and minerals, which suggests that the Kiglapait magma was strongly fractionated. The Upper Zone is subdivided into a number of subzones according to the appearance of new cumulus minerals, such as magnetite (UZb), sulfide (UZc), apatite (UZd), and anti- and mesoperthites (UZe and UZf) (Fig. 51).

Layers containing alkaline feldspars are significantly enriched in Fe and consist of ferrosyenites, which are overlain by the fine-grained rocks of the Upper Border Zone. The UBZ is characterized by

inverse variations in the compositions of minerals in the range from UZf to UZa. This suggests that the UBZ developed downward by means of growing away from the roof, analogously to the Upper Border Zone of the Skaergaard intrusion [Wager and Brown, 1967; McBirney, 1996].

Mineral chemistry. Early in the course of studying this massif, a series of plots were constructed to display the evolution of mineral compositions in different sections, and these data were approximated by generalized trends [Morse, 1979a, 1980]. These trends were eventually tabulated for calculated values of the solidification percentage (PCS) [Morse, 1981]. The evolution of these generalized compositional parameters (*An*, *Fo*, and the Mg number of clinopyroxene) are presented in Fig. 51.

Within the lower half of the LZ, these data exhibit monotonous and insignificant variations in the compositions of the two main minerals: *Pl* ($An_{67} \longrightarrow An_{63}$) and *Ol* ($Fo_{69} \longrightarrow Fo_{67}$). In the uppermost third of the Lower Zone, the *An* and *Fo* contents decrease more significantly: $An_{59} \longrightarrow An_{51}$ and $Fo_{66} \longrightarrow Fo_{59}$. The most remarkable changes take place in the Upper Zone of the Layered Series, in which the *Fo* content decreases to zero and plagioclase gives way to alkaline feldspar containing no more than 20–10% of the anorthite component. The Mg number of the augite is also rapidly decreased. The variations in the composition of titanomagnetite are not as dramatic ($Ulv_{80} \longrightarrow Ulv_{73}$), but it should be recalled that these data represent a reconstruction of the original composition of the oxides, which were re-equilibrated under subsolidus conditions [Morse, 1980].

In the context of geochemical thermometry, the most important minerals are olivine and plagioclase from the lower half of the Lower Zone of the Layered Series (PCS = 4–40%). In fact, the insignificant decrease in the *Fo* and *An* contents in the troctolites (Fig. 51) not so much reflects the actual compositional variations as is caused by the approximation by generalized trends that were translated to the lower part of the intrusion from its upper levels. This is explained by the specifics of Morse's [1981, 1996] genetic reconstructions, which interpreted the structure of the Kiglapait intrusion from the standpoint of the fractional crystallization of a homogeneous magmatic melt. Within the span of this idealized scheme, the compositions of minerals should monotonously evolve starting from the very early solidification stages, and it is convenient to interpret the observed deviations from the model trends as random variations. Nevertheless, an analysis of the primary graphic materials [Morse, 1979a] indicates that these deviations can be of principal importance [Barmina and Ariskin, 2002].

In particular, *Pl* of the composition $An_{64–65}$ and *Ol* corresponding to $Fo_{70–72}$ are present within the solidification range of 30–40%, whereas the generalized trend predicts approximately An_{62} and Fo_{67} at these levels (Fig. 51). At first these differences seem to be insignificant, but here it is worth noting the mere fact of the occurrence of the most primitive compositions. This led us to suggest that the troctolites could have been formed by cumulates that consisted of cumulus minerals only insignificantly different compositionally from the primary crystals entrained by the parental magma. This can be regarded as evidence that the composition and temperature of the intercumulus melt at 4–40% PCS varied insignificantly.

In this situation, the parameters of the initial liquid can be evaluated by the method of geochemical thermometry if troctolites can be found whose major-component composition would vary owing only to the variable proportions of the cumulus and melt. Luckily, Morse's [1981] collection contained a number of samples with such contrasting compositions, which were taken within the Inner Border Zone and the lower half of the Lower Zone in the Layered Series.

Results of geochemical thermometry. For the thermometric calculations, we selected chemical compositions of two samples from the Inner Border Zone (KI3567 and 3623) and four troctolites corresponding to the range of 15–39% PCS (KI3223, 3224, 3649, and 3230) (Table 18). The relative position of their sampling sites in the vertical section are shown in Fig. 51. Additional calculations were conducted for two compositions, including a weighted mean estimate for the Layered Series (Table 18, KIGLAP composition) and the average composition of the marginal facies (MAR), which were regarded as a possible analogue of the parental magma for the Kiglapait intrusion [Nolan and Morse, 1986].

Calculation conditions. The calculations were carried out with one of the latest versions of the COMAGMAT-3.65 (2000) model, which was calibrated to simulate ferrobasaltic melts and was used to evaluate the initial temperatures for the rocks of the Layered Series of the Skaergaard intrusion [Ariskin, 2002, 2003]. Similar to the COMAGMAT-3.5*n* programs [Ariskin, 1999], this modernized model is recommended for application to systems of low and moderate alkalinity (olivine basalts, tholeiites, and ferroandesites). The accuracy of its temperature calculations is comparable with that of the mineral–melt geothermometers (10–15°C), and the major-component compositions are calculated accurate to approximately 0.5 wt %. The differences between the modeled and experimental compositions can only occasionally be greater than 1 mol % for *Ol* and 3 mol % for *Pl*, which makes it possible to use natural mineral compositions as an independent criterion in testing the calculations. This approach can be used if the following two constraints are valid.

First, the natural compositions should not be notably re-equilibrated under subsolidus conditions. It is, however, doubtful that this restriction is true for the Kiglapait troctolites: compare the *Ol* and *Aug* compositions at the boundary of the Lower and Upper zones

Table 18. Weighted mean petrochemical characteristics of the Layered Series and contact zones in comparison with the weakly differentiated troctolites from the Lower Zone of the Kiglapait intrusion

Component	Mean compositions		Inner Border Zone (IBZ)		Troctolies from the Lower Zone of the Layered Series			
	Layered Series, KIGLAP	Contact rocks, MAR (n = 4)	KI3567 (5.7)	KI3623 (5.9)	KI3223 (15.0)	KI3224 (21.0)	KI3649 (35.0)	KI3230 (39.0)
SiO_2	47.60	49.96	48.47	48.09	46.59	48.08	48.88	48.95
TiO_2	0.81	0.30	0.67	0.40	0.12	0.22	0.36	0.20
Al_2O_3	19.52	19.63	18.31	19.17	19.08	23.12	25.29	21.48
FeO	11.11	8.93	11.94	10.66	10.14	7.34	5.90	8.70
MnO	0.15	0.13	0.17	0.14	0.12	0.10	0.07	0.10
MgO	8.06	8.18	8.17	9.60	12.96	8.03	4.11	7.28
CaO	9.30	9.48	8.68	8.59	8.40	9.99	12.14	9.66
Na_2O	3.14	3.11	3.28	3.13	2.43	2.94	3.01	3.40
K_2O	0.22	0.25	0.27	0.20	0.14	0.17	0.23	0.21
P_2O_5	0.09	0.04	0.05	0.02	0.01	0.01	0.01	0.01

Note: The mean composition MAR of the contact rocks is calculated from the data in [Nolan and Morse, 1986], other compositions are from [Morse, 1981]. The stratigraphic setting of rocks of the Inner Border Zone and the troctolites of the Lower Zone is indicated according to the percentage of solidification (PCS) of the massif (vol %) (see Fig. 51). All Fe is given as FeO, the compositions are normalized to 100%.

(Fig. 51). The Mg number of the first crystals of cumulus pyroxene here is 73%, whereas the average *Ol* composition is much more ferrous (Fo_{59}). The compilation of melting-experiment information indicates that high-Ca pyroxene is more magnesian than olivine under subliquidus conditions, but the difference is not as great, commonly no more than 10–15% [Ariskin and Barmina, 2000]. Thus, the forsterite contents observed in natural olivines are shifted relative the initial characteristics by at least a few mol percent. However, in reconstructing the initial conditions, one can use the composition of natural *Pl* crystals, whose cores practically do not change their composition during the postcumulus stage because of the low diffusivity of major components.

Another constraint is concerned with the necessity of estimating total pressure and oxygen fugacity during the emplacement of the parental magma. This is, however, not so crucial for the thermometry of *Ol–Pl* assemblages, because both minerals have roughly similar dependences of their liquidus temperature on pressure (5–7 °C/kbar), and the effect of oxygen fugacity on the olivine composition is within the accuracy of the geothermometers (~0.5 mol % *Fo*/log unit of f_{O_2}, [Ariskin and Barmina, 2000]). Data on mineral assemblages from the contact aureole of the Kiglapait intrusion made it possible to evaluate fairly reliably the pressure under which the parental magma was intruded (2.2–2.3 kbar [Morse, 1990]). Thermodynamic calculations for the observed *Mt–Ilm* assemblages indicate that the redox conditions in the Lower Zone were close to those of the wuestite–magnetite oxygen buffer [Morse, 1980].

In simulating the model liquid lines of descent, we assumed a pressure of 2.2 kbar and redox conditions corresponding to the WM buffer. The calculations were conducted successively as the total percentage of the crystallizing phases for the molten rocks was increased (Table 18). The maximum crystallinity of the modeled systems did not exceed 70–80%, which corresponded to 20–30% intercumulus liquid.

Crystallization sequence. The simulated crystallization sequence of minerals is in good agreement with the initial rock compositions and demonstrates an extended field of *Ol* for the most magnesian sample (KI3223), early *Pl* crystallization for the three aluminous compositions (KI3224, KI3649, and KI3230), and subcotectic relations between olivine and plagioclase for both samples from the Inner Border Zone.

$$\text{KI3223, LZ: } Ol_{89.5}(1343^\circ\text{C}) \longrightarrow Ol_{86.5} + Pl_{70.8}(1258^\circ\text{C}, 11\%) \longrightarrow Ol_{72.5} + Pl_{65.6}(1219^\circ\text{C}, 80\%),$$

$$\text{KI3224, LZ: } Pl_{75.0}(1301^\circ\text{C}) \longrightarrow Ol_{87.6} + Pl_{70.5}(1263^\circ\text{C}, 18\%) \longrightarrow Ol_{74.1} + Pl_{64.7}(1219^\circ\text{C}, 80^\circ\text{C}),$$

$$\text{KI3649, LZ: } Pl_{81.9}(1365^\circ\text{C}) \longrightarrow Ol_{81.4} + Pl_{70.5}(1236^\circ\text{C}, 51\%) \longrightarrow Ol_{67.4} + Pl_{65.4}(1174^\circ\text{C}, 80\%),$$

$$\text{KI3230, LZ: } Pl_{73.5}(1291^\circ\text{C}) \longrightarrow Ol_{84.3} + Pl_{68.4}(1249^\circ\text{C}, 17\%) \longrightarrow Ol_{68.5} + Pl_{59.2}(1183^\circ\text{C}, 80\%),$$

$$\text{KI3567, IBZ: } Ol_{81.1} + Pl_{67.6}(1235^\circ\text{C})$$

$$\longrightarrow Ol_{63.0} + Pl_{57.3}(1146°C, 72\%),$$

KI3623, IBZ: $Ol_{85.4}(1269°C) \longrightarrow Ol_{84.3}$

$+ Pl_{68.7}(1249°C, 3\%) \longrightarrow Ol_{68.5} + Pl_{58.3}(1174°C, 77\%).$

The main characteristic feature of the calculated sequences is the long-lasting concurrent crystallization of *Ol* and *Pl*, which is recorded in the modal composition of samples from the Lower Zone and explains the abundance of troctolites in the Kiglapait intrusion as a whole (Fig. 52). It is interesting that clinopyroxene does not crystallize from troctolite melts even if they have an 80% crystallinity, and the melt has a fairly high temperature (1174–1219°C). This led us to suggest that the initial troctolite mixtures were assemblages of *Ol* and *Pl* crystals coexisting with melt, which was far from saturation with respect to *Aug* and Fe–Ti oxides. These considerations find further support in the modeled liquid lines of descent.

The compositional evolution of the model melts is shown in Fig. 53. Thin lines denote the trajectories of the six selected samples, the heavy line corresponds to the evolutionary trajectory of the KIGLAP weighted mean composition, and the dashed line represents MAR contact rocks. It can be readily seen that the model trajectories of individual rocks converge and intersect at temperatures of about 1240°C. This value should be regarded as the upper limit for the possible temperature of the parental magma, and it is close to the estimate of 1250°C in [Morse, 1979a]. At the same time, the evolutionary lines diverge in *T–X* diagrams at temperature below 1220°C, and, hence, this value can be assumed as the minimum estimate for the initial temperature. The interval of 1220–1240°C is identified fairly reliably, and we believe that the average value of $T = 1230 \pm 10°C$ is the most acceptable as the initial temperature of the Kiglapait magma [Barmina and Ariskin, 2002]. This result (obtained for $P = 2.2$ kbar) is consistent with experimental data on the "primitive" troctolite, which point to its liquidus temperature at 5 kbar equal to 1245°C [Morse *et al.*, 2003].

After estimating the temperature of magma emplacement, it is possible to calculate the composition of the liquid part of the parental magma as an average of the six model melts corresponding to the initial equilibrium at 1230°C. This composition is presented in Table 19 and is demonstrated in Fig. 53 (denoted by an open circle) and can be defined as high-Al ferrobasalt or Al–Fe troctolite magma, considering the low contents of normative diopside in such melts [Olson and Morse, 1990].

Mineral chemistry. Inasmuch as all model trajectories in Fig. 53 represent (at 1230°C) the *Ol* + *Pl* assemblage, the compositions of these cotectic minerals are also assumed to approximate the initial characteristics for the Kiglapait magma. A calculation of the average mineral compositions for this temperature gives 66.7 ± 1.6 mol % *An* in *Pl* and 78.8 ± 1.0 mol % *Fo* in *Ol* (Table 19). This estimate for the compositions of the original plagioclase crystals is in excellent agreement with the data of natural observations (Fig. 51) and experiments [Morse *et al.*, 2003]. At the same time, the calculated composition of olivine was found to be nota-

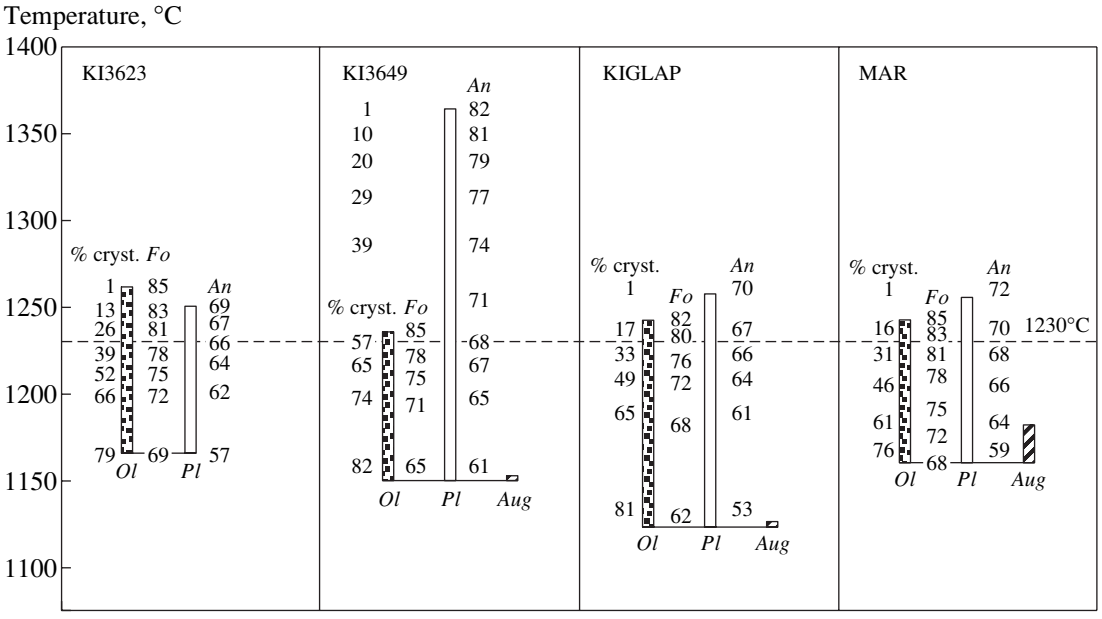

Fig. 52. Crystallization sequence and the evolution of the chemistry of minerals for four troctolites, weighted mean composition of the Kiglapait intrusion (KIGLAP), and the average composition of the marginal rocks (MAR) of the Kiglapait intrusion. The calculations were conducted with the COMAGMAT-3.65 program for a pressure of 2.2 kbar and WM buffer redox conditions [Barmina and Ariskin, 2002]. The rock compositions and the average compositions are given in Table 18. The dashed line corresponds to the estimated emplacement temperature of the Kiglapait parental magma (Fig. 53).

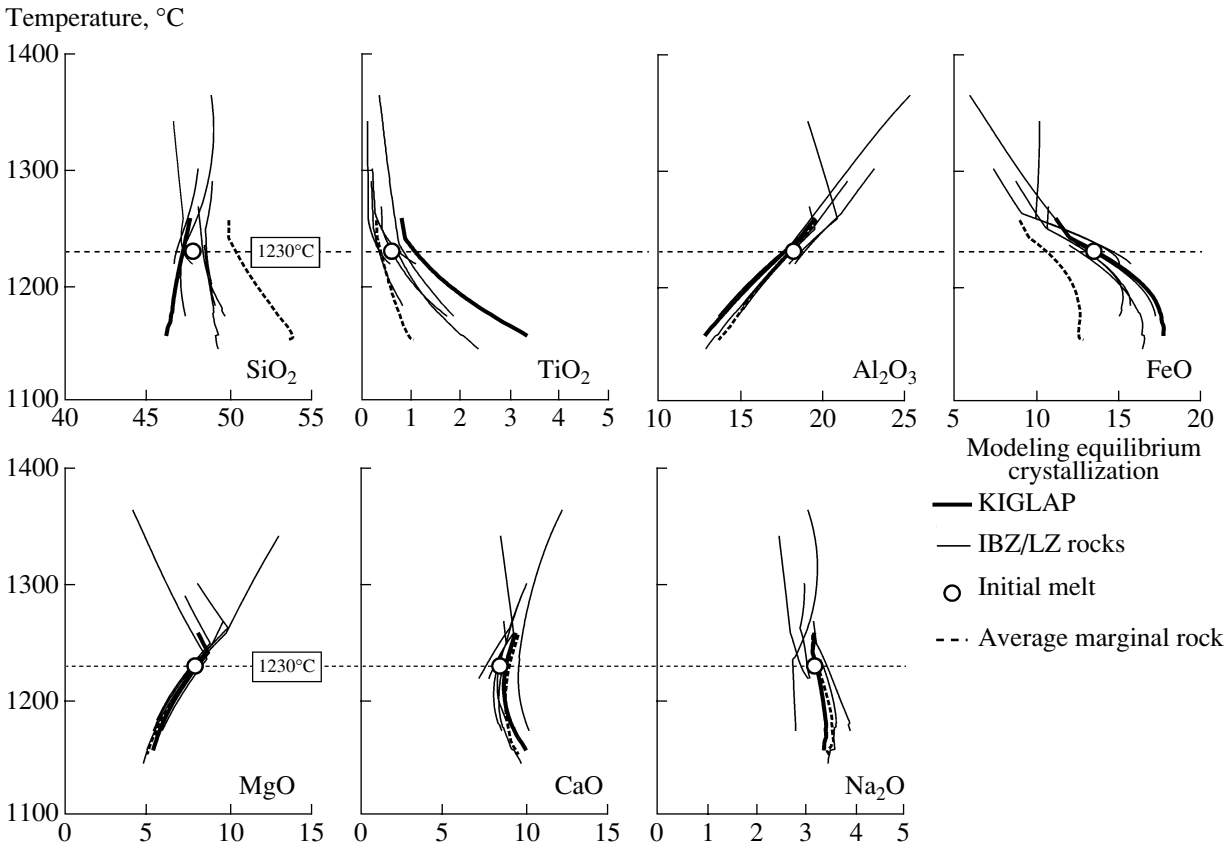

Fig. 53. Evaluated temperature and composition of the magmatic melt representing the liquid constituent of the Kiglapait parental magma. The assumed value of the initial temperature (1230°C) corresponds to the range of convergence and intersections of the calculated liquid lines of descent for the six samples selected (Table 18). The heavy line and dashed line denote the evolutionary trajectories for the weighted mean composition of the intrusion (KIGLAP) and the average composition of the contact rocks (MAR).

bly more magnesian. This is an expectable result, caused mostly by the re-equilibration of the primary crystals during the postumulus stage (see modeled *Ol* compositions in Fig. 51 at a crystallization degree of 80%).

Phase composition of the parental magma. Using the example of the Partridge River intrusion, we have demonstrated that phase equilibrium simulations enable calculations of the modal proportions of crystals and melt in the parental magma. Applying the same approach to the Kiglapait intrusion, we utilized the liquid lines of descent calculated for the weighted average composition of the intrusive body and the probable emplacement temperature of the magma estimated above. Note that the weighted average composition was assumed to correspond to that of the Layered Series (Table 18).

The results of simulations with the COMAGMAT-3.65 program for the KIGLAP composition at a pressure of 2.2 kbar and WM buffer conditions are presented in Table 19 (right-hand column). The modeled *Ol* and *Pl* compositions at 1230°C practically coincide with the compositions calculated for individual rocks, and the Kiglapait magma was concluded to have come into the chamber carrying approximately 25% crystals, mostly plagioclase (20 wt %) and subordinate olivine (~5%). This estimate of the original magma crystallinity can be utilized to evaluate the position of the boundary between the cumulates predominated by intratelluric phases and the cumulates including mineral grains that crystallized in the chamber [Barmina and Ariskin, 2002].

Obviously, at 100% separation and compaction of the primary crystals, the upper boundary of the primary cumulus should correspond to approximately 25% PCS. If the average cumulus crystallinity was 60% (40% intercumulus melt), then the boundary supposedly corresponding to the complete precipitation of the primary crystals should have shifted to 40%. Thus, it is realistic to suggest that the first minerals that were crystallized in the magma chamber appeared in the cumulus starting from a level corresponding to ~40% PCS. This seems to have been responsible for the fast compositional evolution of *Ol* and *Pl* in the upper half of the Lower Zone (Fig. 51).

The role of chilled contact rocks. The medium- and fine-grained gabbroids found in the 1980s near the southern contact of the Kiglapait intrusion with the

Table 19. Chemical and phase characteristics of the parental magma of the Kiglapait intrusion

Component	Results of geochemical thermometry for individual rocks	Simulations for the KIGLAP weighted mean composition
Initial melt composition (wt %) at 1230°C		
SiO_2	47.77 (0.74)	47.17
TiO_2	0.61 (0.19)	1.08
Al_2O_3	18.21 (0.45)	17.70
FeO	13.43 (0.76)	13.51
MnO	0.18 (0.02)	0.19
MgO	7.89 (0.20)	8.03
CaO	8.36 (0.61)	8.73
Na_2O	3.15 (0.31)	3.19
K_2O	0.38 (0.08)	0.28
P_2O_5	0.03 (0.01)	0.12
Original compositions of suspended minerals (mol %)		
Pl	$An_{66.7 \pm 1.6}$	$An_{66.6}$
Ol	$Fo_{78.8 \pm 1.0}$	$Fo_{79.0}$
Phase composition (wt %) of the magma		
Melt	100.0	75.2
Pl	–	20.0
Ol	–	4.8

Note: The geochemical thermometry data are average estimates calculated from the simulation results on phase equilibria for the melts of marginal rocks and primitive troctolites (Table 18); numerals in parentheses correspond to the standard deviations (1σ). For the parental magma (KIGLAP composition), the table lists the composition of its liquid constituent and the relative proportions of the original melt and crystals at the calculated magma emplacement temperature.

Nain anorthosites had chemical parameters approaching the weighted mean composition of the Layered Series [Nolan and Morse, 1986]. This provided grounds to regard these rocks as the chilled marginal facies approximating the composition of the magma that produced the intrusive body. One of the contact-rock samples (KI3763) was used in equilibrium melting experiments to determine the phase proportions in the temperature range of 1192–1250°C at 1 atm pressure [Blundy, 1997]. It was determined that the liquidus assemblage consisted of *Ol* and *Pl*, which should have crystallized at approximately 1240°C (as is approximated for pressures of about 2 kbar). This is in good agreement with the geochemical thermometric estimates. However, the composition of the first crystals of olivine ($Fo_{82–85}$) and plagioclase ($An_{72–74}$) turned out to be notably more primitive than those in rocks in the lower part of the Kiglapait intrusion (Fig. 51). This left uncertain whether the fine-grained facies could be employed as an approximation of the parental Kiglapait magma.

We simulated the equilibrium crystallization of four compositions of the contact gabbroids [Nolan and Morse, 1986] and the average composition of these rocks (MAR, Table 18). The main characteristics of the generalized MAR crystallization trajectory under a pressure of 2.2 kbar and WM redox conditions are presented in Figs. 52 and 53. As can be seen from these data, there are principal differences that make it impossible to interpret the contact facies as the "parental liquid." First, contrary to the determined troctolitic melts (Table 19), the MAR composition is characterized by early augite crystallization, which starts to crystallize at 1178°C at a model crystallinity of 60 wt % (Fig. 52). Second, at the estimated initial temperature of 1230°C, the "generalized" course of crystallization yields about 15% of the troctolite assemblage (Fo_{83} + An_{69}), which is notably different from the natural assemblages (these data differ from them more significantly than the results of geochemical thermometry do). Finally, the liquid lines of descent for MAR definitely indicate that the rocks represent a system oversaturated with respect to SiO_2 and depleted in FeO relative to the parent of the Kiglapait rocks calculated by means of geochemical thermometry (Fig. 53).

3.2.4. Main results on other intrusions

The method of geochemical thermometry of the marginal rocks and weighted mean compositions of intrusive bodies was also utilized to evaluate the phase and chemical characteristics of the parental magmas for the Kamenistyi sill in eastern Kamchatka [Barmina *et al.*, 1989a], Talnakh intrusion in the northwestern Siberian Platform [Krivolutskaya *et al.*, 2001], and the Ioko-Dovyren pluton in northern Transbaikalia [Ariskin *et al.*, 2003]. These bodies have different compositions (from high-alumina diabases to ultramafics) and thicknesses (from 100 m to 3.2 km), but thermometric data for all of them yield a narrow range of magma emplacement temperatures (1170–1200°C) corresponding to a significant initial magma crystallinity for each intrusion (from ~15 to 50 wt %). These results are similar to the data presented above for the Partridge River and Kiglapait intrusions and led us to conclude that the magma emplacement processes and the strong heterogeneity of the original magmatic material are interrelated [Ariskin *et al.*, 2002].

The Kamenistryi sill was discovered among several weakly differentiated bodies exposed in a small mountain spur along the left bank of the Kamenistaya River near its mouth in Cape Kronotskii, Eastern Kamchatka [Barmina *et al.*, 1989a]. The bodies affiliate with the subvolcanic facies of the Paleogene–Eocene Kronotskaya Group, whose volcanic part includes numerous flows of pillow lavas and hyaloclastic rocks of plagiophyric tholeiite basalts, ferrobasalts, ferrobasaltic andesites, and ferroandesites [Khubunaya, 1987].

The Kamenistyi sill is approximately 200 m thick and consists of high-alumina diabases. Its top portion

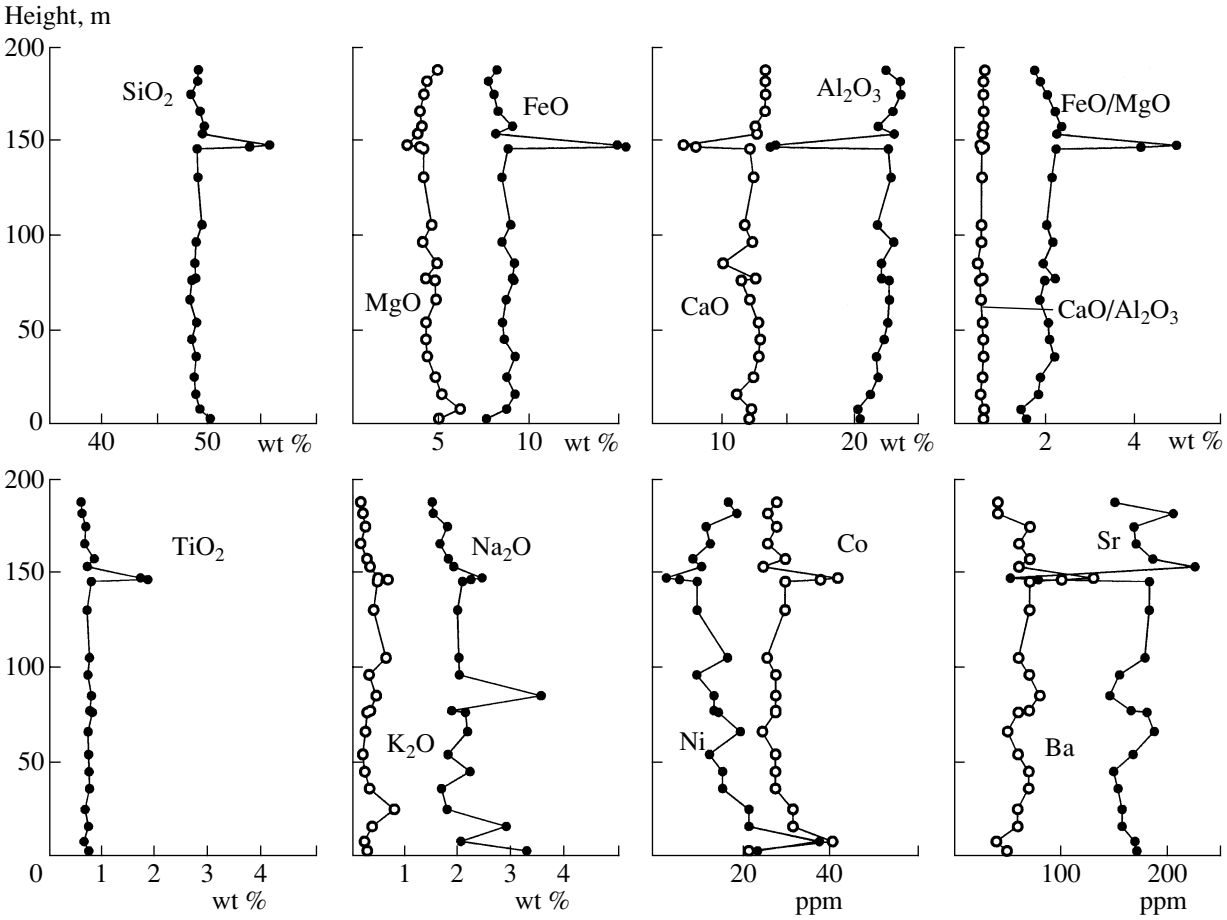

Fig. 54. Variations in major-component and trace-element concentrations and petrochemical ratios in the cross section of the Kamenistyi sill [Barmina *et al.*, 1989a].

includes a layer of magnetite gabbro and ferrodiorites. Of the 24 samples taken from the stratigraphic succession, 15 characterize a 140-m interval of continuous (practically without interruptions) exposures extending upward from the lower contact. The weighted mean composition of the sill (22 wt % Al_2O_3, 4.3 wt % MgO) is close to high-alumina basalt of the Kronotskaya Group [Ariskin and Barmina, 2000].

Mineral chemistry and cryptic layering. Microprobe analyses of plagioclase phenocrysts and large laths indicate that the composition of plagioclase cores varies from An_{79} to An_{91}, and the margins are made up of $An_{65–75}$. The contact rocks of the Kamenistyi sill also contain occasional olivine grains that are fully pseudomorphed and cannot be used to estimate the composition of this mineral. According to petrographic observations, clinopyroxene and magnetite were intercumulus phases crystallized in the rocks of the lower part *in situ*.

Data on major and trace elements indicate that this stratiform body has a cryptic layering at insignificant variations in the major-element concentrations (Fig. 54). These variations are most coherent in the behavior of Ni, demonstrating a monotonous decrease in contents from the bottom toward the ferrodiorite layer and then becoming again roughly equal to the original values near the upper contact. This situation is typical of differentiated traps in the Siberian Platform and was explained by the redistribution and fractionation of *Ol* crystals [Frenkel *et al.*, 1988b, 1989].

These observations led us to hypothesize that the parental magma of the Kamenistyi sill was a heterogeneous mush, strongly enriched in *Pl* crystals at a subordinate amount of *Ol*. The liquid constituent of the magma corresponded to the "tholeiitic" *Ol–Pl* cotectic but not a high-alumina liquid, as could be inferred from the mean intrusion composition. To test this hypothesis, we calculated and compared liquid lines of descent for the weighted mean composition of the Kamenistyi sill and a contact-rock sample relatively enriched in MgO (6.1 wt %) and Ni.

Results of geochemical thermometry. The simulations were conducted using one of the earlier COMAGMAT versions for $P = 1$ atm and redox conditions corresponding to the WM buffer [Barmina *et al.*, 1989a]. Both trajectories show strong oversaturation with respect to plagioclase and the coincidence of trajecto-

Table 20. Modeled parameters of the parental magmas of differentiated sills and large layered intrusions

Component	*VAV*, 1195°C	*TALN*, 1200°C	*KAM*, 1170°C	*PRI*, 1167°C	*SKA*, 1165°C	*DOV*, 1185°C	*KIGL*, 1230°C
SiO_2	49.54	48.75	49.71	47.28	50.01	55.00	47.17
TiO_2	1.19	1.30	1.39	2.69	1.68	0.74	1.08
Al_2O_3	15.57	15.42	14.76	15.80	12.95	15.52	17.70
FeO	11.18	12.00	14.75	16.24	13.24	7.58	13.51
MnO	0.28	0.22	0.26	0.20	0.19	0.14	0.19
MgO	7.91	7.94	6.64	5.67	6.90	7.33	8.03
CaO	11.72	11.43	10.13	8.02	12.40	10.80	8.73
Na_2O	2.12	2.16	1.74	2.86	2.37	1.72	3.19
K_2O	0.36	0.65	0.41	0.97	0.26	1.08	0.28
P_2O_5	0.13	0.14	0.21	0.28	0.15	0.08	0.12
Original crystal-melt proportions, wt %							
Ol (*Fo*)	0.3 (81)	11.3 (80)	0.7 (74)	18.9 (68)	nd (74)	46.5 (85)	4.8 (79)
Pl (*An*)	1.8 (80)	2.7 (78)	41.3 (75)	38.3 (66)	nd (63)	4.6 (80)	20.0 (67)
Total	2.1	14.0	42.0	57.2	nd	51.1	24.8

Note: Intrusions: *VAV*—Vavukan (upper reaches of the Vilyui River, eastern Siberia, thickness h = 100 m [Frenkel *et al.*, 1988b]), *TALN*—Talnakh (northwestern Siberian Platform, h ~ 150 m [Krivolutskaya *et al.*, 2001]), *KAM*—Kamenistyi (Cape Kronotskii, Eastern Kamchatka, h = 200 m [Barmina *et al.*, 1989a]) *PRI*—Partridge River (Minnesota, United States, h = 500 m [this study]), *SKA*—Skaergaard (East Greenland, LS has h = 2.5 km [Ariskin, 1999]), *DOV*—Ioko-Dovyren (northern Transbaikalia, h = 3.2 km [Ariskin *et al.*, 2003]), *KIGL*—Kiglapait (Labrador, h = 9 km [Barmina and Ariskin, 2002]).

ries for most major elements. However, the liquid lines of descent for MgO and Ni exhibit a clear-cut intersection near 1170°C. The composition of the liquid was found to correspond to the *Ol* + *Pl* cotectic and is close to the comagmatic ferrobasalts of the Kronotskaya Group (Table 20, composition KAM). With regard to the relative accuracy of thermometry, the overall crystallinity of the parental magma was estimated to be 42 ± 3 wt %. The intratelluric phase consisted nearly entirely of plagioclase, and the content of primary olivine crystals did not exceed 1 wt %.

The model composition of the "equilibrium" *Pl* crystals (An_{75}) is 5–10% poorer in anorthite than the cores of large phenocrysts. This was due to calculations with an early plagioclase-melt equilibrium model [Drake, 1976b] (see section 2.2.4). The calculated olivine composition corresponds to Fo_{74}. Thus, the main outcome of geochemical thermometry can be formulated as the conclusion that the Kamenistyi parental magma had a temperature of ~1170°C and was a mush with slightly more than 40% *Pl*, approximately 1% *Ol*, and 57 ± 3% ferrobasaltic melt. The accumulation of these early olivine crystals near the bottom of the magma chamber (according to calculations, up to 6 wt % *Ol*) resulted in rocks relatively enriched in MgO and Ni. This can be regarded as "geochemical evidence" that the parental magma contained a cotectic (*Ol* + *Pl*) melt, in spite of the very high bulk alumina content in the magma.

Talnakh intrusion. This intrusion is one of the most famous ore-hosting massifs in the Noril'sk district in the northwestern part of the Siberian Platform. The body is a chonolith with a smoothly convex bottom. The intrusion was traced for 20 km and has a width of 0.5–2 km at a thickness varying from approximately 100 to 200 m [Ryabov *et al.*, 2000]. It has a layered inner structure with systematic changes in cumulus rocks in the vertical cross section. This succession of rocks is commonly represented in the form of the following three major units: Lower Gabbroid Series (LGS), Layered Series (LS), and Upper Gabbroid Series (UGS) [Krivolutskaya *et al.*, 2001]. The LGS comprises contact and taxitic gabbrodolerites; the LS is made up of picrite, olivine, olivine-bearing, and olivine-free gabbrodolerites; and the UGS consists of gabbroids, ferrogabbro, upper contact gabbrodolerites, leucogabbro, and more rare rock varieties. This rock sequence is characteristic of the central portions of the intrusion, whose marginal parts contain no picritic gabbrodolerites and are thus less variable.

The lowermost third of the massif (LGS + the bottom of LS) is the most contrasting compositionally and consists of olivine-rich rocks (up to 50–60 vol % *Ol*) and leucogabbro containing up to 70 vol % *Pl*. These plagioclase-rich gabbroids are characterized by very heterogeneous textures and are commonly referred to as taxitic gabbrodolerites in the literature in Russian or simply as taxites. We draw attention to this fact because the method of geochemical thermometry yields the most reliable results for these rocks of contrasting modal and chemical compositions [Ariskin and Barmina, 2000].

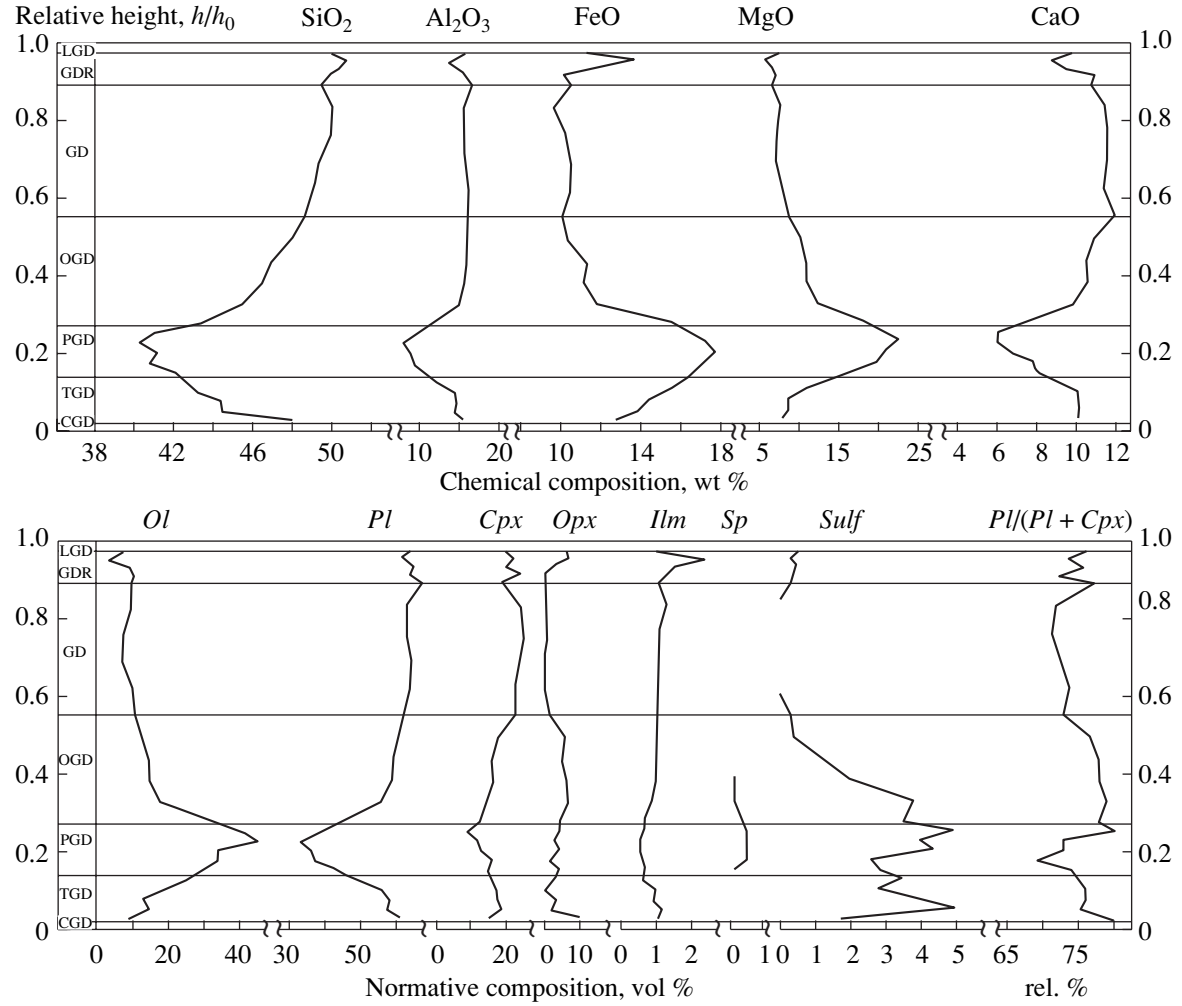

Fig. 55. Variations in the major-component contents and normative compositions of rocks in a generalized cross section of the Talnakh intrusion [Dneprovskaya and Dneprovskii, 1988]. Gabbrodolerites: CGD—contact gabbrodolerites, TGD—taxitic gabbrodolerites, PGD—picritic gabbrodolerites, OGD—olivine gabbrodolerites, GD—olivine-free gabbrodolerites, LGD—leucocratic gabbrodolerites; GDR—granodiorite.

Mineral chemistry and cryptic layering. Here we briefly discuss the variations in the composition of olivine and plagioclase, the two principal minerals that are thought to have been present on the liquidus of the Talnakh magma [Krivolutskaya *et al.*, 2001]. The composition of olivine is systematically varied in different zones of the massif. The maximum *Fo* contents (about 80 mol %) were detected in the taxitic layer, with this mineral containing 75–78 mol % *Fo* in the overlying picritic gabbrodolerites. This parameter continued to decrease to ~70 mol % in the olivine gabbrodolerites and to ~60% near the boundary with olivine-free rocks. The composition of the cumulus *Pl* (large tabular laths) varies from $An_{75–84}$ in the taxitic, picritic, and olivine gabbrodolerites to $An_{56–39}$ in the gabbrodiorites. The intercumulus plagioclase shows smaller variations, approximately from An_{62} to An_{47}.

The variations in the bulk-rock chemistry over the vertical section of the Talnakh intrusion are consistent with the known inner chemical patterns of Siberian trap intrusions [Frenkel *et al.*, 1988b] but differ from them in having higher Mg-O (Fig. 55). These variations are characterized by S-shaped profiles of the MgO, FeO, and Cr_2O_3 distribution with a maximum in the picritic gabbrodolerites (the behavior of Ni is complicated by the abundance of sulfides). The distribution of incompatible elements is characterized by a drastic decrease in the picrite layer and a progressive enrichment at higher levels. The CaO and Al_2O_3 contents also have a clear minimum in the picrites and then increase toward the intrusion roof. All of these features point to a significant role of the redistribution of the intratelluric crystals and further magma fractionation in the chamber.

Inasmuch as our primary task was to determine the original parameters of the Talnakh magma, the following research was centered mostly on the lower part of the massif, from the contact taxites to picritic gabbrod-

olerites with the maximum MgO contents. These layers are characterized by significant variations in the chemistry of the rocks at the SiO_2 contents varying within 5 wt %, Al_2O_3 within ~10 wt %, MgO ~ 15 wt %, and FeO and CaO ~ 7 wt %. These variations could be produced early during the solidification of the intrusive magma by means of the sorting of primary crystals simultaneously with the insignificant fractionation of the original melt. As follows from previous sections, this situation is genetically informative and corresponds to the conditions formulated for the applicability of the geochemical thermometry method.

Results of geochemical thermometry. The geochemical thermometric calculations were conducted using the compositions of 23 gabbrodolerites from three representative drillholes. Modern versions of the COMAGMAT program do not allow for the occurrence of sulfides in the rocks, and this can lead to distortions in the stability fields of minerals and shifts in the model liquid lines of descent. Because of this, the raw chemical analyses should be recalculated to correct the FeO content in the silicate matrix (sulfides are subtracted). The technique of such calculations, based on the overall contents of sulfur and base metals, was described in detail in [Krivolutskaya *et al.*, 2001].

The phase equilibria in the corrected compositions were simulated for a pressure of 0.5 kbar and QFM–0.5 redox conditions. The total water content in the taxites and picrites was assumed to be on the order of 0.1 wt %, which ensured water undersaturation in the melts when they were at 0–70% crystallization [Al'meev and Ariskin, 1996]. The crystallization trajectories were constructed in a successive manner, according to an increase in the degree of magma crystallinity with a crystallization increment of 1 mol %. The maximum crystallinity of the model system did not exceed 80% (20% trapped liquid).

Liquidus *Ol* was identified in 19 of the 23 crystallization sequences at 1250–1540°C. The second phase to crystallize was always *Pl* (at a maximum temperature of 1255°C), and clinopyroxene (*Aug*) was the third. In four compositions, *Ol* and *Pl* crystallized simultaneously at 1200–1235°C. The initial *Aug* crystallization temperature never exceeded 1189°C. An analysis of the liquid lines of descent and a comparison of the simulated and natural *Ol* and *Pl* compositions led us to conclude that the probable temperature of Talnakh magma intrusion was close to 1200°C. The calculated composition of the liquid part of the parental magma appeared to be close to the composition of the contact gabbrodolerites and corresponded to cotectic (*Ol* + *Pl*) tholeiitic ferrobasalt slightly enriched in potassium. The liquid contained approximately 8 wt % MgO and, hence, was more magnesian than the "normal" Siberian dolerite but still a little bit less magnesian than the level of 10–12% commonly thought to determine the picrite-basaltic character of the initial Siberian trap magmas. The calculated average compositions of the intratelluric phases at 1200°C are 81.3 ± 1.1 mol % *Fo* in *Ol* and 80.5 ± 2.4 mol % *An* in *Pl*. These evaluations are in good agreement with the microprobe data.

In order to estimate the phase composition of the parental magma, we carried out simulations for three compositions corresponding to the weighted mean estimates for Talnakh rocks [Dneprovskaya *et al.*, 1987; Czamanske *et al.*, 1995; Krivolutskaya *et al.*, 2001]. In all instances, the calculation results exhibited good agreement between the model liquid compositions at 1200°C at slightly different amounts of equilibrated *Ol* and *Pl* crystals. According to these data, at the moment of its emplacement, the Talnakh magma contained from 7 to 11 wt % intratelluric *Ol* and 3–4% *Pl* phenocrysts. Table 20 reports the chemical and phase characteristics of the original magmatic material calculated for one of the weighted mean compositions [Czamanske *et al.*, 1995].

The Ioko-Dovyren (or Dovyren) dunite–troctolite–gabbronorite pluton is one of the most typical and exhaustively studied layered intrusions in northern Transbaikalia. In spite of its Late Precambrian age (~700 Ma), this intrusion was not metamorphosed and is convenient for petrological–geochemical research [Yaroshevsky *et al.*, 1982; Konnikov, 1986; Kislov, 1998]. The pluton is topographically expressed as mounts Ioko and Dovyren, which are separated by the valley of the Ondoko River (right-hand confluent of the Tyya River). This is a lens-shaped body ~26 ± 3 km. According to geophysical data, it was traced for 4–5 km downward from the modern surface and gradually tapers with depth. The massif is subconformable with its country rocks along the dip and strike (which is nearly vertical because of postmagmatic folding).

The structure of the intrusion varies along its strike. Its central portion (Mount Dovyren) consists of a thick ultramafic body, whereas its southwestern termination (Mount Ioko) is dominated by gabbroids. The phase (modal) layering of the intrusion was thoroughly examined in the ultramafite–mafite part. The main rock types and general succession are usually recognized on the basis of cumulus mineral assemblages [Mironov *et al.*, 1980]. According to these data, the massif was subdivided into a layer of Bottom Plagioperidotites (PP) and five major zones (Fig. 56), corresponding to the upward variations in the cumulus assemblages: *Ol* + *Chr* (Zone A) ⟶ *Ol* + *Pl* + *Chr* (Zone B) ⟶ *Pl* + *Ol* + *Cpx* (Zone C) ⟶ *Pl* + *Ol* + *Cpx* ⟶ *Opx* (Zone D) ⟶ *Pl* + *Opx* + *Cpx* (Zone E). This generalized succession is complicated by thinner intercalations and the cyclic layering of various rock types, often with more "primitive" assemblages overlying more "evolved" ones.

The reader can find a detailed description of these zones in [Ariskin *et al.*, 2003], and here we touch solely upon the Bottom Plagioperidotites, which are of principal importance for further thermometric reconstructions. These rocks are plagioclase lherzolites and com-

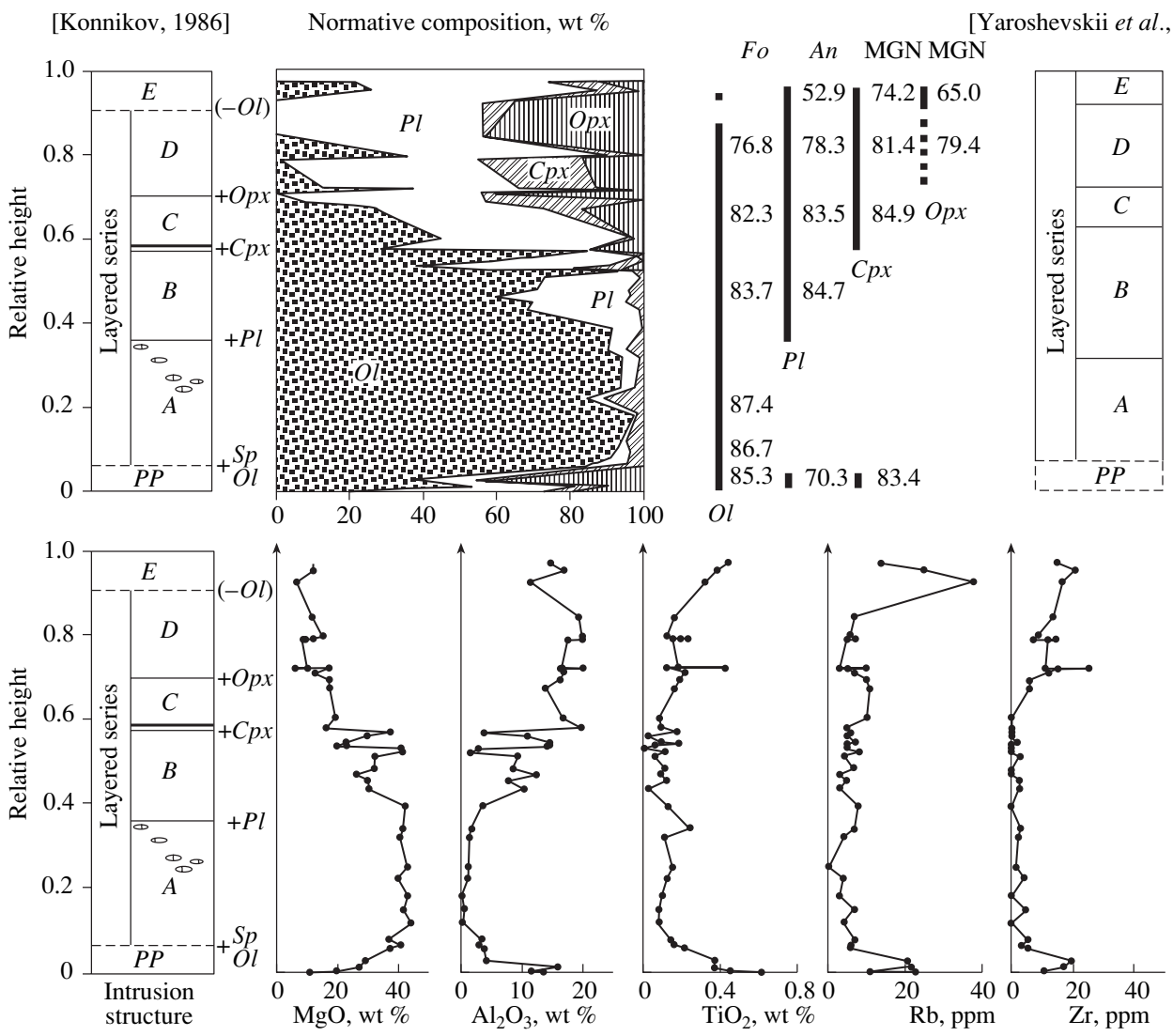

Fig. 56. Principal structural units of the Dovyren intrusion and its mineralogical–geochemical features (after [Yaroshevsky *et al.*, 1982; Konnikov, 1986; Kislov, 1998]). The heavy line in Zone *C* marks the horizon of polysulfide–PGM mineralization.

pose a layer from 160 to 270 m thick. The rocks consist of three cumulus minerals (*Ol* + *Pl* + *Cpx*), with the interstitial space accommodating orthopyroxene and phlogopite. The interstitial minerals occur as oikocrysts with poikilitic inclusions of cumulus minerals, and orthopyroxene commonly corrodes olivine. Because of variations in the proportions of cumulus minerals, the plagioperidotites are sometimes weakly differentiated and grade into olivine gabbronorites and gabbro or, when chilled in contact zones, into picrite-basalts and picrite-dolerites (ophitic gabbro). Chemically, the plagioperidotites are close to the weighted mean composition of the massif.

Mineral chemistry and cryptic layering. Figure 56 demonstrates the tendencies in the compositional variations of the principal cumulus minerals (*Ol*, *Pl*, *Px*) over the cross section of the Layered Series of the Dovyren Massif. These data are average values, which were calculated for each zone based on the data in [Konnikov, 1986]. The Layered Series of the pluton ($A \longrightarrow B \longrightarrow C \longrightarrow D$) is characterized by insignificant variations in the composition of *Ol* (10–12 mol % *Fo*) and *Pl* (~7 mol % *An*) at a systematic decrease in the contents of refractory components upward to the roof. Small changes in the main mineral compositions are very unusual for intrusive magmas. Therewith, the distribution of *Fo* in olivine in the lower part of the dunite layer and plagioperidotites seems to be anomalous. There is an obvious tendency toward upward forsterite enrichment with the transition from the plagoperidotites (85.3 ± 1.4 mol % *Fo*, $n = 11$) to the lower plagiodunites (86.7 ± 1.6 wt %, $n = 15$) and the main dunite zone (87.4 ± 1.5, $n = 60$). This is inconsistent with the normal magma differentiation trends. There are different explanations for such deviations, which result in

different estimates of the primary olivine composition (~Fo_{85} or ~Fo_{87} [Ariskin *et al.*, 2003]). Initially we assumed that the plagioperidotites and chilled contact rocks are inherent members of the Dovyren rock succession, and the earliest (closest to equilibrium) *Ol* crystals had the composition $Fo_{84–85}$, as in the bottom plagioperidotites. The composition of the first liquidus plagioclase crystals seemed to fall into the range of 80–85% *An*.

Some features in the compositional evolution of the rocks are shown in Fig. 56. According to the modal composition of the cumulates, the MgO distribution is controlled by the amount of *Ol* (in the dunites, plagiodunites, and troctolites) and pyroxenes (in the gabbroids), while the Al_2O_3 distribution is controlled by plagioclase. The CaO content sharply increases in the gabbroids, which is correlated with the appearance of cumulus *Aug* but is controlled mainly by an increase in the *Pl* to *Ol* proportion. Another unusual feature of these rocks is an insignificant decrease in the MgO content in the uppermost differentiates, so that the rocks of Zone E contain 10 wt % MgO [Mironov *et al.*, 1980]. Given the insignificant variations in the mineral chemistry (see above), this suggests that there was no efficient fractionation of mafic silicates during the final solidification stages of the Dovyren magma. At the same time, the narrow range of variations in the mineral chemistry may be suggestive of processes like compositional convection of the primitive melt in the cumulus, a process that could have modified the primary composition of the later (more fractionated) differentiation products.

The possibility of postcumulus migration and reequilibration of the pore liquid follows from the behavior of some incompatible elements (Fig. 56). As is exemplified by Ti, Rb, and Zr, their distribution in the vertical section of the massif has an S-shaped configuration with apparent concentration maxima in the bottom plagioperidotites and rocks near the roof. Conversely, the dunites and troctolites are characterized by low concentrations of these elements (they decrease by factors of five to ten), with clear minima of Ti and Zr in Zone *B*. Analyzing the behavior of Ti and Zr, we assumed that the amount of the intercumulus melt was at a minimum in the troctolite zone and was prone to increase downward across the dunite zone toward the bottom plagioperidotites. Thus, the example of the Dovyren intrusion also provides evidence that crystals and melt were redistributed starting from the very early stages of magma solidification. This magma seems to have entrained abundant *Ol* crystals, whose settling in the chamber was coupled with the compaction of the cumulus and the migration of its interstitial liquid. The proportions of the crystals and melt in the parental magma were evaluated by means of thermometric calculations for a number of individual rock compositions and the average composition of the Dovyren rocks [Ariskin *et al.*, 2003].

Selection of initial compositions and simulation conditions. To simulate the original phase equilibria, we selected nine compositions of the contact rocks that corresponded to either individual rock varieties or average compositions from the inner contact zone and from the bottom plagioperidotites. Additionally we used a weighted mean composition of the central portion of the massif (from [Mironov *et al.*, 1980]). Note that the use of average compositions instead of those of naturally existing rocks should not significantly affect the final results of thermodynamic simulations if the same composition of the intercumulus liquid is assumed for the rocks selected. This follows from Eqs. (81) and (82), which demonstrate that these "model rocks" can be expressed as a mechanical mixture of the same assemblages with different proportions of cumulus phases and the same melt. A more serious problem is the possible modification of the original chemical characteristics as a consequence of later oxidation, the effect of fluids, and assimilation processes near the contacts of the intrusion. Here we relied on the remarkable ability of geochemical thermometry to reject crystallization trajectories that significantly deviate from the "main" bundle of cotectic lines [Ariskin and Barmina, 2000].

The liquid lines of descent of each composition were constructed by the COMAGMAT-3.52 program for a pressure of 0.5 kbar and an oxygen fugacity corresponding to the WM buffer. These initial conditions are determined by the emplacement depth of the Dovyren Massif (~1.5 km) and the absence of magnetite in the observed cumulus assemblages. The parental magma was assumed to have been "anhydrous." Given the presence of phlogopite in the bottom plagioperidotites and the significant serpentinization of the dunite layer, this seems unexpected. Nevertheless, judging from the absence of hydrosilicates from the cumulus assemblages of the Layered Series, the Dovyren magma was undersaturated with respect to H_2O. This means that the water concentration in the original melt at $P = 0.5$ kbar could not be higher than a few tenths of a percent [Al'meev and Ariskin, 1996; Dixon *et al.*, 1996]. The crystallization trajectories were simulated up to a crystallinity of 85–90%, which corresponded to the possible presence of 10–15% residual liquid.

The results of geochemical thermometry demonstrate that the chosen "contact rocks" and the weighted mean composition of the massif are characterized by a common temperature–compositional evolution of the intercumulus melt at temperatures below 1200°C. This evolution is consistent with the generalized crystallization sequence of the contact rocks $Ol \longrightarrow Ol + Pl \longrightarrow Ol + Pl + Cpx \longrightarrow Ol + Pl + Cpx + Opx$, which is, in turn, in agreement with the structure of the Layered Series. Figure 57 presents examples of the model crystallization sequences for the chilled ophitic gabbro, olivine–phlogopite gabbronorite, average plagioperidotite, and the weighted mean composition of the intrusion. All of these sequences are predetermined by the

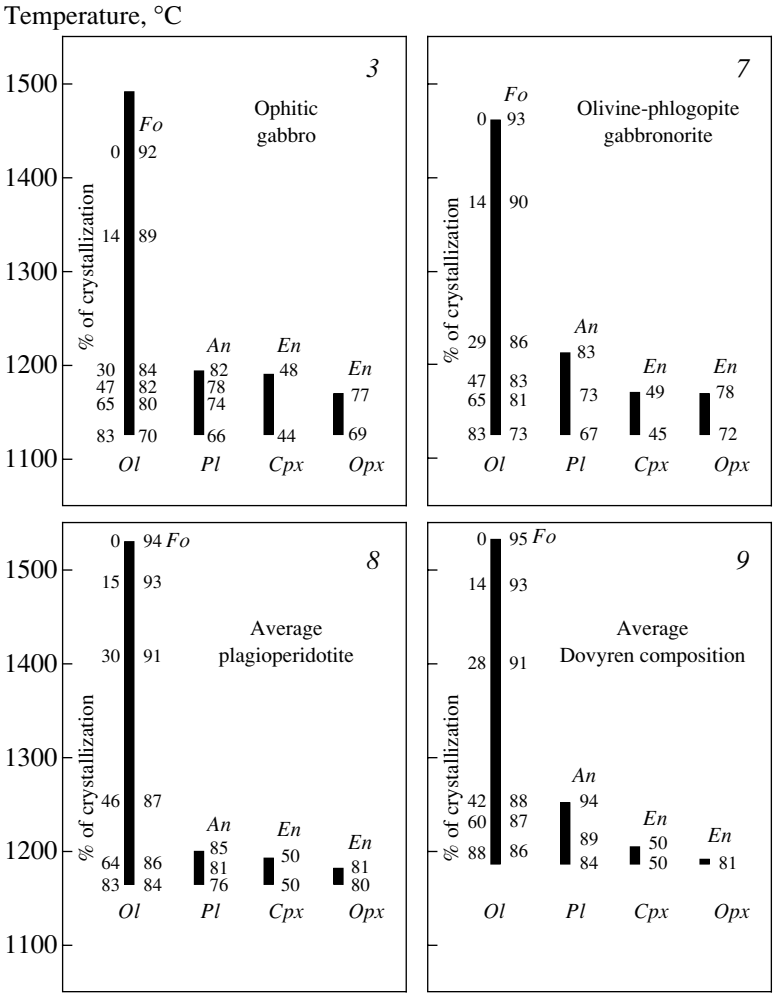

Fig. 57. Modeled sequence of equilibrium crystallization of minerals from the initial melts corresponding to the bottom rocks and the weighted mean composition of the Dovyren Massif (after [Ariskin *et al.*, 2003]). The calculations were carried out with the COMAGMAT-3.52 program for $P = 0.5$ kbar, anhydrous conditions, and f_{O_2} corresponding to the WM buffer. Numerals to the left of the *Ol* lines denote the crystallinity of the modeled system as a function of temperature.

strong oversaturation of the original compositions with respect to olivine and, according to the simulations, suggest that the parental magma contained from 40 to 60 wt % *Ol* crystals.

An important result is that the liquid line of descent for the residual melt of the weighted mean composition of the Dovyren Massif passes through the compositional field of cotectic liquids calculated for the chilled facies and plagioperidotites. The most compact clusters (intersections of the trajectories) correspond to the interval of 1190–1180°C. We believe that an average value of $T = 1185$°C can be assumed as the probable temperature of the melt trapped in the plagioperidotite intercumulus and possibly corresponding to the liquid constituent of the Dovyren parental magma. The major-component composition of this liquid was calculated as an average of all model compositions at 1185°C. The estimated chemical characteristics of this melt correspond to a melt oversaturated with respect to SiO_2 (~55 wt %) and relatively enriched in MgO (~8 wt %) [Ariskin *et al.*, 2003].

Phase composition of the parental magma. In extrapolating the initial temperature of 1185°C to the weighted mean composition of the Dovyren intrusion, we obtained a very high percentage of crystallinity for the system: ~85% (54.3% *Ol*, 23.6% *Pl*, and 6.4% *Cpx*). Obviously, this mixture cannot be referred to as magma (see Section 1.1) and, particularly, it cannot be expected to fractionate in the course of differentiation. Such anomalous characteristics seem to be explained by the overestimation of the volumes of the troctolite and dunite components, because the weighted mean composition of the intrusion was calculated for its cross section with the maximum amount of ultramafic rocks [Mironov *et al.*, 1980].

This led us to turn to the simulation results obtained for the chilled facies and inner-contact rocks, which yield (at the same estimated intrusion temperature and

a close composition of the original liquid) magma crystallinity from 51 to 37 wt %. Provided the magma had a composition corresponding to the average composition of the plagioperidotites, the fraction of the original crystalline material should have been equal to 58%. The most realistic estimate seems to be that for the chilled gabbronorite, because its calculated olivine amount at 1185°C (46.5 wt %) is close to the modal proportion of large *Ol* crystals (~50 vol %) calculated during the petrographic examination of this rock.

Table 20 presents the evaluated composition of the initial liquid and the original modal proportions calculated under the assumption that the Dovyren parental magma was intruded at a temperature of 1185°C (in compliance with geochemical thermometry results), and the bulk composition of this magma corresponded to that of the chilled gabbronorites near the lower intrusion contact (see composition 10 in Table 1 in [Ariskin *et al.*, 2003]).

3.2.5. Main conclusions

The results obtained by the geochemical thermometry of contact rocks and the most primitive cumulates pertain to the problems of the origin of magmatic layering in the differentiated intrusions. The long-lasting discussion of these issues was centered on the hypotheses of crystal settling and *in-situ* crystallization. According to the former concept, most fractionating crystals are thought to nucleate under the roof and, under the effect of gravity, to accumulate on the floor in sediment-like layers [Wager and Brown, 1967; Frenkel *et al.*, 1988b]. The concept of directional (*in situ*) crystallization places less emphasis on gravitational separation and considers magmatic fractionation to be mainly a result of crystal nucleation and growth near the bottom and walls of the magma chamber [Jackson, 1961; Campbell, 1978; McBirney and Noyes, 1979].

It is noteworthy that originally both ideas implied the existence of almost crystal-free, near-liquidus melts. Magma chambers are therewith interpreted as "basins" of a practically homogeneous liquid that contained no suspended crystalline phases and was originally superheated relative to the liquidus. This brought about the opinion that mineral grains can settle only at their homogeneous (volumetric) nucleation in the melt, a process that is, in fact, impossible because of the differences between the adiabatic gradient and the actual dependence of the magma liquidus temperature on pressure [Bartlett, 1969]. These considerations and arguments provided the basis for the hypothesis of a continuous superheating of magma at upper levels and the possibility of its efficient fractionation due to predominant crystallization near the lower solidification front [Campbell, 1978].

Our results indicate that, in analyzing the differentiation mechanisms, it is useful to distinguish between the emplacement of a crystal-poor magma (at a temperature close to the liquidus) and the situation when the initial magmatic material was highly crystallized. The data obtained by the mathematical simulation of crystal–melt equilibria and presented in Table 20 testify that the initial magmatic suspensions could contain from a few percent (differentiated traps of the Siberian Platform) to 15–25% (Talnakh, Kiglapait Massif) and even 40–60% crystals (Kamenistyi sill and the Partridge River intrusion).

These differences can be accounted for by the cooling of the basaltic magma during its injection. This scenario for the pre-chamber evolution of the phase magma compositions finds support in the results of dynamic calculations simulating the emplacement of a nonisothermal magma into a funnel-shaped chamber [Sharapov *et al.*, 1997]. According to the evaluations of these authors, the filling of such a chamber at a rapid discharge of the magmatic material (of about 100–200 m^3/s) results in lower average magma crystallinity corresponding to a content of the solid phase equal to 10–15%, a moderate discharge of 10–100 m^3/s yields 25–30% suspended crystals, whereas slow emplacement with a rate of 0.2–10 m^3/s generates highly crystallized magmas containing at least of 40% crystals.

It follows that traditional concepts of the instantaneous injection of a superheated melt into a chamber are oversimplified, which puts forth the problem of the validity of thermal convection and differentiation schemes that admit the homogeneity of the original magma. The settling of intratelluric crystals and the compaction of the primary cumulates should, perhaps, be recognized as an important initial stage of mass transfer processes in magma chambers. This conclusion remains valid irrespective of whether the subsequent fractionation of the magmatic melt proceeded by the mechanism of sedimentation of mineral grains that nucleated near the roof or by means of *in-situ* crystallization directed upward from the floor.

Another important observation is as follows: for all of the intrusions discussed above, the results of geochemical thermometry yield average (equilibrium) compositions of early olivine crystals that are notably more magnesian than the compositions of this mineral in the rock. This is explained by the known effect of re-equilibration of the primary crystals via their reactions with iron-enriched intercumulus liquid [Barnes, 1986; Calokwu and Grant, 1987]. The results of thermodynamic simulations make it possible to estimate this effect qualitatively or semiquantitatively with regard to the extent of re-equilibration of mineral grains as functions of the cumulus porosity and composition.

Our research demonstrates that the process of re-equilibration in the course of cumulus cooling takes place not only in the contact rocks and the most primitive cumulates but also in the rocks of the layered series, in which it can be pronounced even more clearly, because the FeO/MgO ratio in the residual liquids is increased during the magma fractionation process. A

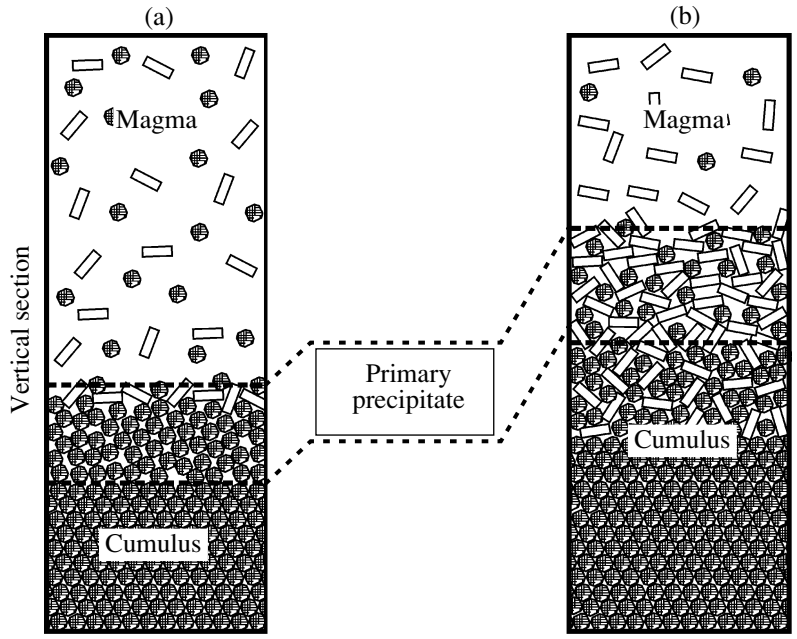

Fig. 58. Scheme of the evolution of the phase composition of the residual magmas and cumulus near the front of an accumulation of the crystalline material. Plots (a) and (b) illustrate different stages of filling the magmatic chamber with crystallizing minerals.

glaring example of this phenomenon is offered by the differentiated traps of the Siberian Platform [Barmina *et al.*, 1989b]. However, in applying the method of geochemical thermometry, one should be aware that the condition of the closure of the primary cumulus system is not always valid. In large layered intrusions, it is quite probable that the intercumulus melts can migrate through the cumulus and lead to the complete or partial re-equilibration (and even recrystallization) of the mineral assemblages [Irvine, 1980; Hunter, 1996]. Geochemical thermometry can still be utilized in this situation, but the simulation results should be interpreted bearing in mind that they can pertain to the integral effect of cooling and infiltration of the pore liquid.

3.3. Geochemical Thermometry of Differentiated Rocks

This section presents examples of the geochemical thermometry of rocks from the layered series of intrusive bodies. The main task of these simulations was to assay the fractionation trend of the intrusive magma, including the temperature evolution and changes in the chemistry of differentiated melts that were entrapped in the intercumulus [Ariskin and Barmina, 2000]. Simultaneously, the initial composition of the cumulus phases are found, along with the relative proportions of crystals and melt in the original magmatic suspension. This makes it possible to track the variations not only in the modal composition of the cumulates but also in the magma itself in which crystal separation proceeds.

For the first time, the method of the successive geochemical thermometry of differentiated rocks in the vertical sections of intrusive bodies was tuned in application to the Vel'minskii sill in eastern Siberia [Frenkel *et al.*, 1988a, 1988b; Barmina *et al.*, 1989a]. The method was underlain by the hypothesis that, regardless of the assumed differentiation mechanism (directional crystallization or crystal settling), the bulk of the rocks was successively formed from below upward, which implies a directed change in the composition of both the minerals and the melt. This leads to an important consequence: by averaging the composition of the overlying portion of the intrusion, one can calculate the bulk composition of the parental melt–crystal mixture ($\cong$ residual magma) for each of the rocks. In fact, this idea was exploited and developed in the approach proposed by Wager [1960] for the calculation of the successive magma compositions of the Skaergaard intrusion. However, in contrast to Wager's approach, we regard magma not as a homogeneous system but as a suspension of crystals in a magmatic liquid, so that the relative amounts of the crystals and liquid could be deduced from the results of geochemical thermometry.

The physical meaning of these simulations is illustrated in Fig. 58, which presents a scheme for the changes in the phase compositions of the residual heterogeneous magmas and coexisting cumulus mixtures when the chamber is filled with a crystalline precipitate. This mush of primary crystals and melt could be formed at the front of the accumulation of the crystalline material by the mechanism of sedimentation convection [Trubitsyn and Kharybin, 1997], see discussion in [Ariskin *et al.*, 2003]. The differences in the bulk composition of the rock and residual magma at each level can be attributed to the variations in the relative

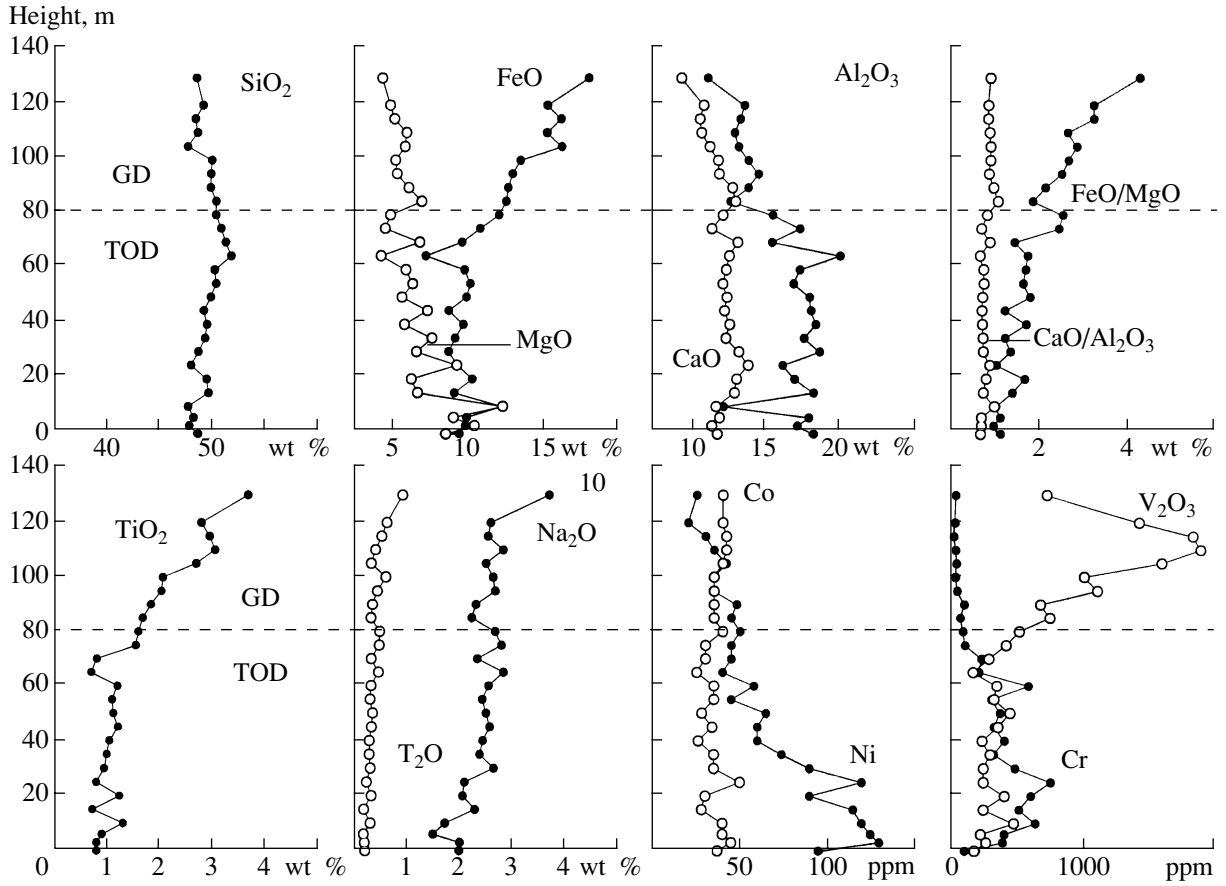

Fig. 59. Variations in the major- and trace-element concentrations and petrochemical ratios in the vertical section of the Vel'minskii sill. GD—gabbrodolerite, TOD—taxito-ophitic dolerite.

proportions of minerals and liquid but not the compositions of these phases. As was mentioned above, this situation allows one to use the technique of geochemical thermometry and provides grounds to hope that the estimates of the thermodynamic parameters obtained with phase equilibria models will be realistic.

With reference to this situation, the method involves numerical simulating the liquid lines of descent for a pair of original compositions, one of which is the bulk composition of the rock (at a specified level in the vertical section), and the other is the weighted mean composition of the overlying portion of the intrusion. The intersection of these trajectories in composition–temperature space should uniquely determine the conditions under which the rock was produced, the phase composition of the residual magma, and the chemical composition of the melt from which the minerals composing the rock crystallized [Frenkel *et al.*, 1988a, 1988b].

3.3.1. Dolerite sills in the Siberian Platform

The Vel'minskii sill offers an example of cryptic layering, which resulted from the differentiation of a tholeiite basalt magma in a tabular-shaped chamber. This trap intrusion was traced for a distance of about 20 km along the right-hand bank of the Podkamennaya Tunguska River about 250 km upstream from its confluence with the Yenisei [Lebedev, 1962]. The intrusion has a stratiform morphology with the maximum apparent thickness of its exposed vertical section of approximately 140–150 m. Although no upper inner-contact facies was found, geological observations suggest that this facies was no thicker than a few meters. The lower contact can be examined only in low-water years.

The layering of the sill is pronounced in the variations in rock textures and compositions [Koptev-Dvornikov *et al.*, 1976]. The textural setting of augite in the rocks was employed as a petrographic criterion for distinguishing two principal types of the Vel'minskii rocks: taxito-ophitic dolerites and overlying prismatic-granular gabbrodolerites. The boundary between these petrographic varieties is spatially restricted to the upper third of the intrusion (Fig. 59) and is of facies nature: within 1–2 m from it, augite becomes progressively more euhedral and its amount relative to plagioclase simultaneously increases. The gabbrodolerites grade into ferrogabrodolerites, which are much richer in ore

minerals. The upper part of the ferrogabbrodolerite layer includes lenses of pegmatoid ferrogabbro.

Mineral chemistry and cryptic layering. The main rock-forming minerals of the sill are olivine, plagioclase, high-Ca clinopyroxene, and titanomagnetite. According to the morphology of mineral grains, textural patterns, and chemical compositions of minerals, they were subdivided into two textural–groups [Koptev-Dvornikov *et al.*, 1979]. Group I comprises the supposedly high-temperature assemblage of the cores of tabular crystals of calcic *Pl*, magnesian and Cr-rich oikocrysts of *Aug*, and *Ol*. Euhedral mineral grains assigned to group I compose roughly half of the rock by volume and make up an open framework whose voids are filled with group-II aggregates. Textural group II includes the outermost zones of plagioclase laths, the relatively Fe-rich and Cr-poor rims of large augite crystals and its small grains, orthopyroxene grains, ore minerals, and interstitial biotite and granophyre. Microprobe analyses indicate that the differences between the compositions of the same minerals in groups I and II are no less than 8–12 mol % *En* in *Aug* and *An* in *Pl*.

The compositions of rocks of the Vel'minskii sill show systematic variations in the contents of major and trace elements (Fig. 59). These are shown as an upward decrease in the contents of MgO, Al_2O_3, CaO, Ni, and Cr at simultaneous enrichment in FeO, TiO_2, alkalis, and other incompatible elements. The chemical trends are complicated by local fluctuations in the concentrations of major oxides and trace elements (more Al_2O_3—less FeO and MgO, higher Ni—-higher MgO). This testifies that the chemical variations are correlated with those in the mineralogy of the rocks.

Selecting original compositions and simulation conditions. The thermometric simulations were carried out with the compositions of 27 selected samples, which were taken near Vel'minskii Rapids from a vertical exposure of the intrusion with a step of 3–5 m (Fig. 59). On the basis of these data, we calculated 26 residual magma compositions following the scheme in Fig. 58. Table 21 presents two examples of such pairs: taxitoophitic dolerite B-2/76 (sampled at a distance of $h = 3$ m upward from the bottom) and gabbrodolerite B-20/76 ($h = 90$ m). The complete set of analyses was published in [Frenkel *et al.*, 1988a, 1988b].

The evaluation of the thickness of the eroded overlying rocks yielded a depth of sill formation equal to approximately 2000 m; further simulations were carried out at a pressure of 1 atm. There are no data on the oxygen fugacity during the crystallization of the Vel'minskii dolerites. Because of this, we carried out the simulations at an assumed oxygen fugacity corresponding to the WM buffer, which ensured *Mt* crystallization from the ferrogabbrodolerite melts in the upper portion of the intrusion. The liquid lines of descent were constructed with the THOLEMAG program (the 1987 version of COMAGMAT) with an increment of 1 mol %, to a crystallinity of $\varphi_{cr} = 80\%$.

Table 21. Examples of compositional pairs representing the rocks and tied residual magmas of the Vel'minskii sill, and their original phase characteristics calculated from the results of geochemical thermometry

Component	$h = 3$ m		$h = 90$ m	
	B-2/76	magma	B-20/76	magma
SiO_2	47.79	49.42	49.80	48.90
TiO_2	0.82	1.63	1.83	2.69
Al_2O_3	17.14	15.69	13.82	13.25
FeO	9.88	11.69	12.72	15.24
MnO	0.21	0.22	0.23	0.26
MgO	10.49	6.30	6.06	5.22
CaO	11.39	12.04	12.76	11.00
Na_2O	2.02	2.50	2.32	2.75
K_2O	0.20	0.39	0.34	0.53
P_2O_5	0.06	0.13	0.12	0.17
Results of geochemical thermometry				
T, °C	1160		1140	
Ol	16.3	2.3	0.7	1.0
Pl	39.0	17.1	22.6	17.9
Aug	4.7	–	18.9	9.2
Mt			0.3	1.9
Melt	40.0	80.6	57.5	70.0

Note: h is the height from the bottom of the exposed rock sequence. The original proportions of solid phases and melt are given in wt % (after [Barmina *et al.*, 1989a]).

The results of geochemical thermometry for two compositions from Table 21 are demonstrated in Fig. 60. It can clearly be seen that the intersections of the model liquid lines of descent are identified quite confidently and point to a common temperature range of the Vel'minskii magma crystallization equal to ~1160–1135°C [Barmina *et al.*, 1989a]. At the same time, when the whole set of compositions was examined, we encountered certain difficulties related to the too small sampling intervals. Evidently, when the overall temperature range (~25°C) is commensurable with the number of sampling sites, the difference between the rock formation temperatures for neighboring rock samples is approximately 1°C, which is one order of magnitude smaller than the sensitivity of geochemical thermometric techniques (10–15°C). Because of this, we did not focus on the evaluation of the absolute temperatures for each dolerite sample but instead attempted to track changes in the original phase and chemical characteristics of the rocks and magma at a presumably monotonous temperature decrease from 1160 to 1135°C with an increment of $\Delta T \approx 1$°C.

We determined that the composition of the residual magmatic melt exhibits a coherent trend from below upward (i.e., from higher to lower temperatures), which

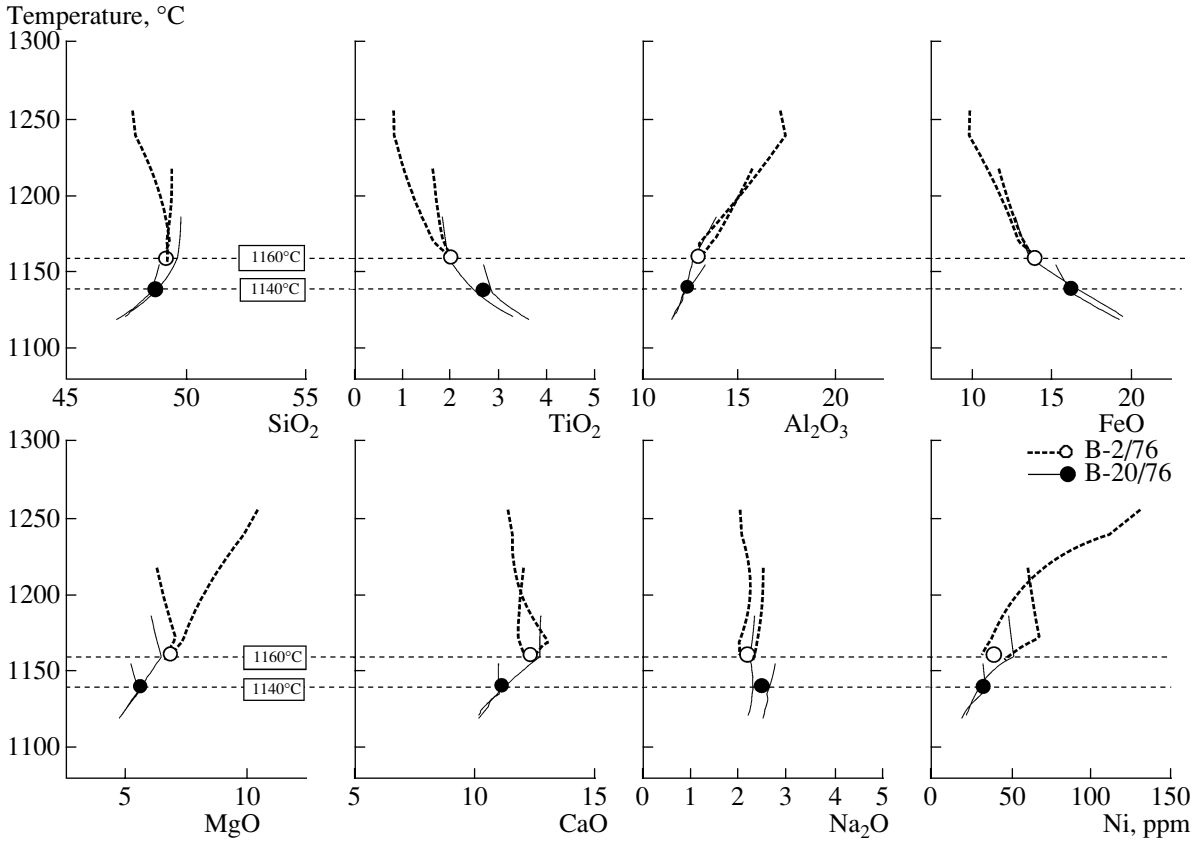

Fig. 60. Geochemical thermometric results for two dolerites and the residual magmas of the Vel'minskii trap intrusion. The simulations were conducted with the THOLEMAG program (an earlier version of COMAGMAT) for $P = 1$ atm and WM buffer conditions [Barmina *et al.*, 1989a]. See Table 21 for the initial compositions. The compositions of the differentiated melt at 1160 and 1140°C are averages of the liquids calculated for the each rock and the linked residual magma at the corresponding temperature.

is expressed in the systematic enrichment in FeO, TiO_2, and alkalis and depletion in SiO_2, Al_2O_3, CaO, MgO, and Ni (Fig. 60). The estimated original modal proportions in the dolerite "cumulus" and the corresponding residual magmas point to the presence of the *Ol* + *Pl* + *Aug* cotectic assemblage starting from very early differentiation stages in the chamber (see examples in Table 21).

Complete data on all sampling sites (Fig. 61) demonstrate that the relatively high-temperature dolerites from the bottom part of the layered series are triminералic cumulates (*Ol–Pl–Aug*–melt, Fig. 61a). The original proportions of minerals and liquid significantly vary: the amount of cumulus *Pl* is 20–47 vol %, the pyroxene content was 5–14%, and the cumulus *Ol* content was approximately 5% (with a maximum value of 17% in rocks near the intrusion bottom). The transition to the gabbrodolerites is marked by a strong increase in the fraction of cumulus clinopyroxene and a simultaneous decrease in the amount of *Pl* at a general decrease in the amount of primary *Ol* grains to 1–2%. Cumulus *Mt* also appears in the rocks starting from roughly the same level. Note that the transition zone is characterized by a sharp increase in the amount of cumulus phases and a decrease in the trapped melt fraction.

It is no less interesting to track the evolution of the phase compositions of the Vel'minskii magma in the process of its fractionation (Fig. 61b). As can be seen from this plot, at the initial moment, the magma representing the weighted mean composition of the exposed part of the sill should have contained approximately 20 vol % suspended crystals, and this value increased to 26% for the middle part of the taxito-ophitic dolerite zone. Then the crystallinity of this suspension decrease toward the level at which gabbrodolerite appears, whose lower boundary is marked by a drastic increase in the amount of suspended phases. The final stage is characterized by an increase in the magma crystallinity to approximately 35%.

Compositions of cumulus phases. Figure 62 illustrates the variations in the composition of the original *Pl* and *Ol* crystals. Circles correspond to the compositions of the highest temperature *Aug*, *Pl*, and *Ol* crystals detected in 14 samples (microprobe data). The trajectories were constructed based on the results of geochemical thermometry, and one of them corresponds to the dolerite, and the other represents the model magma at

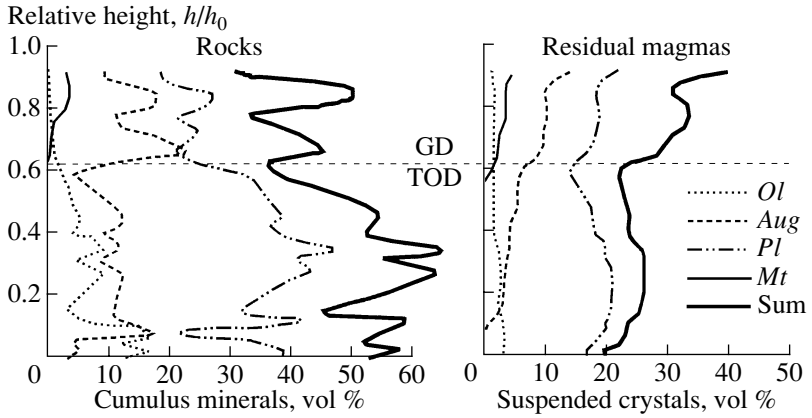

Fig. 61. Variations in the contents of cumulus minerals and suspended crystals with the formation of the observed succession of rocks of the Vel'minskii sill. Sum is the total amount: for rocks—cumulus minerals, for residual magmas—suspended crystals; GD—gabbrodolerite, TOD—taxito-ophitic dolerite.

each level. The shaded area shows the difference between these values that correspond to the uncertainty of the method, which usually does not exceed 2–4 mol % end member.

The model and observed compositions of the highest temperature *Pl* cores are in good agreement in the lower part of the succession, while in its upper part, the calculated *Pl* compositions are, on average, 3–5 mol % richer in *An* than the analyzed *Pl* grains from the rocks (Fig. 62a). A comparative analysis of data on the magnesian clinopyroxene also demonstrates similarities between their model and natural characteristics [Barmina *et al.*, 1989a]. This led us to conclude that the cores of primary *Pl* and *Aug* grains preserve a "record" of the original melt–crystal equilibrium conditions during the origin of the cumulus framework of the rock.

The calculated and analytical data on the olivine show significant discrepancies (Fig. 62b). The compositions of *Ol* grains analyzed in the rocks are systematically poorer in *Fo* by 15–25 mol % than the expected compositions of primary olivine crystals in equilibrium with the intercumulus liquid. These differences are one order of magnitude greater than the uncertainties in the calculated *Ol* compositions related to the use of the *Fo* and *Fa* geothermometers. It is also hard to explain the discrepancies in the general directions of the compositional trends for *Ol*. According to geochemical thermometric results, the *Fo* content in the cumulative *Ol* should monotonously decrease upward, whereas analytical data point to a notable increase in this parameter with the transition to gabbrodolerites (Fig. 62b). It is also pertinent to mention that such local "backtrackings" in the compositions of mafic minerals are typical of many differentiated intrusions and are usually interpreted as resulting from additional injections of a high temperature magma.

An analysis of all available geochemical thermometric data led us to conclude that the differences between the observed and model compositions are correlated with the amount of the iron-enriched intercumulus liquid. This provides sound evidence that the main cause of the changes in the original olivine composition was diffusion-controlled Fe^{2+} and Mg^{2+} exchange between the primary crystals and melt during the solidification of the melt–crystal mixture. This effect can explain why *Ol* compositions become more magnesian at the boundary between TOD and GD (Fig. 62b). This phenomenon is definitely correlated with a decrease in the fraction of the intercumulus liquid near the bottom of the gabbrodolerite layer (Fig. 61b). Thus, there is no need to invoke additional injections of a more magnesian melt to account for the seeming increase in the Mg number of the magmatic melt.

Results of geochemical thermometry obtained for other differentiated sills. We conducted further thermometric simulations for three trap intrusions that

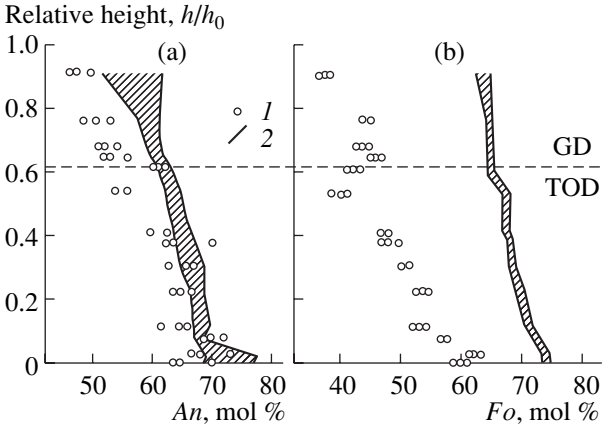

Fig. 62. Evolution of the compositions of (a) plagioclase and (b) olivine in the vertical section of the Vel'minskii sill. (*1*) Compositions of the most primitive *Ol* crystals and *Pl* cores (microprobe data); (*2*) original compositions of cumulus *Ol* and *Pl* calculated by means of geochemical thermometry.

were thoroughly sampled from their lower to upper contacts [Frenkel *et al.*, 1988b]. These were the Kuz'movskii (h = 85 m, in the valley of the Podkamennaya Tunguska River), Vilyuiskii (h = 150 m, in the valley of the Vilyui River), and Vuvakanskii (h = 100 m, in the valley of the Vilyui River) dolerite sills. The Kuz'movskii sill is weakly differentiated, and its cryptic layering was identified based on the variations in the contents of major and trace elements. The Vilyuiskii and Vavukanskii intrusions are differentiated more contrastingly and exhibit a clearly observable transition from taxito-ophitic dolerites to gabbrodolerites.

The main distinctive feature of all of these intrusions that make them different from the Vel'minskii sill is the elevated Mg number (the average MgO contents range from 8 to 9 wt %). Our research indicates that the relatively high MgO content did not result from the richness of the parental magmas in *Ol* and *Aug* crystals but rather points to the more primitive composition of the initial liquid. This is confirmed by the occurrence of the so-called poikilophitic dolerites (which can be interpreted as the highest temperature rocks) in the lower portion of the intrusion. They consist of a cotectic assemblage of early *Ol* and *Pl* crystals cemented by large *Cpx* oikocrysts, which crystallized from the interstitial melt.

The materials obtained on the structures and the compositions of the Kuz'movskii, Vilyuiskii, and Vavukanskii intrusions were originally used to test the convective–cumulative model for the intra-chamber differentiation of trap magmas and were later utilized for thermometric reconstructions [Frenkel *et al.*, 1988b, 1989]. Here we touch upon only some results of this research that pertain to the method of geochemical thermometry.

(1) The attempts to use the method of thermometry of contact rocks with the utilization of the weighted mean compositions of the differentiated sills eventually failed. This was caused by the fact that the composition of the poikilophitic dolerites near the bottom was close to the composition of the intrusive bodies (i.e., to the composition of the parental magma). As a result, the model trajectories appeared to be nearly parallel liquid lines of descent without clear intersections in composition–temperature space.

(2) Because of this, in evaluating the crystallinity of the trap magmas, it is necessary to rely on the results of forward modeling of the structure of intrusive traps based on the convective–cumulative model [Frenkel *et al.*, 1989]. According to these data, the parental magmas were subcotectic (*Ol* + *Pl*) systems and contained no more than 8% intratelluric phenocrysts (see, for example, the data on the Vavukanskii intrusion in Table 20).

(3) The application of the method of paired (rock + magma) geochemical thermometry to the subsequent derivatives proved efficient, because the estimates obtained for the phase evolution of the cumulus and residual magmas were practically identical with the results of the forward computer simulations of the intra-chamber differentiation. The most significant results of the thermometric calculations are presented in Fig. 63.

The evolution of the phase composition (primary liquidus assemblages) of the cumulus is illustrated by the first set of the plots. In considering these dependences, one should be aware of the figurative sense of the term *Cumulates* in application to the bottom poikilophitic dolerites, because their contents of primary *Ol* and *Pl* crystals are no higher than 25%. In general, the rocks of the lower zone are characterized by a progressive accumulation of cumulus crystals, with this process reaching a maximum (45–55%) in the middle portions of the vertical sections. These data demonstrate that the first cumulus pyroxene appears at different levels, which coincides with petrographic evidence of the transition from the poikilitic (*Ol* + *Pl*) to taxito-ophitic (*Ol* + *Pl* + *Aug*) dolerites. The boundaries between the taxito-ophitic dolerites and gabbrodolerites in the Vilyuiskii and Vavukanskii sills are marked by an increase in the amount of cumulus clinopyroxene relative to plagioclase.

The evolution of the phase composition of the residual magmas (right-hand set of plots in Fig. 63) also shows similarities between different intrusions, for which the crystallinity of the residual magmas always systematically increased in the process of differentiation from a few percent near the contacts of the intrusions to 30–40% in their middle parts. It can be concluded that the phase difference between the cumulus and residual are at a minimum during the final solidification stages of the intrusions. Another of their distinctive features is that the increase in the crystallinity of the residual magmas is mostly caused by the accumulation of *Pl* crystals, and the amount of *Ol* and *Aug* crystals in the magmatic suspension never exceeds 10%.

So far as we know, these estimates still remain the only example of the complex genetic interpretation not only of the dolerites of differentiated sills but also of intrusive basites in general. This approach proved informative and simple in studying relatively thin bodies [Frenkel *et al.*, 1988a, 1988b; Ariskin and Barmina, 2000]. At the same time, its applicability to larger plutons is still questionable, because most layered complexes have laterally complicated inner structures, which makes it impossible to extrapolate data obtained on typical or representative sections to the whole volume of the magmatic reservoir. Nevertheless, there is another modification of geochemical thermometry of successive magmatic derivatives that allows one to estimate the phase characteristics of the cumulates even if the plausibility of the calculated bulk compositions of the parental magmas is doubtful. This approach will be considered using the example of the thermometry of rocks from the Layered Series of the Skaergaard intrusion [Ariskin, 2002, 2003].

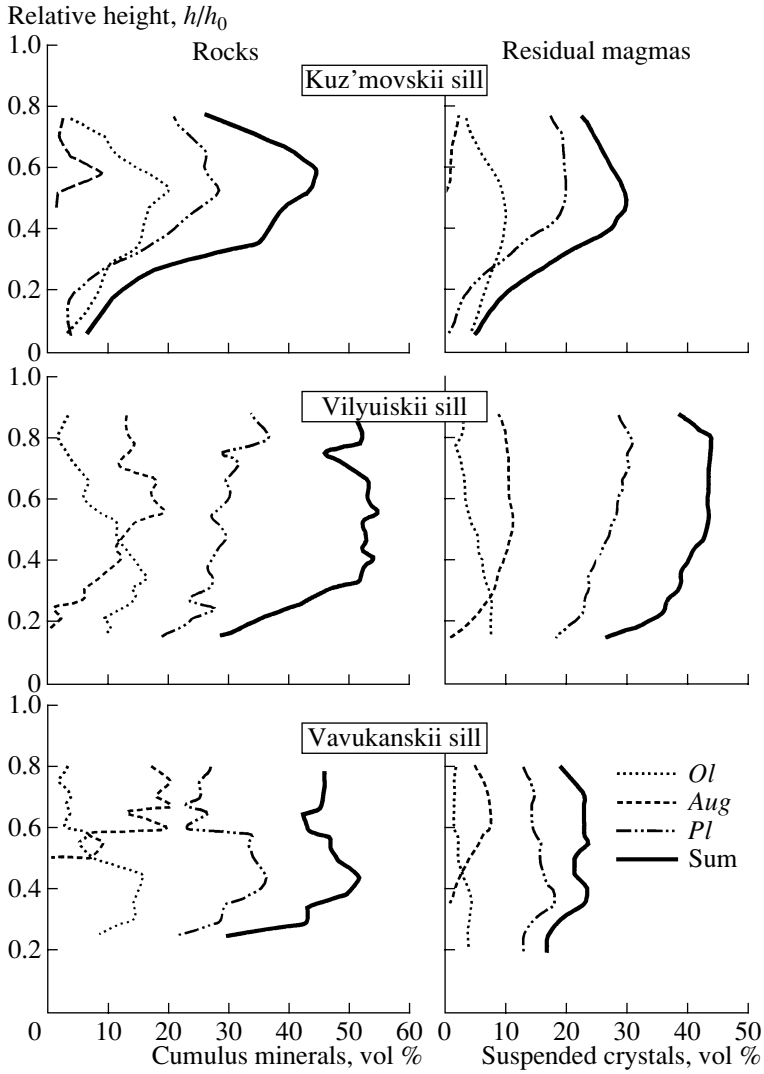

Fig. 63. Variations in the contents of cumulus minerals and suspended crystals with the formation of the observed succession of rocks of the Kuz'movskii, Vilyuiskii, and Vavukanskii differentiated sills. Sum is the total amounts of original cumulus minerals of the rocks or suspended crystals in the coexisting residual magmas.

3.3.2. Layered Series of the Skaergaard intrusion

The modal composition of cumulates and the chemical evolution of residual melts can be reconstructed using only the compositions of rocks sampled along the vertical section of the magmatic body. It is natural to assume that the bulk compositions of rocks collected within the same zone or horizon present information on the compositionally similar trapped liquids and the same original cumulus assemblage. In this situation, a search for the cluster of intersections of liquid lines of descent is justified, and the probable composition of the residual melt within a given zone (horizon) can be calculated as an average of a number of modeled liquid compositions at the calculated temperature of the original equilibrium. A disadvantage of this method is the absence of a modeled trajectory for the bulk composition of the residual magma including differentiated (i.e., intercumulus) melt and suspended crystals. This precludes estimating its original modal composition. However, the chemical characteristics of the liquidus assemblage can be simulated unambiguously. Preparatory to systematic geochemical thermometry simulations for the rocks of the Layered Series of the Skaergaard intrusion, we conducted a series of testing simulations with different COMAGMAT versions.

Additional calibrations and preliminary simulations. The main problems in the application of the COMAGMAT-3.5 program [Ariskin and Barmina, 1999] to the differentiated rock of the Skaergaard intrusion are caused by the low-temperature character (~1115–1080°C) of cumulus assemblages from the LZc, MZ, and UZa zones [McBirney, 1996]. These values lie outside the range of the experimental temperatures (1120–1350°C) at which equilibrium equations

for *Ol*, *Pl*, and pyroxenes were calibrated (see Section 2.2.4). Therefore, at temperatures lower than 1100°C, simulations with the COMAGMAT-3.5 model resulted in a systematic shift of the calculated phase boundaries, as follows from the excessive enlargement of the *Aug* field at the sacrifice of *Pl* and *Pig*. In order to minimize this effect, we revised and extended the basic set of experimental data and simultaneously increased the proportion of experiments at temperatures of ≤1100°C and lower. This work and the corresponding recalibrations were carried out using the INFOREX-4.0 database, and the mineral–melt geothermometers newly designed for mafic minerals and plagioclase formed the empirical background of the COMAGMAT-3.65 model [Ariskin, 2003]. The testing of this program against the results of independent experiments has revealed an insignificant improvement in the accuracy of the temperature calculations, although the modeled *Pl* compositions and phase relations between *Aug* and *Pig* became more realistic. Further support for the efficiency of the COMAGMAT-3.65 is provided by the results of computer simulations of the crystallization of the melts that represent the average compositions of the principal structural units of the Skaergaard intrusion (Figs. 43, 64).

The testing simulations were conducted for the average compositions of the five main zones of the Layered Series (LZa, LZb, LZc, MZ, and UZa) and their equivalents in the Marginal Border Series (LZa*, LZb*, LZc*, MZ*, and UZa*) [Ariskin, 2002, 2003]. The simulations were conducted at $P = 1$ kbar for systems closed or opened with respect to oxygen (from QFM + 1 to QFM – 2) at an assumed water content in the melt equal to 0.1 wt %. The modeled crystallization sequences show both common features and principal differences (Fig. 64).

There is a remarkable similarity between the LS rocks and their MBS equivalents in the order of minerals that crystallized at each zone, which is in good agreement with the assumption that both series crystallized from the same magma. For example, the LZa and LZb compositions show small fields of *Ol* crystallization, which is followed by *Pl* and *Aug*, with the crystallization field of clinopyroxene notably expanding in the LZb rocks, which correlates with the appearance of abundant granular augite (Fig. 43). The LZc trajectories are characterized by the early crystallization of *Ilm* and *Mt*, which is also consistent with the observed mineralogy of rocks in this zone. Similar phase relations were obtained for the rocks of the Upper and Middle zones (compare with their MBS equivalents), except that olivine was found to be completely dissolved via its reaction with the residual liquid.

It is interesting to consider the behavior of pigeonite. In the rocks of the Marginal Border Series, this mineral crystallized earlier than in the Layered Series, and this resulted in the relatively early dissolution of olivine. As for oxide-rich gabbros, both series (LZc $\longrightarrow$ UZa and LZc* $\longrightarrow$ UZa*) demonstrate the almost simultaneous precipitation of magnetite and ilmenite, although ilmenite crystallized slightly earlier in the LS rocks compared to MBS. Thus, the simulations conducted at QFM conditions are consistent with the overall structure of the massif, with the only exception of *Ol* behavior modeled for the rocks of the Upper Zone.

The point is that complete *Ol* dissolution during the final crystallization stages of UZa rocks implies that this mineral should be absent not only from the rocks of the Middle Zone but also from the more evolved rocks of the Upper Zone. However, olivine "reappearance" is considered to be the main petrographic criterion for distinguishing between MZ and UZa zones [Wager and Deer, 1939; McBirney, 1989, 1996]. In an attempt to settle these contradictions within the framework of phase equilibria constraints, we conducted an additional set of calculations simulating equilibrium crystallization under conditions closed with respect to oxygen, using the same average compositions of the main zones of the Layered Series.

The results of simulations in a closed system demonstrate the significant expansion of the *Ol* stability field, with this mineral remaining in the LZc and UZa rocks in amounts of 4–10 wt % up to a crystallinity of about 80%. Important results were also obtained for the proportions of Fe–Ti oxides. The calculations with the COMAGMAT-3.65 program confirmed the conclusion that the amount of *Mt* crystallizing in a closed system is approximately two-thirds of that calculated under conditions buffered with respect to oxygen [Ariskin *et al.*, 1988b; Toplis and Carroll, 1996]. The bulk proportion of *Ilm* in the closed system was remarkably increased, so that the overall *Ilm*/*Mt* ratio was modified in favor of ilmenite. This led us to suggest that the Skaergaard magma could have crystallized in a closed system, because ilmenite is more abundant than magnetite in the Layered Series [McBirney, 1989]. Moreover, the results provide evidence that the closure of the natural system with respect to oxygen could have stabilized olivine on the liquidus and preclude its complete dissolution during the final solidification stages, as is typical of rocks in the Upper Zone of the Layered Series.

Results of geochemical thermometry. As follows from the introduction to this section, to conduct thermometric calculations for a specified vertical section (irrespective of whether it is real or generalized), it is necessary to subdivide the available petrochemical data into compositional groups for which it is reasonable to assume similar compositions of the intercumulus liquids. Data on the Skaergaard intrusion can be subdivided fairly reliably [McBirney, 1989, 1996].

Selecting samples and simulation conditions. The 65 samples selected for the calculations are distributed among the five zones of the Layered Series in the following manner: LZa ($n = 8$), LZb ($n = 16$), LZc ($n = 11$), MZ ($n = 20$), and UZa ($n = 10$) [McBirney, 1998].

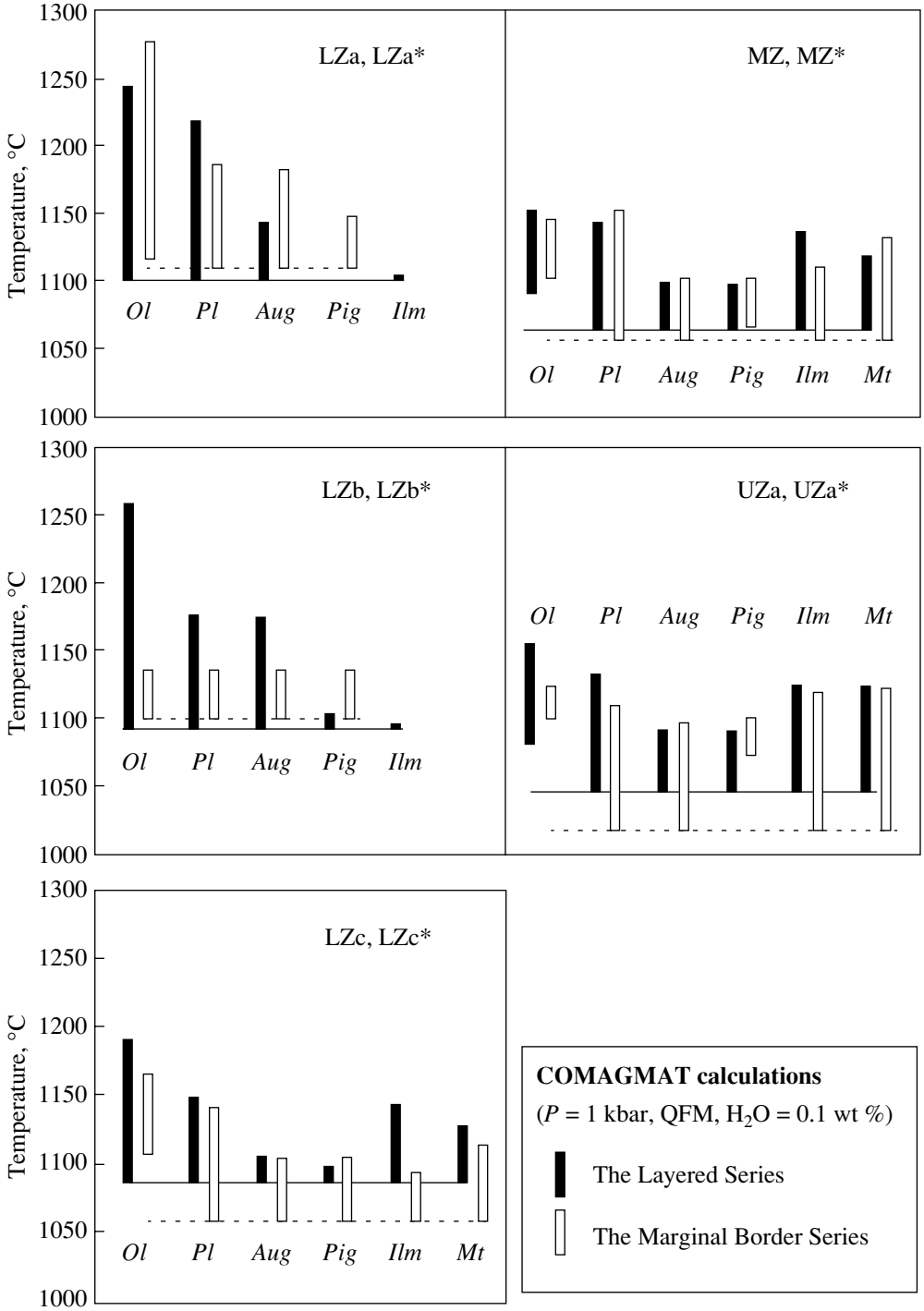

Fig. 64. Mineral crystallization sequences simulated for the average compositions of the principal zones of the Layered Series and their equivalents in the Marginal Border Series [Ariskin, 2003]. Equilibrium crystallization was simulated with the COMAGMAT-3.65 program at a pressure of P = 1 kbar, water content of 0.1 wt % in the original system, and redox conditions corresponding to the QFM buffer.

This selection includes no differentiated rocks from UZb, UZc, and SH because our models still cannot account for apatite crystallization. In interpreting the results of the computer simulations, we also used data on the geochemical thermometry of six contact rocks from the Marginal Border Series discussed in Section 3.2.1.

The simulations were conducted in the isobaric mode (P = 1 kbar) and with the assumption that the rocks contained no more than 0.1 wt % primary mag-

matic H_2O. The choice of the pressure was based on the analysis of phase relations between the polymorphs of silica and ferrous pyroxenes in the Sandwich Horizon, with these relations pointing to a pressure of 600 ± 100 bar and a temperature of 970 ± 20°C [Lindsley *et al.*, 1969]. Judging from the density of the overlying gabbros and basalts, this corresponds to a depth of approximately 2 km for the Sandwich Horizon and places LZa at 4.5 and UZa at 3 km below the original surface. Thus, the Lower Zone of the Layered Series was formed under a pressure of approximately 1.5 kbar, and the boundary between the Middle and Upper zones corresponds to a pressure of ~0.9 kbar.

In contrast to simulations for other intrusive bodies, in conducting the geochemical thermometry of the layered rocks of the Skaergaard intrusion, we did not specify beforehand the oxygen fugacity in the magma. The simulations by the COMAGMAT-3.65 program were performed with the FeO and Fe_2O_3 contents measured in the rocks (these data were made available for us courtesy of A. McBirney of the University of Oregon). This approach implies that the system was ideally closed but can result in overestimating the Fe_2O_3 content because of rock weathering, which is hopefully minimized by the "freshness" of the samples and the absence of apparent traces of alterations [McBirney, 1998]. This approach also opens the possibility of evaluating the probable oxygen fugacity in the initial melt by solving the inverse problem: the calculation of f_{O_2} values at a given temperature and the residual liquid composition. Summarizing these data on discrete zones of the Layered Series, it is possible to reproduce the general evolution of the oxygen fugacity in the process of the Skaergaard magma differentiation [Ariskin, 2002, 2003].

LZa zone. The results of computer simulations for five starting compositions with MgO > 9.5 wt % point to a wide field of crystallization of cumulus olivine: *Ol* (1322–1258°C) ⟶ *Pl* (1237–1193°C) ⟶ *Aug* ± *Mt* (1140–1110°C) ⟶ *Pig* (1125–1110°C). Two samples demonstrate subcotectic relations between *Ol* and *Pl* at 1230–1200°C, and titanomagnetite was the first to appear on the liquidus (at 1190°C) for one sample. Except for one of these subcotectic samples and magnetite gabbro (whose affiliation with the LZa zone is problematic), the calculated liquid lines of descent compose a single family of six cotectics, which maximally converge within the temperature range of 1140–1150°C. The average composition of this cluster at 1145°C is presented in Table 22 and shown in Fig. 65, along with the calculation results for LZb. The average *Ol* and *Pl* compositions estimated for the six samples at 1445°C are $Fo_{74.9 \pm 1.5}$ and $An_{66.3 \pm 1.9}$, with the *An* content in *Pl* being in good agreement with data on the natural rocks (Fig. 43). The modeled *Ol* composition appeared to be approximately 7 mol % more magnesian than the observed one. We believe that, as in other differentiated intrusions, these differences were caused by late diffusion re-equilibration. The average $\log f_{O_2}$ value, calculated from thermometric data for the rocks of the LZa zone at 1145°C, is –7.5 ± 0.6. This value is about 1.5 logarithmic units higher than that of the QFM buffer and is consistent with the results of measurements [Kersting *et al.*, 1989]. In Fig. 65 this value is shown together with the estimate obtained for the overlying LZb rocks.

LZb zone. Three principal crystallization sequences were established for this zone. Four compositions indicate the following order: *Ol* (1370–1240°C) ⟶ *Pl* (1220–1170°C) ⟶ *Aug* ± *Mt* (1160–1110°C) ⟶ *Pig* (<1130°C). For five samples, augite appeared on the liquidus at temperatures of 1200–1170°C simultaneously with olivine or immediately after it; and plagioclase was the first to crystallize (at 1250–1190°C) in seven samples. Titanomagnetite was the fourth crystallizing mineral, and pigeonite and ilmenite were identified only during later stages, at temperatures below ~1120 and 1100°C, respectively. The results of these simulations are in agreement with the conclusion that *Aug* crystallized and accumulated as the third cotectic phase, along with olivine and plagioclase [Wager and Brown, 1967; McBirney, 1989]. The calculated liquid lines of descent form a clear-cut cluster at temperatures below 1140°C. The most compact cluster of intersecting trajectories was identified visually at 1125 ± 5°C (Fig. 65). The average compositions of cumulus minerals at this temperature are reported in Table 22. The average oxygen fugacity during the crystallization of the LZb rocks was evaluated as $\log f_{O_2} = -7.4 \pm 0.7$.

LZc zone. Compared with rocks from the LZa and LZb zones, the simulation results for the LZc compositions show an even greater diversity of the crystallization sequences of minerals on the liquidus. This is caused by the presence of abundant oxides, so that *Ilm* and *Mt* were the first to crystallize (at 1270–1170°C) in six samples. The crystallization sequence of silicate minerals varied (*Ol* ⟶ *Pl* ⟶ *Aug* + *Pig* or *Ol* ⟶ *Aug* + *Pig* ⟶ *Pl*), and pyroxenes were never observed at temperatures above 1110°C. This temperature was assumed as the upper stability limit of the primary cumulus assemblage *Ol* + *Pl* + *Aug* + *Mt* + *Ilm*. The reliability of evaluations of the composition of the trapped liquid for these rocks depends on the accuracy of prediction not only for the crystallization sequence but also for the *Mt* and *Ilm* proportions, which control the SiO_2 and FeO covariations in the residual melt. Luckily, the modal proportions of Fe-Ti oxides were previously calculated for all eleven samples of magnetite–ilmenite gabbro from the LZc zone [McBirney, 1998]. A comparison of these data with the calculation results indicate that the COMAGMAT-3.65 model is able to fairly well predict the bulk *Mt* and *Ilm* proportions after the solidification of the "modeled rocks." This adds confidence to the reliability of the evolutionary trajectories calculated for the differentiated liquid (Fig. 66).

Table 22. Thermodynamic characteristics of intercumulus melts and the compositions of minerals in the original assemblages, calculated for the main zones of the Layered Series in the Skaergaard intrusion

Component	LZa (n = 6)*	LZb (n = 14)	LZc (n = 9)	MZ (n = 17)	UZa (n = 8)
	1145**	1125	1100	1090	1085
	–7.5 ± 0.6***	–7.4 ± 0.7	–8.9 ± 0.4	–9.8 ± 0.4	–10.3 ± 0.6
Compositions (wt %) of the intercumulus liquids					
SiO_2	49.26 ± 0.76	50.06 ± 1.25	48.04 ± 1.49	49.05 ± 0.86	50.31 ± 1.05
TiO_2	2.50 ± 0.58	2.83 ± 0.76	5.50 ± 0.63	5.25 ± 0.40	4.68 ± 0.24
Al_2O_3	12.74 ± 0.23	11.97 ± 0.77	10.26 ± 0.92	10.35 ± 0.90	11.05 ± 0.31
FeO	14.84 ± 0.81	15.73 ± 0.72	17.05 ± 0.73	17.50 ± 0.55	17.31 ± 0.58
MnO	0.20 ± 0.01	0.21 ± 0.04	0.22 ± 0.04	0.23 ± 0.04	0.24 ± 0.02
MgO	6.29 ± 0.23	5.56 ± 0.32	4.82 ± 0.26	4.00 ± 0.18	3.35 ± 0.19
CaO	11.02 ± 0.54	10.27 ± 0.59	11.00 ± 1.16	10.20 ± 0.78	9.01 ± 0.50
Na_2O	2.59 ± 0.32	2.73 ± 0.34	2.57 ± 0.34	2.80 ± 0.40	3.40 ± 0.29
K_2O	0.39 ± 0.07	0.42 ± 0.22	0.38 ± 0.17	0.39 ± 0.16	0.49 ± 0.14
P_2O_5	0.17 ± 0.06	0.22 ± 0.12	0.15 ± 0.06	0.21 ± 0.15	0.17 ± 0.06
Equilibrium compositions (wt %) of the cumulus minerals					
Ol	*Fo* (74.9 ± 1.5)	*Fo* (72.1 ± 2.1)	*Fo* (64.0 ± 1.5)	see Note	*Fo* (52.5 ± 2.5)
Pl	*An* (66.3 ± 1.9)	*An* (61.9 ± 2.1)	*An* (57.4 ± 2.1)	*An* (54.2 ± 2.9)	*An* (48.0 ± 3.1)
Aug		*En* (47.0 ± 1.4)	*En* (42.2 ± 1.8)	*En* (39.5 ± 1.1)	*En* (38.0 ± 1.9)
		Fs (13.6 ± 1.3)	*Fs* (16.8 ± 0.6)	*Fs* (20.2 ± 0.7)	*Fs* (22.6 ± 1.0)
		Wo (39.4 ± 0.9)	*Wo* (41.0 ± 1.7)	*Wo* (40.5 ± 1.0)	*Wo* (39.4 ± 1.2)
				En (54.3 ± 1.4)	*En* (51.4 ± 1.6)
Pig			see Note	*Fs* (34.1 ± 1.5)	*Fs* (37.7 ± 1.4)
				Wo (11.6 ± 0.7)	*Wo* (10.9 ± 0.3)
Ilm			*Il* (91.4 ± 3.9)	*Il* (93.8 ± 2.8)	*Il* (93.7 ± 2.5)
Mt			*Ulv* (54.0 ± 6.6)	*Ulv* (72.3 ± 4.9)	*Ulv* (81.4 ± 6.7)

Note: All compositions are average values (±1σ) calculated for the maximum convergence and intersection points of the modeled trajectories (see Figs. 65 and 66). In four initial bulk-rock compositions from the LZc zone *Pig* was calculated to be present among the original cumulus minerals ($En_{59.1 \pm 0.9}Fs_{29.2 \pm 0.3}Wo_{11.7 \pm 0.9}$). For five compositions from the Middle Zone, *Ol* was simulated in amounts of 2–3 wt % ($Fo_{56.6 \pm 1.4}$). The values of *Il* and *Ulv* characterize the $FeTiO_3$ and Fe_2TiO_4 activities calculated by the equation from [Stormer, 1983]. * Zone, ** temperature (°C), *** $\log f_{O_2}$.

The modeled lines of the LZc rocks form a distinct intersection near 1100°C, which corresponds to melts somewhat depleted in SiO_2 and enriched in TiO_2 and FeO compared to the intercumulus liquid simulated for the underlying LZb zone (Table 22). The original compositions of *Ol*, *Pl*, and pyroxene in equilibrium with the "average intercumulus melt" of the LZc rocks are consistent with the general trend of depletion in refractory components toward the roof. The modeled *Ilm* and *Mt* compositions are listed in Table 22 as $FeTiO_3$ and Fe_2TiO_4 activities calculated following the method in [Strormer, 1983]. They suggest the occurrence of nearly stoichiometric ilmenite and moderately ferrous titanomagnetite, which is consistent with the shift in the redox conditions of the primary equilibrium toward lower oxygen fugacity values (~QFM, Fig. 66].

MZ zone. Twenty samples were selected to conduct geochemical thermometry for the Middle Zone [Ariskin, 2002, 2003]. The differences in starting compositions and the extent of iron oxidation of the rocks predetermined the diversity of the modeled crystallization sequences, in which six minerals (*Ol*, *Pl*, *Aug*, *Pig*, *Ilm*, and *Mt*) change or replace one another within a narrow temperature range, practically within the accuracy of the COMAGMAT-3.65 model (10–15°C). An important result was the fact that all *Ol*-free samples contained some amounts of olivine during the early and middle crystallization stages. However, this mineral was completely dissolved at 50–70% solidification of the rock via its reactions with pyroxenes, oxides, and melt. It is worth noting that the appearance of low-Ca pyroxene corresponded to a crystallinity of ~20–40%, which is consistent with the presence of this mineral

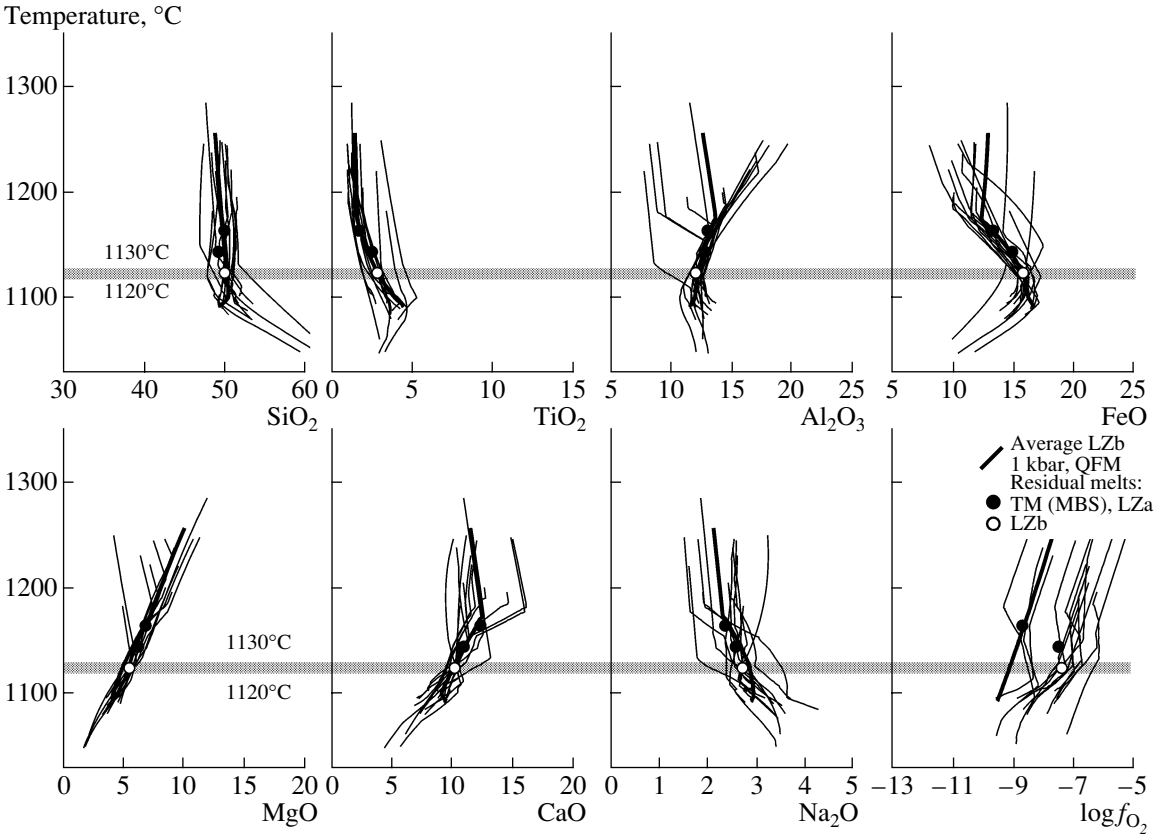

Fig. 65. Results of geochemical thermometry of rocks from the LZb zone. Thin lines correspond to the equilibrium crystallization trajectories calculated for systems closed with respect to oxygen. The value of $T = 1125 \pm 5$°C is assumed as the temperature of the original *Ol–Pl–Aug* assemblage in equilibrium with the intercumulus melt, whose composition is listed in Table 22. The heavier line corresponds to the modeling result for the average composition of the LZb zone under QFM buffer conditions (Fig. 64). For comparison, the initial melt compositions estimated in rocks of the Marginal Border Series (MBS) and the LZa zone are presented.

among the primary cumulus phases according to the petrographic subdivision of the Layered Series (Fig. 43).

The convergence of the modeled liquid lines of descent for the MZ rocks is no less clear than that for the LZc rocks, with the most compact cluster of intersections occurring at temperatures below 1100°C. The problem, however, is that the "parallelism" of the evolutionary lines for multiphase assemblages at low temperatures precludes unambiguously determining the temperature and composition of the intercumulus melt. We assumed a value of 1090°C as the probable primary equilibrium temperature, at which the modeled composition of *Pl* (a phase that was least strongly affected by subsolidus re-equilibration) is the closest to the composition observed in the rocks. The average trapped melt composition, calculated for 1090°C, is shown in Fig. 66 and listed in Table 22, along with the modeled compositions of the original cumulus phases. It is interesting that, according to our simulations, ilmenite became slightly richer in $FeTiO_3$, whereas the activity of the ulvospinel component in Ti-magnetite considerably increased (Ulv_{72} in MZ as compared to Ulv_{54} in LZc). This suggests a rapid decrease in the oxygen fugacity to $\log f_{O_2}$ values below the QFM buffer (Fig. 66), which is consistent with the data of earlier researchers (see the reviews in [McBirney, 1996; Ariskin, 2003]).

UZa zone. The simulation of phase equilibria for ten UZa rocks yielded the lowest cotectic temperatures for the examined part of the Layered Series, and none of the compositions yielded liquidus temperatures above 1200°C. The modeled crystallization sequences are similar to those simulated for the MZ zone, and all of them begin with the brief crystallization of olivine or the $Ol + Pl \pm$ oxides assemblage. Two samples with the highest FeO contents (35 and 46 wt %) yielded anomalously wide fields of magnetite crystallization and were excluded from further considerations. Both pyroxenes crystallized nearly simultaneously at temperatures below 1100°C, and the *Pig* field was slightly decreased compared to that in the MZ simulations. This resulted in an increase in the modal proportion of *Ol*. The liquid lines of descent for the UZa rocks composed a fairly compact cluster within the temperature interval of 1090–1080°C. The average composition of this residual liquid at 1085°C points to an insignificant increase

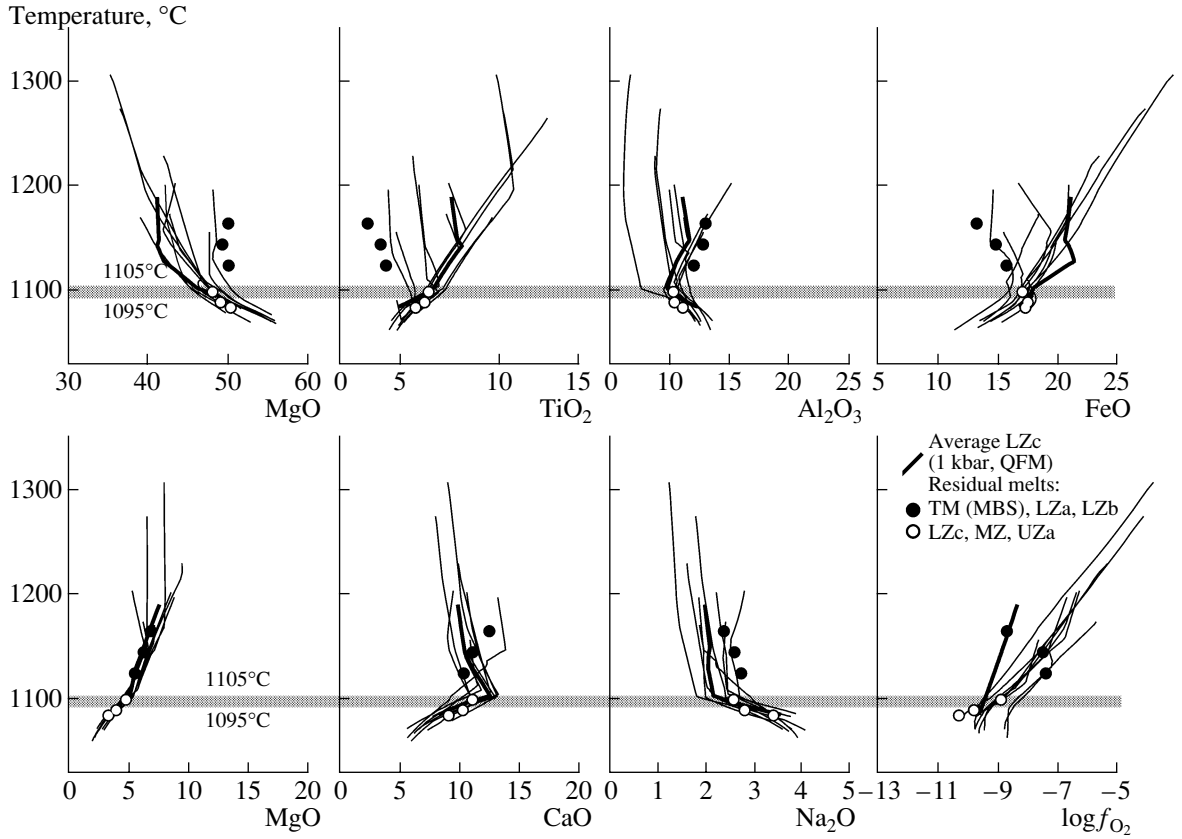

Fig. 66. Results of geochemical thermometry of rocks from the LZc zone. The value of $T = 1100 \pm 5$°C is assumed as the temperature of the original *Ol–Pl–Aug–Ilm–Mt* assemblage in equilibrium with the intercumulus melt, whose composition is listed in Table 22. The heavier line corresponds to the modeling result for the average composition of the LZc zone under QFM buffer conditions (Fig. 64). For comparison, the diagram shows the compositions of the melts entrapped in the primitive cumulates of the Marginal Border Series (MBS) and the rocks overlying and underlying the LZc zone.

in the SiO_2 and FeO contents (Table 22). This melt can be regarded as the most evolved derivative, which is characterized by the lowest MgO and CaO contents at an elevated alkalinity. The anorthite content in plagioclase in equilibrium with the modeled melt ($An_{48.0 \pm 3.1}$) corresponds to that observed in the rock, whereas the calculated olivine is much more magnesian ($Fo_{52 \pm 2.5}$ against Fo_{40}). The composition of ilmenite does not vary, and magnetite practically passes into the ulvospinel stability field and is characterized by high Fe_2TiO_4 activities (0.81 ± 0.7). This is consistent with the established tendency toward a rapid decrease in the oxygen fugacity in the lower portion of the Upper Zone, which corresponds, according to simulations for the closed system, to $\log f_{O_2} = -10.3 \pm 0.6$ (Table 22, Fig. 66).

Discussion. The geochemical thermometry of the Layered Series rocks reproduced the probable range of the "formation temperatures" that represent the melts trapped in the intercumulus: from approximately 1145 ± 10°C for the LZa zone to 1085 ± 10°C for the UZa zone. The oxygen fugacity, which was calculated simultaneously and had been controlled by the residual liquid composition, corresponded to $\log f_{O_2}$ values from 1–1.5 units above QFM for LZa/LZb rocks to QFM and lower values starting from the LZc zone. However, the main output of our simulations was the estimation of the residual melt compositions, which could define a common evolutionary trend for the Skaergaard magma (Table 22). These liquids demonstrate strong enrichment in FeO (up to ~18 wt %) and TiO_2 (up to ~5.5 wt %), so that there is a temptation to draw an analogy with the evolutionary trends of Fe- and Ti-enriched tholeiitic magmas, the so-called Fe–Ti basalts [Brooks *et al.*, 1991]. It is, however, hard to reconcile this interpretation with data on the melts derived for the rocks from the Marginal Border Series, which correspond to common tholeiitic ferrobasalts (Table 15).

The results of geochemical thermometry do not confirm the conclusion made in [Wager and Brown, 1967] that the differentiated melts were monotonously depleted in SiO_2 starting from the lower parts of the Lower Zone. Conversely, these results demonstrate that the silica content in the residual liquids slightly increased within the LZa zone (Fig. 65), which is consistent with the experimental data on the crystallization

of the *Ol–Pl* assemblage in tholeiitic systems [Grove and Baker, 1984; Ariskin and Barmina, 2000]. When the LZb rock were produced, the silica content in the melt started to decrease (in response to the settling of the *Ol + Pl + Aug* assemblage), as is manifested by the low SiO_2 contents of the melts that gave rise to the overlying rocks in the LZc zone (Fig. 66, Table 22). This trend is relatively short: the intercumulus of the overlying rocks shows, again, a trend with SiO_2 enrichment (in spite of a decrease in the bulk silicity of the rocks), which was caused by the massive crystallization of magnetite and ilmenite (*Ol + Pl + Aug* + oxides ± *Pig*). It is worth noting that the SiO_2 enrichment recognized in the LZb ⟶ UZa rocks is not as significant as could be anticipated at *Mt* crystallization in systems buffered with respect to f_{O_2}. This is correlated with the absence of significant FeO variations (Table 22), which can be regarded as evidence that the Skaergaard magma evolved in a system closed with respect to oxygen [Osborn, 1959; Presnall, 1966; Toplis and Carroll, 1996].

At the same time, it is pertinent to mention that the almost three orders of magnitude decrease in the oxygen fugacity within a temperature range of about 60°C (Table 22) cannot be explained only by the evolution of the residual melts during closed-system crystallization. This decrease is so significant that the progressive iron reduction in the melt can be accounted for only by the partial "opening" of the system late in the intra-chamber process. The term "openness" implies here that the oxygen fugacity was not determined from the outside (there are simply no mineral buffers able to cause such a significant f_{O_2} decrease) but rather that some reducing agent or fluid (perhaps, hydrogen-bearing) acted, whose nature still has to be clarified [Ariskin, 2003].

A significant controversy in the thermometric data concerns the compositional gap between the melts of the LZa/LZb rocks and those of the oxide-rich gabbros from the LZc ⟶ UZa zones (Table 22). The gap is manifested in the drastic change in the CaO and SiO_2 contents (Fig. 66), which is hard to explain from the standpoint of the fractionation of a common parental magma. In principle, this controversy can be accounted for by the calculation uncertainties of the COMAGMAT-3.65 program and the insufficient "resolution" of the method at low temperatures. However, a noteworthy fact here is the nearly twofold increase in the TiO_2 content of the trapped liquid with the transition from the LZb to LZc rocks, a change that extends far beyond the uncertainties of the computational model [Ariskin and Barmina, 2000]. To explain this fact, the crystallization schemes should admit 40–50% solidification of the system and the efficient redistribution of the strongly fractionated intercumulus liquid within the chamber. These considerations lead to the idea of the possibility of compositional convection in the crystal–melt mush, a process manifested in the expelling and migration of the interstitial liquid [Tait and Jaupart, 1992, 1996]. Thus, this compositional gap may have a genetic sense as a geochemical indicator of the onset of convection flows in the cumulus [Ariskin, 2003].

3.3.3. Main conclusions

Geochemical thermometry is an efficient method that was thoroughly tested and approved in application to genetically interpreting intrusive basites. This method is underlain by the comparative analysis of the results of computer simulations of the equilibrium crystallization of melts corresponding to cumulates observed in nature. Irrespective of whether these rocks are from the marginal facies or layered series of intrusions, the proposed thermometric techniques enable one to calculate the temperatures and compositions of their initial interstitial liquid, the primary modal proportions and composition of the cumulus minerals, and the average porosity of this cumulus.

An important result of geochemical thermometry of the most primitive rocks of intrusive bodies is the possibility of translating the parameters obtained for the intercumulus melt onto the initial intrusion temperatures and the composition of the liquid part of the parental magma. Simultaneously the possibility is opened for evaluating the phase composition of this original magmatic suspension. However, such calculations are possible only for bodies of substratiform morphology, whose average composition can be reliably evaluated (such as the Partridge River, Kamenistyi, Talnakh, and other intrusions, see Table 20). For some of them, the parental magma was determined to have been highly crystalline, which is consistent with the absent (for the Partridge River intrusion) or weak (for the Kamenistyi sill) fractionation in the chamber.

If the layered series of the massif is sampled in much detail, the method of geochemical thermometry makes it possible to calculate the temperatures and compositions of the differentiated (trapped or residual) melts starting from the lowest sampling level. This task can be fulfilled for any sample by using the calculated residual heterogeneous magma compositions or the compositions of several "neighboring" rocks from nearby portions of the vertical section. In the former situation, it is necessary to evaluate the weighted mean composition of the overlying part of the vertical section for each sample. In the latter case, a group of rocks should be selected for which it is reasonable to assume the same composition of the intercumulus liquid.

The efficiency and informativeness of the former approach was demonstrated above in application to doleritic sills in the Siberian Platform. The other modification of thermometry was designed for differentiated rocks and can be utilized to reconstruct only the chemical characteristics of the residual melts and suspended minerals that provide no information on the variations in the proportions of melt and crystals in the residual magma. This is exemplified by the application of ther-

mometric calculations to the Layered Series rocks of the Skaergaard intrusion (Table 22). Obviously, it is most expedient to merge both approaches controlling the phase equilibria calculations for natural rocks by simulating the liquid lines of descent for the respective residual magmas.

In any event, the efficiency of geochemical thermometry depends on the preparatory location of the selected samples relative to certain zones and layers in the vertical sections of the intrusive bodies. At the same time, it is easy to imagine a situation when information on the conditions under which the rocks were produced can be deduced from data on a single sample, which was examined but whose exact geological setting is unknown. For this purpose, one has to mentally subdivide the rock into fractions enriched in different sorts of crystals, determine the bulk compositions of these fractions, and use these characteristics as the starting compositions to simulate the equilibrium crystallization. By definition, these "imaginary" cumulates should have been produced by a common magma (melt–crystal mixture) at the same temperature. The intersections of the modeled trajectories in such schemes should be clear and unambiguous.

It is still hard to say whether this problem can be solved via the physical fragmentation or crushing of a single rock followed by the chemical studies of fractions subdivided according to the size of mineral grains. We are not aware of any methodical research of this kind. However, there is a natural magmatic material for which this problem can be solved. This is regolith, a thin layer of finely fragmented and mixed material on the surface of planetary bodies affected by meteoritic impacts. For example, the lunar regolith contains mineral and rock fragments most of which were probably produced by the destruction of the same bodies (flows, lava sheets, and sills) or relatively large fragments of igneous rocks. This situation is favorable for applying geochemical thermometric techniques. If the number of the initial compositions is large enough, the results acquire a statistical (probabilistic) character [Ariskin and Barmina, 2000].

It is also worth mentioning that the approach proposed in this chapter merges and develops traditional methods of petrological interpretations that are based on the use of experimental data within the framework of the laws of the equilibrium partitioning of components in melt–crystal systems. Evidently, the uncertainties and inaccuracies of simulations with the COMAGMAT, MELTS, and other similar programs sometimes leave uncertain the plausibility of the estimated crystallization parameters. Nevertheless, our experience in the use of phase equilibrium models testifies that the accuracies of predicting the temperatures, modal proportions, and chemical compositions for basaltic systems approach more and more closely the level of purely experimental uncertainties. In this sense, the methodological development of geochemical thermometry techniques is not only relevant but also highly promising in the context of further progress in modern methods for genetic interpreting igneous rocks.

CHAPTER 4. COMPUTER SIMULATION OF FRACTIONAL CRYSTALLIZATION OF BASALT MAGMAS

The problems of fractionation of the main types of basaltic magmas constitute the core of igneous petrology. This is due to the scale of manifestations of basaltic magmatism and the particular role of basic melts as the parent of various volcanic and intrusive rocks. The origin of this chemical diversity (in the broad sense, the magmatic evolutionary trend) is traditionally explained by the separation of crystalline phases in a liquid [Bowen, 1928]. However, the physical mechanisms and the scale of this phase separation can vary, and their chemical consequences can not always be explained within the scope of simple "Bowen's" fractional crystallization [Irvine, 1980; O'Hara and Mathews, 1981; Frenkel *et al.*, 1988b; Langmuir, 1989; Kelemen, 1990].

Nevertheless, the concept of perfect fractional crystallization proved fruitful and is still widely employed in genetic interpretations of the volcanic associations and layered series of intrusive complexes. This suggests that there should be certain common features in the physical situations in the magma feeder systems and chambers that predetermined the magma evolution along fractionation lines. The most important of these features seems to be the stirring and mixing of the bulk of the crystallizing magmatic system, a process caused by the high efficiency of sedimentation convection compared with simple crystal settling [Frenkel *et al.*, 1988b].

The idea of sedimentation convection was first put forth by Hess [1960], who suggested the existence of vertical flows in the Stillwater magma in the form of upward and downward currents of magmatic suspensions depleted or enriched in crystalline material. Nearly 40 years later, hydrodynamic simulations were conducted that not only confirmed this prediction but made it possible to evaluate some physical characteristics of this mass transfer mechanism [Trubitsyn and Kharybin, 1997]. These results also provided a physicochemical basis for the interpretation of the dynamics of trap magma differentiation modeled according to the convective–cumulative mechanism [Frenkel *et al.*, 1988b, 1989].

Thus, studying the perfect fractional crystallization of a magma coupled with its convective stirring remains of keen interest, although the COMAGMAT program is able to simulate more complicated processes occurring within the scope of partial and intermediate fractionation [Ariskin and Barmina, 2000]. In this chapter, we will discuss some examples of constructing fractional crystallization trajectories that pertain to disputable issues in the evolution of tholeiitic and calc–alkaline

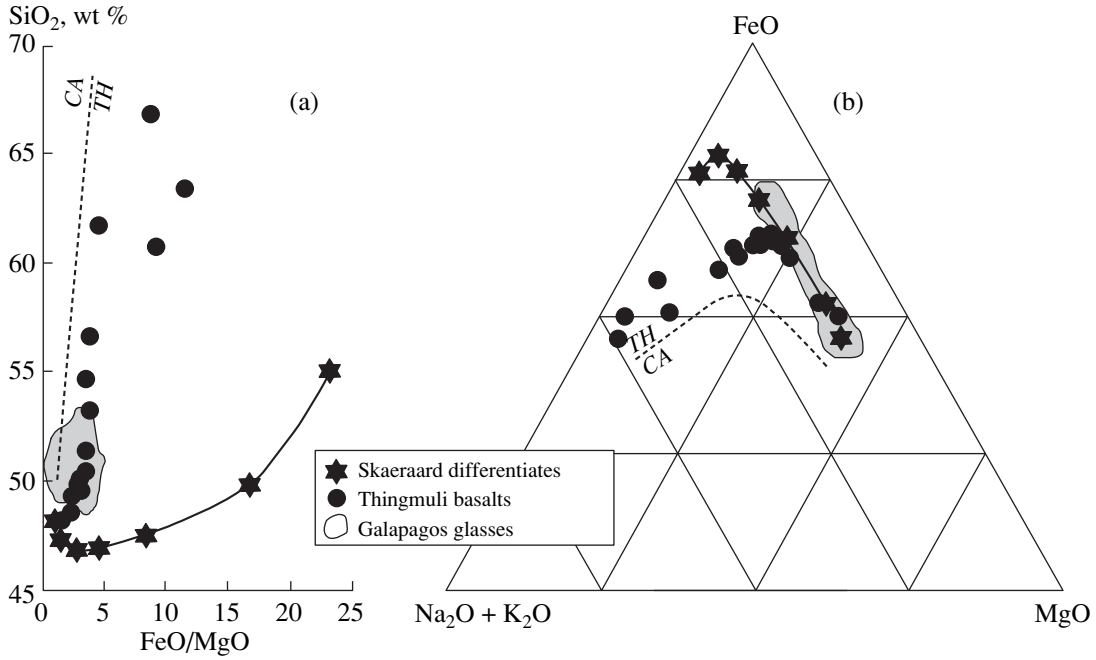

Fig. 67. Discrimination diagrams for the tholeiitic (*TH*) and calc–alkaline (*CA*) series. (a) After Miyashiro [1974]; (b) after [Irvine and Baragar, 1971]).

magmas. An analysis of the results of these simulations indicates that the comparison of fractionation lines modeled under different redox conditions and pressures makes it possible to derive information on the thermodynamic parameters of the crystallization process that are recorded in the form of the direction of and bends on the petrochemical trends.

4.1. Fractional Crystallization of Tholeiitic Magmas under Low Pressures

4.1.1. Tholeiitic trends and their phase interpretation

The main distinctive feature of tholeiitic series is the progressive enrichment of the residual melts in iron oxides during their early and intermediate fractionation stages and the subsequent depletion of these components during the late stage (Fig. 67). The Fe enrichment resulted from the low-pressure fractionation of basaltic magma, when the crystallizing assemblage was characterized by the predominance of plagioclase over mafic minerals (see the crystallization proportions of the *Ol–Pl* and *Ol–Pl–Px ± Mt* cotectic in Table 13). The phase interpretation of these features was considered in detail in [Grove and Baker, 1984]. Based on the results of experiments in basaltic and andesitic systems, these researchers proposed a generalized diagram for the evolution of tholeiitic and calc–alkaline magmas (Fig. 68). This phase diagram was constructed by projecting the compositions of experimental glasses quenched in the presence of various *Pl*-bearing assemblages (the *Ol* field corresponds here to the *Ol–Pl* cotectic, the *Ol–Aug* curve corresponds to the *Ol–Pl–Aug* cotectic, etc.) onto the OLIV–CPX–QTZ plane.

An important feature of this diagram is the occurrence of a temperature maximum (point *T*), located between reaction points *A* (*Ol* + *Pl* + *Aug* + *Pig* + *l*) and *B* (*Ol* + *Pl* + *Opx* + *Pig* + *l*). This maximum acts as a natural barrier separating the evolutionary paths of magmatic melts with different normative *Cpx* contents. As can be seen from Fig. 68, the fractionation of tholeiite-like original melts proceeds via the crystallization of the *Ol–Pl*, *Ol–Pl–Aug*, and *Ol–Pl–Aug–Pig* assemblages. In this process, the FeO content in the melts is monotonously increased and becomes particularly significant after passing reaction point *A*. The silica content of the derivative liquids increases insignificantly early in the course of crystallization and can slightly decrease at point *A*. This scheme was later refined and detailed [Tormey *et al.*, 1987; Grove, 1993] and is in good agreement with the mineralogy of the "pigeonite series" [Kuno, 1950, 1960] and numerous data on the melting of oceanic tholeiites.

Iron enrichment versus silica enrichment. Figure 67 demonstrates only three examples of the typical evolution of tholeiitic magmas of two volcanic series (Thingmuli basalts and Galapagos glasses) and the succession of residual magmas of the Skaergaard intrusion [Wager and Brown, 1967]. These data clearly demonstrate the essence of discussions concerning the evolution of tholeiitic magmas. The main problems here are as follows: (i) the maximum possible degree of iron enrichment, (ii) the directions of the

silica trends, and (iii) the relative proportions of silica-enriched derivatives.

It is pertinent to recall the principal discussion between Bowen and Fenner [Bowen, 1928; Fenner, 1929]. The differences between how these researchers interpreted the evolutionary paths of basaltic magmas stemmed, in essence, from their phase interpretations. Bowen originally relied upon data on the *Ab–An–Di* system. Fractionation in this system results in albite-rich melts, which led Bowen to conclude that basaltic magmas should inevitably evolve with enrichment in silica and alkalis. Fenner noted that this reasoning is also applicable to clinopyroxene solid solutions, whose fractionation should give rise to iron-enriched melts. Thus, the differences between the *Bowen's* and *Fenner's* differentiation trends are underlain by the estimated relative roles of plagioclase and Fe–Mg silicates during the crystallization of basaltic magmas. According to the results of modern investigations of phase equilibria in silicate systems, this alternative is interpreted as a result of the dependence of these trends on the initial composition and crystallization conditions.

Shi [1993] published data on the stability of the *Ol–Pl–Aug* assemblage in the Na_2O–CaO–FeO–MgO–Al_2O_3–SiO_2 system at a temperature of 1100°C and a pressure of 1 atm. These results include the compositions of isothermal liquids in equilibrium with the gabbroic assemblage and make it possible to evaluate the possible evolutionary trajectories of the modeled magma depending on the composition. It was revealed that the stability field of the *Ol–Pl–Aug* assemblage in a Na_2O–SiO_2 diagram spans the range of ~38–52 wt % SiO_2 at a melt alkalinity of approximately 2 wt % and ~40–60 wt % SiO_2 at ~6 wt % Na_2O in the liquid (Fig. 69). Considering data on the chemistry of the minerals, this suggests the possibility of the evolution of basaltic magmas with the formation of both *Ne*-normative and SiO_2-oversaturated melts.

These conclusions are consistent with data on the melt compositions of natural samples, which characterize the stability of the *Ol + Pl + Aug ± Pig* and *Mt + Pl + Aug ± Pig ± Ol* assemblages (Fig. 69). They include experiments (extracted from the INFOREX database) that lasted for at least 12 h and produced experimental glasses with total alkalinity $Na_2O + K_2O \le 6$ wt %. As can be seen in this plot, natural cotectics permit the possibility of both enrichment and depletion in silica during clinopyroxene crystallization, but the predominant tendency is still SiO_2 depletion in the liquid. If magnetite appears on the liquidus of *Pl*- and *Aug*-bearing assemblages, the compositions of the residual melts notably shift toward higher SiO_2 contents. This leads to the conclusion that the final fractionation stages of systems with low and moderate alkalinity are anticipated to be characterized by SiO_2 depletion and FeO enrichment if no magnetite is present among the crystallizing minerals. The precipitation of iron oxides should result in a change in the fractionation trend with SiO_2 enrichment in the liquid. The FeO behavior is ambiguous. As will be demonstrated below, the evolution in the content of this component is controlled by the f_{O_2} regime.

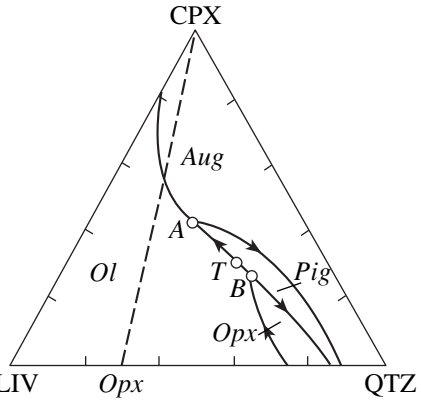

Fig. 68. Phase diagram of basaltic and andesitic melts saturated with respect to *Pl*, *Ol*, and *Px* under dry conditions and P = 1 atm [Grove and Baker, 1984]. *T* is the temperature maximum separating the evolutionary paths through reaction points *A* (*Ol + Pl + Aug + Pig + l*) and *B* (*Ol + Pl + Opx + Pig + l*).

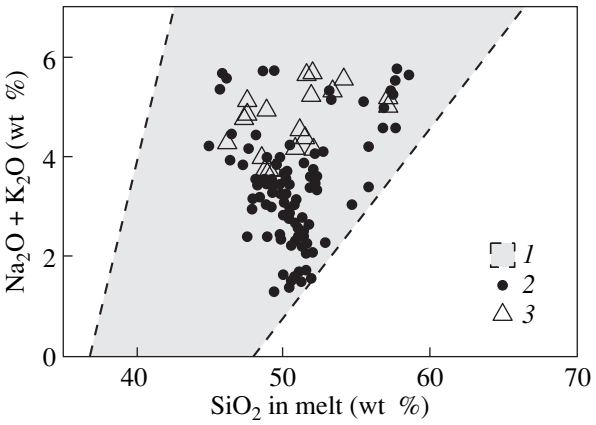

Fig. 69. Compositions of melts corresponding to the stability of *Ol*, *Pl*, and *Aug* under dry conditions and P = 1 atm. (*1*) *Ol + Pl + Aug* assemblage in the Na_2O–CaO–FeO–MgO–Al_2O_3–SiO_2 system at 1100°C [Shi, 1993]; natural basalts and andesites: (*2*) *Ol + Pl + Aug ± Pig*, (*3*) *Mt ± Pl + Aug ± Pig ± Ol*; information from the INFOREX-4.0 database on runs that lasted for more than 12 h.

Petrological observations indicate that natural rocks exhibit both tendencies: enrichment in silica and alkalis is typical of the final evolutionary stages of tholeiitic and calc–alkaline series, while FeO enrichment is characteristic of the early and intermediate crystallization stages of tholeiites [Ariskin and Barmina, 2000]. The extent of FeO enrichment and the behavior of SiO_2 during the early fractionation of tholeiitic magmas can be different in accordance with the differences in the evolutionary trends of volcanic series and the residual

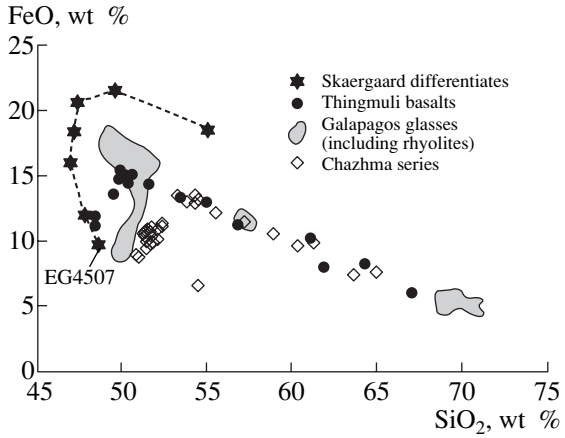

Fig. 70. Relationships between the Fenner evolution of the Skaergaard magma and the Bowen trend for tholeiitic volcanic series. The Chazhma suite consist of mesocratic and leucocratic rocks of the Chazhma sill, Eastern Kamchatka [Barmina *et al.*, 1988], see Section 4.1.3.

magma compositions estimated for differentiated intrusions.

Differences in the trends of intrusive and volcanic rocks. Using the average compositions and relative volumes of the principal zones of the Layered Series in the Skaergaard intrusion (Fig. 43), Wager *et al.* calculated residual melt compositions that approximated the evolution of the parental magma in the course of its differentiation in the chamber [Wager and Deer, 1939; Wager and Brown, 1967]. According to these mass-balance constraints, the calculated compositional series exhibits a monotonous increase in the sum of Fe oxides (FeO from 9.6 to 18.2 wt %) during the major stage of solidification of the massif ($0 < F < 88\%$) with a complimentary decrease in SiO_2 from 48.1 to 46.9 wt %. Further crystallization ($88 < F < 98\%$) is characterized by insignificant enrichment in FeO (to 21.7 wt %) and SiO_2 (49.8 wt %). During the final stages, the modeled derivatives had very unusual compositions: at F = 99.3%, the FeO and SiO_2 contents in the residual liquid are, respectively, 18.5 and 55.0 wt % (Fig. 70). For several decades, this trend was considered to be a standard for the evolution of tholeiitic magmas along the trajectory of the maximum Fe enrichment. Later, this trend was substantiated by mass-balance calculations for some other intrusions (see, for example, [Morse, 1981]) and is still regarded as the main argument in support of the Fenner evolution.

Paradoxically, tholeiitic basalts and natural glasses are known to include compositions strongly enriched in iron (up to 18–19 wt % FeO [Brooks *et al.*, 1991]), but no volcanic equivalents of the "Skaergaard ferroandesites" have ever been found [Toplis and Carroll, 1996]. Most volcanic series are characterized by moderate enrichment in FeO (usually to 13–15%) in the range of basaltic compositions, but this is not accompanied by a simultaneous decrease in SiO_2 (see, for example, [Carmichael, 1964] (Fig. 70). At the same time, it is known that the results of melting experiments with the Skaergaard cumulates [McBirney and Naslund, 1990] at temperatures of about 1100°C gave rise to SiO_2-poor melts that were anomalously enriched in FeO (see Section 3.2.1). The possibility of the origin of such liquids in nature follows from finds of silica-depleted ferrobasalts in the dike complex associated with the Skaergaard intrusion [Brooks and Nielsen, 1978].

A physicochemical explanation of these facts was proposed by Osborn [1959], who experimented with the $MgO–FeO–Fe_2O_3–SiO_2$ system and has established that the differences between the crystallization trends of the melts can be accounted for by the magnetite crystallization proportions, which are controlled by the redox conditions. When crystallization proceeds in a closed system (i.e., a system with a constant bulk composition and FeO/Fe_2O_3 ratio), *Mt* crystallization does not result in melt depletion in FeO, while crystallization at a constant oxygen fugacity leads to a rapid decrease in the FeO content in the melt due to an enhanced proportion of crystallizing magnetite. Analysis of these chemical features led Osborn to conclude that the intrachamber differentiation of tholeiitic magmas (in particular, for the Skaergaard magma) could occur in a closed system, whereas the parental magmas of volcanic series could fractionate under conditions buffered with respect to f_{O_2}. This conclusion was also supported by experimental data on the $CaO–MgO–FeO–Fe_2O_3–SiO_2$ system [Presnall, 1966; Eggler and Osborn, 1982] and the results of numerous melting experiments with natural basalt and andesite samples [Ariskin, 1998].

Effect of magnetite crystallization. The experimental demonstration of andesite and dacite origin via the crystallization of *Mt*-bearing assemblages (Fig. 24) initiated the comprehensive exploring of this problem, including a comparative analysis of geological observations, mass-balance calculations, considerations of the thermodynamic aspects of magnetite crystallization, and the development and interpretation of numerical models for fractional crystallization. These issues were somewhat clarified by the results of the direct modeling of the fractional crystallization of the Thingmuli olivine tholeiite under QFM buffer conditions [Ghiorso and Carmichael, 1985].

In their simulations, these researchers used one of the early versions of the MELTS computer program [Ghiorso, 1985] to model, at pressures of $P \le 2$ kbar and a low H_2O content in the starting system (0.1 wt %), the crystallization sequence of minerals in the Thingmuli lavas [Carmichael, 1964, 1967]: *Ol* ⟶ *Pl* ⟶ *Aug* *Mt* ⟶ *Opx* (*Pig* in natural samples). The main outcome of these calculations was determining that the modeled liquid lines of descent reproduced accurately enough the petrochemical trends characteristic of this volcanic series, first of all, the FeO versus SiO_2 evolution, including the sharp bend at FeO ~ 15 wt %

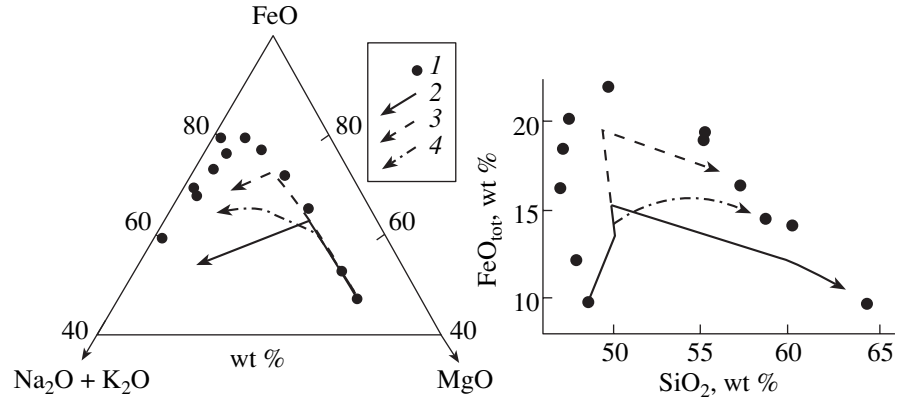

Fig. 71. First simulations of fractional crystallization for an assumed Skaergaard magma composition. (*1*) Differentiated melts after [Wager and Brown, 1967], calculations with the THOLEMAG model [Ariskin *et al.*, 1988b]: (*2*) QFM buffer, (*3*) IW buffer, (*4*) closed system. Chilled gabbro EG4507 was used as an approximation of the initial magma.

(Fig. 70). The overall amount of derivatives with SiO_2 contents higher than 60 wt % was calculated to be 12 wt % of the parent; the process was associated with the crystallization of approximately 6 wt % titanomagnetite. These conclusions have found support from the results of simulating the crystallization of the Thingmuli tholeiite with the THOLEMAG program [Ariskin *et al.*, 1988b].

Problems were encountered in interpreting the first results of simulating the fractional crystallization of the Skaergaard magma. The starting composition selected for these simulations was that of a chilled gabbro (sample EG4507, Table 14). The calculations were conducted at $P = 1$ atm and different redox regimes, including both oxygen buffers (IW/QFM), and conditions closed with respect to oxygen [Ariskin *et al.*, 1988b]. Despite the imperfection of the magnetite model utilized in these simulations (see Section 2.2.5), the modeling results realistically reproduced the observed crystallization sequence of the Skaergaard magma (Fig. 43),

$$Ol + Pl \longrightarrow Ol + Pl + Aug \longrightarrow Ol + Pl + Aug + Pig$$
$$\longrightarrow Pl + Aug + Pig + Mt \text{ (QFM)}$$
$$Ol + Pl \longrightarrow Ol + Pl + Aug \longrightarrow Ol + Pl + Aug + Mt$$
$$\longrightarrow Ol + Pl + Aug + Mt + Ilm \text{ (IW)},$$

except for ilmenite, which crystallized only under the reduced conditions of the iron–wuestite buffer. The modeled *Ol*, *Pl*, *Aug*, and *Pig* compositions were close enough to the compositions of the analogous minerals in the natural rocks, but the simulated fractionation trends and the residual magma compositions of the Skaergaard intrusion [Wager and Brown, 1967] appeared to be principally different (Fig. 71).

In an AFM diagram, these natural and modeled lines nearly coincided and indicated significant Fe enrichment and MgO depletion until the appearance of magnetite. Magnetite crystallization under IW and QFM conditions resulted in a bend in the Fenner trend toward rapid FeO depletion and alkali enrichment in the melt. The maximum Fe enrichment in the melt was observed under the most reduced conditions and attained ~20 wt % FeO (Fig. 71). In a closed system, the tendency toward FeO enrichment in the melt was less clearly pronounced, because magnetite appearance was associated with a deceleration in melt enrichment in Fe due to an approximately 1.5–2 times lower crystallization proportion of this mineral than that in the open system. Differences in the directions of the trends are revealed when these results are compared in a FeO–SiO_2 diagram (Fig. 71). It can be said that they correlate with the differences between intrusive and volcanic tholeiitic series discussed above:

(1) The modeled trends show silica enrichment starting from the early stages of magma fractionation. Judging from the crystallization proportions of the *Ol–Pl* cotectic (Table 13), it is reasonable to anticipate that the melt could become depleted in SiO_2 (Fig. 70) only if *Ol* was crystallized with *Pl* of a composition more sodic than An_{55}. Plagioclase of this composition first appears during the intermediate crystallization stages of the Skaergaard magma, shortly after the onset of clinopyroxene crystallization (Fig. 43).

(2) Regardless of the redox conditions of crystallization, magnetite crystallization should result in melt enrichment in SiO_2 (Fig. 71). However, Wager's mass-balance calculations suggest that the silicity of the derivatives starts to increase at a "stratigraphic" level much higher than that at which *Mt* first appears (supposedly as a cumulus mineral).

Problems of Skaergaard magma fractionation. Hunter and Sparks [1987] also noted that the calculated residual magma compositions [Wager and Brown, 1967] are in conflict with experimental data on phase equilibria in basaltic systems. The discrepancies include both the degree of Fe enrichment and the silica depletion trend, which is inconsistent with the low SiO_2 content (44–46%) in the crystallization products of the *Ol–Pl–Cpx* ± *Mt* gabbroic assemblage. The derivatives

of the Skaergaard magma were suggested to be, in fact, the products of tholeiitic magma evolution giving rise to the ferrobasalt—basaltic andesite—icelandite (ferroandesite)—dacite series, as is typical of volcanic suites. During its early and intermediate stages, this process was characterized by the crystallization of the *Ol–Pl ± Cpx* assemblage, which caused monotonous FeO enrichment in the melt at a roughly unchanging content of SiO_2. The onset of *Mt* crystallization results in strong melt depletion in FeO and complementary enrichment in SiO_2 [Hunter and Sparks, 1987].

It is important to stress that, in calculating the new series of the "Skaergaard magmas," Hunter and Sparks [1987] used another sample of chilled gabbro (KT-39 [Hoover, 1989b]), which contained ~50 wt % SiO_2 (the value normalized to the anhydrous basis, Table 15). Because of this, the derivatives obtained with the use of gabbroic components were systematically higher in silica compared with the data in [Wager and Brown, 1967]. Moreover, these calculations were conducted ignoring the possibility that the cumulus could contain some amount of the trapped melt and the magma could carry suspended crystals.

In the mid-1990s, these problems attracted the attention of Toplis and Carroll [1995, 1996], who conducted a series of melting experiments with synthetic compositions approximating the most primitive ferrobasalts from dikes comagmatic with the Skaergaard intrusion [Toplis and Carroll, 1995]. The results of these experiments within a broad f_{O_2} range were presented in the form of dependences of the crystallization sequences on the bulk degree of crystallization, melt composition, and redox conditions (ΔQFM). Using this parametrization and the calculated modal proportions, these authors developed an empirical model that made it possible to examine ferrobasaltic magma fractionation in systems buffered and closed with respect to oxygen [Toplis and Carroll, 1996]. The main conclusions of this research confirmed the results in [Ariskin *et al.*, 1988b]: none of the modeled lines of fractionation reproduced the canonical trend for the Skaergaard residual magmas, and the direction of the calculated trends corresponded to the tendency identified for volcanic series (Fig. 70).

At the same time, these data show discrepancies with the results in [Ghiorso and Carmichael, 1985; Ariskin *et al.*, 1988b] concerning the estimated parameters of magnetite crystallization. Toplis and Carroll [1996] postulated an unexpectedly high *Mt* crystallization proportion: it was decreased from ~40 to 5 wt % under the conditions of the oxygen buffers (20–25% on average) and from 30 to 10 wt % (15% on average) in a closed system. Consequently, iron depletion and silica enrichment in a FeO–SiO_2 diagram appeared to be more significant, and the drastic FeO depletion of the melt occurred irrespective of whether the system was open or closed to oxygen.

Concluding this excursion into the problem, it is pertinent to mention that attempts to revise traditional ideas concerning the evolutionary trends of the Skaergaard magma inevitably provoke controversy among petrologists. These discussions still have not resolved the conflict between the arguments put forth by opponents of the new interpretation [McBirney and Naslund, 1990; Morse, 1990; Brooks and Nielsen, 1990] and the data on phase equilibria utilized in [Ariskin *et al.*, 1988b; Hunter and Sparks, 1987, 1990; Toplis and Carroll, 1996]. Apparently, these issues can be settled by determining the starting conditions of the intra–chamber differentiation (including estimates of the temperature and crystallinity of the parental magma) and developing more accurate models for phase equilibria, including the crystallization of *Mt*- and *Ilm*-bearing mineral assemblages. After calibrating more realistic models of magnetite and ilmenite crystallization, new simulations were conducted to model Skaergaard magma fractionation [Ariskin and Barmina, 1999, 2000]. These results are discussed below in light of data on the geochemical thermometry of rocks from the Marginal Border Series and the Layered Series of the Skaergaard intrusion (Chapter 3).

4.1.2. Simulation of Skaergaard magma fractionation

The simulations were carried out with two starting compositions: (1) TMav, corresponding to the average of the experimental and theoretical estimates of the intercumulus liquid composition in MBS rocks, and (2) KT-39, which represents the chilled gabbro (Table 15). The fractional crystallization was simulated at 1 atm, in systems open (QFM/WM) and closed with respect to oxygen, with a crystallization increment of $\Delta\varphi_{cr}$ = 1 mol %, up to the maximum degree of fractionation equal to 80%.

Systems buffered with respect to f_{O_2}. The crystallization sequence of minerals as a function of temperature is shown in Fig. 72. According to these data, the liquidus temperatures are 1158°C at QFM and 1163°C at WM for the TMav composition and are slightly higher for KT-39 (1170 and 1174°C, respectively). The modeled crystallization sequence for TMav is independent of redox conditions and is $Ol + Pl + Aug \longrightarrow Pl + Aug + Mt$. The only difference is the earlier crystallization of magnetite under QFM conditions. The phase relations for KT-39 are more complicated: the crystallization of silicates also does not depend on f_{O_2}, but ilmenite starts to crystallize earlier under more reduced (WM) conditions. The evolution of mineral compositions shown in Fig. 72 demonstrates that the liquidus olivine falls within the range of 74–76 mol % *Fo*, whereas the plagioclase contains 62–63 mol % *An*. The modeled clinopyroxene composition varies from $En_{44}Wo_{41}$ near the liquidus to $En_{26}Wo_{30}$ during late crystallization stages. The titanomagnetite and ilmenite

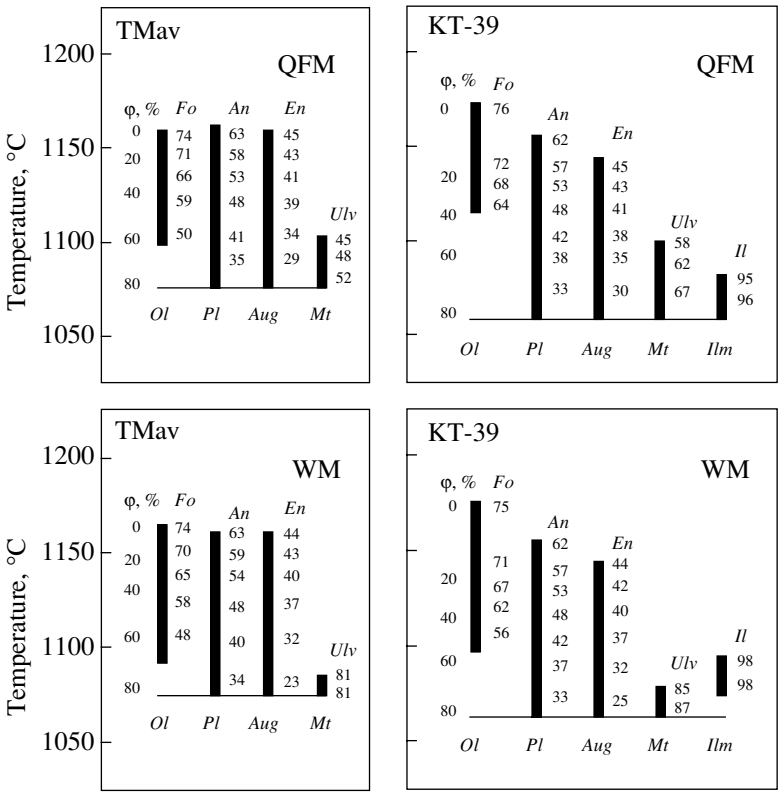

Fig. 72. Crystallization sequence of minerals during the perfect fractionation of two magmas proposed to be parental to the Skaergaard intrusion. The calculations were conducted with the COMAGMAT-3.51 program at $P = 1$ atm and variable redox conditions: (*1*, *2*) TMav initial melt (average between TM and the experimental composition in Table 15); (*3*, *4*) chilled gabbro KT-39. The compositions of silicates are in mol %, *Ulv* and *Il* are the activities of Fe–Ti oxide components calculated after [Stormer, 1983].

compositions correlate with changes in the redox conditions.

Figure 73 compares the covariation in FeO and SiO_2 in the modeled melts corresponding to the fractionation of TMav and KT-39 compositions under QFM conditions. Each of these compositions corresponds to two evolutionary lines: the upper line demonstrates the results of calculations with the basic COMAGMAT-3.51 model (without temperature correction), and the lower one represents the corrected results. The corrections involved the artificial decrease in the *Ol*, *Pl*, and *Aug* crystallization temperatures by 10°C as the *Mt* and *Ilm* liquidus temperatures were increased by 15°C. Thus, the relative increase in the magnetite liquidus temperature was +25°C, which corresponds to the maximum inaccuracies related to the use of the COMAGMAT program. As can be seen from these diagrams, such an increase in the modeled temperatures for *Mt* results in a decrease in the degree of Fe enrichment in the melt by 1.5–2.5 wt % at the same SiO_2 contents. This is commensurable with the effect of a change in $\log f_{O_2}$ by 0.5–1 logarithmic units.

In addition, Fig. 73 demonstrates the canonical differentiation trend of the Skaergaard magma [Wager and Brown, 1967], the compositions of some dikes comagmatic with the Skaergaard Massif [Brooks and Nielsen,

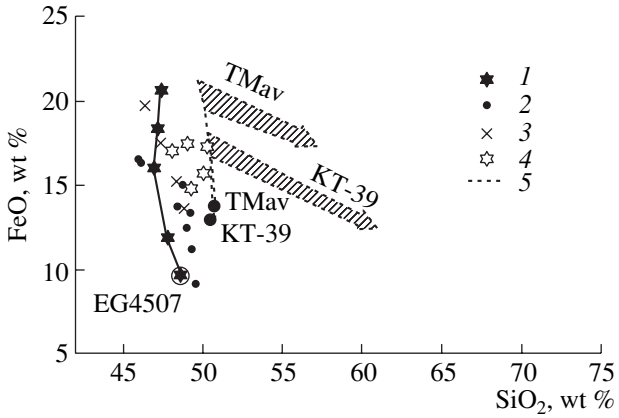

Fig. 73. Natural differentiation trends versus modeled fractionation lines of the Skaergaard magma. (*1*) Canonical trend [Wager and Brown, 1967]; (*2*) compositions of comagmatic dikes [Brooks and Nielsen, 1978, 1990]; (*3*, *4*) intercumulus liquid compositions for Layered Series rocks: (*3*) data of melting experiments [McBirney and Nakamura, 1973; McBirney and Naslund, 1990], (*4*) data of geochemical thermometry (Table 22); (*5*) simulation of fractional crystallization for TMav and KT-39 compositions (Table 15). The calculations were conducted with the COMAGMAT-3.51 program at $P = 1$ atm and QFM conditions. The shaded fields cover the range of uncertainties due to the use of the magnetite model [Ariskin and Barmina, 1999].

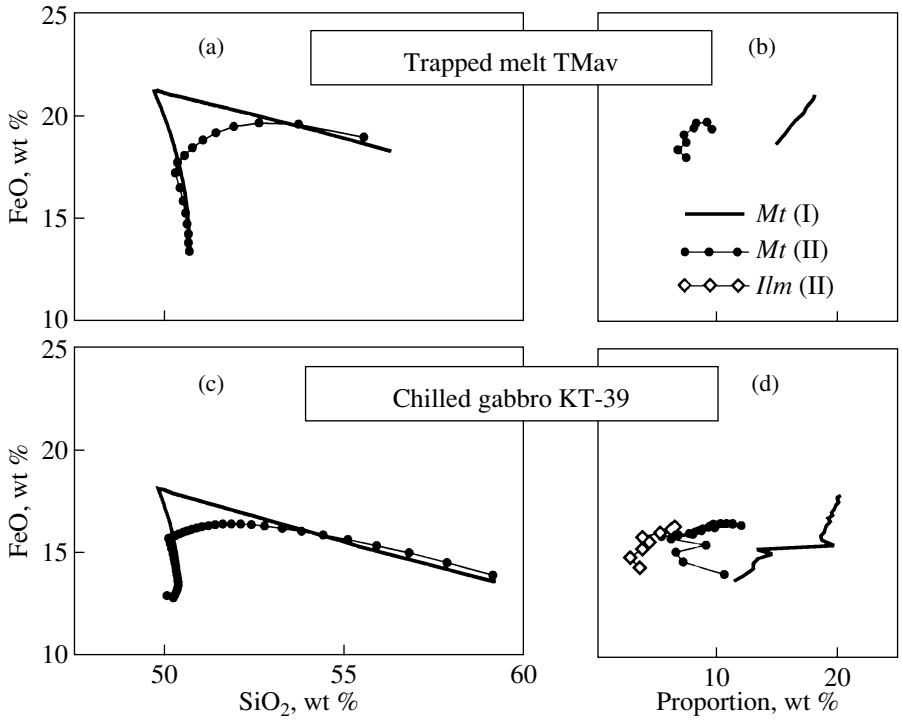

Fig. 74. Evolution of the derivative liquid compositions and crystallization proportions of Fe–Ti oxides during the fractionation of the Skaergaard melts in systems open and closed with respect to oxygen. Calculations were conducted with the COMAGMAT-3.51 program at P = 1 atm under the following conditions: (*I*) QFM; (*II*) closed system (original $Fe^{2+}/\Sigma Fe$ ratio = 0.86 corresponds to the QFM buffer at the liquidus temperature): (a, b) initial TMav melt, (c, d) chilled gabbro KT-39.

1978, 1990], the estimated compositions of the intercumulus liquid for the Layered Series rocks (experimental data from [McBirney and Nakamura, 1973; McBirney and Naslund, 1990], and the results of geochemical thermometry from Table 22. A comparison of the natural and experimental trends leads to two conclusions: (i) the simulated evolutionary lines demonstrate weak (if any) SiO_2 depletion compared with the differentiation trends proposed for the Skaergaard magma and (ii) the modeled trajectories have inflection points corresponding to the onset of titanomagnetite crystallization.

At the same time, this comparison emphasizes the differences between the two chosen parental magma compositions, which are manifested in the behavior of Fe–Ti oxides. KT-39 composition, which is relatively enriched in TiO_2 (Table 15), is characterized by the appearance of ilmenite (Fig. 72) and a lower degree of Fe enrichment. In the case of TMav, ilmenite does not appear at all, but the degree of FeO enrichment is high, up to 20–22 wt %. Hence, it can be hypothesized that the natural initial melt of the Layered Series rocks should have possessed TiO_2 contents sufficient for *Ilm* crystallization (at least 2.5 wt % TiO_2) and have been slightly depleted in SiO_2 compared with TMav and KT-39 compositions, which explains the tendency toward melt enrichment in FeO without an increase in SiO_2.

These speculations are supported by the data of geochemical thermometry of Layered Series rocks (Table 22). In Fig. 73, these compositions lie between the natural trends and modeled trajectories. The uncertainties of the thermometric calculations preclude their approximating by a general "course of differentiation," but the relative position of the data points leaves no doubt that the source was depleted in SiO_2 and enriched in TiO_2. It is interesting that this conclusion is consistent with the systematic differences in the crystallization sequences of minerals determined for the average compositions of the Layered Series and their equivalents from the Marginal Border Series (Fig. 64) [Ariskin, 2003].

Systems closed to oxygen. In modeling the fractional crystallization of TMav and KT-39 compositions in closed systems, we postulated initial ratio $Fe^{2+}/\Sigma Fe$ = 0.86, which corresponded to that of the QFM buffer at the liquidus temperature of these systems. Other parameters corresponded to the calculations at buffered f_{O_2} conditions discussed above. The most important results are presented in Fig. 74. As can be seen from these data, the FeO–SiO_2 evolutionary lines remain practically the same as in our earlier models (Fig. 71) and suggest lower degrees of Fe enrichment than in the crystallization trajectories for the open system. These differences were caused by a decrease in the *Mt* crystal-

lization proportion: the right-hand plots in Fig. 74 indicate that the amount of *Mt* crystallized in a closed system is two-thirds of that calculated under the oxygen pressure.

In general, the results of simulating fractional crystallization in systems closed to oxygen and a comparison of these results with natural trends are consistent with the conclusions drawn for the open systems. According to these calculations, the maximum degree of Fe enrichment in the melts does not exceed 20 wt %, the appearance of Fe–Ti oxides results in enrichment in SiO_2, and the source of the melts of the Layered Series cumulates should have been less silicic than follows from the TMav and KT-39 compositions. In any event, it seems to be hardly probable that the problem of Skaergaard magma differentiation can be solved within the framework of the concepts of the openness or closure of the system with respect to oxygen [Ariskin, 2003].

Analyzing the possible reasons for the chemical differences between the intercumulus liquids in the marginal facies and the rocks of the Layered Series is beyond the scope of this publication. We believe that progress in techniques for the simulation of crystallization processes and their systematic application to studying the full vertical section of the Skaergaard intrusion will shed light onto this problem, as well as on other aspects of genetic reconstructions for this very interesting intrusion.

4.1.3. Simulation of ferrodiorites from the Chazhma sill, Eastern Kamchatka

The example of Skaergaard magma differentiation has demonstrated that it is difficult to draw direct analogies between the inner structures of intrusive bodies and the petrochemistry of volcanic suites, mostly because of the uncertainties in the conditions and mechanisms of intra–chamber differentiation. At the same time, there are layered bodies whose rock compositions display sublinear trends like those of andesite–basalt series [Sparks, 1988; Wiebe, 1994; Koroleva and Oleinikov, 1998]. This makes it possible to examine them using the same techniques of petrological interpretations elaborated for volcanic associations. A typical body of this type is the Chazhma sill in the northeastern tip of Kronotskii Peninsula, Kamchatka, Russia [Barmina *et al.*, 1988]. The example of the Chazhma differentiated suite is utilized to demonstrate the possibility of redoximetry of rocks that approximate the compositions of derivative liquids during the fractionation of *Mt*-bearing mineral assemblages [Ariskin and Barmina, 1999].

Geologic setting and inner structure. The Chazhma sill is exposed as craggy cliffs extending along the Pacific coast for ~1.5-km. The outcrops trend from southwest to northeast and expose the subvolcanic body from its upper to the lower contact in the breaker zone. The thickness of the sill varies from 25 to 40 m. It includes numerous leucocratic layers and segregations, sharply contrasting with the host diabases (plagiodolerites). The morphology of these segregations varies: these are usually lamina and beds elongated along the strike of the vein or cutting across it. Their thicknesses vary from a few centimeters to 1.5 m. The leucocratic beds often bend and have swells and pinches. The contacts of the beds are sharp, although sometimes they grade into the host rocks. The segregations also often have the shapes of lenses, schlieren, and tongues.

The mesocratic plagiodolerites dominate in the lower portion of the sill. These are massive porphyritic rocks with 20–30% plagioclase phenocrysts and occasional olivine grains. The groundmass consists of plagioclase, clinopyroxene, iron oxides, and minor amounts of glassy mesostasis and has a doleritic or, in places, poikilophitic texture. The amount of *Pl* phenocrysts in the dolerites increases upward from the sill bottom, and this is associated with the appearance of the first leucocratic beds. The embedded rocks retain their porphyritic texture, but their groundmass contains insignificant amounts of hornblende, biotite, and apatite. The contents of granophyre and glassy material is significantly increased. The texture of the leucocratic rocks approaches a micropegmatitic one.

The chemistry of minerals from the Chazhma sill was analyzed on an X-ray microprobe [Barmina *et al.*, 1988]. The plagioclase comprises two morphological varieties: large phenocrysts, whose composition varies from An_{65} to An_{80}, and smaller grains, which crystallized *in situ* and whose composition is close to that of the rims of the phenocrysts: $An_{50–65}$. The composition of microlites in the mesostasis is $An_{20–30}$. The size and amount of *Pl* phenocrysts in the leucocratic rocks decreases, and their composition becomes progressively more sodic, $An_{50–60}$. The groundmass plagioclase varies from An_{35} to An_{50}, and microlites in the mesostasis consist of $An_{5–20}$.

Pyroxene occurs as large equant crystals, which become subhedral in the upper part of the vertical section. They are zonal, with high-temperature cores and low-temperature outer rims. The plagiodolerites are dominated by augite, whose composition varies as $En_{35–50}Fs_{15–20}Wo_{35–45}$. The rocks of the leucocratic layers commonly contain abundant subcalcic pigeonite and augite.

Olivine can be identified optically as single equant grains only in the mesocratic dolerites. These crystals are nearly completely replaced by aggregates of water-bearing minerals. Magnetite was found in all of the samples in the form of small euhedral crystals and large skeletal grains. The composition of this mineral calculated on the *Ulv–Mt* basis varies in the range $20 \le x_{Uly} \le 80$ mol %, with the rocks of leucocratic layers containing ulvospinel-richest grains.

The chemical composition of rocks from the Chazhma sill is characterized in Table 23 and in the variation diagrams in Fig. 75. The mesocratic dolerites

Table 23. Compositions of the rocks and assumed parental melts used to simulate the formation of ferrodiorites in the Chazhma sill by means of fractional crystallization

Component	Plagiodolerite and the most primitive melt		Fine-grained rocks from leucocratic layers			
	PD	PD-30	GD-1 (n = 2)	GD-2 (n = 4)	DR (n = 3)	GR (n = 3)
SiO_2	51.69	51.70	53.78	54.65	59.45	64.33
TiO_2	1.28	1.87	1.92	1.92	1.44	0.93
Al_2O_3	18.47	13.65	14.11	14.20	14.28	15.10
FeO	10.24	14.43	13.47	12.91	10.32	7.48
MnO	0.16	0.22	0.21	0.23	0.25	0.16
MgO	4.15	5.30	3.95	3.60	2.44	1.25
CaO	10.22	9.28	8.16	7.52	5.67	3.46
Na_2O	2.52	2.09	2.66	3.03	3.33	3.79
K_2O	1.04	1.11	1.41	1.55	2.18	3.20
P_2O_5	0.24	0.35	0.33	0.38	0.64	0.30

Note: All natural and modeled compositions are normalized to 100 wt % (all Fe as FeO). PD—average plagiodolerite (n = 22), PD-30—melt calculated by means of removal of 28.7 wt % *Pl* ($An_{61.6}$) and 1.3 wt % *Ol* ($Fo_{70.4}$); GD-1—average "primitive" ferrogabbrodiorite (it was utilized as the starting composition for simulations whose results are shown in Fig. 76); GD-2—average "normal" ferrogabbrodiorite; DR—average ferrodiorite; GR—average granophyre. Numerals in parentheses show the numbers of samples.

compose a compact group with compositional variations caused by variable contents of Al_2O_3 (16.9–20.5 wt %) and FeO (8.5–11.5 wt %). The rocks are characterized by enrichment in FeO at an insignificant increase in the SiO_2 content. The leucocratic gabbro and diorites compose a continuous series of Bowen's type, which is characterized by an increase in the contents of SiO_2 and alkalis coupled with a monotonous decrease in the contents of FeO, TiO_2, MgO, and CaO (Fig. 75). The most silicic rocks of the leucocratic layers contain 64–65 wt % SiO_2 and 7.5 wt % FeO, while the intermediate compositions are close to those of ferroandesites from Thingmuli volcano (Fig. 70). Given the subvolcanic nature and textures of these rocks, they are referred to as ferrodiorites.

The mechanism that has produced the ferrodiorites and the nature of genetic links between these rocks and the host plagiodolerites are the key problems in the petrology of the Chazhma sill. The genesis of these rocks can, perhaps, be explained by the differentiation of a high-Al basaltic parent in a magma chamber. However, this hypothesis is at variance with data on the chemistry of the chilled contact diabases, which are notably poorer in SiO_2 than the weighted mean composition of the sill (calculated with regard for leucocratic layers) and are practically identical to the mesocratic dolerite compositions (Table 23). Along with the occurrence of the leucocratic segregations in the form of veins, this suggests that the melts corresponding to the ferrodiorites had been formed prior to injection into the magma chamber. At the same time, facies relationships between the leucocratic and mesocratic rocks testify that the strongly differentiated materials were injected into the chamber practically simultaneously with the emplacement or just after it, as the body began to crystallize.

Fractional crystallization simulation. To clarify the possible crystallization links between the ferrodiorites and host rocks, we simulated the fractional crystallization of the melt of composition corresponding to the average plagiodolerite of the Chazhma sill (Table 23). These preliminary simulations were carried out with the THOLEMAG program [Barmina *et al.*, 1988] as a precursor of the COMAGMAT model. The course of fractionation was calculated at QFM conditions with corrections of the modeled *Mt* temperatures (they were decreased by 20–30°C).

According to the simulation results, the first mineral to crystallize at 1236°C was plagioclase of composition An_{79}. After 22% *Pl* ($An_{79} \longrightarrow An_{70}$) had crystallized, olivine of composition Fo_{70} appeared on the liquidus at a temperature of approximately 1150°C. In the temperature range of 1137–1132°C, olivine was replaced by titanomagnetite and augite ($En_{43}Fs_{20}Wo_{37}$), after which *Pig* ($En_{61}Fs_{30}Wo_9$) started to crystallize at 1126°C. This calculated crystallization sequence is consistent with the mineral assemblages and textural relations inferred from petrological observations, and the modeled mineral compositions appeared to be close to the microprobe data. Considering the clearly pronounced petrochemical trends, this led us to suggest that the leucocratic gabbro, ferrodiorites, and host plagiodolerites affiliate with a single magmatic series that was formed by the crystallization mechanism [Barmina *et al.*, 1988].

This conclusion is confirmed by the correspondence between the observed trends of differentiation of the Chazhma rocks and the liquid lines of descent calculated for the average plagiodolerite melt (Fig. 75). Each bend of the natural trends corresponds to an inflection

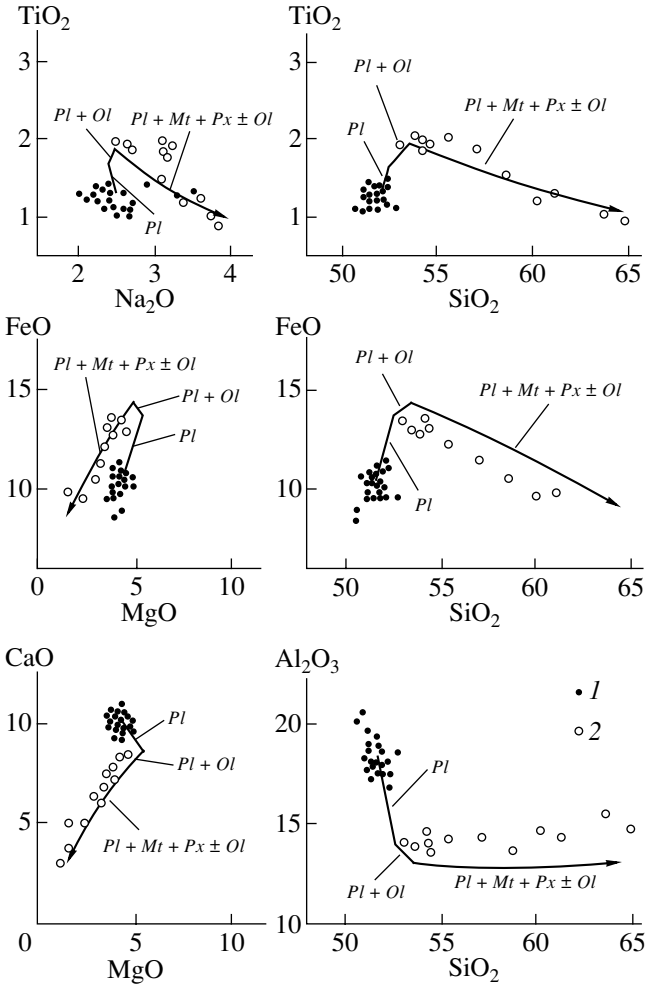

Fig. 75. Differentiation trends of rocks from the Chazhma sill and the modeled lines of fractional crystallization calculated for the average "plagiodolerite" as the assumed parental magma [Barmina, 1988]. (*1*) Mesocratic plagiodolerites; (*2*) leucocratic layers.

in the modeled lines related to a change in the modal composition of the crystallizing mineral assemblages. The fact that the data points of the leucocratic rocks cluster close to the lines of cotectic control suggests that these rocks are compositionally close to the liquid fractions derived from the assumed basaltic parent and contain very insignificant amounts of accumulated crystals. This is also consistent with the low amount of *Pl* phenocrysts in the ferrodiorites.

The first calculations carried out for the Chazhma suite have demonstrated the high potentiality of the developed phase equilibrium model and the role of magnetite in the genesis of petrochemical trends. However, these results left uncertain the redox conditions of the crystallization process. The QFM buffer was chosen based on general considerations, which were underlain by known concepts concerning the crystallization conditions of tholeiitic magmas (see, for example, [Carmichael and Ghiorso, 1986]). Moreover, the later studying of the petrology and geochemistry of the Kronotskii basalts and their hypabyssal analogues has demonstrated that the predominance of Al_2O_3-enriched compositions was not caused by the occurrence of high-Al magmas but is a consequence of the mechanical accumulation of *Pl* crystals in the ferrobasaltic liquids similar to island-arc tholeiites [Barmina *et al.*, 1989a, 1992].

From this standpoint, the crystallization link between the plagiodolerites and ferrodiorites of the Chazhma sill implies that the latter rocks are the product of the fractional crystallization of the ferrobasaltic melt that composed the liquid part of the parental plagiophyric magma. The composition of this original melt can be estimated by the method of geochemical thermometry (see open circle in Fig. 76), but we attempted to evaluate the redox conditions under which the Chazhma ferrodiorites were produced using only natural rock compositions.

Redoximetry of the Chazhma ferrodiorites. If the rocks of the leucocratic layers are assumed to represent the liquids generated by the fractionation of a basaltic parent, their liquidus mineral assemblage should have

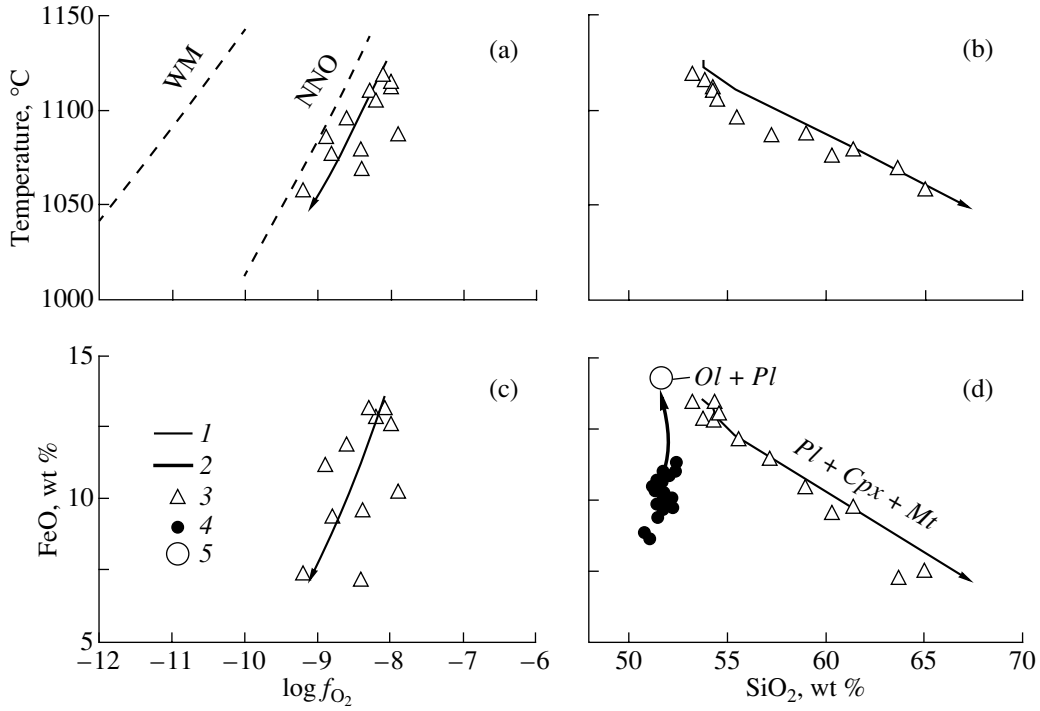

Fig. 76. Evaluated redox conditions and the results of simulating the genesis of the Chazhma ferrodiorites with the COMAGMAT-3.51 program [Ariskin and Barmina, 1999]. (a, b) *Pl* and *Mt* crystallization temperatures: (a) as a function of f_{O_2}, (b) as a function of SiO_2; (c, d) FeO contents in the melts: (c) as a function of f_{O_2}, (d) as a function of SiO_2. (*1*, *2*) Liquid lines of descent at NNO + 0.5: (*1*) fractionation of GD-1 composition, (*2*) equilibrium crystallization of PD composition (Table 23); (*3*) ferrodiorites; (*4*) plagiodolerites; (*5*) product of 30% crystallization of PD composition.

been *Pl* + *Aug* + *Mt* ± *Ol* ± *Pig*. In this situation, the temperature at which any rock was formed can be evaluated with the *Pl*–melt geothermometer, whose accuracy is 10–15°C and which is virtually independent of f_{O_2}. As can be seen from Fig. 76b, these temperatures range from 1125°C for the ferrogabbrodiorites to 1050°C for the granophyres. With regard for the condition of simultaneous saturation with respect to all cotectic phases, the calculated *Pl* temperatures should coincide with the *Mt* crystallization temperatures. This enabled us to undertake a search for f_{O_2} values at which the condition $T_{Pl} = T_{Mt}$ is fulfilled.

Within the scope of this method, thermometric calculations were conducted for each leucocratic rock (14 samples) within the range of $-10 \le \log f_{O_2} \le -7$. These calculations yielded $\log f_{O_2}$ values at which the modeled temperatures of the *Mt*–melt equilibrium differed from the *Pl* temperatures by no more than 1°C. These data are presented in Fig. 76a and demonstrate an insignificant but reliably identified decrease in f_{O_2} from 10^{-8} to 10^{-9} bar with decreasing temperature. The calculated trend corresponds to the parameters of the NNO + 0.5 buffer, and these values can be regarded as the redox conditions under which the Chazhma ferrodiorites were produced.

The accuracy of the $\log f_{O_2}$ evaluations is determined by the dependence of the magnetite liquidus temperature on oxygen fugacity. As follows from the data presented in Section 2.2.5, this dependence is 15–30°C/$\log f_{O_2}$. At an average calculation error of the magnetite crystallization temperature of 15°C, the uncertainty in the absolute $\log f_{O_2}$ estimates is 0.5–1 logarithmic units. However, this is valid at a good accuracy of the plagioclase temperature calculations. The uncertainty in the f_{O_2} estimates increases if the calculation inaccuracies of the *Pl* and *Mt* temperatures have different signs, and, conversely, decreases if they have the same sign.

As an independent criterion of the accuracy of the oxygen fugacity reconstructions, one can use the result of computer simulations of the fractional crystallization of the melt corresponding to the average "primitive" ferrogabbrodiorite (Table 23, GD-1). As can be seen from Fig. 76d, the modeled line of fractionation realistically reproduces the Bowen trend of Fe depletion and SiO_2 enrichment under NNO + 0.5 conditions.

The modeled conditions under which the Chazhma ferrodiorites were formed not only testify to the crystallization nature of the genetic relations between the ferrodiorites and parental ferrobasalts but also confirm that the oxygen fugacity controlling the magma crystallization process can be evaluated in such a manner. Geological relationships indicate that this fractionation took place during a prechamber stage, which was followed by the practically simultaneous injection of the plagiodolerite magma and the formation of the leucocratic layers and tongues. The origin of the silicic derivatives can be explained by the extensive crystallization of the basalt parent in the boundary zones of magma conduit or an intermediate chamber, which was accompanied by the segregation of low-melting residues from the crystallization products via the mechanism of compositional convection [McBirney *et al.*, 1985; Tait and Jaupart, 1992].

4.2. Polybaric Fractionation of Tholeiitic Magmas

In previous sections, we considered examples of tholeiitic magma fractionation in relatively small chambers at $P \leq 2$ kbar. It was established that, under these conditions, thermodynamic simulation techniques can realistically reproduce the Fenner trend of FeO enrichment and the Bowen tendency toward the origin of SiO_2-rich derivatives. The transition between these two trends is controlled by the extent of system closure with respect to oxygen, and this opens the possibility of using modeled liquid lines of descent to evaluate the redox conditions of crystallization.

It is more difficult to solve such problems for polybaric fractionation. This is related, to some extent, to the techniques utilized to simulate mineral–melt equilibria under elevated pressures (our approach is quite primitive, see Section 2.2.6). However, the main problem is the uncertainty of the experimental data obtained at high parameters. Although pressure can be monitored in these experiments accurate to a few kilobars, there are larger interlaboratory differences in piston–cylinder pressure calibration at high temperatures. The oxygen fugacity is commonly not controlled at all, whereas the effect of encapsulating material and thermocouples on the stability of the mineral assemblages may be significant. This situation is further complicated by the effect of minor water contents on the phase equilibria [Falloon *et al.*, 2001]. Moreover, the formation of equilibrium crystals in runs at higher pressures and temperatures is often a problem, because the scale of heterogeneity introduced by quench solid phases can be greater than that of the pockets of segregated melt. This provokes doubts in the equilibrium character of the experimental products.

Thus, the quality of experimental information provided by high-pressure experiments is notably lower than that obtained under atmospheric pressure, which affects the accuracy of the developed phase equilibria models. The first results of computer simulations by the MELTS program led to the pessimistic conclusion that data of high-pressure experiments in natural systems do not allow the development of realistic phase equilibrium models that could be applied to a wide range of *P–T* conditions [Ghiorso, 1997]. We believe that this situation is not as desperate if the task is not formulated as the development of a "supersystem of computer modeling" [Ghiorso and Sack, 1995], but instead attention is focused on solving specific problems and selecting an appropriate experimental database for the calibrations. Thus, the blame (often justified) on the quality of the programs simulating phase equilibria at elevated pressures does not mean that it is senseless to continue attempts to develop new techniques for the genetic interpretation of mafic rocks on the basis of polybaric crystallization models.

O'Hara [1965] was the first to consider in much detail the petrogenetic aspects of fractional crystallization of basaltic magmas under the effect of changing pressures. The main conclusion of this research was as follows: the chemical and modal mineral compositions of most basalts provide information on the shallow-depth crystallization conditions. The further estimates of the effect of the high-pressure process were presented in a series of early publications by Green and Ringwood, but the majority of experimental data on basaltic phase diagrams was obtained in the 1980s and 1990s (see the reviews in [Hess, 1992; Herzberg, 1995]). As a result, the stability fields of principal cotectic assemblages were constrained at $P \leq 30$ kbar, and this opened up the possibility of constructing generalized *P–T* diagrams for basaltic systems [Stolper, 1980; Takahashi and Kushiro, 1983] and extrapolating data on the peridotite melting to still-unexplored compositions [Ryabchikov, 1994; Kinzler and Grove, 1992a, 1992b, 1993; Hirschmann *et al.*, 1998, 1999].

This information was commonly utilized to construct various barometric diagrams that could be used to project basalt glass compositions. This resulted in the opinion that the evolution of tholeiitic magmas in mid-oceanic ridges proceeded under relatively shallow-depth conditions, at $P < 5$ kbar [Presnall *et al.*, 1979; Stolper, 1980; Thompson, 1987; Kadik *et al.*, 1990]. At the same time, some aspects of the fractional crystallization of tholeiites under elevated pressures remained outside the scope of the experimental approach. Understanding the general direction of the polybaric crystallization trends is insufficient for the genetic interpretations of natural igneous suites. To solve these problems, semiempirical magma fractionation models were proposed, which were based on the parametrization of experimental cotectics (see, for example, [Grove *et al.*, 1992; Yang *et al.*, 1996]). Our simulations of the polybaric fractionation of tholeiitic magmas in the Central Atlantic were among the first attempts to study these phenomena with a thermodynamically coherent crystallization model [Ariskin *et al.*, 1990, 1992].

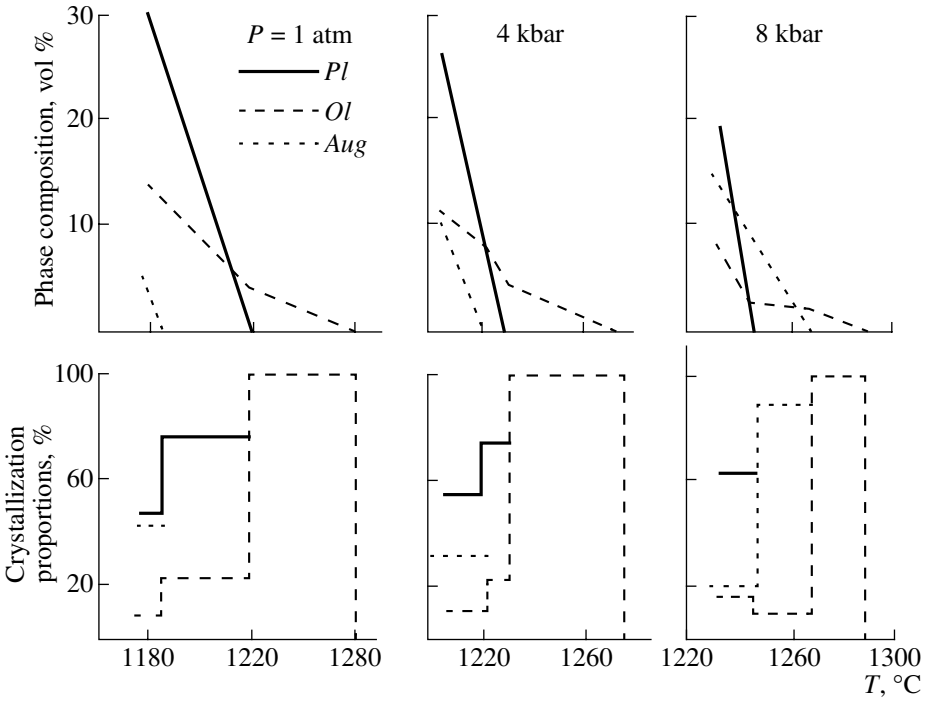

Fig. 77. Evolution of the phase composition of the system and the crystallization proportions of minerals during the equilibrium solidification of a high-Mg basalt [Bender *et al.*, 1978]. The polybaric calculations were conducted with the THOLEMAG program [Ariskin *et al.*, 1990].

4.2.1. Chemical sequences of polybaric crystallization

When discussing the calibration of the COMAGMAT program for the effect of pressure, it was mentioned that the model had been calibrated on three sets of experimental data on the melting of high-Mg oceanic tholeiites at pressures from 1 atm to 15 kbar [Bender *et al.*, 1978; Green *et al.*, 1979; Fujii and Bougault, 1983]. This was caused by the fact that the THOLEMAG version of the program was designed to solve genetic problems related to the fractionation of primitive magmas in mid-oceanic ridges. Using the THOLEMAG program, we conducted a series of polybaric calculations of equilibrium and fractional crystallization for high-Mg tholeiitic melt 527-1-1, which contained 10.8 wt % MgO [Bender *et al.*, 1978]. The calculations were conducted for a pressure of 1 atm and 2, 4, 6, 8, and 10 kbar under WM buffer conditions, with a crystallization increment of 2 mol % [Ariskin *et al.*, 1990]. Despite the imperfection of the early model, it managed to reproduce realistically enough the expansion of the clinopyroxene crystallization field with increasing pressure and the changes in the mineral assemblages (Fig. 30). However, the most important and even somewhat unexpected results were obtained on the evolution of the phase composition of the system and the crystallization proportions of minerals (Fig. 77).

The narrowing of the overall interval of the crystallization temperatures of minerals with increasing pressure demonstrated in this figure (compare the upper plots for 1 atm and 8 kbar) is caused by the earlier crystallization of *Cpx* and was extensively discussed in the literature (see reviews in [Hess, 1992; Herzberg, 1995]). More questions are provoked by the character of changes in the crystallization proportions shown in the lower series of plots. As can be seen from these data, the amount of *Pl* crystallized at the *Ol–Pl–Aug* cotectic monotonously increased from 48 vol % at 1 atm to 62 vol % at 8 kbar. At the same time, the proportion of *Aug* decreased within the same interval from 42 to 20%. This result has important petrological consequences and deserves more detailed consideration.

Evolution of the crystallization proportions. The relative decrease in the *Pl* temperature at a pressure increase in a closed system is coupled with complementary Al_2O_3 enrichment in the melt late in the crystallization process. With reference to the genesis of oceanic tholeiites, this effect was examined experimentally with the use of a synthetic analogue of plagioclase lherzolite [Presnall *et al.*, 1979]. For the fields of four- and five-phase equilibria, these authors established a monotonous enrichment of the liquid in alumina with a pressure increase to 9.3 kbar, which led to the conclusion that the amount of crystallizing plagioclase should be significantly decreased with increasing pressure. This conclusion is consistent with the data portrayed in the upper set of plots in Fig. 77.

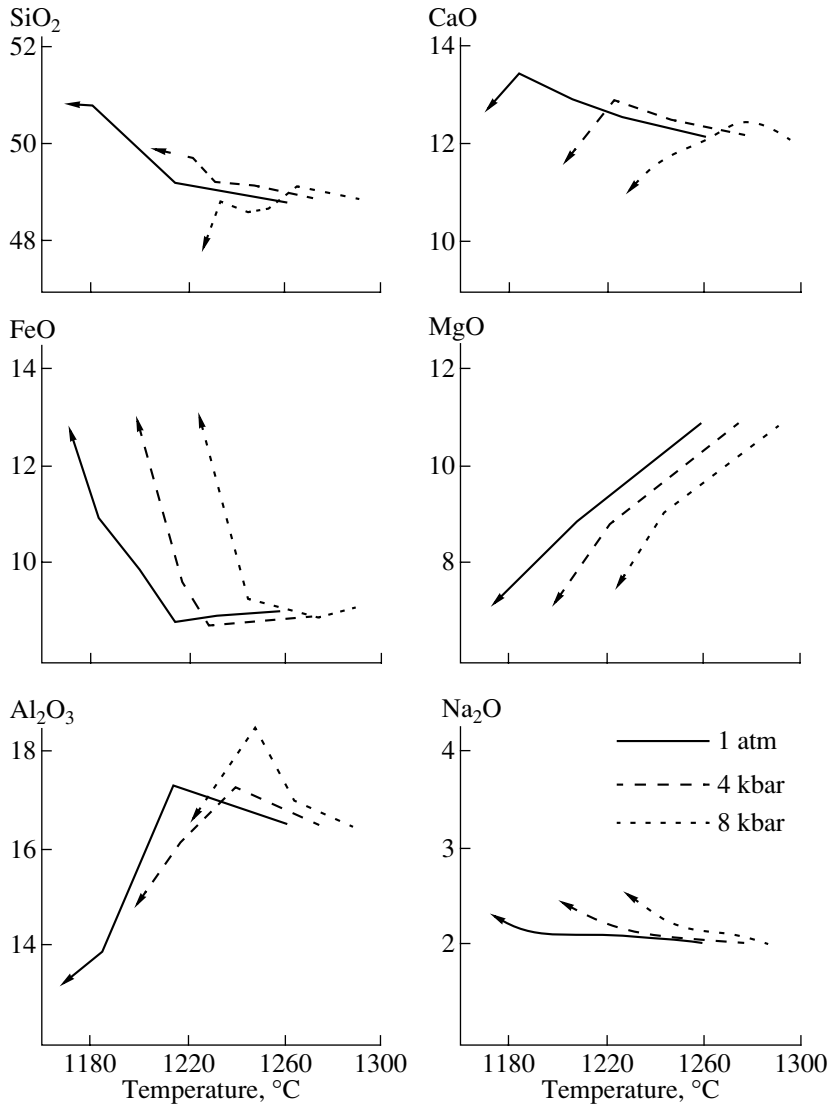

Fig. 78. Evolutionary lines of residual melts during the fractional crystallization of the primitive tholeiitic melt [Bender *et al.*, 1978]. The polybaric calculations were conducted with the THOLEMAG program [Ariskin *et al.*, 1990].

It seems, however, unjustified to extrapolate these results to the crystallization proportions of minerals. The point is that, proceeding from the general decrease in the *Pl* amount in liquidus assemblages, some researchers arrived at the conclusion that the percentage of *Pl* in the crystallizing material decreased with increasing pressure [Grove and Baker, 1984]. This conclusion implies that similar variations in the *Pl* crystallization proportions with pressure predetermine the possibility of deriving high-Al melts from a basaltic magma. Our calculations point to the opposite tendency (see the lower plots in Fig. 77): a decrease in the overall *Pl* amount in the system and complementary enrichment of the melt in Al_2O_3 prior to *Pl* crystallization lead to an increase in the proportion of this mineral relative to *Aug* during the cotectic crystallization of both minerals.

This means that the crystallization of the *Ol–Pl–Aug* assemblage under elevated pressures should result in the depletion of the residual melt in Al_2O_3, a process that is pronounced even more contrastingly than at lower pressures.

The evolution of the melt composition during the fractional crystallization of the same primitive tholeiite at pressures of 1 atm, 4 and 8 kbar is demonstrated in Fig. 78. The fractionation was simulated by means of the complete removal of crystallizing phases from the system with an increment $\Delta\varphi_{cr} = 2$ mol %. As can be seen from these data, a pressure increase significantly affects the trends of the concentrations of certain components, with Al_2O_3 strongly enriching the melt during the crystallization of the *Ol–Aug* cotectic at 8 kbar. This suggests that high-Al melts can be produced under elevated pressures but only if *Pl* is absent from the liquidus

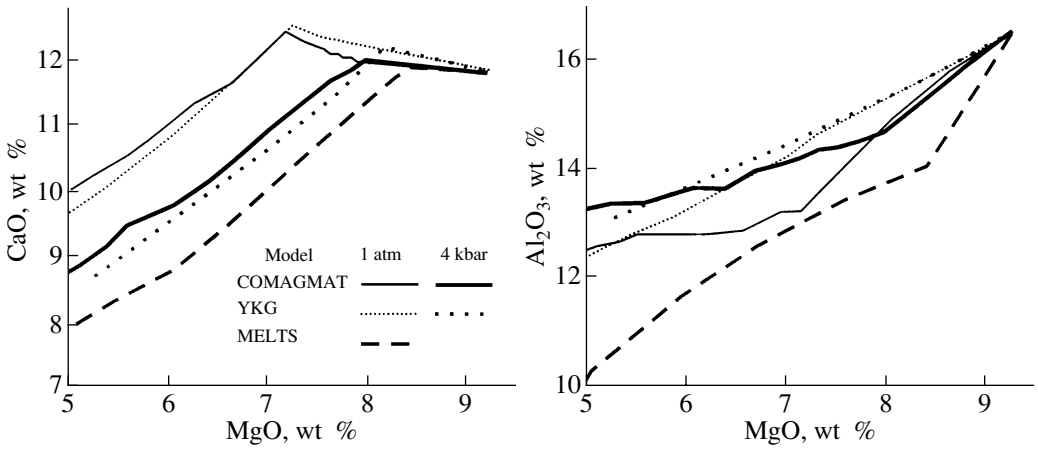

Fig. 79. Verification of fractional crystallization lines for the melt of oceanic tholeiite ALV-2004-3-1, calculated by different models [Yang *et al.*, 1996].

assemblages (this problem will be discussed in detail in Section 4.3). It seems to be important for our further analysis to consider data on the CaO contents. This component demonstrates a systematic and the strongest dependence on pressure (Fig. 78).

The cause of this phenomenon is self-evident: relatively early *Aug* crystallization under high-pressure conditions leads to a drastic depletion of the melt in CaO, which is directly correlated with pressure and the depth at which crystallization differentiation proceeds. This led us to draw the preliminary conclusion that the most calcic tholeiitic melts correspond to the shallowest crystallization conditions of the parental magmas, whereas CaO-depleted basalts mark the high-pressure stage of their fractionation [Ariskin *et al.*, 1990; Grove *et al.*, 1992].

The evolution of the SiO_2 content in the melt also correlates with the crystallization of pyroxenes. During the crystallization of the *Ol–Pl* cotectic, the melt becomes enriched in SiO_2, but the earlier crystallization of *Aug* under elevated pressures can significantly hamper or even prevent this trend of silica enrichment. It is more difficult to assay how realistic the significant SiO_2 enrichment is during the final fractionation stages at 8 kbar. First we believed that this is an artifact of the calculations caused by the uncertainty of the olivine and pyroxene relations under high-pressure conditions. However, the analysis of the dependence of experimental cotectics on pressure indicates that the liquid line of descent at 0.8 GPa can produce SiO_2-poor tholeiite basalt and, by extended fractional crystallization, alkali basalts and even nepheline-normative trachytes (see [Hess, 1992, p. 79]).

Thus, the computer simulation of the high-pressure crystallization of a primitive tholeiite melt demonstrates that pressure affects mostly the evolution of the Al_2O_3 and CaO contents, which can be regarded as characteristic components useful for the purposes of barometry of basaltic melts. This places more stringent requirements upon the accuracy of Al_2O_3 and CaO determination in the modeled melts.

Additional testing of the COMAGMAT program. As followed from the calibrating method for the high-temperature version of the model, the position of the inflection point on the CaO evolutionary line depends on the accuracy with which the *Aug* appearance on the liquidus at 1 atm is calculated and the extrapolation accuracy of this modeled temperature to elevated pressures (Section 2.2.6). When analyzing the data of Fig. 21, we mentioned that the model used for the *Aug*–melt equilibrium works well in application not only with oceanic tholeiites but also with other basaltic systems of moderate alkalinity. The results of independent testing of augite geothermometers proposed by different authors [Nielsen and Dungan, 1983; Ariskin *et al.*, 1987; Weaver and Langmuir, 1990] indicate that our *Aug*–melt geothermometers developed in 1986 show the best agreement with experimental data and natural observations [Danyushevsky *et al.*, 1996].

The realism of the high-pressure simulations with the COMAGMAT program can be assayed from the results of another independent testing [Yang *et al.*, 1996]. These researchers experimentally examined the stability of the *Ol–Pl* and *Ol–Pl–Aug* assemblages in oceanic tholeiite melts and combined these data with the results obtained by other authors at pressures from 1 atm to 10 kbar. The results of 190 experiments were used to develop empirical dependences of the temperature and the contents of selected "independent" melt components (Al, Ca, and Mg) on the system composition and pressure. The calibrated dependences were combined with the parametrization for the *Ol–Pl* and *Ol–Pl–Aug* cotectics in the model that was utilized to construct polybaric fractionation lines of oceanic tholeiites (YKG model).

Figure 79 compares the CaO and Al_2O_3 evolutionary trends calculated at 1 atm and 4 kbar for the same starting composition with the YKG [Yang *et al.*, 1996],

MELTS [Ghiorso and Sack, 1995], and COMAGMAT-3.0 [Ariskin *et al.*, 1993] models. As can be seen, the inflection points on the CaO evolutionary trends practically coincide for the YKG and COMAGMAT models at the same pressures. The differences between the Al_2O_3 trends are definitely caused by the "nonthermodynamic" form of equations in the YKG model, which are poorly sensitive to changes in the crystallizing assemblages. The results obtained with the MELTS program yield significant overestimates for the onset of *Aug* crystallization temperature even at $P = 1$ atm.

4.2.2. Pressure evaluation for tholeiitic glasses from the Mid-Atlantic Ridge

The high-pressure COMAGMAT model (its earlier THOLEMAG version) was used for the comparative analysis and genetic interpretation of basaltic glasses from Holes 332 and 418A drilled in the axial zone and the western flank of the Mid-Atlantic Ridge. This choice was dictated by the following reasons. First of all, quenched glasses from Hole 332 can be regarded as reference material for controlling the results of computerized barometry, because their sampling is fairly representative and the composition of their hypothetical parental melt was evaluated [LeRoex *et al.*, 1981; Dmitriev *et al.*, 1984]. Moreover, it is petrologically interesting to compare the evolutionary trends and estimated formation conditions of the magmatic melts corresponding to the initial (Hole 418A) and late (Hole 332) stages of seafloor opening in the Central Atlantic [Mirlin and Suschevskaya, 1990].

Barometry of glasses from Hole 332. Holes 332A and 332B were drilled in the course of Leg 37 of the R/V *Glomar Challenger* within a narrow 3-km valley 30 km west of the Mid-Atlantic Ridge axis at a point at 36°52′ N. The distance between the two holes is no more than 100 m, and, thus, the core recovered from them (~400 m from Hole 332A and 700 m from Hole 332B) can be reliably enough considered to represent a continuous (virtually without gaps) vertical section of the second seismic layer (below we will refer to the holes as Hole 332). The composition of the core is characterized by 860 silicate analyses of the basalts, picrites, and quenched glasses [*Init. Rep. DSDP*, 1977], and the data on the glasses include approximately 130 microprobe analyses. To evaluate the pressure during the crystallization of the corresponding melts, we utilized the method involving the calculation of lines of fractionation for an assumed parental magma under different pressure followed by a comparison of the modeled trends with the compositions of the quenched glasses [Ariskin *et al.*, 1990, 1992].

Primitive inclusions in Cr-spinel from a dredged sample of picritic basalt [LeRoex *et al.*, 1981] and in olivine (Fo_{91}) from magnesian basalt recovered by Hole 332 [Dmitriev *et al.*, 1984] provided data for estimating the compositions of the parent and supposedly initial melts that gave rise to tholeiitic basalts in this province.

Table 24. Compositions of melts parental to basalts from Holes 332 and 418A that were used in simulating polybaric fractionation

Component	TOR-1 (Hole 332)	MB (Hole 418A)
SiO_2	49.32	49.37
TiO_2	0.60	1.12
Al_2O_3	15.10	15.02
FeO	7.65	9.77
MnO	0.20	0.19
MgO	13.08	10.61
CaO	12.38	11.72
Na_2O	1.61	1.99
K_2O	0.06	0.07
P_2O_5	–	0.13
FeO/MgO	0.585	0.921
CaO/Al_2O_3	0.820	0.780

Note: All compositions are normalized to 100%; TOR-1 is a refractory melt inclusion in *Ol* from Hole 332 [Dmitriev *et al.*, 1984], MB is magnesian basalt from Hole 418A (sample 85-1, 145–148 [*Init. Rep. DSDP*, 1977]).

For the purposes of computer simulations, we selected a starting composition that corresponded to the most magnesian composition TOR-1 (Table 24). The fractionation lines were calculated for WM buffer conditions at pressures of 1 atm and 2, 4, 6, and 8 kbar. The crystallization sequences of minerals at different pressures are shown in the *P–T* diagram of Fig. 80a.

As can be seen in the diagram, *Ol* is a liquidus phase throughout the whole pressure interval of interest. Plagioclase is the second mineral to crystallize at $P <$ 6 kbar, with clinopyroxene crystallizing as the second phase at higher pressures. At 1 atm $\le P \le$ 6 kbar, an increase in the absolute crystallization temperature of *Aug* is ~60°C. The point of clinopyroxene appearance on the liquidus is therewith shifted for 40°C relative to *Ol* and *Pl*. This is a significant increase, which is three to four times greater than the uncertainty of the temperature estimates with mineral–melt geothermometers. This makes it possible to use this effect with the purposes of barometry of Aug-bearing assemblages with an accuracy of 1.5–2 kbar (absolute errors). The utilization of certain phase diagrams for projecting glass compositions from the same province allows distinguishing compositional groups for which the relative pressure differences can be evaluated more accurately.

To support this statement, we compared the trends of quenched glasses from Hole 332 and modeled polybaric fractionation trajectories in a CaO/Al_2O_3–MgO diagram (Fig. 81), which was recommended for constructing the most pressure-sensitive and informative plots (see Fig. 78). The following two principal conclusions can be drawn from the position of the natural compositions relative to the modeled cotectics: (1) the

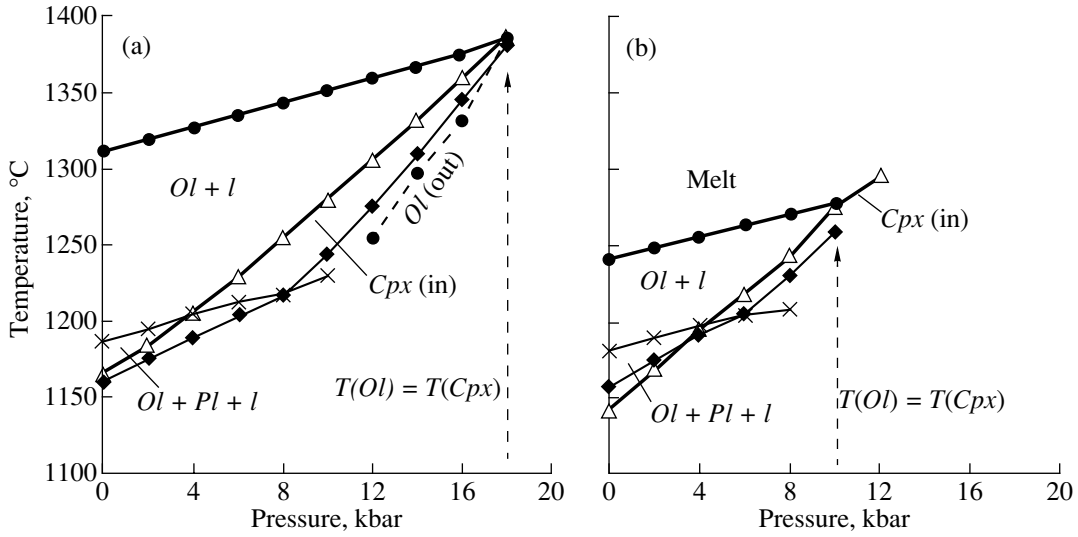

Fig. 80. *P–T* diagrams for the parental tholeiitic magmas calculated based on the simulation of fractional crystallization under pressures from 1 atm to 8 kbar. (a) Hole 332 (composition TOR-1), (b) Hole 418A (composition MB).

observed diversity of the glass compositions can be explained by the fractionation of the same initial melt TOR-1 within a pressure range of 1–7 kbar and (2) most of the glasses define clear-cut trends close to the fractionation lines calculated at pressures of 2–3 and 6 kbar, respectively.

Thus, petrochemical data on basalts from Hole 332 can be interpreted without invoking the idea of two different parental tholeiitic magmas. A more plausible explanation seems to be differences in the pressure during the crystallization of a common basaltic parent similar to TOR-1. The pressure differences for the subseries were 3–4 kbar. This led us to the conclusion that there were two magma chambers occurred at different levels (with a depth difference of 9–12 km), at which the melt TOR-1 and its derivatives fractionated.

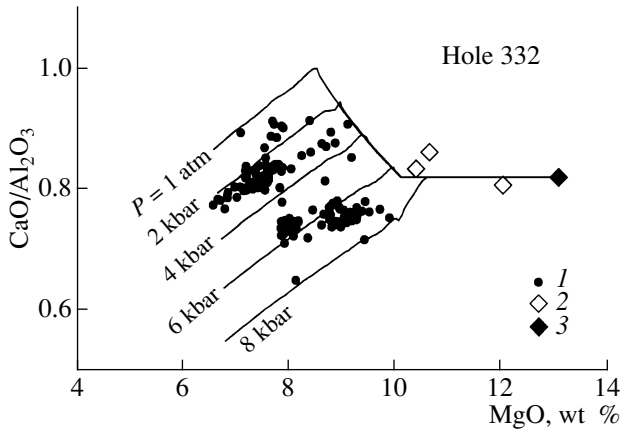

Fig. 81. Evolution of the melt composition during the fractional crystallization of TOR-1 in comparison with the compositions of quenched glasses from Hole 332. (*1*) Glasses; (*2*) melt inclusions in spinel [LeRoex *et al.*, 1981]; (*3*) TOR-1 (inclusion in *Ol*) [Dmitriev *et al.*, 1984].

These speculations and considerations are underlain by data on phase equilibria and can be important for the geodynamic reconstructions of magmatism near the axial zone of the Mid-Atlantic ridge. At the same time, when using this information, one should be aware that, inpostulating the composition of the initial melt close to the composition of the most primitive liquids (such as TOR-1 [Dmitriev *et al.*, 1984]), we had to assume that they to arrived directly from the magma generation zones to relatively shallow-sitting chambers. In this situation, it is reasonable to expect an equiprobable distribution of the derivatives over the compositional range and their equal frequencies of occurrence. However, the data in Fig. 81 demonstrate the absence or rarity of intermediate fractions corresponding to high-Mg melts.

It is natural to explain this fact by the processes of deep-seated crystallization accompanied by the settling of mafic minerals. Ignoring this possibility, it is difficult to account for the absence of basaltic glasses with "low-pressure" CaO/Al_2O_3 ratios and MgO contents within the range of 8–10 wt %. This leads to the following two-stage scenario for the origin of basaltic assemblages from Hole 332. The earliest melts underwent high-pressure crystallization (perhaps, with the participation of *Aug*, see Fig. 80a) and gave rise to magnesian melts, whose further fractionation resulted in the diversity of compositions corresponding to the relatively "high-pressure" and "low-pressure" basaltic glasses.

Returning to Fig. 81, we can hypothesize that these parental magmas corresponded to the fractionation products of the primary melt TOR-1 at $P > 8$ kbar and contained ~10 wt % MgO. Correspondingly, the barometric grid should be corrected with regard for the

decrease in the Mg-number of the initial melt. This should have resulted in an insignificant but systematic shift in the pressure estimates toward lower values. This situation is considered below with reference to the barometry of quenched glasses from Hole 418A.

Barometry of glasses from Hole 418A. Hole 418A was drilled during Leg 53 of the R/V *Glomar Challenger* near the southern margin of the Bermuda Rise. The drilling was accomplished with the aim of examining rocks belonging to ancient domains (dated at ~110 Ma) of the Atlantic oceanic crust. The hole reached a depth of 544 m and yielded approximately 390 m of drill core [*Init. Rep. DSDP*, 1980]. The massive basalts (25%) and pillow lavas (75%) differ in phenocryst assemblages, extent of brecciation, and the degree of alteration, but the suite of the quenched glasses seems to show several common features. In contrast to glasses from Hole 332, these glasses are characterized by a continuous interval of compositions (virtually without compositional gaps), elevated FeO/MgO ratios, and relatively high TiO_2 content at lower contents of Al_2O_3 and K_2O (Fig. 82). These compositions provide no reasons for subdividing them into high- and low-Ca groups, a fact testifying to insignificant pressure variations during the fractionation of the initial magmatic melt. The composition of the parental magma remains, however, uncertain, which hampers barometric reconstructions for this suite.

The relatively MgO-enriched glasses from Hole 418A contain no more than 8.5 wt % MgO and can hardly correspond to the initial primitive melt. The composition of this liquid can be evaluated using independent information, including the compositions of the most refractory phases contained in the magnesian basalts. If olivine was the first silicate mineral to crystallize from the primitive liquid, the magnesian Ol-rich basalts can be regarded as an approximation of the composition parental to the glasses and basalts of this province, provided that this liquidus *Ol* was close to the most magnesian *Ol* in rocks from Hole 418A.

The magnesian basalt 418A, 85-1, 145-148 from the bottom of this hole (Table 24, MB) can be considered as a rock matching this criterion. Under atmospheric pressure and WM buffer conditions, the liquidus phase of this composition is *Ol*, which was calculated to have started crystallizing at 1259°C and contained 87.1 mol % *Fo*. This composition is close to that of the most magnesian *Ol* found in the lavas from Hole 418A and containing 87.9 mol % *Fo* [*Init. Rep. DSDP*, 1980]. The *P–T* diagram calculated for melt MB is presented in Fig. 80b, and the results of comparing the modeled lines for polybaric fractionation and the observed compositional variations of the quenched glasses are shown in Fig. 82.

As can be seen from this diagram, the tholeiitic glasses cluster along the *Ol* + *Pl* and *Ol* + *Pl* + *Aug* cotectic lines corresponding to the narrow pressure range of 2–5 kbar. The compositional variations span the whole

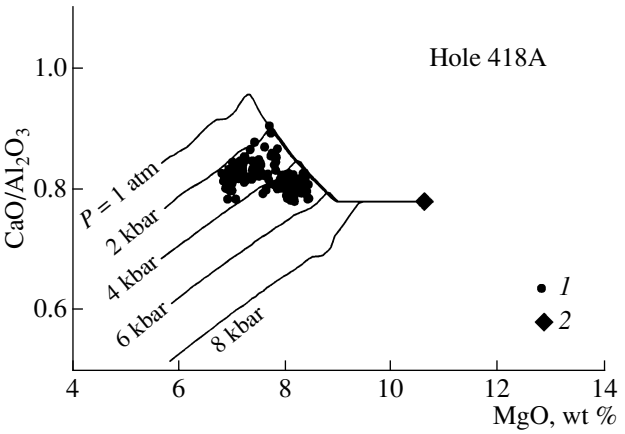

Fig. 82. Evolution of the melt composition during the fractional crystallization of MB in comparison with the compositions of quenched glasses from Hole 418A. (*1*) Glasses; (*2*) assumed initial melt composition (Table 24, MB).

range of the crystallization conditions of the *Ol* + *Pl* cotectic, which makes these data principally different from the data obtained when the TOR-1 initial melt was used (Fig. 81). This result also justifies the choice of composition MB as that of the probable initial melt.

Comparing Figs. 81 and 82, one can see that they differ not only in starting compositions and pressure estimates but also in the general configuration of compositional fields of basaltic glasses. The glass compositions from Hole 332 show a discrete distribution with trends corresponding to lines of the *Ol* + *Pl* + *Aug* cotectic control at different pressures. Conversely, the character of trends for glasses from Hole 418A suggests monotonous magma fractionation at a pressure from ~5 to 2 kbar, a process that was, perhaps, associated with the ascent and decompression of the initial magmatic melt. The reality and importance of decompression fractionation will be demonstrated in the last section of this chapter by the example of magmatic evolution of Klyuchevskoi volcano in Kamchatka. It is also pertinent to mention that the compositions of quenched glasses from Holes 332 and 418 suggest insignificant degrees of fractionation of the proposed parents, no more than 30–40%, regardless of the baric crystallization regime. This is consistent with earlier estimates, based on the results of melting experiments with primitive oceanic tholeiites, e.g., [Kadik *et al.*, 1990].

The proposed technique of barometry of oceanic basaltic glasses was further developed by Sushchevskaya *et al.* and yielded estimates for the differentiation conditions of tholeiitic magmas in the Transatlantic Geotravers, East Pacific Rise, the equatorial segment of the Mid-Atlantic Ridge, mid-oceanic ridges in the Indian Ocean, and the junction zone between the Mid-Atlantic and North Weddell ridges [Sushchevskaya and Tsekhonya, 1994; Sushchevskaya *et al.*, 1996a, 1996b, 1998a, 1998b]. Over the past years, the barometry of MORB glasses with the COMAGMAT program was

conducted to reconstruct magmatism in the southern portion of the Mid-Atlantic Ridge [LeRoex *et al.*, 2002a, 2002b].

4.3. Decompression Fractionation of Island-Arc High-Magnesia Basalts

This section presents the results of a petrological–geochemical study of basaltic lavas from Klyuchevskoi volcano in eastern Kamchatka, Russia. These materials are employed to validate the hypothesis that high-alumina basalts from this volcano were generated via the decompression fractional crystallization of a high-magnesia basaltic parent. All principal results of this research were presented and generalized in our earlier publications [Ariskin *et al.*, 1995; Ariskin, 1999] and are described below only briefly, with some additions from the monograph [Ariskin and Barmina, 2000].

Problems related to the genesis of high-alumina magmas. Examining the elevated (up to 18 wt %) Al_2O_3 contents in some aphyric volcanics in northern California, Tilley [1950] was the first to recognize high-alumina basalts (hereafter, HAB) as one of the main types of basaltic magmas. Kuno [1960] proposed a set of mineralogical and petrochemical criteria for distinguishing between high-alumina basalts and associated tholeiitic and alkaline rocks. He also formulated the problem of the genesis of HAB, believing that these rocks correspond to the primary magma that was derived by means of the partial melting of a mantle source. Later an alternative viewpoint was put forth, according to which magma enrichment in Al_2O_3 can be caused by a delay in plagioclase crystallization in hydrous picrite–basalt magmas [Yoder and Tilley, 1962]. Over the succeeding decades, the alternative of the primary or non-primary character of high-Al magmas was the core of discussions about the genesis of HAB (see reviews in [Crawford *et al.*, 1987; Kadik *et al.*, 1990; Myers and Johnston, 1996]).

In a number of hypotheses proposed to account for the genesis of high-Al basalts, these rocks were considered to be (1) partial melts derived from the subducted oceanic crust [Babansky *et al.*, 1983; Baker and Eggler, 1983; Brophy and Marsh, 1986; Johnson, 1986]; (2) fractionation products of mantle magmas [Perfit *et al.*, 1980; Kay and Kay, 1985; Nye and Reid, 1986; Uto, 1986; Gust and Perfit, 1987; Kadik *et al.*, 1989, 1990; Draper and Johnson, 1992]; (3) products of the re-equilibration of the ascending primary melts with the country rocks composing the magma conduit walls [Kelemen and Ghiorso, 1986; Kelement, 1990]; and (4) cumulates that were formed via plagioclase accumulation [Crawford *et al.*, 1987; Plank and Langmuir, 1988; Brophy, 1988, 1989; Fournelle and Marsh, 1991].

In this context, geological observations are important that testify that many volcanic centers in island arcs are characterized by a close association of HABs and high-Mg basalts (hereafter, HMB), containing more than 10 wt % MgO [Pertif *et al.*, 1980] and *Fo*-rich olivine ($Fo_{88–92}$) [Kay and Kay, 1985]. Analogous associations were also found at Okmok and Makushin volcanoes in the Aleutians [Nye and Reid, 1986; Gust and Perfit, 1987], Klyuchevskoi volcano [Khrenov *et al.*, 1990; Khubunaya *et al.*, 1993; Ozerov *et al.*, 1996], and in many other volcanic provinces.

Despite their relative rarity, high-Mg basalts attracted attention as potential parental magmas derived from mantle peridotites. This hypothesis was explored in a series of experimental studies centered on examining the phase equilibria in island-arc HMB under pressures from 1 atm to 20 kbar [Gust and Perfit, 1987; Kadik *et al.*, 1989, 1990; Draper and Johnston, 1992]. These researchers have established that the products of HMB fractionation under pressures of more than 8 kbar and anhydrous conditions can contain 16–18 wt % Al_2O_3 and show petrochemical characteristics similar to those of natural high-Al basalts. However, in terms of the CaO and MgO contents, the rocks of island-arc HMB and HAB suites have no analogues among experimental quenched glasses [Draper and Johnston, 1992]. This left unsettled the problem of the possibility and conditions of the polybaric fractionation of primary magmas.

The aim of our research was to utilize a complex of petrological and geochemical data (including computer simulation techniques) to explore the possibility of the origin of HAB from a high-Mg basaltic parent via the decompressional fractionation of a hydrous magma at undersaturated conditions [Ariskin *et al.*, 1995]. As the model object, we chose the lava series of Klyuchevskoi volcano. These lavas define a continuous trend from high-Mg to high-Al basalts [Khrenov *et al.*, 1990; Kersting and Arculus, 1994].

4.3.1. Petrology of Klyuchevskoi volcano, eastern Kamchatka

Geologic setting and structure. Klyuchevskoi is the main volcano of the Kurile–Kamchatka volcanic zone and is one of the world's most active volcanoes according to the volume of its erupted products [Fedotov *et al.*, 1990]. This vast volcanic center is located within the Eastern Kamchatka Volcanic Belt and rises to a height of 4800 m. It developed on the slope of the older volcano Kamen' at approximately 7 ka [Melekestsev *et al.*, 1991]. Starting from the very first descriptions of the volcano in 17th century until 1932, its eruptive activity was noted to be restricted exclusively to the summit crater. The eruptions were explosive or, more rarely, explosive–extrusive, so that the pyroclastic material significantly dominates volumetrically over lava flows in the volcanic edifice. A drastic change in the character of the volcanic activity occurred in 1932: simultaneously with the continuing activity in the central crater, eruptions started in the slopes of the volcano with an average frequency of once every four years [Fedotov *et al.*, 1990]. Since this time,

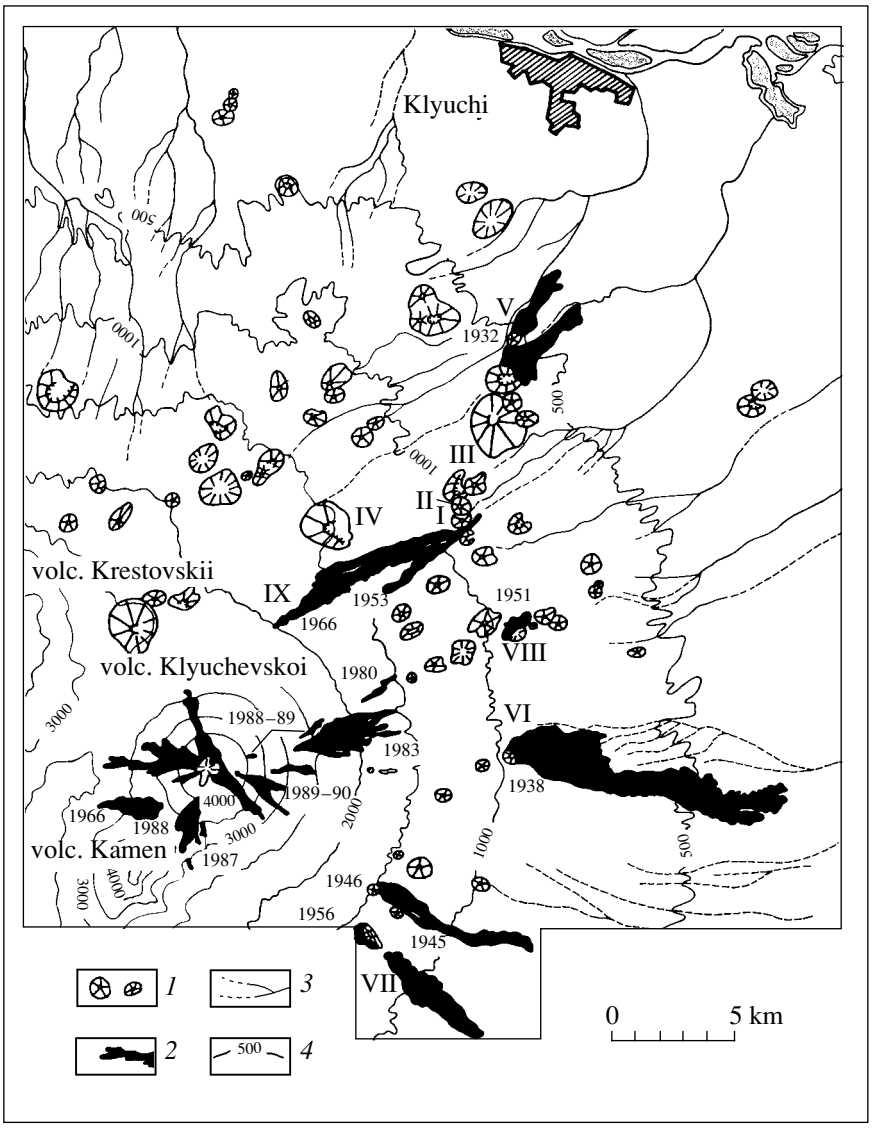

Fig. 83. Location map of Klyuchevskoi volcano boccas (modified after V.N. Dvigalo, Institute of Volcanology, Petropavlovsk-Kamchatskii, Russia). (*1*) Cinder cones: (I) Bulochka, (II) Novograblenov, (III) Luchitskii, (IV) Slyunin; (*2*) 1932–1990 lava flows and their eruption years: (V) Tuila, (VI) Bilyukai, (VII) Zavaritskii, (VIII) Bylinkina, (IX) Piip; (*3*) dry riverbeds; (*4*) contour lines.

more than 20 significant flank eruptions have occurred, which gave rise to long, from a few hundred meters to 7–8 km, lava flows and produced more than 100 cinder cones on the slopes.

The volcanic edifice is dominated by aluminous basalts (90%), with the rest of the volcanics affiliating with magnesian and intermediate varieties. Along with lavas from summit eruptions, the material of flank fissure eruptions is one of the main sources of petrological information. These fissures are spatially restricted to the northeastern, eastern, and southeastern sectors of the volcano (Fig. 83), where magma exposures occur at topographic heights of 450–4000 m. Starting from 1984, the crater has been characterized by a high magma level, and the height of the flank fissures also increased: after 1987, most eruptions took place at heights no lower than 2800 m.

According to Gorshkov [1956], the magma chamber of the Klyuchevskoi volcano is located at a depth of 50–60 km and has the shape of a flat lens ~30 km in diameter and a thickness of no less than 10–12 km. This concept was further developed in later papers, in which seismic "shadows" beneath Klyuchevskoi volcano were interpreted as a combination of a huge mantle diapir and a vertical magma conduit rising from the upper boundary of the diapir at depths of 60–70 km [Ermakov *et al.*, 1971]. Reliable seismic data are now available only on the uppermost 25 km of the Klyuchevskoi plumbing system [Fedotov *et al.*, 1988]. According to this information, the most seismically active portion of

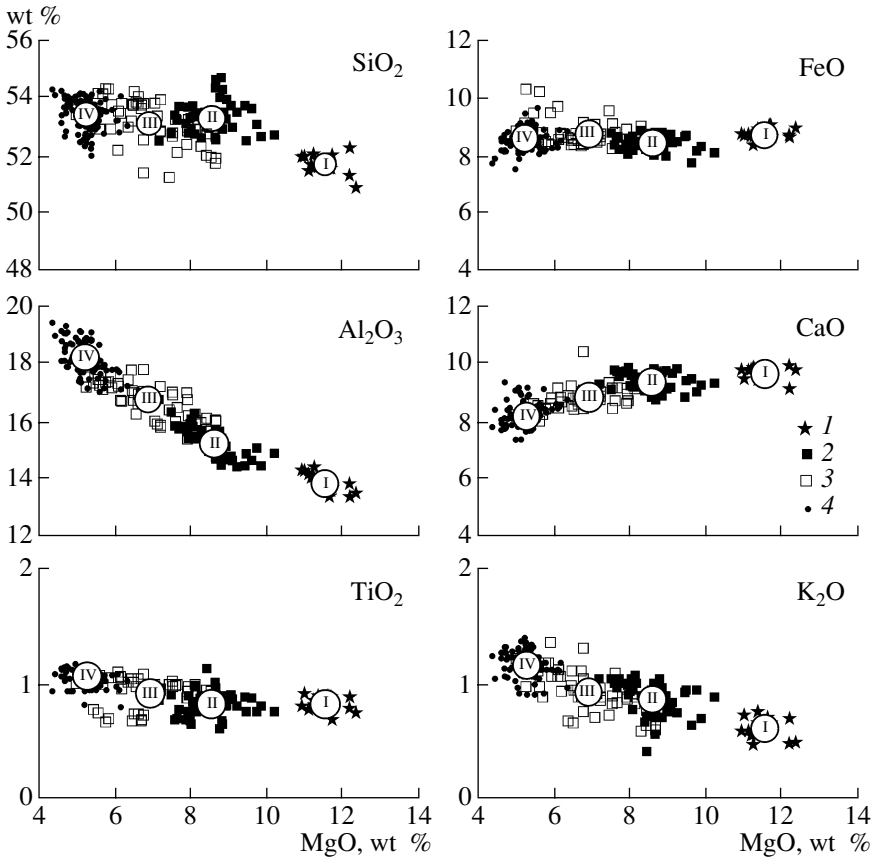

Fig. 84. Variation diagrams for the eruption products of Klyuchevskoi volcano. The diagram is based on 242 rock compositions, including data of the authors, A.P. Khrenov, and V.N. Andreev. (*1–4*) Types of basalts: (*1*) high-magnesia (HMB), (*2*) magnesian (MB), (*3*) aluminous (AB), (*4*) high- alumina (HAB); (I–IV) average compositions (see Table 25).

this zone has a diameter of 5 km and is characterized by a seismic area ~3 km across at depths from 5 to 20 km. This area is interpreted as a zone of plastic rocks around the main feeder of the volcano. An important conclusion drawn from geophysical evidence is that the seismically active zone includes no aseismic area more than 5 km in diameter that could be interpreted as a large intermediate magma chamber. This conclusion is consistent with the roughly similar intensities of earthquakes at depths of 0–25 km [Fedotov *et al.*, 1988]. Geophysical data on Klyuchevskoi volcano suggest that this magmatic system is fed from the mantle in the absence of large crustal or peripheral chambers at the magma conduit [Ozerov *et al.*, 1997].

Petrochemistry of the Klyuchevskoi lavas. Our research is based on a collection of 45 rocks sampled from cinder cones and fissures in the lower part of Klyuchevskoi volcano, within the elevation range of 500–2000 m (Fig. 83). This interval includes old cones with an age of approximately 2000 ka and the products of historical eruptions, such as Tuila (1932), Bilyukai (1938), Bylinkina (1951), Belyankina (1953), and Piipa (1966). The samples collected here represent practically all compositional varieties of basalts of Klyuchevskoi volcano and can be used for to develop and test computer models for crystallization differentiation.

Rock descriptions. The lavas of Klyuchevskoi volcano are vesicular or massive porphyritic basalts with phenocrysts of *Ol*, *Cpx*, and *Pl*, whose sizes range from 0.1 to 1 mm. The rocks contain occasional olivine and pyroxene grains up to 5–7 mm across. All rock types contain abundant glomerocrysts, which can be as large as 10 mm. The mineral assemblages change in modal composition from *Ol–Cpx* (with the predominance of *Ol* in the most magnesian basalts and *Cpx* in aluminous basalts) to *Pl*-rich in HAB. Plagioclase grains were also occasionally found in magnesian basalts. Orthopyroxene is rare: its single grains or, in places, aggregates with *Pl* and *Cpx* are contained only in aluminous basalts. This mineral was identified by detailed microprobe analysis as solid-phase inclusions in *Ol* and *Cpx* from high-Mg and high-Al basalts [Khubunaya *et al.*, 1993; Ozerov, 2000]. Cr-rich spinel occurs as inclusions in olivine, particularly from magnesian basalts. The high-Al basalts are characterized by finely disseminated titanomagnetite, sometimes in aggregates with *Ol* and *Cpx*, and inclusions of this mineral in *Pl*.

The content of phenocrysts is 3–7 vol % in HMB and magnesian varieties and as high as 20% in HAB. For further consideration, it is important to mention that the high-Al basalts, which are dominated by porphyritic rocks, also include microphyric, up to subaphyric varieties. The groundmass of the basalts varies from vitrophyric to intersertal in texture and is dominated by thin plagioclase laths and fine intergrowths of *Ol*, *Cpx* (*Aug* or *Pig*) and titanomagnetite. The mesostasis consists of weakly altered devitrified glass, which has an andesite-dacite composition in the aluminous basalts [Ozerov, 2000].

Petrochemcial systematics of the Klyuchevskoi basalts. The variability of the rocks erupted by Klyuchevskoi volcano is illustrated in the variation diagrams constructed for 242 basaltic compositions (Fig. 84). This selection includes the authors' data, analyses compiled by A.P. Khrenov, and a few analyses of lavas collected from the summit eruptions by V.N. Andreev (of the Institute of Volcanology, Far East Division, Russian Academy of Sciences, Petropavlovsk-Kamchatskii). According to these data, the lava suite of Klyuchevskoi volcano varies from high-Mg (~12% MgO, 13.5% Al_2O_3) to high-Al (4–5% MgO, 18–19% Al_2O_3) basalts and defines continuous trends in major- and trace-element variation diagrams. Nevertheless, in papers on the volcano published in the Russian literature, this suite has long been subdivided into magnesian and aluminous basalts, with the boundary between them drawn at approximately 7% MgO and 16–17% Al_2O_3 [Khrenov *et al.*, 1990]. Using methods for the hierarchical classification of igneous rocks, we subdivided the Kyuchevskoi basalts into four major groups with specific petrochemical characteristics (Table 25) [Ariskin *et al.*, 1995]. These groups are *high-magnesia* (HMB, n = 15 samples), *magnesian* (MB, n = 46), *aluminous* (AB, n = 50), and *high-alumina* (HAB, n = 131) basalts. The average compositions of these groups are also demonstrated in Fig. 84.

The transition from HMB to HAB is generally characterized by a systematic increase in the contents of SiO_2, TiO_2, Al_2O_3, Na_2O, K_2O, and P_2O_5 and a monotonous decrease in the concentrations of MgO and CaO at a roughly constant FeO content, because of which the Mg number of the rocks MGN monotonously decreases from 70 to 50 in the most aluminous compositions. These data indicate that the leading process that was responsible for the formation of the Klyuchevskoi lava suite could have been the fractionation of the parental HMB magma via the crystallization of mafic minerals

Table 25. Chemical and normative compositions of the main types of the Klyuchevskoi basalts [Ariskin *et al.*, 1995]

Component	High magnesia basalt, HMB (type I, n = 15)	Magnesian basalt, MB (type II, n = 46)	Aluminous basalt, AB (type III, n = 50)	High alumina basalt, HAB (type IV, n = 131)
SiO_2	51.76 (0.34)	53.39 (0.55)	53.22 (0.78)	53.50 (0.48)
TiO_2	0.86 (0.07)	0.84 (0.11)	0.95 (0.13)	1.09 (0.07)
Al_2O_3	13.86 (0.33)	15.29 (0.55)	16.79 (0.66)	18.26 (0.50)
FeO	8.83 (0.18)	8.52 (0.24)	8.83 (0.47)	8.67 (0.33)
MnO	0.17 (0.01)	0.17 (0.02)	0.17 (0.04)	0.16 (0.02)
MgO	11.55 (0.43)	8.58 (0.65)	6.89 (1.00)	5.24 (0.34)
CaO	9.73 (0.20)	9.41 (0.30)	8.91 (0.46)	8.22 (0.38)
Na_2O	2.47 (0.18)	2.72 (0.24)	3.11 (0.32)	3.45 (0.20)
K_2O	0.63 (0.09)	0.90 (0.15)	0.96 (0.19)	1.20 (0.10)
P_2O_5	0.15 (0.02)	0.18 (0.03)	0.18 (0.04)	0.20 (0.04)
Mg/(Mg + Fe)	0.699	0.641	0.580	0.517
Ca/(Ca + Al)	0.561	0.528	0.491	0.450
CIPW, wt %				
Or	3.72	5.32	5.67	7.09
Ab	20.90	23.01	26.31	29.19
An	24.88	26.86	29.02	30.80
Di	18.18	15.24	11.54	7.20
Hy	17.93	25.04	21.96	21.15
Ol	12.42	2.52	3.28	2.02
Ilm	1.63	1.60	1.80	2.07
Ap	0.36	0.43	0.43	0.47

Note: All compositions are normalized to 100 wt %; numerals in parentheses are the standard deviations (1σ) for each average composition.

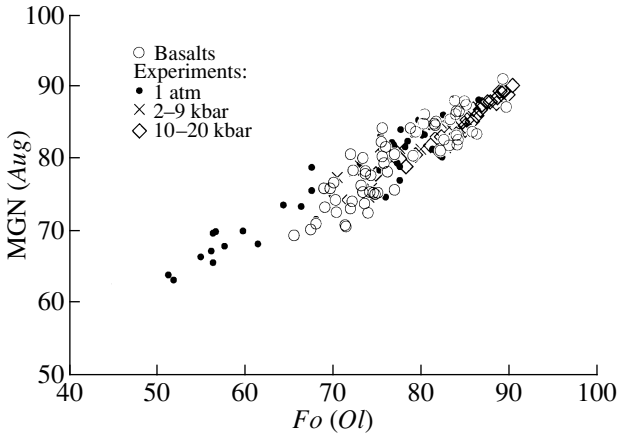

Fig. 85. Compositions of coexisting olivine and clinopyroxene occurring in the Klyuchevskoi basalts and obtained in melting experiments. Natural compositions are from [Ariskin *et al.,* 1995]. Experimental mineral compositions were retrieved from the INFOREX-4.0 database [Ariskin *et al.*, 1997] and include the results from 20 papers: 55 runs carried out at P = 1 atm and 44 runs in the range of 2–20 kbar. This set of experiments represents runs with durations of no less than 12 h and glasses with ($Na_2O + K_2O$) < 5 wt %.

in the absence or very insignificant crystallization of plagioclase. This is supported by changes in the normative composition of the main groups (Table 25).

The most typical feature of these variations with the HMB ⟶ HAB transition is the systematic enrichment in plagioclase components at a decrease in the contents of olivine and diopside. If the petrochemical types accurately approximate the compositional evolution during the fractional crystallization of the HMB magma, it can be concluded that the main crystallizing phases were *Ol* and *Cpx*. During the early stages (HMB ⟶ MB), the crystallizing assemblages were dominated by olivine, while the transition to more aluminous compositions (MB ⟶ AB) seems to have been marked by an increase in the proportion of *Aug* and the crystallization of minor *Opx* amounts. These conclusions receive further support from the compositional evolution of phenocrysts and mineral inclusions (see below).

The evolution in the trace-element composition is also systematic. The Ni, Co, Cr, and Sc contents monotonously decrease with decreasing MgO and increasing Al_2O_3 [Kersting and Arculus, 1994; Ariskin *et al.*, 1995]. This process is coupled with melt enrichment in incompatible elements (Ba, Rb, and Li) and LREE. It is worth noting the behavior of Sr: this element is also enriched in high-alumina basalts but to a lesser degree than typical incompatible elements. An even weaker enrichment is characteristic of HREE. The scale of these variations is in agreement with the hypothesis of fractionation, which could attain up to 40–50% of the original mass of the HMB magma, judging from the degrees of K, P, Li, and La enrichment.

It is important to emphasize that some elements (Sr, Sc, and Yb) show no linear correlations with the Ni contents but instead exhibit smoothly curved trends. This feature of the Klyuchevskoi basalts was first noted in diagrams showing correlations between the contents of compatible elements and TiO_2 [Kersting and Arculus, 1994] and suggests that intermediate basaltic derivatives could not be produced by the mixing of HMB and HAB magmas. Another observation concerns Cu and V, elements with variable valences. Our data indicate that the contents of Cu are not correlated with the contents of MgO and Ni or with any other magma fractionation parameters. The Cu contents in HMB vary insignificantly, but the transition to less magnesian and more aluminous compositions is marked by a diverging "fan" of Cu contents, including areas both enriched and depleted in this element. A similar distribution is also typical of V. This suggests that the redox conditions were unstable during the evolution of the magma-generating system of Klyuchevskoi volcano.

Chemistry of rock-forming minerals. Earlier researchers have revealed two main characteristics of the observed phenocrysts. First, it was determined that the rocks contain very magnesian assemblages of clinopyroxene (MGN = 87–90) and olivine (MGN = 88–92) with numerous inclusions of Cr-rich spinel and occasional *Opx* (MGN ~ 89 and lower), particularly in HMB and MB. Second, the cores of the phenocrysts and mineral inclusions in all rock types show wide compositional ranges of *Ol*, *Cpx*, and *Opx*: from MGN = ~90 to 65–70. The composition of plagioclase varies from $An_{84–85}$ to ~An_{60}. These phenocrysts occur in aluminous basalts and HAB, often in aggregates with mafic minerals.

The compositional trends of the minerals coexisting as glomerocrysts and occurring as crystalline inclusions are discussed based on the data from [Ariskin *et al.*, 1995; Ozerov, 2000]. Interest in glomerophyric aggregates is caused by their nature: these could be cotectic assemblages that crystallized simultaneously from the parental or derivative magmatic melts. If these minerals contained silicate and Fe-oxide inclusions, these phases were also considered to be cotectic.

Figure 85 compares the Mg-numbers of the olivine and augite that coexisted in the Klyuchevskoi basalts and those synthesized by different researchers in melting experiments with natural basalts. The experimental data were compiled from 20 papers, including 55 low-pressure (P = 1 atm) and 44 high-pressure ($2 \le P \le 20$ kbar) experiments conducted in systems of low and moderate alkalinity ($Na_2O = K_2O \le 5$ wt %). Using the search subroutine of the INFOREX system, we selected only those of the low- and high-pressure experiments that lasted for no less than 48 and 12 h, respectively. Both trends overlap within the range of $65 \le MGN \le 90$, although the scatter of the MGN of *Aug* is notably higher at roughly the same *Fo* contents.

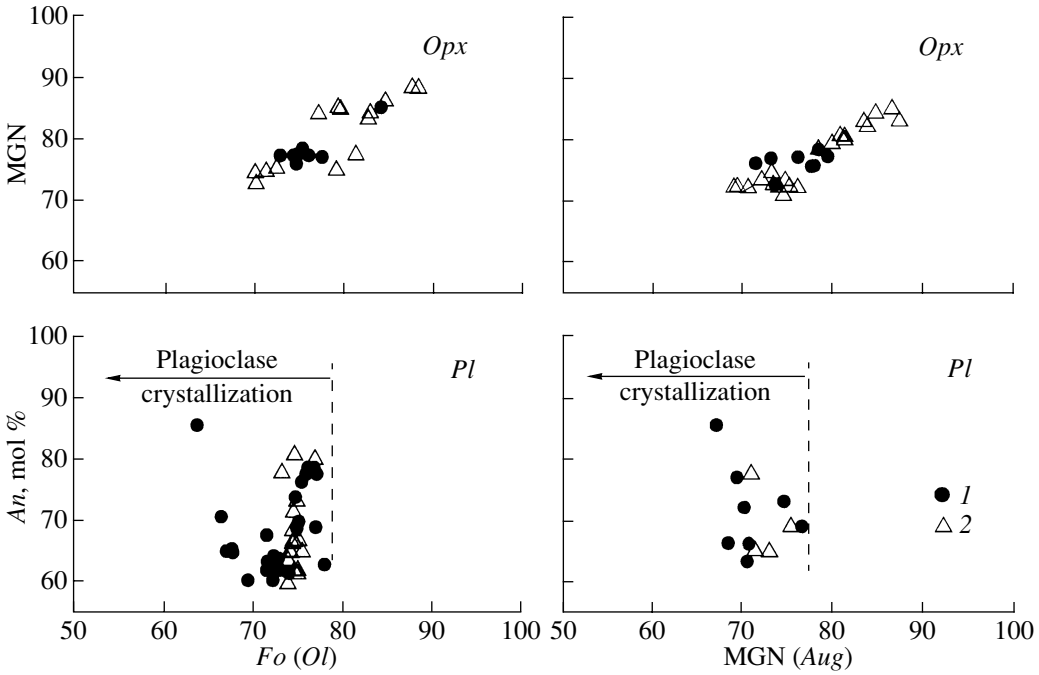

Fig. 86. Compositions of *Opx* and *Pl* occurring as aggregates or inclusions in *Ol* and *Cpx* in the basalts of Klyuchevskoi volcano. (*1*) Authors' data; (*2*) mineral inclusions from high-Al basalts of the Zavaritsky bocca [Ozerov, 2000]; $An = 100 \times Ca/(Ca + Na + K)$.

Important information can be deduced from the distribution of experimental compositions as a function of pressure. As can be seen from Fig. 85, the data of most experiments at $P = 1$ atm fall within the field of the most ferrous compositions, due to the fact that clinopyroxene is the third phase to crystallize under low pressures. Within the pressure range of 2–9 kbar, *Cpx* with MGN = 74–85, and *Aug* with MGN > 80 was synthesized in high-temperature ($T > 1200$°C) experiments under pressures of P = 8–9 kbar. The overwhelming majority of the most magnesian clinopyroxenes with MGN ≤ 90 were obtained in high-pressure experiments at $P > 15$ kbar, with the high-pressure assemblage of *Ol* and *Aug* always being in equilibrium with the high-Mg basaltic melt containing >10 wt % MgO.

Hence, the identity of the natural and experimental compositional trends for olivine and clinopyroxene can be regarded as an argument in favor of the fractionation of the initial HMB melt and may be used to preliminarily evaluate the pressure during the crystallization of the Klyuchevskoi magmas. Judging by the compositional ranges of the natural *Ol* and *Aug*, fractional crystallization could proceed under pressures varying from approximately 15–20 to 2–5 kbar. Independent evidence in support of these estimates will be given below, in considering the results of computer simulations of the phase relations and fractional crystallization of the HMB magma.

The compositions of *Opx* and *Pl* found in aggregates and as inclusions in each other are shown in Fig. 86. These data are presented in terms of the *Fo* contents in *Ol* and MGN of *Aug*, the main two phases of the original cotectic assemblage. The upper pair of plots in Fig. 86 illustrates the evolution of the orthopyroxene compositions. Clearly pronounced trends within the range of 72 ≤ MGN ≤ 89 leave no doubt that *Opx* was present in the crystallizing assemblage starting from the early fractionation stages of the initial melt. Petrographic evidence indicates that *Opx* is scarce in the lavas, and its content in the basalts of the HMB ⟶ MB ⟶ AB succession does not exceed a few percent.

The distribution of *Pl* compositions is no less informative. At a broad scatter of the *An* contents, this mineral does not exhibit any significant correlation with the compositions of mafic minerals. The average Mg-number of *Ol*, *Aug*, and *Opx* in aggregates and inclusions in *Pl* is ~75 and does not exceed 77–78. Obviously, these values mark the first appearance of *Pl* as a crystallizing phase, while the most ferrous compositions with MGN ~ 65 seem to correspond to the final fractionation stages in the system.

Spinel inclusions in olivine demonstrate a systematic decrease in the Cr_2O_3 contents with *Ol* depletion in *Fo*. This is consistent with the hypothesis of primitive magma fractional crystallization [Ariskin *et al.*, 1995; Ozerov, 2000]. No chromite inclusions were found in the plagioclase, but the rocks contain numerous pyroxene–plagioclase–magnetite aggregates, which are abundant in HAB. This suggests cotectic relations between *Pl* and Ti-*Mt*. The sharp transition from Cr-spinel to titanomagnetite occurs within the same range of the MGN of *Ol* as that corresponding to the begin-

ning of *Pl* crystallization: 75–77% *Fo* (Fig. 86). These observations point to the practically simultaneous precipitation of *Pl* and *Mt* late in the process of Klyuchevskoi magma fractionation.

The results obtained on the compositions of aggregates of coexisting (cotectic) minerals and crystalline inclusions led us to the following two principal conclusions. First, the systematic variations in the compositions of the minerals are in agreement with the successive fractionation of the initial HMB melt:

$$Ol(Fo_{90–92}) + Aug(\mathrm{MGN}_{89–91}) \pm Sp(\mathrm{CRN}_{70–72})$$
$$\Rightarrow Ol(Fo_{87–88}) + Aug(\mathrm{MGN}_{86–87})$$
$$\pm Opx(\mathrm{MGN}_{88–89}) \pm Sp(\mathrm{CRN}_{65–70})$$
$$\Rightarrow Ol(Fo_{75–77}) + Aug(\mathrm{MGN}_{79–80}) \pm Opx(\mathrm{MGN}_{78–79})$$
$$+ Sp(\mathrm{CRN}_{20–30}) + Pl(An_{65–77}).$$

This sequence of crystallization does not depend on the age of the fissures and points to the homogeneity (stability) of the mantle source of the primary Klyuchevskoi magma (see below).

Second, the wide variations in the compositions of mafic minerals even within individual samples suggest that, when erupted, these basalts were unequilibrated assemblages of a melt and suspended minerals. This implies that melts and crystals corresponding to different fractionation stages of the parental magmas could be efficiently mixed in the feeder of the volcano [Ozerov *et al.*, 1996; Ariskin and Barmina, 2000].

4.3.2. Simulation of the formation of high-alumina basalts

In order to explore the possibility for the Klyuchevskoi HAB to origin via the polybaric fractionation of a HMB melt, we carried out the following sequence of simulations with the COMAGMAT-3.0 program [Ariskin *et al.*, 1995]. The first *P–T* diagrams for the main rock types at anhydrous conditions made it possible to establish the general characteristics of the trends that resulted from the equilibrium crystallization of an average HMB under different pressures. Then we considered the effect of pressure variations and the presence of water on the calculated liquid lines of descent. This allowed us to construct trajectories of the decompressional fractionation for the initial HMB melt in an H_2O-undersaturated system. Comparing the modeled lines of fractionation with the petrochemical trends of natural rocks, we evaluated the polybaric fractionation conditions of the parental high-Mg magma.

The choice of an average HMB as an analogue of the parental magma (type I in Table 25) is inferred from the petrochemical and geochemical data (see above). Further support came from the calculations of the *Ol* composition on the liquidus of the high-Mg parent. For example, Khubunaya *et al.* [1993] used the geothermometers from [Ford *et al.*, 1983] to evaluate the MGN of *Ol* in equilibrium with the HMB melt from the Bulochka fissure and obtained $Fo_{89.7}$. Closely similar values of $Fo_{89.3–90.0}$ were calculated for the average HMB at pressures from 1 atm to 15 kbar and QFM conditions [Ariskin *et al.*, 1999]. These estimates are consistent with the most magnesian compositions identified for the *Ol–Aug–Sp* cotectic (Fig. 85) and justify the use of the average Klyuchevskoi HMB in simulating the conditions under which the high-Al basalts were generated.

Preparatory to the consideration of the simulation results, it should be mentioned that a disadvantage of the COMAGMAT program is the absence of Cr-spinel crystallization and the insufficient stability of the scheme in simulating the peritectic relations between *Opx*, *Ol*, and *Aug* (particularly under elevated pressures). Nevertheless, considering the distinctive features of the Klyuchevskoi basalts, which are strongly dominated by *Ol*, *Cpx*, and *Pl* phenocrysts, the application of the high-pressure version of the COMAGMAT model (which was developed for tholeiitic systems) seems to be justified (see Section 2.2.6).

Calculation of *P–T* diagrams for the main basalt types. Figure 87 demonstrates modeled diagrams characterizing phase relations for the four main petrochemical types of the Klyuchevskoi basalts (Table 25). The diagrams were constructed based on the initial crystallization temperatures of minerals calculated for the course of equilibrium crystallization in different isobaric sections (1 atm $\le P \le$ 20 kbar, anhydrous conditions). For our further considerations, the results obtained for high-Mg basalts are the most important. At $P \sim 18$ kbar, the initial HMB melt is saturated with respect to olivine ($Fo_{90.3}$) and augite (MGN = 89.8), i.e., phases corresponding to the most primitive assemblage found in the lavas of Klyuchevskoi volcano (Figs. 85, 86). These relationships can be regarded as indicating that the fractionation of the parental HMB magma started at depths of more than 55 km, which is in agreement with geophysical estimates of the depth of the Klyuchevskoi magma plumbing system [Gorshkov, 1956].

In this context, it is expedient to consider the compositional lines calculated for the high-Mg melt at different pressures. These data for Al_2O_3, CaO, and MgO are presented in Fig. 88 (two upper plots). A characteristic feature of the modeled trends is the presence of inflection points in the CaO–MgO plots, which are related to the onset of clinopyroxene crystallization. Under pressures of about 20 kbar, the strong depletion of the melt in CaO occurs during the early stages and is caused by *Cpx* appearance on the liquidus. Analyzing the alumina content evolution, it can be seen than the high-Al residual melts (>18 wt % Al_2O_3) can be generated in this system at $P \ge 10$ kbar, and their compositions in Al_2O_3–MgO diagrams are close to the compositions of the Klyuchevskoi basalts. However, the natural trend of the CaO contents is inconsistent with the calculated lines of isobaric fractionation.

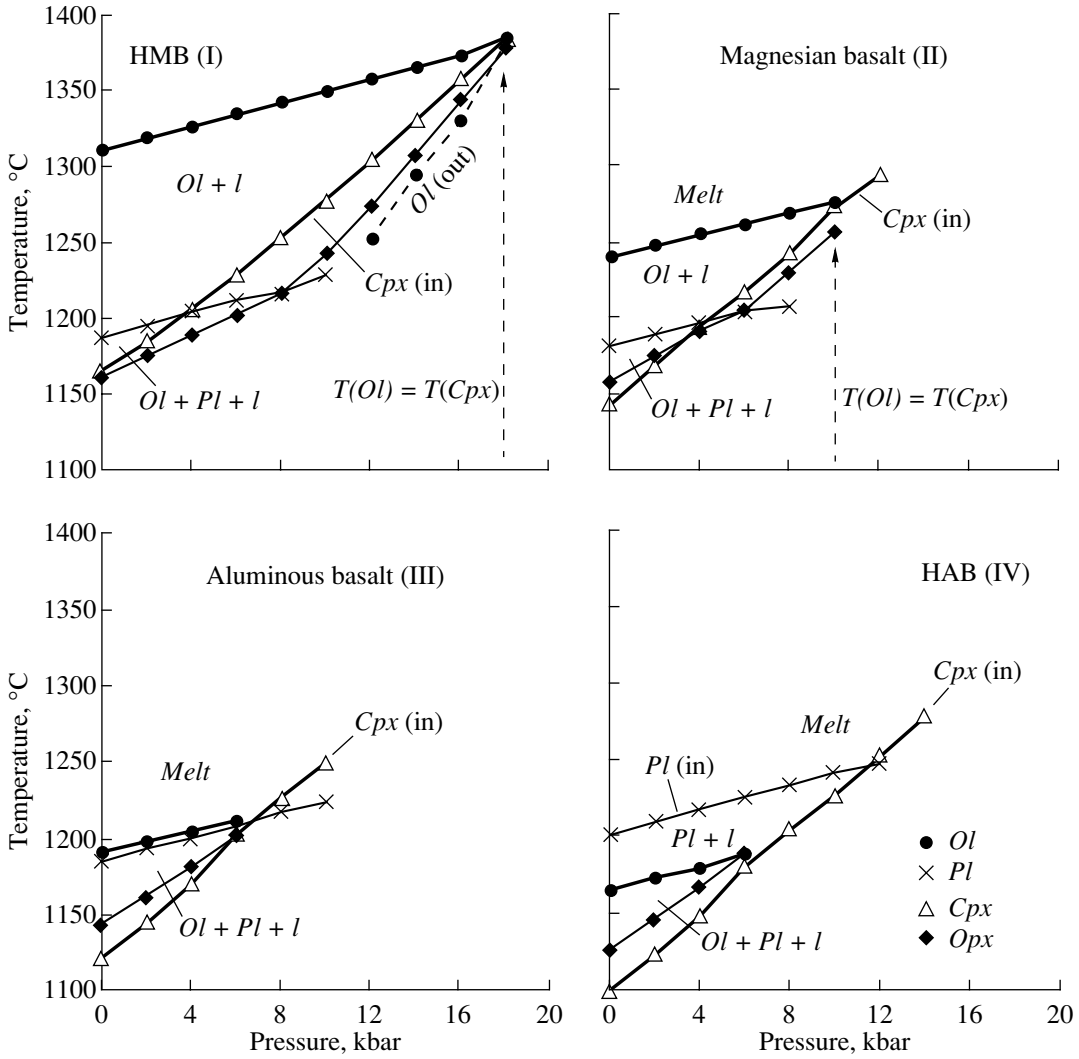

Fig. 87. Anhydrous *P–T* phase relations of the typical Klyuchevskoi basalts calculated with the COMAGMAT-3.0 program. The diagrams were constructed from the isobaric equilibrium crystallization sequences calculated for four initial melts (see Table 25) at pressures of 1 atm and 2–20 kbar. The calculations were carried out with a crystallization increment $\Delta\varphi_{cr}$ = 1 mol % up to a total percentage of crystallization of φ_{cr}^{max} = 60%. The basic version of COMAGMAT-3.0 was slightly modified through small changes in "high-pressure parameters" for *Aug* and *Opx* [Ariskin, 1999]

As can be seen from the CaO–MgO diagrams, the trend for the Klyuchevskoi basalts intersects the calculated isobaric lines, and this precludes the pressure estimating, as was done above for oceanic tholeiites (see Section 4.2.2). This situation will not change if the liquid lines of descent calculated at equilibrium crystallization are replaced with the fractionation trajectories. It is also scarcely probable that these differences are caused by some imperfections of the COMAGMAT program, because this model is able to accurately predict the evolution of the CaO content as a function of MgO (Fig. 79). A similar problem was encountered by the experimentalists dealing with phase relations in high-Mg basalts from Okmok volcano in the Aleutians [Draper and Johnston, 1992]. These data are presented in the lower pair of diagrams in Fig. 88 and testify that the drastic decrease in the CaO contents in the experimental glasses occurs at lower MgO contents compared to the natural sample compositions.

In principle, these discrepancies (particularly the enrichment in alumina) can be resolved if there is a mechanism permitting *Ol* to be a liquidus phase until high-Al compositions are attained [Draper and Johnston, 1992]. However, experimental data on melting HABs indicate that such systems under anhydrous conditions are characterized by the crystallization of excess *Pl* up to pressures of about 15–17 kbar [Baker and Eggler, 1983; Johnston, 1986]. As can be seen from the calculated phase diagram for the average HAB these estimates are decreased to approximately 12 kbar

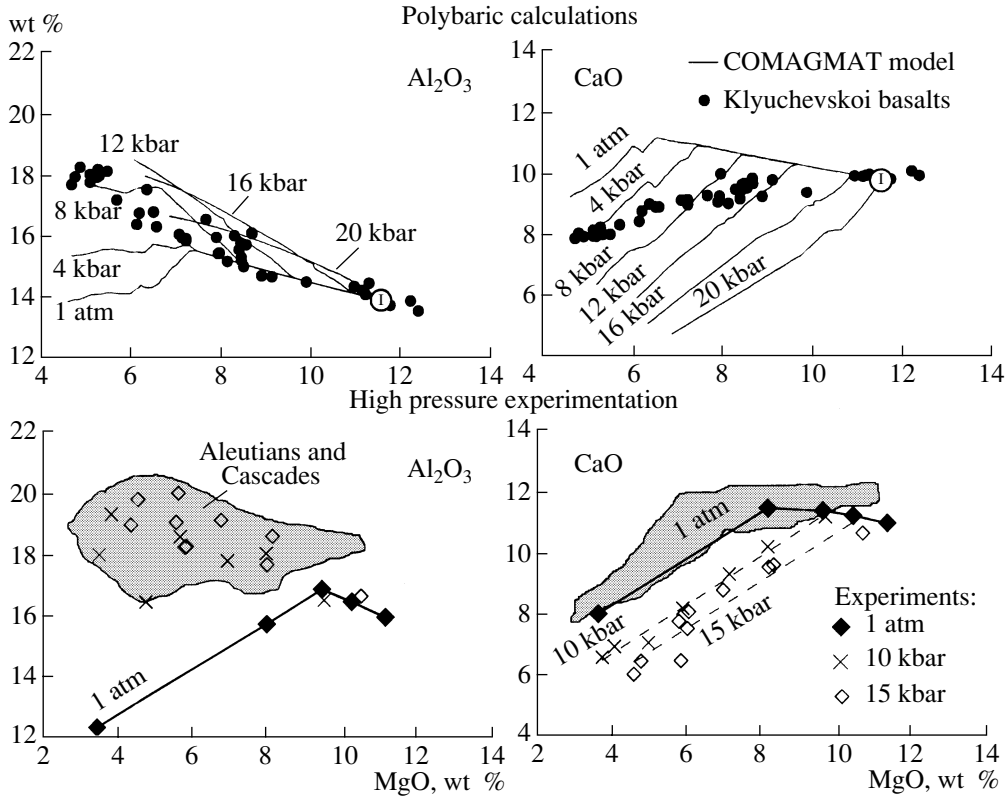

Fig. 88. Calculated and experimental liquid lines of descent for high-magnesia basalts from Klyuchevskoi volcano, Kamchatka, and Okmok volcano, Aleutians. The calculations of the equilibrium crystallization of the average Klyuchevskoi HMB were carried out using the COMAGMAT-3.0 model [Ariskin *et al.*, 1993, 1995]. The experimental compositions of the glasses and natural HAB, Aleutians and Cascades, are compiled from [Draper and Johnston, 1992].

(Fig. 87, composition IV). Attempts to settle this inconsistence resulted in two hypotheses [Draper and Johnston, 1992]: either *Ol* is in reaction relationships with the HAB melts (which precludes the appearance of this mineral as a liquidus phase), or the *Ol* crystallization field expands at the expense of *Pl* because the presence of water in the system.

Later considerations of the results of melting experiments on HAB and HMB compositions led to the conclusion that the *Ol*–melt reaction at high pressures can hardly account for the absence of liquidus olivine in high–alumina basalts. Thus, some amount of water is necessary to enable the origin of HAB via the fractionation of mafic minerals [Myers and Johnston, 1996]. As will be shown below, this conclusion holds for the Klyuchevskoi basalts with one exception. Mineralogical, petrochemical, and geochemical lines of evidence indicate that the origin of the Klyuchevskoi suite was controlled by *Ol* and *Cpx* crystallization, with these minerals occurring in cotectic relations throughout the whole range of compositions derived by the fractionation of the parental magma.

The problem is that this conclusion should be consistent with the structure of the modeled *P–T* diagrams (Fig. 87). In fact, at 8–18 kbar (i.e., the conditions under which the high-Al residual melts were probably generated), the HMB composition is characterized by a broad *Ol* crystallization field, which should lead to melt enrichment in CaO. This is, however, in conflict with the data of natural observations (Fig. 88). To resolve this problem we assumed that the HMB parent of Klyuchevskoi volcano had fractionated under polybaric conditions, starting from high pressures decreasing simultaneously with the process of magma crystallization. This decompressional hypothesis is consistent with the isobaric diagrams that suggest a systematic pressure decrease for the *Ol–Aug* cotectic with the transition from high-Mg to aluminous compositions (Fig. 87).

Simulation method for decompressional fractionation. In order to explore this hypothesis numerically, we conducted two series of simulations. The first set included the calculations of the fractional crystallization of the average Klyuchevskoi HMB in the process of decompression of the initial melt under anhydrous conditions. Varying the rate of the pressure decrease during fractionation, we could use the results of these simulations to evaluate the $dP/d\varphi$ at which the modeled CaO–MgO trends produce the best fit to the natural trends. The other series of polybaric simulations was carried out at the determined "optimal" rate of the pres-

sure decrease at variable H_2O contents in the initial high-Mg parent. This enabled us to evaluate the water content at which the modeled Al_2O_3–MgO trends coincided with the observed ones. This combination of anhydrous and hydrous polybaric calculations made it possible to constrain the most important parameters of the decompressional fractionation at water-undersaturated conditions that were responsible for the formation of the lava suite of Klyuchevskoi volcano.

These operations with phase equilibria models constitute a new technique of genetic reconstructions in application to mafic volcanic rocks and deserve certain comments. In fact, the proposed approach is based on the simulations of the fractionation of initial melts at a specified incremental net of external conditions (pressure, oxygen fugacity, and water content). The next step is the selection of an optimum model consistent with the observed geochemical and mineralogical characteristics of the Klyuchevskoi basalts. The main criterion of the validity of this model (in the sense of evaluating the fractionation conditions) is the agreement between the calculated and observed major- and trace-element variations. The results of these simulations are interpreted based on two assumptions.

First, at a reliable approximation of the initial magma, the compositions of the modeled fractionation products should be compared exclusively with the compositions of natural glasses, aphyric rocks, or genetically informative melt inclusions in minerals. In this sense, the Klyuchevskoi lava suite is pretty acceptable, if not ideal, because the total amount of original crystals in these rocks rarely exceeds 5–15 vol %.

Second, the calculated crystallization sequence and the liquid lines of descent are functions of the degree of fractionation and time (for dynamic models), i.e., each residual melt is derived from more primitive liquid at a strictly specified stage. However, the eruptions of the Klyuchevskoi volcano do not show any clearly pronounced temporal succession of basalts belonging to different petrochemical types: although the lavas are generally prone to become more silicic and aluminous with time, sometimes magnesian basalts were erupted after aluminous lavas, e.g., [Khrenov *et al.*, 1990]. Because of this we do not regard the Klyuchevskoi lavas as a suite resulting from the simple one-stage fractionation of the same parental magma but, instead, believe that the absence of a significant scattering in the rock compositions relative to the general petrochemical trends (Fig. 84) suggests the similarity of the compositions of the parental magmas and the stability of the conditions of their fractionation throughout the evolutionary history of this volcanic center.

This interpretation does not deny the importance of the mixing of derivative melts corresponding to distinct fractionation stages or formed in different times. In any event, the bulk major- and trace-element compositions of the hybrid basalts also should not significantly deviate from the main lines of cotectic control, e.g., [Nielsen, 1990].

Decompressional fractionation in anhydrous system. The fact that natural CaO–MgO trends intersect the calculated lines of isobaric crystallization (Fig. 88) suggest that the natural proportion of clinopyroxene that crystallized with Ol was lower than that simulated one. This could be caused by the contraction of the phase volume of *Cpx* due to a pressure decrease as the parental HMB magma ascended to the surface and fractionated. We simulated the decompressional process under anhydrous conditions starting from $P \sim 19$ kbar, which corresponded to the *Ol* and *Aug* saturation point (Fig. 87), to $P \sim 1$–2 kbar. In the course of these calculations, the rate of decompression $dP/d\varphi$ was the main variable parameter characterizing the assumed pressure change per 1 mol % melt crystallization. In the upper pair of plots in Fig. 89, the calculated lines of decompressional fractionation are compared with the observed suite of the Klyuchevskoi lavas.

The calculated trajectories indicate that the derivatives modeled at a high decompression rate $dP/d\varphi = -0.6$ kbar/% cryst. (rapid contraction of the *Cpx* field) are richer in CaO than the natural compositions. If the *Cpx* volume slowly contracts, at $dP/d\varphi = -0.2$ kbar/% cryst., the CaO content decreases more rapidly than it does in the Klyuchevskoi basalts.

At an intermediate decompression rate of $dP/d\varphi = -0.4$ kbar/% cryst., the modeled liquid lines of descent produce the best fit to the natural Al_2O_3–MgO and CaO–MgO trends. However, the final stage of fractionation is, again, characterized by notable deviations, manifested in the cessation of melt enrichment in Al_2O_3 and an increase in CaO (Fig. 89). Corrections for the water contents in the melts allowed us to minimize these discrepancies.

Decompressional fractionation in the presence of water. This mechanism was explored using the "hydrous" version of the COMAGMAT-3.0 program (see Section 2.2.7). In searching for the optimum conditions of fractional crystallization, the calculations were carried over a much more closely spaced grid of parameters: $-0.50 \le dP/d\varphi \le -0.30$ (with an increment of 0.02 kbar/% cryst.) and initial water contents of $0.2 \le H_2O \le 2.0$ wt % (with an increment of 0.20 wt %). In some instances, this "probing" grid was converged even more, because complicated reaction relations between *Ol*, *Aug*, and *Opx* under high pressures made the system very sensitive to even minor changes in the input parameters. Sometimes this resulted in the disappearance of one of the phases from the modeled crystallization sequence. This somewhat decreased the predicting ability of the model, and the computer simulation itself acquired some features of optimization with the simultaneous use of numerous geochemical and mineralogical criteria. Finally, we considered almost 600 combinations of the calculation parameters. The principal

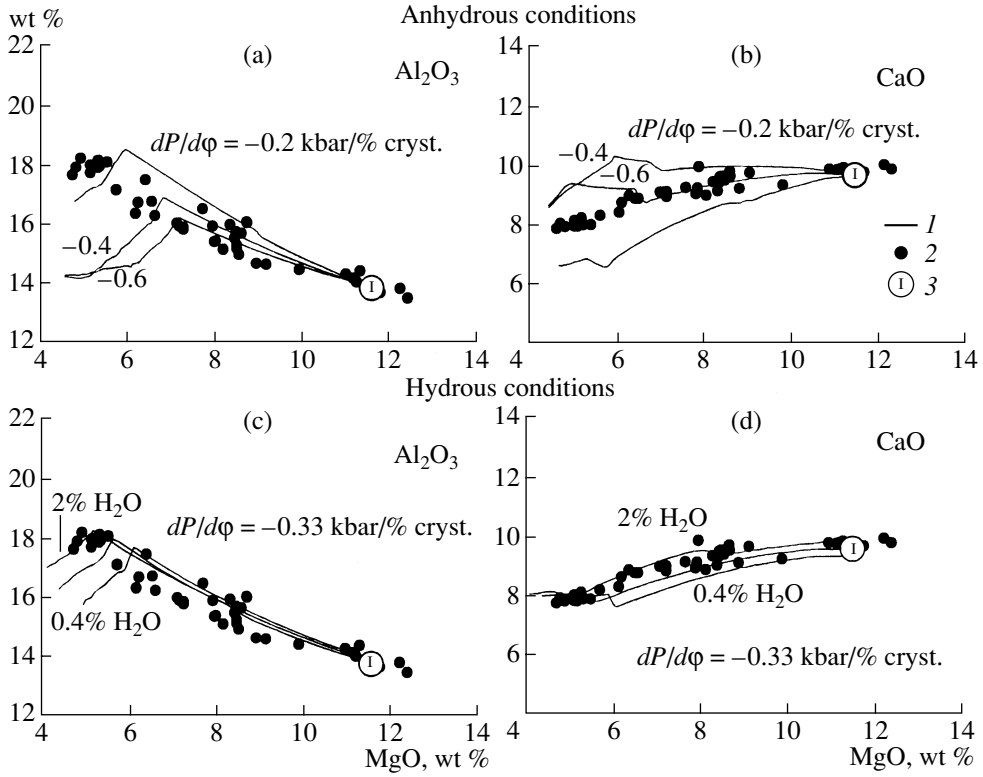

Fig. 89. Liquid lines of descent calculated for the decompressional fractionation of anhydrous and hydrous high-magnesia basalt. (a, b) Anhydrous conditions (initial pressure P_{in} = 18 kbar, final pressure P_{fin} = 1 kbar, $dP/d\varphi_{cr}$ = –0.2, –0.4, and –0.6 kbar/% cryst.); (c, d) the system contains from 0.4 to 2 wt % H_2O (initial pressure P_{in} = 19.3 kbar, final pressure P_{fin} = 1.5 kbar, $dP/d\varphi$ = –0.33 kbar/% cryst.). (*1*) Calculations with the COMAGMAT-3.0 model; (*2*) basalts of Klyuchevskoi volcano; (*3*) average HMB.

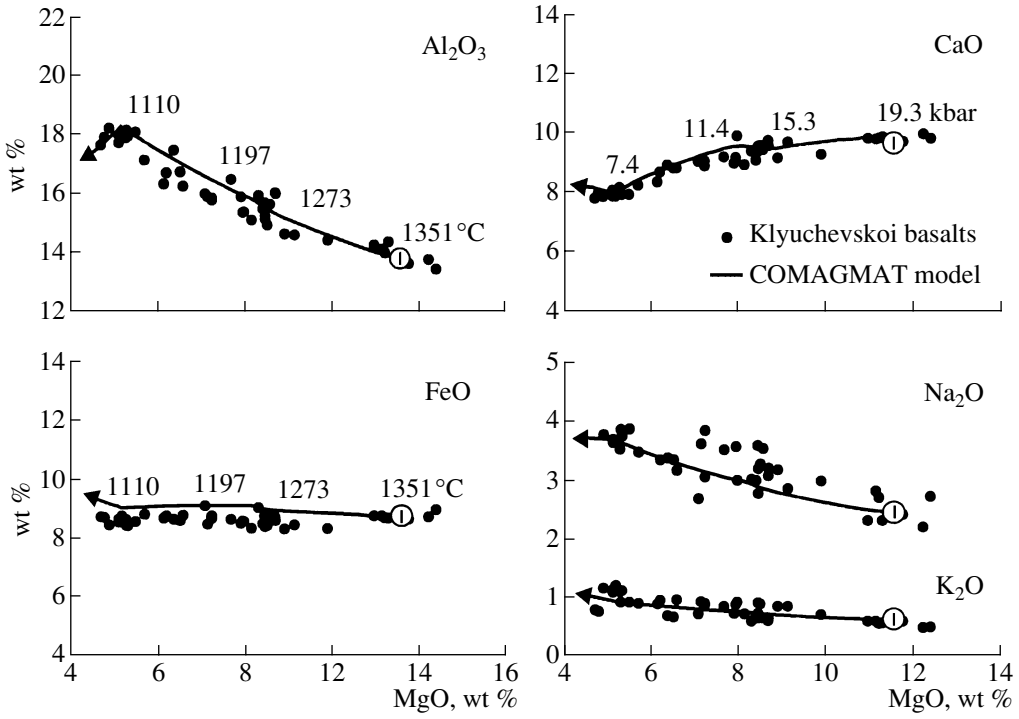

Fig. 90. Modeled trends of decompressional fractionation for the average Klyuchevskoi high-Mg basalt (Type I from Table 25). The calculations were carried out using the COMAGMAT-3.0 model and assuming a crystallization increment of 1 mol %, initial pressure of P = 19.3 kbar, the rate of decompression $dP/d\varphi_{cr}$ = –0.33 (kbar/mol %), initial water content of 2 wt %, and QFM buffer [Ariskin *et al.*, 1993, 1995]. The values near the calculated lines represent the temperature and pressure decrease during the decompressional fractionation.

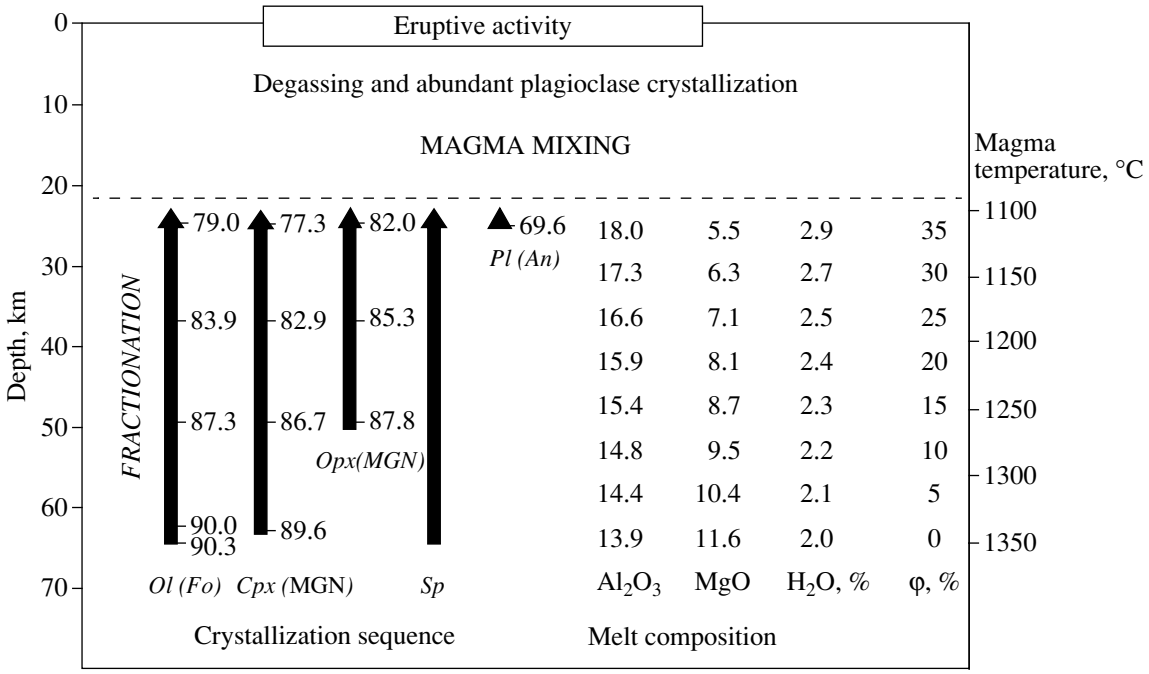

Fig. 91. Modeled crystallization sequence and compositional evolution during the decompressional fractionation of the average Klyuchevskoi high-Mg basalt as a function of depth, magma temperature, and the degree of fractionation φ. See captions to Fig. 90 for the calculation conditions. This plot demonstrates that the HAB melts are formed at depths of 20 km. At shallower depths, these melts take part in the processes of mixing with other (even more primitive) differentiates and undergo, due to water degassing, massive *Pl* crystallization, which is responsible for the observed variations in the modal and chemical composition of the high-alumina, aluminous, and, probably, magnesian basalts.

results of the forward modeling are presented in the lower plots of Fig. 89.

Compositional evolution of the melt. According to these simulations, the optimum model for the fractionation of the parental HMB magma corresponds to an initial water content of approximately 2 wt % and a decompression rate $dP/d\varphi$ = –0.33 kbar/% cryst. At these input parameters, the calculated liquid lines of descent best reproduce the petrochemical trends in Al_2O_3–MgO and CaO–MgO diagrams (Fig. 89). The derivatives modeled at water contents of <1 wt % show insignificant but systematic deviations from the natural CaO–MgO trend and have Al_2O_3 contents notably lower than those typical of HAB.

Figure 90 clearly demonstrates the relationships between the evolutionary trends and the fractionation conditions inferred from the optimal model. The modeled trajectories are marked with the *P–T* values corresponding to a number of crystallization stages. Thus, each composition on the fractionation line may be assigned to unique pressure and temperature values, which is a principal difference between the decompression and isobaric models. These data demonstrate that the high-alumina Klyuchevskoi basalts were produced by low-temperature (1110°C) melts, which were formed under pressure of about 7 kbar after ~36% crystallization of the parental HMB magma.

The crystallization sequence and variations in the chemistry of minerals with decreasing temperature and pressure at the optimal parameters are shown in Fig. 91. The right-hand part of this plot demonstrates the com-

Table 26. Composition of the average HAB from Klyuchevskoi volcano and the modeled high-alumina melt

Component	HAB	MD
SiO_2	53.50	53.23
TiO_2	1.09	1.13
Al_2O_3	18.26	18.16
FeO	8.67	9.10
MnO	0.16	0.15
MgO	5.24	5.29
CaO	8.22	8.14
Na_2O	3.45	3.65
K_2O	1.20	0.93
P_2O_5	0.20	0.22

Note: See Table 25 for the HAB composition (type IV); MD is the modeled derivative melt at the onset of plagioclase crystallization at *P* = 7 kbar and *T* = 1110°C (Figs. 90, 91).

positional characteristics of the residual melts corresponding to different fractionation stages. As follows from these data, the parental HMB magma started to crystallize with the *Ol–Aug* cotectic under a pressure of 19 kbar and a temperature of about 1350°C. Olivine and augite crystallized in the proportion of approximately 2 : 3 up to 1260°C (15 kbar, φ_{cr} = 15 wt %), when magnesian *Opx* (MGN = 87.8) joined the liquidus minerals. Continued fractionation is inferred from the increased amount of crystallizing *Aug* (up to 80–90%) at an *Ol* proportion decreasing to 10–15 wt %. The amount of *Opx* in the crystallizing assemblage did not exceed 2 wt %. The more efficient separation of *Aug* resulted in the CaO–MgO trend bending toward a greater decrease in the CaO content (Fig. 91).

Plagioclase started to crystallize at pressure of ~7 kbar, a temperature of 1110°C, and a water content of 3 wt % in the residual melt. During this stage, the bulk degree of fractionation of the system is 36% of the original melt, and the olivine composition is slightly more magnesian (Fo_{79}) than that determined by microprobe analyses ($Fo_{75–77}$). However, the most significant deviations of the modeled compositions of the observed minerals occurred at $T < 1150$°C. This led us to think that the low-temperature simulations conducted with the COMAGMAT model for water-bearing systems cannot provide an exact correspondence between the compositions of coexisting olivine and pyroxenes (the effect of water on the *Pl* composition is also ignored). Nevertheless, the main conclusion that melts close to HAB in composition were generated during a high-pressure crystallization process seems to be justified (compare the compositions of the average HAB and the modeled high-alumina melt in Table 26). If the water content in the calculated HAB is decreased, the point of the onset of *Pl* crystallization is shifted toward lower pressures. However, at the optimal values of 1.5–2.0 wt % H_2O and a decompression rate $dP/d\varphi$ = –0.33 kbar/% cryst., the estimated starting pressure of *Pl* crystallization never decreases below 5 kbar.

4.3.3. Main conclusions and implications

One of the main results of this study is the conclusion that the assemblage of phenocrysts, crystal aggregates, and mineral inclusions observed in the Klyuchevskoi lavas was formed by a high-pressure crystallization process. This conclusion is independent of the accuracy of the computer model used to simulate the phase equilibria but is based on the analysis of experimental information on the compositions of highly magnesian clinopyroxene and olivine that coexisted at $P >$ 10–15 kbar (Fig. 85). These parameters are notably higher than P = 5–9 kbar obtained by means of graphical projecting onto barometric diagrams [Kersting and Arculus, 1994], but the pressure estimates are confirmed by the results of computer simulation of the polybaric crystallization of the parental HMB magma at water-undersaturated conditions (Figs. 87–90).

A comparison of the petrochemical trends exhibited by the Klyuchevskoi basalts and the modeled liquid lines of descent indicates that the optimal model for the formation of the volcanic suite is the polybaric fractionation of the HMB magma at an average rate of decompression of $dP/d\varphi$ = –0.33 kbar per 1% crystallization, with ~2 wt % water in the initial melt. These estimates, obtained by simulating phase equilibria, are close to the results of directly analyzing the water contents in melt inclusions in olivine from the Klyuchevskoi basalts [Sobolev and Chaussidon, 1996].

According to our model, the proposed parental magma started to crystallize with the formation of olivine and clinopyroxene (in the presence of spinel) under pressures of approximately 19 kbar and a temperature of ~1350°C. These minerals are joined by magnesian *Opx* at P ~ 15 kbar and T ~ 1260°C, although its percentage in the crystallizing assemblage was no higher than a few percent, so that it did not significantly affect the lines of the *Ol–Aug* cotectic control. The enrichment of the melt in water resulted in a significant delay of plagioclase crystallization and the formation of high-alumina liquids, that contained >18 wt % Al_2O_3 (Fig. 91) [Ariskin *et al.*, 1995; Ariskin, 1999].

Final crystallization stages of the Klyuchevskoi magmas. This trend of alumina enrichment terminated when *Pl* began to crystallize at a pressure of 7 kbar, temperature of 1110°C, and a water content in the melt of ~3 wt %. During this stage, the compositional range of the modeled liquids corresponded to the observed diversity of the Klyuchevskoi lava compositions. These polybaric calculations under optimal model parameters were cut off at ~1050°C and 4 kbar, which corresponded to ~46% fractionation of the original melt. This was done deliberately, because the COMAGMAT-3.0 program could not guarantee the plausibility of the modeled liquid lines of descent at lower temperatures and higher water contents. According to more advanced calculations, further crystallization should lead to the rapid saturation of the system with water (3.6–3.8 wt % H_2O) and its subsequent degassing at a pressure of 1.5 kbar and a temperature of ~1000°C.

The final evolutionary stages of the high-alumina melts were recently explored by analyzing melt inclusions in *Ol* ($Fo_{71–79}$), *Cpx* (MGN = 70–81), and *Pl* ($An_{47–84}$) [Mironov *et al.*, 2001]. These data indicate that the phenocrysts were formed at 1145–1030°C and pressures lower than 3.5 kbar. The average pressure during their crystallization was estimated to be ~1.5 kbar, and the water content in the high-alumina derivative melts could attain 5 wt %. It was also established that the final product of HAB magma crystallization should have been dacite melts, which, however, were not found among the Klyuchevskoi rocks and occur only as melt inclusions. These results are mostly

in good agreement with the data of decompression simulations with the COMAGMAT program. The differences between the pressure estimates attributed to the formation conditions of the most aluminous liquids ($P \sim 7$ kbar, according to [Ariskin *et al.*, 1995], and $P \leq 3.5$ kbar, according to [Mironov *et al.*, 2001]), are within the uncertainties of the modeling techniques and the results obtained on the melt inclusions.

The proposed scenario for the pressure- and temperature dependent compositional evolution of the Klyuchevskoi magmas presented in Fig. 91 was not intended to be a comprehensive model of the magmatic evolution of this volcano, because it does not allow for the multistage character of magma fractionation, mixing, degassing, and other processes. In essence, this scheme is thermodynamic and demonstrates the range of external conditions under which the magma generating system could pass from one state (that corresponded to the proposed high-Mg parent) to another (corresponding to the observed compositions of the high-Al basalts). The fractionation dynamics is accounted for implicitly, through introducing a parameter characterizing the rate of decompression $dP/d\varphi$. Evidently, the assumed optimal values $dP/d\varphi$ are related to the speed at which primitive Klyuchevskoi magmas could rise to the surface. Because of this, the degree of pressure decrease per percent crystallized should be taken into account when deriving more rigorous dynamic and geophysical models of the evolution of this volcanic center.

Given the uncertainties of the polybaric calculations, the estimates of the thermodynamic parameters should be regarded cautiously. Nevertheless, the formulation of the problem itself and the development of the model for decompression fractionation seem to be relevant and significant. We hope that the results of our research will attract the attention of petrologists to the proposed mechanism of polybaric fractionation and the possibilities opened by the application of modern models of phase equilibria to the study of this still inadequately poorly understood process.

GENERAL DISCUSSION

This publication is a synthesis of the results of petrological studies conducted by our team starting from the early 1980s and centered on the computer simulating phase equilibria during the crystallization of basaltic magmas. Over these years, we gained significant experience in developing magma crystallization models for estimating the genetic link and formation conditions of various intrusive and volcanic rocks. This experience provides us with a methodological basis for predetermining the avenues for the further development of models of equilibrium and fractional crystallization and their application. Because of this, we least of all wished that the data presented in this publication were regarded merely as a compilation of the results published in earlier papers. This monograph was conceived rather as a guide for researchers appreciating the efficiency and potentialities of modern computational petrology. This predetermined the necessity of detailed descriptions of the experimental and thermodynamic fundamentals of the models and the attention focused on the issues related to the calibration and testing of mineral–melt geothermometers (see Chapters 1 and 2).

These sections provide the reader with insight into the building blocks of modern models designed to simulate magma differentiation processes. In our model, the system involves an experimental database on the melting of igneous rocks (INFOREX) and an algorithm proposed for solving the equilibrium problem in application to crystallizing magmas (models of the COMAGMAT series). Another important component of this system is procedures for modeling the dynamics of heat and mass transfer in a magma chamber which allow one to explore the diversity of igneous processes [Frenkel *et al.*, 1988b, 1989; Ariskin and Barmina, 2000].

In this publication, we do not discuss successive dynamic models, placing emphasis on examples of utilizing the crystallization routine of the COMAGMAT program. This algorithm has received wide recognition from petrologists but, regretfully, only part of its potentialities is currently used, and it is still often utilized for purposes lying outside its specified range of applicability. The data and considerations presented in this publication will, hopefully, allow the user to assay the actual potential of the COMAGMAT model and the reliability of results obtained with it.

An important aspect of genetic interpretations underlain by magma crystallization models is the necessity of the complex petrological–geochemical exploring of the objects. The easy orientation in this information and the ability to accurately compare the data of observations and thermodynamic simulations open the possibility of the fairly precise reconstructing of the magma differentiation conditions with the use of computer modeling techniques. Without this basis, the simulations of crystallization may become a sort of computer game of virtual petrology, whose results have very little relevance to the actual processes of magma fractionation.

Comparing and testing crystallization models. Here it is relevant to address the question often asked by those who compare the results of simulations with the COMAGMAT program and the currently popular MELTS model: Why COMAGMAT can often reproduce more realistically the liquid lines of descent of terrestrial basalts, in spite of the utilization of a simplified approximation of the solid-solution thermodynamics and an explicit algorithm for minimizing the Gibbs free energy? This can be explained by two reasons. First,

unlike our American colleagues, we had no intention of developing a "supersystem" of computer modeling, in the sense that it could be used throughout the whole range of the compositions of natural melts and temperatures from 500 to 1800°C (in some cosmochemical papers, the MELTS program was utilized at even higher parameters).

Conversely, our approach relies on the maximally accurate calibration of models for a specified compositional range, corresponding to the diversity of rocks representing a given geological object. Our many-years' of experience in modeling demonstrates that this approach can yield calculated temperatures with an accuracy of about 10°C and compositions accurate to 1–5 mol % for minerals and ~0.5 wt % for melts (depending on the proportions of crystals and melt). As an example, it should be mentioned that COMAGMAT is most applicable to tholeiitic systems, the LUNAMAG program works better with lunar basaltic melts, whereas METEOMOD was designed specially for simulating the equilibrium and fractional melting of ordinary chondrites [Ariskin and Barmina, 2000].

The principal importance of this comment is illustrated by the results obtained by testing the MELTS [Ghiorso and Sack, 1995], MAGPOX [Longhi, 1991], and COMAGMAT-3.0 [Ariskin *et al.*, 1993] programs, which were recently published in [Slater *et al.*, 2003; Thompson *et al.*, 2003]. These researchers conducted calculations of equilibrium crystallization for three "Martian" and lunar samples, which were examined experimentally, and compared these results with those obtained with the three aforementioned programs. The main conclusion was that the MELTS and MAGPOX models produce the best fit with experimental data, while the COMAGMAT program yields inaccurate characteristics for most parameters. The problem is, however, that this formal conclusion ignored the selection of experimental compositions used for calibrating the crystallization models. The former two programs were designed using the compositions of iron-enriched systems, which are close to the melting products of "Martian" meteorites and lunar mare basalts. In calibrating the COMAGMAT model, we did not utilize these data at all in order to best simulate terrestrial tholeiitic systems (Chapter 2). Thus, the petrological worth of the comparison conducted in [Slater *et al.*, 2003; Thompson *et al.*, 2003] provokes serious doubt, leaving alone the inaccurateness of the use of the out-of-date version of the COMAGMAT-3.0 program for estimating the effect of oxygen fugacity.

Significance of the geochemical thermometry technique. In this publication, much attention is paid to the fundamentals of the method of geochemical thermometry and the results of thermometric calculations for intrusive basites (Chapter 3). The name of the method puts emphasis on the technical aspect, related to evaluating the temperature of the intercumulus melt [Frenkel *et al.*, 1988a] but inadequately little reveals the potential of these simulations in the context of genetic reconstructions. Simultaneously with the temperature estimates, the initial melt composition for each sample is calculated, which makes it possible to confirm or refute cotectic links within the rock associations in question. Sometimes it is also possible to assay the evolution of the chemical and phase composition of the magma during its differentiation in the chamber. Thus, the method of geochemical thermometry was developed to combine traditional thermometric techniques for the main rock-forming minerals, and this enables the user to retrieve maximum genetic information assuming the equilibrium distribution of components between the melt and crystals.

The thermometry of contact rocks and primitive cumulates of the differentiated series of layered intrusions (Skaergaard, Partridge River, Talnakh, Kamenistyi, and Yoko-Dovyren) indicates that their parental magmas were emplaced within an incredibly narrow temperature range (~1170–1200°C) with melts of relatively little varying compositions, close to ferrobasalts of tholeiitic series (Table 20). The only exception is the magma of the Kiglapait intrusion, which had a higher temperature (~1230°C) when injected into the chamber, and whose liquid portion compositionally corresponded to Early Proterozoic Al–Fe troctolite magmas [Olson and Morse, 1990; Barmina and Ariskin, 2002]. Much more contrasting estimates were obtained for the phase compositions of the parental magmas. The data in Table 20 testify that the original magmatic suspensions could contain crystals in amounts from a few percent (the differentiated traps of the Siberian Platform) to 15–25% (the Talnakh and Kiglapait massifs) and even 40–60% (the Kamenistyi sill and Partridge River intrusion). This means that traditional concepts of the instantaneous emplacement of an overheated or liquidus melt into the crust are not realistic and calls for the revision of magma differentiation hypotheses underlain by thermal convection of a homogeneous liquid in the chamber [Barlett, 1969].

If there is a thoroughly sampled layered series, the method of geochemical thermometry makes it possible to calculate the evolution of the temperature and composition of differentiated (trapped or residual) melts starting from the lowermost level of sampling of the intrusion. This task can be achieved by using the compositions of the residual magmas or the numerous compositions of "neighboring" rocks in the vertical section of the intrusion. The efficiency and informativeness of this approach was illustrated by the examples of dolerite sills in the Siberian Platform and the Layered Series of the Skaergaard intrusion (see Section 3.3). Although the data obtained for these bodies are of a reconnaissance and preliminary character, we believe that this version of geochemical thermometry developed for differentiated rocks has good potentialities in the context of reconstructing the chemical and phase characteristics of intrachamber differentiation [Ariskin, 2003].

Problems related to the fractionation of tholeiitic magmas were addressed to in Sections 4.1 and 4.2. We tried to demonstrate how the configuration and direction of petrochemical trends can be used to evaluate the thermodynamic parameters controlling the magma crystallization process. It was demonstrated that this problem can be resolved by simulating the perfect fractionation of the parental magma at different P–T–f_{O_2}–H_2O parameters and then comparing the modeled evolutionary lines with available petrochemical data. This approach is not new and, in fact, is based on exhausting the lines of phase control with regard for the initial conditions. Bowen [1928] was the first to justify the application of this technique, but the possibilities of its systematic utilization were opened only lately thanks to the thorough calibration of the thermodynamic basis of the COMAGMAT model, including the more systematic accounting for the effects of pressure and water on phase equilibria [Ariskin and Barmina, 2000].

Significant difficulties were caused by the necessity of developing accurate models for the crystallization of Fe–Ti oxides and accounting for the effect of oxygen fugacity on the liquid lines of descent. Several users noted that earlier versions the COMAGMAT model and its analogues developed by other researchers insufficiently accurately predicted the crystallization conditions of magnetite and ilmenite. We managed to solve this problem in the late 1990s, when models were developed (COMAGMAT-3.5 and higher) that now are able to calculate the crystallization temperatures of these minerals accurate to 10–15°C depending on the oxygen fugacity [Ariskin and Barmina, 1999]. This made it possible to perform investigations of the effects of systems open or closed with respect to oxygen on basalt magma fractionation trends. This provided the basis for the development of a new method for estimating the redox conditions of the origin of basalt–andesite–dacite associations. It is based on the calculations of the f_{O_2} values at which the modeled *Pl*–melt and *Mt*–melt temperatures are equal, if a series of cotectic rock compositions is available. At an accuracy of the calculated magnetite temperatures of 15°C, the uncertainties in the absolute f_{O_2} evaluations are 0.5–1 logarithmic units. The results of redoximetry of ferrodiorites from the Chazhma sill in Eastern Kamchatka demonstrated that the original melts of these rocks were derived under relatively oxidized conditions of NNO + 0.5. The major-element trends of perfect fractionation modeled at these parameters are in good agreement with those revealed by rocks and approximating the Bowen evolution of the Chazhma magma.

The high-pressure version of the COMAGMAT-3.0 model was used to develop a technique for the barometry of the glasses of oceanic tholeiites. This approach involves the calculation of the liquid lines of descent for a parental melt at different pressures, followed by a comparison of the modeled trends with variations of the glass compositions in a CaO/Al_2O_3–MgO diagram. The results of the barometry for glasses from Hole 332, which was drilled near the axial zone of the Mid-Atlantic Ridge, suggest the occurrence of two main depth levels (differing by 9–12 km), which corresponded to the fractionation of a primitive melt similar to TOR-1 in relatively small magma chambers. The characteristic features of the trends of glasses recovered by Hole 418A in the western MAR flank point to the monotonous fractionation of a magnesian basaltic melt within a pressure range of 5–2 kbar, perhaps during the ascent and decompression of the proposed parental melt.

The decompression fractionation model for primitive calc–alkaline magmas was examined in application to the suite of the magnesian and high-alumina lavas of the Klyuchevskoi volcano (Section 4.3). We used data on the geochemistry, mineralogy, and phase relations in the Klyuchevskoi basalts to confirm the conclusion that the HAB were produced by the polybaric fractional crystallization of initial melts of HMB type. Then we developed a decompression version of the COMAGMAT model with regard for the changes in the liquidus assemblages and compositions over a pressure interval of 20 kbar to 1 atm and initial water contents of 1–2 wt %. This program was utilized to conduct hundreds of calculations of the crystallization of a high-magnesia parent, and this allowed us to evaluate the most probable conditions of the polybaric process.

According to these estimates, the optimal model for the genesis of this igneous suite involves the fractionation of the high-magnesia magma with an average rate of decompression $dP/d\varphi$ = –0.33 kbar/% cryst. at a water content of 2 wt % in the initial melt. The starting conditions were estimated to correspond to the crystallization of olivine, clinopyroxene, and spinel at P ~ 19 kbar and T ~ 1350°C. The successive enrichment of the melt in H_2O resulted in a delay of plagioclase crystallization and the formation of high-Al derivatives. The line of Al_2O_3 enrichment terminates as soon as plagioclase appears on the liquidus at a pressure of 7 kbar, a temperature of 1110°C, and 3 wt % H_2O in the residual liquid. During this stage, the modeled liquid compositions should represent the entire range of the compositional diversity of the Klyuchevskoi lavas, and further crystallization results in the rapid saturation of the system with water with its subsequent degassing at pressures of approximately 1.5 kbar. It was the first attempt of computer simulations of this type ever conducted with the purposes of igneous petrology [Ariskin *et al.*, 1995]. The mechanism of decompressional fractionation and the respective calculations with the COMAGMAT program were recently utilized to reconstruct the polybaric conditions that were responsible for the formation of the Mt. Buller igneous suite in southeastern Australia [Soesoo, 2000].

As an additional comment on the data of the polybaric simulations, it should be mentioned that currently existing models of high-pressure crystallization, such

as MELTS and COMAGMAT, provoked certain criticism, particularly concerning the evaluation of changes in the modal composition of cotectic assemblages and the corresponding solid residuals. These discrepancies are caused by difficulties in attaining consistency between the results of experiments at high pressures, because the reproducibility of these data is much worse than that of 1-atm experiments. This explains why the idea was expressed over the past years that it is principally impossible to develop internally consistent and realistic models simulating polybaric melting and crystallization [Ghiorso, 1997]. It was also proposed [Falloon *et al.*, 2001] to completely revise the available high-pressure experimental database. This skepticism has certain grounds (see introduction to Section 4.2). It is, however, worth noting that the methods of barometry and computer simulations that are based on the principles of phase control in fact utilize the same effect of the expansion of the stability field of high-Ca pyroxene relative to olivine and plagioclase. This effect was estimated to be approximately 15°C/kbar. In other words, at uncertainties of the calculated high-pressure equilibrium temperatures of about 30°C, it is hardly probable that the application of geobarometry to natural melts can result in errors in excess of 2 kbar.

ACKNOWLEDGMENTS

The authors are deeply indebted to M.Ya. Frenkel (1943–1993) and Prof. A.A. Yaroshevsky, who were pioneers in computer simulating the crystallization differentiation of basaltic magmas and supervised our research team for many years. Special thanks are due to our friends E.V. Koptev-Dvornikov, B.S. Kireev, and S.A. Khubunaya, who shared the first successes in the computer simulation of differentiated intrusions and volcanic suites. We appreciate the invaluable help of R.R. Al'meev, G.S. Nikolaev, S.S. Meshalkin, and T.I. Tsekhonya in the further development of this research avenue. It is hard to overestimate the enthusiasm of our colleagues N.A. Krivolutskaya, E.G. Konnikov, A.Yu. Ozerov, N.M. Sushchevskaya, and C.I. Chalokwu, who not only believed in the significant potential of the COMAGMAT model but also highly professionally utilized the results of the phase equilibrium calculations in the genetic reconstructions for various magmatic objects. Significant influence on the materials presented in this publication was exerted by discussions with L.V. Danyushevsky, J. Longhi, O.I. Lukanin, A. McBirney, B. Marsh, R. Nielsen, I.D. Ryabchikov, A.V. Sobolev, V.N. Sharapov, and O.I. Yakovlev. These studies were financially supported from grants of the National Science Foundation (NSF EAR-9206647), International Science Foundation (M1N000 and M1N300), and the Russian Foundation for Basic Research (94-05-16098, 96-05-64231, 96-89054, 99-05-64875, 00-05-78046, and 02-05-64118). A.A.A. thanks the Foundation for Support of National Science for financing of this research in 2001–2003.

REFERENCES

1. V. M. Agoshkov, "Modeling of Crystal Growth from Magmatic Melt in an Open System," Geochem. Int. **40** (Suppl. 1), 82–91 (2002).
2. R. R. Al'meev and A. A. Ariskin, "Mineral: Melt Equilibria in a Hydrous Basaltic System: Computer Modeling," Geochem. Int. **34**, 563–573 (1996).
3. A. A. Ariskin, "Calculation of Titanomagnetite Stability on the Liquidus of Basalts and Andesites with Special Reference to Tholeiitic Magma Differentiation," Geochem. Int. **36**, 15–23 (1998).
4. A. A. Ariskin, "Phase Equilibria Modeling in Igneous Petrology: Use of COMAGMAT Model for Simulating Fractionation of Ferro-basaltic Magmas and the Genesis of High-alumina Basalt," J. Volcanol. Geotherm. Res. **90**, 115–162 (1999).
5. A. A. Ariskin, "Geochemical Thermometry of the Layered Series Rocks of the Skaergaard Intrusion," Petrology **10**, 495–518 (2002).
6. A. A. Ariskin, "The Compositional Evolution of Differentiated Liquids from the Skaergaard Layered Series as Determined by Geochemical Thermometry," Russ. J. Earth Sci. **5**, 1–29 (2003).
7. A. A. Ariskin and G. S. Barmina, "Equilibria Thermometry between Plagioclases and Basalt or Andesite Magmas," Geochem. Int. **27** (10), 129–134 (1990).
8. A. A. Ariskin and G. S. Barmina, "An Empirical Model for the Calculation of Spinel–Melt Equilibrium in Mafic Igneous Systems at Atmospheric Pressure: II. Fe–Ti Oxides," Contrib. Mineral. Petrol. **134**, 251–263 (1999).
9. A. A. Ariskin and G. S. Barmina, *Modeling Phase Equilibria during the Crystallization of Basaltic Magmas* (Nauka, Moscow, 2000) [in Russian].
10. A. A. Ariskin and G. S. Nikolaev, "An Empirical Model for the Calculation of Spinel–Melt Equilibrium in Mafic Igneous Systems at Atmospheric Pressure: I. Chromian Spinels," Contrib. Mineral. Petrol. **123**, 282–292 (1996).
11. A. A. Ariskin and M. Ya. Frenkel, "Computer Simulation of the Fractional Crystallization of Basic Silicate Melts," Geokhimiya, No. 3, 338–356 (1982).
12. A. A. Ariskin, G. S. Barmina, and M. Ya. Frenkel, "Computer Simulation of Basalt Magma Crystallization at a Fixed Oxygen Fugacity," Geochem. Int. **24** (6), 85–98 (1987).
13. A. A. Ariskin, G. S. Barmina, and M. Ya. Frenkel, "A Crystallization Mechanism for the Tholeiitic Series," Int. Geol. Rev. **30**, 382–389 (1988a).
14. A. A. Ariskin, A. Deutsch, and M. Ostermann, "The Sudbury Igneous Complex: Simulating Phase Equilibria and in Situ Differentiation for two Proposed Parental Magmas," Geol. Soc. Am. Spec. Pap. **339**, 373–387 (1999).
15. A. A. Ariskin, M. Ya. Frenkel, and T. I. Tsekhonya, "High-Pressure Fractional Crystallization of Tholeiitic Magmas," Geochem. Int. **27** (9), 10–20 (1990).

16. A. A. Ariskin, E. G. Konnikov, and E. V. Kislov, "Modeling of Equilibrium Crystallization of Ultramafic Rocks with Application to the Problems of Phase Layering in the Dovyren Pluton, Northern Baikal Region, Russia," Geochem. Int. **41**, 107–129 (2003).

17. A. A. Ariskin, T. I. Tsekhonya, and M. Ya. Frenkel, "Computerized Barometry and Genetic Interpretation of Central Atlantic Basalt Glasses," Geochem. Int. **29** (2), 117–125 (1992).

18. A. A. Ariskin, G. S. Barmina, M. Ya. Frenkel, and R. L. Nielsen, "COMAGMAT: A Fortran Program to Model Magma Differentiation Processes," Comput. Geosci. **19**, 1155–1170 (1993).

19. A. A. Ariskin, G. S. Barmina, M. Ya. Frenkel, and A. A. Yaroshevsky, "Simulating Low-Pressure Tholeiite-Magma Fractional Crystallization," Geochem. Int. **25** (4), 21–37 (1988b).

20. A. A. Ariskin, G. S. Barmina, N. A. Krivolutskaya, and E. G. Konnikov, "Parental Magmas of Differentiated Intrusions: Composition, Temperature, and Crystallization Percentage," in *Proceedings of All-Russia Scientific Conference Geology, Geochemistry, and Geophysics at the Turn of the 21th Century, 2002*, Vol. 2, p. 36.

21. A. A. Ariskin, G. S. Barmina, A. Yu. Ozerov, and R. L. Nielsen, "Genesis of High-Alumina Basalts from Klyuchevskoi Volcano," Petrology **3,** 449–472 (1995).

22. A. A. Ariskin, K. V. Bouadze, S. S. Meshalkin, and T. I. Tsekhonya, "INFOREX: A Database on Experimental Studies of Phase Relations in Silicate Systems," Am. Mineral. **77**, 668–669 (1992).

23. A. A. Ariskin, M. I. Petaev, A. A. Borisov, and G. S. Barmina, "METEOMOD: A Numerical Model for the Calculation of Melting–Crystallization Relationships in Meteoritic Igneous Systems," Meteoritics Planet. Sci. **32** (1), 123–133 (1997a).

24. A. A. Ariskin, G. S. Barmina, S. S. Meshalkin, *et al.*, "INFOREX-3.0: A Database on Experimental Phase Equilibria in Igneous Rocks and Synthetic Systems. II. Data Description and Petrological Applications," Comput. Geosci. **22**, 1073–1082 (1996).

25. A. A. Ariskin, S. S. Meshalkin, R. R. Almeev, *et al.*, "INFOREX Information Retrieval System: Analysis and Processing of Experimental Data on Phase Equilibria in Igneous Rocks," Petrology **5**, 28–36 (1997b).

26. J. V. Auwera and J. Longhi, "Experimental Study of a Jotunite (Hypersthene Monzodiorite): Constraints on the Parent Magma Composition and Crystallization Conditions (P, T, f_{O_2}) of the Bjerkreim–Sokndal Layered Intrusion (Norway)," Contrib. Mineral. Petrol. **118**, 60–78 (1994).

27. A. D. Babansky, I. D. Ryabchikov, and O. A. Bogatikov, *The Evolution of Calc-Alkaline Magmas* (Nauka, Moscow, 1983) [in Russian].

28. D. R. Baker and D. H. Eggler, "Fractionation Paths of Atka (Aleutians) High-Alumina Basalts: Constraints from Phase Relations," J. Volcanol. Geotherm. Res. **18**, 387–404 (1983).

29. L. L. Baker and M. J. Rutherford, "The Effect of Dissolved Water on the Oxidation State of Silicic Melts," Geochim. Cosmochim. Acta **60**, 2179–2187 (1996).

30. G. S. Barmina and A. A. Ariskin, "Estimation of Chemical and Phase Characteristics for the Initial Magma of the Kiglapait Troctolite Intrusion, Labrador, Canada," Geochem. Int. **40**, 972–983 (2002).

31. G. S. Barmina, A. A. Ariskin, and M. Ya. Frenkel, "Petrochemical Types and Crystallization Conditions of the Kronotsky Peninsula Plagiodolerite (Eastern Kamchatka)," Geochem. Int. **26** (9), 24–37 (1989a).

32. G. S. Barmina, A. A. Ariskin, and G. M. Kolesov, "Simulating the REE Patterns of Hypabyssal Rocks in the Kronotsky Series, Eastern Kamchatka," Geochem. Int. **29** (3), 45–54 (1992).

33. G. S. Barmina, A. A. Ariskin, M. Ya. Frenkel, and N. N. Kononkova, "Origin of the Chazhma Sill Ferrodiorites," Geochem. Int. **25** (5), 110–114 (1988).

34. G. S. Barmina, A. A. Ariskin, E. V. Koptev-Dvornikov, and M. Ya. Frenkel, "Estimates of the Primary Compositions of Cumulate Minerals in Differentiated Traps," Geochem. Int. **26** (3), 32–42 (1989b).

35. G. S. Barmina, M. Ya. Frenkel, A. A. Yaroshevsky, and A. A. Ariskin, "Crystallization-related Redistribution of Trace Elements in Stratiform Intrusions," in *Dynamic Models of Physical Geochemistry* (Nauka, Novosibirsk, 1982), pp. 45–55.

36. S. J. Barnes, "The Effect of Trapped Liquid Crystallization on Cumulus Mineral Compositions in Layered Intrusions," Contrib. Mineral. Petrol. **93**, 524–531 (1986).

37. R. W. Bartlett, "Magma Convection, Temperature Distribution, and Differentiation," Am. J. Sci. **267**, 1067–1082 (1969).

38. J. F. Bender, F. N. Hodges, and A. E. Bence, "Petrogenesis of Basalts from the Project Famous Area: Experimental Study from 0 to 15 kbar," Earth Planet. Sci. Lett. **41**, 277–302 (1978).

39. G. W. Bergantz, "Melt Fraction Diagrams: The Link between Chemical and Transport Models," Rev. Mineral. **24**, 239–257 (1990).

40. R. G. Berman, "Internally-Consistent Thermodynamic Data for Minerals in the System Na_2O–K_2O–CaO–MgO–FeO–Fe_2O_3–Al_2O_3–SiO_2–TiO_2–H_2O–CO_2," J. Petrol. **29**, 445–522 (1988).

41. J. Blundy, "Experimental Study of a Kiglapait Marginal Rock and Implications for Trace Element Partitioning in Layered Intrusions," Chem. Geol. **141**, 73–92 (1997).

42. J. D. Blundy and B. J. Wood, "Crystal-Chemical Controls on the Partitioning of Sr and Ba between Plagioclase Feldspar, Silicate Melts, and Hydrothermal Solutions," Geochim. Cosmochim. Acta **55**, 193–209 (1991).

43. J. D. Blundy and B. J. Wood, "Partitioning of Strontium between Plagioclase and Melt: Reply to the Comment by S. A. Morse," Geochim. Cosmochim. Acta **56**, 1739–1741 (1992).

44. S. V. Bolikhovskaya, M. O. Vasil'yeva, and E. V. Koptev-Dvornikov, "Simulating Low-Ca Pyroxene Crystallization in Basite Systems: New Geothermometer Versions," Geochem. Int. **33** (12), 1–19 (1996).

45. A. A. Borisov, "Temperature Dependence of Redox Reactions Involving Variable-Valence Elements in Model and Natural Melts, Geochem. Int. **25** (12), 85–93 (1988).

46. A. A. Borisov and A. I. Shapkin, "A New Empirical Equation Rating Fe^{3+}/Fe^{2+} in Magmas to Their Composition, Oxygen Fugacity, and Temperature," Geochem. Int. **27** (1), 111–116 (1990).

47. M. V. Borisov and Yu. V. Shvarov, *Thermodynamics of Geochemical Processes* (Mosk. Gos. Univ., Moscow, 1992) [in Russian].

48. Y. Bottinga and D. F. Weill, "The Viscosity of Magmatic Silicate Liquids: A Model for Calculation," Am. J. Sci., **272**, 438–475 (1972).

49. N. L. Bowen, *The Evolution of the Igneous Rocks* (Princeton Univ. Press, Princeton, New Jersey, 1928).

50. N. L. Bowen and J. F. Schairer, "The System MgO–FeO–SiO_2," Am. J. Sci. **29**, 151–217 (1935).

51. R. S. Bradley, "Thermodynamic Calculations on Phase Equilibria Involving Fused Salts: I. General Theory and Application to Equilibria Involving Calcium Carbonate at High Pressures," Am. J. Sci. **260**, 374–382 (1962a).

52. R. S. Bradley, "Thermodynamic Calculations on Phase Equilibria Involving Fused Salts: II. Solid Solutions and Applications to Olivines," Am. J. Sci. **260**, 550–554 (1962b).

53. R. S. Bradley, "Thermodynamic Calculations on Phase Equilibria Involving Fused Salts: III. Application to Polymeric Anions," Am. J. Sci. **262**, 541–544 (1964).

54. C. K. Brooks and T. F. D. Nielsen, "Early Stages in the Differentiation of the Skaergaard Magma as Revealed by a Closely Related Suite of Dike Rocks," Lithos **11**, 1–14 (1978).

55. C. K. Brooks and T. F. D. Nielsen, "The Differentiation of the Skaergaard Intrusion: A Discussion of Hunter and Sparks (Contrib. Mineral. Petrol. 95: 451–461)," Contrib. Mineral. Petrol. **104**, 244–247 (1990).

56. C. K. Brooks, L. M. Larsen, and T. F. D. Nielsen, "Importance of Iron-Rich Tholeiitic Magmas at Divergent Plate Margins: A Reappraisal," Geology **19**, 269–272 (1991).

57. J. G. Brophy, "Basalt Convection and Plagioclase Retention: A Model for the Generation of High-Alumina Basalt," J. Geol. **97**, 319–329 (1988).

58. J. G. Brophy, "Can High-Alumina Arc Basalt Be Derived from Low-Alumina Arc Basalt?: Evidence from Kanaga Island, Aleutian Arc, Alaska," Geology **17**, 333–336 (1989).

59. J. G. Brophy and B. D. Marsh, "On the Origin of High-Alumina Arc Basalt and the Mechanics of Melt Extraction," J. Petrol. **27**, 763–789 (1986).

60. C. W. Burnham, "Development of the Burnham Model for Prediction of the H_2O Solubility in Magmas," in *Volatiles in Magmas*, Ed. by M. R. Carroll and J. R. Holloway, Rev. Mineral. **30**, 123–129 (1994).

61. I. H. Campbell, "Some Problems with the Cumulus Theory," Lithos **11**, 311–323 (1978).

62. M. Z. Camur and A. I. Kilinc, "Empirical Solution Model for Alkalic to Tholeiitic Basic Magmas," J. Petrol. **36**, 497–514 (1995).

63. I. S. E. Carmichael, "The Petrology of Thingmuli, a Tertiary Volcano in Eastern Iceland," J. Petrol. **5**, 435–460 (1964).

64. I. S. E. Carmichael, "The Mineralogy of Thingmuli, a Tertiary Volcano in Eastern Iceland," Am. Mineral. **52**, 1815–1841 (1967).

65. I. S. E. Carmichael and M. S. Ghiorso, "Oxidation–Reduction Relations in Basic Magma: A Case for Homogeneous Equilibria," Earth and Planet. Sci. Lett. **78**, 200–210 (1986).

66. I. S. E. Carmichael and M. S. Ghiorso, "The Effect of Oxygen Fugacity on the Redox State of Natural Liquids and Their Crystallizing Phases," in *Modern Methods of Igneous Petrology: Understanding Magmatic Processes*, Ed. by J. Nicholls and J. K. Russell, Rev. Mineral. **24**, 191–212 (1990).

67. C. I. Chalokwu and N. K. Grant, "Reequilibration of Olivine with Trapped Liquid in the Duluth Complex, Minnesota," Geology **15**, 71–74 (1987).

68. C. I. Chalokwu and N. K. Grant, "Petrology of the Partridge River Intrusion, Duluth Complex, Minnesota: 1. Relationships between Mineral Compositions, Density, and Trapped Liquid Abundance," J. Petrol. **31**, 265–293 (1990).

69. C. I. Chalokwu, A. A. Ariskin, and E. V. Koptev-Dvornikov, "Forward Modeling of the Incompatible Element Enrichment at the Base of the Partridge River Intrusion, Duluth Complex, Minnesota: Magma Dynamics in a Lower Mushy Zone," Geochim. Cosmochim. Acta **60**, 4997–5011 (1996).

70. C. I. Chalokwu, N. K. Grant, A. A. Ariskin, and G. S. Barmina, "Simulation of Primary Phase Relations and Mineral Compositions in the Partridge River Intrusion, Duluth Complex, Minnesota: Implications for the Parent Magma Composition," Contrib. Mineral. Petrol. **114**, 539–549 (1993).

71. *Classification and Nomenclature of Igneous Rocks* (Nedra, Moscow, 1981) [in Russian].

72. A. J. Crawford, T. J. Falloon, and S. Eggins, "The Origin of Island Arc High-Alumina Basalts," Contrib. Mineral. Petrol. **97**, 417–430 (1987).

73. G. K. Czamanske, T. E. Zen'ko, V. A. Fedorenko, *et al.*, "Petrographic and Geochemical Characterization of Ore-Bearing Intrusions of the Noril'sk Type, Siberia, with Discussion of Their Origin," Resour. Geol. Spec. Issue, No. 18, 1–45 (1995).

74. L. V. Danyushevsky, F. N. Della-Pasqua, and S. Sokolov, "Re-equilibration of Melt Inclusions Trapped by Magnesian Olivine Phenocrysts from Subduction-Related Magmas: Petrological Implications," Contrib. Mineral. Petrol. **138**, 68–83 (2000).

75. L. V. Danyushevsky, A. V. Sobolev, and L. V. Dmitriev, "Estimation of the Pressure of Crystallization and H_2O Content of MORB and BABB Glasses: Calibration of an Empirical Technique," Contrib. Mineral. Petrol. **57**, 185–204 (1996).

76. L. V. Danyushevsky, M. A. M. Gee, E. G. Nisbet, and M. J. Cheadle, "Olivine-Hosted Melt Inclusions in Belingwe Komatiites: Implications for Cooling History, Parental Magma Composition, and Its H_2O Content," Geochim. Cosmochim. Acta **66** (Suppl. 15A), A725 (2002).

77. L. V. Danyushevsky, M. R. Perfit, S. M. Eggins, and T. J. Falloon, "Crustal Origin for 'Ultra-Depleted' and 'Plagioclase' Signatures in MORB Olivine-Hosted Melt Inclusions: Evidence from the Siqueiros Transform Fault, East Pacific Rise," Contrib. Mineral. Petrol. **144**, 619–637 (2003).

78. D. J. DePaolo, "Trace Element and Isotopic Effects of Combined Wallrock Assimilation and Fractional Crystallization," Earth Planet. Sci. Lett. **53**, 189–202 (1981).

79. D. B. Dingwell, "Redox Viscosimetry of Some Fe-Bearing Silicate Melts," Am. Mineral. **76**, 1560–1562 (1991).

80. J. E. Dixon, E. M. Stolper, and J. R. Holloway, "An Experimental Study of Water and Carbon Dioxide Solubilities in Mid-Ocean Ridge Basaltic Liquids: 1. Calibration and Solubility Models," J. Petrol. **36**, 1607–1631 (1996).

81. L. V. Dmitriev, A. V. Sobolev, N. M. Sushchevskaya, *et al.*, "Evolution of Tholeiitic Magmatism in Oceanic Rift Zones," in *Proceedings of 27th International Geological Congress* (Nauka, Moscow, 1984), Vol. 6: *Oceanic Geology*, Part 1, pp. 147–154.

82. M. B. Dneprovskaya and N. V. Dneprovskii, "Quantitative Approximation of Geochemical Relations in Geological Structures by Random Functions: An Example from the Talnakh Pluton," Geokhimiya, No. 1, 128 (1988).

83. M. B. Dneprovskaya, M. Ya. Frenkel, and A. A. Yaroshevskii, "A Quantitative Stratification Model of the Talnakh Pluton, Noril'sk Area," in *Modeling of Ore-Forming Systems* (Nauka, Novosibirsk, 1987), pp. 96–106 [in Russian].

84. M. J. Drake, "Evolution of Major Mineral Element Abundances during Fractional Crystallization of a Model Lunar Composition," Geochim. Cosmochim. Acta **40**, 401–411 (1976a).

85. M. J. Drake, "Plagioclase–Melt Equilibria," Geochim. Cosmochim. Acta **40**, 457–465 (1976b).

86. M. J. Drake and D. F. Weill, "Partition of Sr, Ba, Ca, Y, Eu^{2+}, Eu^{3+}, and other REE between Plagioclase Feldspar and Magmatic Liquid: An Experimental Study," Geochim. Cosmochim. Acta **39**, 689–712 (1975).

87. D. S. Draper and A. D. Johnston, "Anhydrous *P–T* Phase Relations of an Aleutian High-MgO Basalt: An Investigation of the Role of Olivine–Liquid Reaction in the Generation of Arc High-Alumina Basalts," Contrib. Mineral. Petrol. **112**, 501–519 (1992).

88. D. H. Eggler and E. F. Osborn, "Experimental Studies of the System MgO–FeO–Fe_2O_3–$NaAlSi_3O_8$–$CaAl_2Si_2O_8$–SiO_2: A Model for Subalkaline Magmas," Am. J. Sci. **282**, 1012–1041 (1982).

89. V. A. Ermakov, P. P. Firstov, and V. P. Shirokov, "The Petrogenesis of the Klyuchevskaya Volcanic Family," in *Volcanism and the Earth's Interiors* (Nauka, Moscow, 1971), pp. 152–156 [in Russian].

90. T. J. Falloon, L. V. Danyushevsky, and D. H. Green, "Peridotite Melting at 1 GPa: Reversal Experiments on Partial Melt Compositions Produced by Peridotite: Basalt Sandwich Experiments," J. Petrol. **42**, 2363–2390 (2001).

91. S. A. Fedotov, A. P. Khrenov, and N. A. Zharinov, "The Activity of Klyuchevskoi Volcano in the Years 1932–1986 and the Prospects for the Future," Volkanol. Seismol. **9**, 501–521 (1990).

92. S. A. Fedotov, N. A. Zharinov, and V. I. Gorel'chik, "Klyuchevskoi Volcano: Deformation, Earthquakes, and Activity Model," Volkanol. Seismol., No. 2, 3–42 (1988).

93. G. D. Feoktistov, "Computerized Physicochemical Simulation of the Equilibrium Crystallization of a Silicate Melt" Dokl. Akad. Nauk SSSR **271** (3), 720–724 (1983).

94. G. D. Feoktistov, "Computer Simulation of the Crystallization of a Trap Melt under Hypabyssal Conditions in the Presence of Water," in *Petrology of Fluid–Silicate Systems* (Nauka, Novosibirsk, 1987), pp. 111–120 [in Russian].

95. C. E. Ford, D. J. Russel, J. A. Craven, and M. R. Fisk, "Olivine–Liquid Equilibria: Temperature, Pressure, and Composition Dependence of Crystal/Liquid Cation Partition Coefficients for Mg, Fe^{2+}, Ca, and Mn," J. Petrol. **24**, 256–265 (1983).

96. J. Fournelle and B. D. Marsh, "Shisalkin Volcano: Aleutian High-alumina Basalts and the Question of Plagioclase Accumulation," Geology **19**, 234–237 (1991).

97. W. J. French and E. P. Cameron, "Calculation of the Temperature of Crystallization of Silicates from Basaltic Melts," Mineral. Mag. **44**, 19–26 (1981).

98. M. Ya. Frenkel, "Geochemical Structure of a Stratiform Intrusion," in *Dynamic Models in Physical Geochemistry* (Nauka, Novosibirsk, 1982), pp. 19–30 [in Russian].

99. M. Ya. Frenkel, *Thermal and Chemical Dynamics of Differentiation of Basic Magmas* (Nauka, Moscow, 1995) [in Russian].

100. M. Ya. Frenkel and A. A. Ariskin, "A Computer Algorithm for Equilibration in a Crystallizing Basalt Magma," Geochem. Int. **21** (5), 63–73 (1984).

101. M. Ya. Frenkel and A. A. Ariskin, "Computer Simulation of Basalt–Magma Equilibrium and Fractional Crystallization," Geochem. Int. **22** (3), 73–84 (1985).

102. M. Ya. Frenkel, A. A. Ariskin, G. S. Barmina, *et al.*, "Geochemical Thermometry of Magmatic Rocks: Principles and Example," Geochem. Int. **25** (6), 35–50 (1988a).

103. M. Ya. Frenkel, A. A. Yaroshevsky, A. A. Ariskin, G. S. Barmina, E. V. Koptev-Dvornikov, and B. S. Kireev, *Dynamics of the In Situ Differentiation of Basic Magmas* (Nauka, Moscow, 1988b) [in Russian].

104. M. Ya. Frenkel, A. A. Yaroshevsky, A. A. Ariskin, *et al.*, "Convective–Cumulative Model Simulating the Formation Process of Stratified Intrusions," in *Magma–Crust Interactions and Evolution*, Ed. by B. Bonin (Theophrastus, Athens, 1989), pp. 3–88.

105. R. F. Fudali, "Oxygen Fugacities of Basaltic and Andesitic Magmas," Geochim. Cosmochim. Acta **29**, 1063–1075 (1965).

106. T. Fujii and H. Bougault, "Melting Relations of a Magnesian Abyssal Tholeiite and the Origin of MORBs," Earth Planet. Sci. Lett. **62**, 283–295 (1983).

107. G. A. Gaetani, D. J. Cherniak, and E. B. Watson, "Diffusive Reequilibration of CaO in Olivine-Hosted Melt

Inclusions," Geochim. Cosmochim. Acta **66** (Suppl. 15A), A254 (2002).

108. P. W. Gast, "Trace Element Fractionation and the Origin of Tholeiitic and Alkaline Magma Types," Geochim. Cosmochim. Acta **32**, 1057–1086 (1968).
109. *Geological Dictionary* (Nedra, Moscow, 1978), Vol. 1.
110. M. S. Ghiorso, "Chemical Mass Transfer in Magmatic Processes: I. Thermodynamic Relations and Numeric Algorithms," Contrib. Mineral. Petrol. **90**, 107–120 (1985).
111. M. S. Ghiorso, "Modeling Magmatic Systems: Thermodynamic Relations," in *Thermodynamic Modeling of Geological Materials: Minerals, Fluids and Melts*, Rev. Mineral. **17**, 443–465 (1987).
112. M. S. Ghiorso, "Algorithms for the Estimation of Phase Stability in Heterogeneous Thermodynamic Systems," Geochim. Cosmochim. Acta **58**, 5489–5501 (1994).
113. M. S. Ghiorso, "Thermodynamic Models of Igneous Processes," Annu. Rev. Earth Planet. Sci. **25**, 221–241 (1997).
114. M. S. Ghiorso and I. S. E. Carmichael, "Chemical Mass Transfer in Magmatic Processes: II. Applications in Equilibrium Crystallization, Fractionation, and Assimilation," Contrib. Mineral. Petrol. **90**, 121–141 (1985).
115. M. S. Ghiorso and I. S. E. Carmichael, "Modeling Magmatic Systems: Petrologic Applications," in *Thermodynamic Modeling of Geological Materials: Minerals, Fluids and Melts*, Rev. Mineral. **17**, 467–499 (1987).
116. M. S. Ghiorso and R. O. Sack, "Chemical Mass Transfer in Magmatic Processes: IV. A Revised and Internally Consistent Thermodynamic Model for the Interpolation and Extrapolation of Liquid–Solid Equilibria in Magmatic Systems at Elevated Temperatures and Pressures," Contrib. Mineral. Petrol. **119**, 197–212 (1995).
117. M. S. Ghiorso, I. S. E. Carmichael, M. L. Rivers, and R. O. Sack, "The Gibbs Free Energy of Mixing of Natural Liquids: An Expanded Regular Solution Approximation for the Calculation of Magmatic Intensive Variables," Contrib. Mineral. Petrol. **84**, 107–145 (1983).
118. G. S. Gorshkov, "Magma Generation Depth of Klyuchevskoi Volcano," Dokl. Akad. Nauk SSSR **106** (4), 703–705 (1956).
119. N. K. Grant and C. I. Chalokwu, "Petrology of the Partridge River Intrusion, Duluth Complex, Minnesota: II. Geochemistry and Strontium Isotope Systematics in Drill Core DDH-221," J. Petrol. **33**, 1007–1038 (1992).
120. D. H. Green, W. O. Hibberson, and A. L. Jaques, "Petrogenesis of Mid-Ocean Ridge Basalts," in *The Earth: Its Origin, Structure, and Evolution* (Academic, London, 1979), pp. 265–299.
121. L. P. Greenland, "An Equation for Trace Element Distribution during Magmatic Crystallization," Am. Mineral. **55**, 455–465 (1970).
122. T. L. Grove, "Corrections to Expressions for Calculating Mineral Components in 'Origin of Calc–Alkaline Series Lavas at Medicine Lake Volcano by Fractionation, Assimilation, and Mixing' and 'Experimental Petrology of Normal MORB near the Kane Fracture Zone: 22°–25° N, Mid-Atlantic Ridge'", Contrib. Mineral. Petrol. **114**, 422–424 (1993).
123. T. L. Grove and M. B. Baker, "Phase Equilibrium Controls on the Tholeiitic versus Calc–Alkaline Differentiation Trends," J. Geophys. Res. **89B**, 3253–3274 (1984).
124. T. L. Grove and W. B. Bryan, "Fractionation of Pyroxene-Phyric Morb at Low Pressure: An Experimental Study," Contrib. Mineral. Petrol. **84**, 293–309 (1983).
125. T. L. Grove and T. C. Juster, "Experimental Investigations of Low-Ca Pyroxene Stability and Olivine–Pyroxene–Liquid Equilibria at 1 Atm in Natural Basaltic and Andesitic Liquids," Contrib. Mineral. Petrol. **103**, 287–305 (1989).
126. T. L. Grove, D. C. Gerlach, and T. W. Sando, "Origin of Calc–Alkaline Series Lavas at Medicine Lake Volcano by Fractionation, Assimilation, and Mixing," Contrib. Mineral. Petrol. **80**, 160–182 (1982).
127. T. L. Grove, R. J. Kinzler, and W. B. Bryan, "Natural and Experimental Phase Relations of Lavas from Serocki Volcano," in *Proceedings of Ocean Drilling Program: Scientific Results* (1990), Vol. 106/109, pp. 9–17.
128. T. L. Grove, R. J. Kinzler, and W. B. Bryan, "Fractionation of Mid-Ocean Ridge Basalt (MORB)," in *Mantle Flow and Melt Generation at Mid-Ocean Ridges*, Ed. by J. P. Morgan, D. K. Blackman, and J. M. Sinton (AGU, Washington, 1992), Geophys. Monogr. Ser. **71**, 281–310.
129. D. A. Gust and M. R. Perfit, "Phase Relations on a High-Mg Basalt from the Aleutian Island Arc: Implications for Primary Island Arc Basalts and High-Al Basalts," Contrib. Mineral. Petrol. **97**, 7–18 (1987).
130. D. L. Hamilton, C. W. Burnham, and E. F. Osborn, "The Solubility of Water and Effects of Oxygen Fugacity and Water Content on Crystallization in Mafic Magmas," J. Petrol. **5**, 21–39 (1964).
131. E. Harvie, J. P. Greenberg, and J. H. Weare, "A Chemical Equilibrium Algorithm for Highly Nonideal Multiphase System: Free Energy Minimization," Geochim. Cosmochim. Acta **51**, 13–21 (1987).
132. D. E. Hay and R. F. Wendlandt, "The Origin of Kenya Rift Plateau-Type Flood Phonolites: Evidence from Geochemical Studies for Fusion of Lower Crust Modified by Alkali Basaltic Magmatism," J. Geophys. Res. **100** (B1), 411–422 (1995).
133. C. Herzberg, "Phase Equilibria of Common Rocks in the Crust and Mantle," in *Rock Physics and Phase Relations: A Handbook of Physical Constants*, Ed. by T. J. Ahrens (AGU, Washington, 1995), pp. 166–177.
134. H. H. Hess, "Stillwater Igneous Complex, Montana: A Quantitative Mineralogical Study," Geol. Soc. Am. Mem. **80**, 1–230 (1960).
135. P. C. Hess, "Polymerization Model for Silicate Melts," in *Physics of Magmatic Processes*, Ed. by R. B. Hargraves (1980), pp. 1–48.
136. P. C. Hess "Phase Equilibria Constraints on the Origin of Ocean Floor Basalts," in *Mantle Flow and Melt Generation at Mid-Ocean Ridges*, Ed. by J. P. Morgan, D. K. Blackman, and J. M. Sinton (AGU, Washington, 1992), Geophys. Monogr. Ser. **71**, 67–102 (1992).
137. P. C. Hess, "Thermodynamic Mixing Properties and the Structure of Silicate Melts," in *Structure, Dynamics and*

Properties of Silicate Melts, Ed. by J. F. Stebbins, P. F. McMillian, and D. B. Dingwell, Rev. Mineral. **32**, 145–189 (1995).

138. R. Hill and P. Roeder, "The Crystallization of Spinel from Basaltic Liquid as a Function of Oxygen Fugacity," J. Geology **82**, 709–729 (1974).
139. M. M. Hirschmann, M. S. Ghiorso, L. E. Wasylenki, *et al.*, "Calculation of Peridotite Partial Melting from Thermodynamic Models of Minerals and Melts: I. Review of Methods and Comparison to Experiments," J. Petrol. **39**, 1091–1115 (1998).
140. M. M. Hirschmann, M. S. Ghiorso, and E. M. Stolper, "Calculation of Peridotite Partial Melting from Thermodynamic Models of Minerals and Melts: II. Isobaric Variations in Melts near the Solidus and Owing to Variable Source Composition," J. Petrol. **40**, 297–313 (1999).
141. J. D. Hoover, "Petrology of the Marginal Border Series of the Skaergaard Intrusion," J. Petrol. **30**, 399–439 (1989a).
142. J. D. Hoover, "The Chilled Marginal Gabbro and Other Contact Rocks of the Skaergaard Intrusion," J. Petrol. **30**, 441–476 (1989b).
143. R. H. Hunter, "Texture Development in Cumulate Rocks," in *Layered Intrusions* (Elsevier, 1996), Dev. Petrol. **15**, 77–101 (1996).
144. R. H. Hunter and R. S. J. Sparks, "The Differentiation of the Skaergaard Intrusion," Contrib. Mineral. Petrol. **95**, 451–461 (1987).
145. R. H. Hunter and R. S. J. Sparks, "The Differentiation of the Skaergaard Intrusion: Replies to A. R. McBirney and H. R. Naslund, to S. A. Morse, to C. K. Brooks and T. F. D. Nielsen," Contrib. Mineral. Petrol. **104**, 248–254 (1990).
146. *Initial Reports Deep Sea Drilling Project* (US Government Printing Office, Washington, 1977), Vol. 37.
147. *Initial Reports Deep Sea Drilling Project* (US Government Printing Office, Washington, 1980), Vols. 51, 52.
148. T. N. Irvine, "Magmatic Infiltration Metasomatism, Double-Diffusive Fractional Crystallization, and Adcumulus Growth in the Maskox Intrusion and Other Layered Intrusions," in *Physics of Magmatic Processes*, Ed. by R. B. Hargraves (Princeton Univ. Press, New York, 1980), pp. 325–384.
149. T. N. Irvine and W. R. A. Baragar, "A Guide to the Chemical Classification of the Common Volcanic Rocks," Can. J. Earth Sci. **8**, 523–548 (1971).
150. A. J. Irving, "A Review of Experimental Studies of Crystal/Liquid Trace Element Partitioning," Geochim. Cosmochim. Acta **42A**, 743–770 (1978).
151. E. D. Jackson, "Primary Textures and Mineral Associations in the Ultramafic Zone of the Stillwater Complex, Montana," US Geol. Surv. Prof. Pap. **358**, 1–106 (1961).
152. C. Jaupart and S. Tait, "Dynamics of Differentiation in Magma Reservoirs," J. Geophys. Res. **100**, 17615–17636 (1995).
153. A. D. Johnston, "Anhydrous *P–T* Phase Relations of Near-Primary High-Alumina Basalt from the South Sandwich Islands: *Implications for the Origin of Island Arcs and Tonalite–Trondhjemite*, Contrib. Mineral. Petrol. **92**, 24–38 (1986).
154. J. H. Jones, "Experimental Trace Element Partitioning," in *Rock Physics and Phase Relations: A Handbook of Physical Constants*, Ed. by T. J. Ahrens (AGU, 1995), pp. 73–104.
155. N. W. Jones, "Petrology of Some Logan Diabase Sills, Cook County, Minnesota," Minn. Geol. Surv. Rep. Invest. **29**, 40 (1984).
156. T. C. Juster and T. L. Grove, "Experimental Constraints on the Generation the Fe–Ti Basalts, Andesites, and Rhyodacites at the Galapagos Spreading Center, 85° W and 95° W," Geophys. Res. **94B**, 9251–9274 (1989).
157. A. A. Kadik, E. B. Lebedev, and N. I. Khitarov, *Water in Magmatic Melts* (Nauka, Moscow, 1971) [in Russian].
158. A. A. Kadik, O. A. Lukanin, and I. V. Lapin, *Physicochemical Conditions of the Evolution of Basalt Magmas in Shallow Chambers* (Nauka, Moscow, 1990) [in Russian].
159. A. A. Kadik, A. P. Maksimov, and B. V. Ivanov, *Physicochemical Conditions of Crystallization and Genesis of Andesites* (Nauka, Moscow, 1986) [in Russian].
160. A. A. Kadik, M. Rosenhauer, and O. A. Lukanin, "An Experimental Study of the Pressure Effect on the Crystallization of Magnesian and Aluminous Basaltoids in Kamchatka," Geokhimiya, No. 12, 1748–1762 (1989).
161. I. K. Karpov, *Computerized Physicochemical Modeling in Geochemistry* (Nauka, Novosibirsk, 1981) [in Russian].
162. I. K. Karpov, A. I. Kiselev, and F. A. Letnikov, *Computerized Modeling of Mineral Formation in Nature* (Nedra, Moscow, 1976) [in Russian].
163. S. M. Kay and R.W. Kay, "Aleutian Tholeiitic and Calc–Alkaline Magma Series: I. The Mafic Phenocrysts," Contrib. Mineral. Petrol. **90**, 276–296 (1985).
164. P. B. Kelemen, "Reaction between Ultramafic Rock and Fractionating Basalt Magma: I. Phase Relations, the Origin of Calc–Alkaline Magma Series, and the Formation of Discordant Dunite," J. Petrol. **31**, 51–98 (1990).
165. P. B. Kelemen and M. S. Ghiorso, "Assimilation of Peridotite in Zoned Calc–Alkaline Plutonic Complexes: Evidence from the Big Jim Complex, Washington Cascades," Contrib. Mineral. Petrol. **94**, 12–28 (1986).
166. W. Q. Kennedy, "Trends of Differentiation in Basaltic Magmas," Am. J. Sci. **25**, 239–256 (1933).
167. G. C. Kennedy, "Equilibrium between Volatiles and Iron Oxides in Igneous Rocks," Am. J. Sci. **246**, 529–549 (1948).
168. A. K. Kennedy, T. L. Grove, and R. W. Johnson, "Experimental and Major Element Constraints on the Evolution of Lavas from Lihir Island, Papua New Guinea," Contrib. Mineral. Petrol. **104**, 722–734 (1990).
169. A. B. Kersting and R. J. Arculus, "Klyuchevskoy Volcano, Kamchatka, Russia: The Role of High-Flux Recharge, Tapped, and Fractionated Magma Chamber(s) in the Genesis of High-Al_2O_3 from High-MgO Basalt," J. Petrol. **35**, 1–41 (1994).
170. A. B. Kersting, R. J. Arculus, J. W. Delano, and D. Loureiro, "Electrochemical Measurements Bearing

on the Oxidation State of the Skaergaard Layered Intrusion," Contrib. Mineral. Petrol. **102**, 376–388 (1989).

171. A. P. Khrenov, V. S. Antipin, L. A. Chuvashova, and E. V. Smirnova, "Petrochemistry and Geochemistry of Klyuchevskoi Basalts," Volkanol. Seismol. **11**, 285–304 (1990).
172. S. A. Khubunaya, *High-Alumina Plagiotholeiitic Formation of Island Arcs* (Nauka, Moscow, 1987) [in Russian].
173. S. A. Khubunaya, S. O. Bogoyavlenskii, T. Yu. Novgorodtseva, and A. I. Okrugina, "Mineralogy of Magnesian Basalts and Intra-Chamber Magma Fractionation of Klyuchevskoi Volcano," Volkanol. Seismol., No. 3, 46–68 (1993).
174. A. Kilinc, I. S. E. Carmichael, M. Rivers, and R. O. Sack, "The Ferric–Ferrous Ratio of Natural Silicate Liquids Equilibrated in Air," Contrib. Mineral. Petrol. **83**, 136–140 (1983).
175. R. J. Kinzler and T. L. Grove, "Primary Magmas of Mid-Ocean Ridge Basalts: 1. Experiments and Methods," J. Geophys. Res. **97**, 6885–6906 (1992a).
176. R. J. Kinzler and T. L. Grove, "Primary Magmas of Mid-Ocean Ridge Basalts: 2. Applications," J. Geophys. Res. **97**, 6907–6926 (1992b).
177. R. J. Kinzler and T. L. Grove, "Corrections and Further Discussion of the Primary Magmas of Mid-ocean Ridge Basalts, 1and 2," J. Geophys. Res. **98**, 22339–22347 (1993).
178. E. V. Kislov, *The Yoko–Dovyrenskii Layered Pluton* (Buryat. Nauchn. Tsentr Sib. Otd. Ross. Akad. Nauk, Ulan-Ude, 1998) [in Russian].
179. E. G. Konnikov, *Differentiated Ultrabasic–Basic Complexes in the Precambrian of Transbaikalia* (Nauka, Novosibirsk, 1986) [in Russian].
180. E. V. Koptev-Dvornikov, G. S. Barmina, M. Ya. Frenkel, and A. A. Yaroshevsky, "The Geology of a Differentiated Trap Intrusion at the Vel'minskii Rapids, Podkamennaya Tunguska River," Geol. Geofiz., No. 4, 50–56 (1976).
181. E. V. Koptev-Dvornikov, A. A. Yaroshevsky, and M. Ya. Frenkel, "Fractional Crystallization of an Intrusive Magma: Reality of the Sedimentation Model," Geochem. Int. **16** (2), 85–101 (1979).
182. O. V. Koroleva and B. V. Oleinikov, "Geochemistry and Genesis of Monzonitoids of the Dzhaltul'skii Trap Intrusion, Northwest Siberian Platform," Geol. Geofiz. **39**, 178–189 (1998).
183. D. S. Korzhinsky, "Acid–Basic Interaction of Components in Silicate Melts and Cotectic Lines," Dokl. Akad. Nauk SSSR **128** (2), 383–386 (1959).
184. S. M. Kravchenko, *Fractionation of Trace Elements during Differentiation of Basitic Magmas* (Nauka, Moscow, 1977) [in Russian].
185. V. C. Kress and I. S. E. Carmichael, "Stoichiometry of the Iron Oxidation Reaction in Silicate Melt," Am. Mineral. **73**, 1267–1274 (1988).
186. V. C. Kress and I. S. E. Carmichael, "The Lime–Iron–Silicate Melt System: Redox and Volume Systematics," Geochim. Cosmochim. Acta **53**, 2883–2892 (1989).
187. V. C. Kress and I. S. E. Carmichael, "The Compressibility of Silicate Liquids Containing Fe_2O_3 and the Effect of Composition, Temperature, Oxygen Fugacity, and Pressure on Their Redox States," Contrib. Mineral. Petrol. **108**, 82–92 (1991).
188. N. A. Krivolutskaya, A. A. Ariskin, S. F. Sluzhenikin, and D. M. Turovtsev, "Geochemical Thermometry of Rocks of the Talnakh Intrusion: Assessment of the Melt Composition and the Crystallinity of the Parental Magma," Petrology **9**, 389–414 (2001).
189. H. Kuno, "Petrology of Hakone Volcano and the Adjacent Areas," Geol. Soc. Am. Bull. **61**, 957–1020 (1950).
190. H. Kuno, "High-alumina Basalt," J. Petrol. **1**, 121–145 (1960).
191. Yu. A. Kuznetsov, *Problems in the Formation and Analysis of Magmatites. Selected Works* (Nauka, Novosibirsk, 1990), Vol. 3 [in Russian].
192. C. H. Langmuir, "Geochemical Consequence of in Situ Crystallization," Nature **340**, 199–205 (1989).
193. C. H. Langmuir and G. N. Hanson, "Calculating Mineral–Melt Equilibria with Stoichiometry, Mass Balance, and Single-Component Distribution Coefficients," in *Thermodynamics of Minerals and Melts*, Ed. by R. C. Newton, A. Navrotsky, and B. J. Wood, Adv. Phys. Geochem. **1**, 247–271 (1981).
194. C. H. Langmuir, E. M. Klein, and T. Plank, "Petrological Systematics of Mid-Ocean Ridge Basalts: Constraints on Melt Generation beneath Mid-ocean Ridges," in *Mantle Flow and Melt Generation at Mid-Ocean Ridges*, Ed. by J. P. Morgan, D. K. Blackman, and J. M. Sinton (AGU, Washington, 1992), Vol. 71 of Geophys. Monogr. Ser., pp. 183–280 (1992).
195. I. V. Lapin, O. A. Lukanin, and A. A. Kadik, "The Effect of Oxidation Regime on the Near-Surface Crystallization and Differentiation of Iceland Basalts," Geokhimiya, No. 6, 747–760 (1985).
196. A. P. Lebedev, "Trap Association in the Lower Reaches of the Podkamennaya Tunguska River," in *Petrography of Eastern Siberia* (Akad. Nauk SSSR, Moscow, 1962), Vol. 1, pp. 71–117 [in Russian].
197. I. Lee and E. M. Ripley, "Genesis of Cu–Ni Sulfide Mineralization of the South Kawishiwi Intrusion, Spruce Road Area, Duluth Complex, Minnesota," Can. Mineral. **33**, 723–743 (1995).
198. A. P. LeRoex, A. J. Erlank, and H. D. Needham, "Geochemical and Mineralogical Evidence for the Occurrence of at Least Three Distinct Magma Types in the FAMOUS Region," Contrib. Mineral. Petrol. **77**, 24–37 (1981).
199. P. J. LeRoux, A. P. LeRoex, and J.-G. Schilling, "Crystallization Processes beneath the Southern Mid-Atlantic Ridge (40°–55° S), Evidence for High-Pressure Initiation of Crystallization," Contrib. Mineral. Petrol. **142**, 582–602 (2002a).
200. P. J. LeRoux, A. P. LeRoex, and J.-G. Schilling, "MORB Melting Processes beneath the Southern Mid-Atlantic Ridge (40°–55° S): A Role for Mantle Plume-Derived Pyroxenite," Contrib. Mineral. Petrol. **144**, 206–229 (2002b).
201. D. H. Lindsley, G. M. Brown, and I. D. Muir, "Conditions of the Ferrowollastonite–Ferrohedenbergite Inversion in the Skaergaard Intrusion, East Greenland," Mineral. Soc. Am. Spec. Publ. **2**, 193–201 (1969).

202. J. Longhi, "Magma Oceanography: 2. Chemical Evolution and Crustal Formation," Lunar Planet. Sci. **8**, 601–621 (1977).

203. J. Longhi, "Comparative Liquidus Equilibria of Hypersthene-normative Basalts at Low Pressure," Am. Mineral. **76**, 785–800 (1991).

204. J. Longhi, D. Walker, and J. F. Hays, "The Distribution of Fe and Mg between Olivine and Lunar Basaltic Liquids," Geochim. Cosmochim. Acta **42**, 1545–1558 (1978).

205. T. P. Loomis, "An Empirical Model for Plagioclase Equilibrium in Hydrous Melts," Geochim. Cosmochim. Acta **43**, 1753–1759 (1979).

206. O. A. Lukanin, "Interpretation of the Bimodal Rock Distribution in Volcanic Associations," Geokhimiya, No. 3, 348–359 (1985).

207. S. Maaloe, "Quantitative Aspects of Fractional Crystallization of Major Elements," J. Geol. **84**, 81–96 (1976).

208. G. A. Mahood and D. R. Baker, "Experimental Constraints on Depths of Fractionation of Mildly Alkalic Basalts and Associated Felsic Rocks: Pantelleria, Strait of Sicily," Contrib. Mineral. Petrol. **93**, 251–264 (1986).

209. B. D. Marsh, "Magma Chambers," Annu. Rev. Earth Planet. Sci. **17**, 439–474 (1989a).

210. B. D. Marsh, "On Convective Style and Vigor in Sheet-Like Magma Chambers," J. Petrol. **30**, 479–530 (1989b).

211. A. R. McBirney, "The Skaergaard Layered Series: I. Structure and Average Compositions," J. Petrol. **30**, 363–397 (1989).

212. A. R. McBirney, "The Skaergaard Intrusion," in *Layered Intrusions* (Elsevier, 1996), Dev. Petrol. **15**, 147–180 (1996).

213. A. R. McBirney, "The Skaergaard Layered Series: V. Included Trace Elements," J. Petrol. **39**, 255–276 (1998).

214. A. R. McBirney and Y. Nakamura, "Immiscibility in Late Stage Magmas of the Skaergaard Intrusion," Carnegie Inst. Yearbook **72**, 348–352 (1973).

215. A. R. McBirney and H. R. Naslund, "The Differentiation of the Skaergaard Intrusion: A Discussion of Hunter and Sparks (Contrib. Mineral. Petrol. 95: 451–461)," Contrib. Mineral. Petrol. **104**, 235–240 (1990).

216. A. R. McBirney and R. M. Noyes, "Crystallization and Layering of the Skaergaard Intrusion," J. Petrol. **20**, 487–554 (1979).

217. A. R. McBirney, H. R. Baker, and R. H. Nilson, "Liquid Fractionation: I. Basic Principles and Experimental Simulation," J. Volcanol. Geotherm. Res. **26**, 1–24 (1985).

218. W. L. McIntire, "Trace Element Partition Coefficient: A Review of Theory and Applications to Geology," Geochim. Cosmochim. Acta **27**, 1209–1264 (1963).

219. I. V. Melekestsev, A. P. Khrenov, and N. N. Kozhemyaka, "Tectonic Position and General Description of Volcanoes of Northern Group and Sredinnyi Range," in *Active Volcanoes of Kamchatka* (Nauka, Moscow, 1991), Vol. 1, pp. 79–81 [in Russian].

220. S. S. Meshalkin and A. A. Ariskin, "INFOREX-3.0: A Database on Experimental Phase Equilibria in Igneous Rocks and Synthetic Systems: I. Datafile and Management System Structure," Comput. Geosci. **22**, 1061–1071 (1996).

221. S. S. Meshalkin, A. A. Ariskin, G. S. Barmina, *et al.*, "Development of a Database on Experimental Crystal–Melt Equilibria for Igneous Rocks: INFOREX System, Version 3.0," Geochem. Int. **34** (2), 85–90 (1996).

222. J. D. Miller, Jr. and E. M. Ripley, "Layered Intrusions of the Duluth Complex, Minnesota, USA," in *Layered Intrusions* (Elsevier, 1996), Dev. Petrol. **15**, 257–301 (1996).

223. J. D. Miller and P. W. Weiblen, "Anorthositic Rocks of the Duluth Complex: Examples of Rocks Formed from Plagioclase Crystal Mushes," J. Petrol. **31**, 295–340 (1990).

224. E. G. Mirlin and N. M. Sushchevskaya, "Spatiotemporal Heterogeneity of Ocean Formation and Its Structural and Petrologic Consequences: Evidence from the Atlantic Ocean," in *Oceanic Magmatism and Tectonics* (Nauka, Moscow, 1990), pp. 108–122 [in Russian].

225. N. L. Mironov, M. V. Portnyagin, P. Y. Pletchov, and S. A. Khubunaya, "Final Stages of Magma Evolution in Klyuchevskoy Volcano, Kamchatka: Evidence from Melt Inclusions in Minerals of High-alumina Basalts," Petrology **9**, 46–62 (2001).

226. Yu. V. Mironov, D. A. Ionov, G. S. Krivoplyasov, *et al.*, "Structure of the Ioko–Davyren Layered Dunite–Troctolite–Gabbro–Norite Pluton, Northern Baikal Area," Dokl. Akad. Nauk SSSR **250** (5), 1228–1232 (1980).

227. A. Miyashiro, "Volcanic Rock Series in Island Arcs and Active Continental Margins," Am. J. Sci. **274**, 321–355 (1974).

228. A. Mogessie, E. F. Stumpfl, and P. W. Weiblen, "The Role of Fluids in the Formation of Platinum-Group Minerals, Duluth Complex, Minnesota: Mineralogic, Textural, and Chemical Evidence," Econ. Geol. **86**, 1506–1518 (1991).

229. G. Moore, K. Righter, and I. S. E. Carmichael, "The Effect of Dissolved Water on the Oxidation State of Iron in Natural Silicate Liquids," Contrib. Mineral. Petrol. **120**, 170–179 (1995).

230. S. A. Morse, "Kiglapait Geochemistry: I. Systematics, Sampling, and Density," J. Petrol. **20**, 555–590 (1979a).

231. S. A. Morse, "Kiglapait Geochemistry: II. Petrography," J. Petrol. **20**, 591–624 (1979b).

232. S. A. Morse, "Kiglapait Mineralogy: II. Fe–Ti Oxide Minerals and the Activities of Oxygen and Silica," J. Petrol. **21**, 685–719 (1980).

233. S. A. Morse, "Kiglapait Geochemistry: IV. The Major Elements," Geochim. Cosmochim. Acta **45**, 461–479 (1981).

234. S. A. Morse, "The Differentiation of the Skaergaard Intrusion: A Discussion of Hunter and Sparks (Contrib. Mineral. Petrol. 95: 451–461)," Contrib. Mineral. Petrol. **104**, 240–244 (1990).

235. S. A. Morse, "Kiglapait Mineralogy: III. Olivine Compositions and Rayleigh Fractionation Models," J. Petrol. **37**, 591–624 (1996).

236. S. A. Morse, D. C. Banks, and J. B. Brady, "Kiglapait Magma Evolution: Mantle to Labrador to Lab," Geophys. Res. Abstracts **5**, 07325 (2003).

237. J. D. Myers and A. D. Johnston, "Phase Equilibria Constraints on Models of Subduction Zone Magmatism," in *Subduction Top to Bottom*, Ed. by G. E. Bebout, D. W. Scholl, S. H. Kirby, and J. P. Platt (AGU, Washington, 1996), Geophys. Monogr. Ser. **96**, 229–249 (1996).

238. B. O. Mysen, "Experimental, in Situ, High-temperature Studies of Properties and Structure of Silicate Melts Relevant to Magmatic Processes," Eur. J. Mineral. **7**, 745–766 (1995).

239. B. O. Mysen, "Relations between Structure, Redox Equilibria of Iron, and Properties of Magmatic Liquids," in *Physical Chemistry of Magmas*, Ed. by L. L. Perchuk and I. Kushiro, Adv. Phys. Geochem. **9**, 41–98 (1991).

240. B. O. Mysen, D. Virgo, E.-R. Neumann, and F. A. Seifert, "Redox Equilibria and the Structural States of Ferric and Ferrous Iron in Melts in the System CaO–MgO–Al_2O_3–SiO_2–FeO: Relationships between Redox Equilibria, Melt Structure and Liquidus Phase Equilibria," Am. Mineral. **70**, 317–331 (1985).

241. M. Nakamura and M. Shimakita, "Dissolution Origin and Syn-Entrapment Compositional Change of Melt Inclusion in Plagioclase," Earth Planet. Sci. Lett. **161**, 119–133 (1998).

242. H. D. Nathan and C. K. Vankirk, "A Model of Magmatic Crystallization," J. Petrol. **19** (1), 66–94 (1978).

243. R. L. Nielsen, "Simulation of Igneous Differentiation Processes," in *Modern Methods of Igneous Petrology: Understanding Magmatic Processes*, Ed. by J. Nicholls and J. K. Russell, Rev. Mineral. **24,** 63–105 (1990).

244. R. L. Nielsen and M. J. Drake, "Pyroxene–Melt Equilibria," Geochim. Cosmochim. Acta **43**, 1259–1272 (1979).

245. R. L. Nielsen and M. A. Dungan, "Low-Pressure Mineral–Melt Equilibria in Natural Anhydrous Mafic Systems," Contrib. Mineral. Petrol. **84**, 310–326 (1983).

246. R. L. Nielsen, L. M. Forsythe, W. E. Gallahan, and M. R. Fisk, "Major- and Trace-Element Magnetite–Melt Equilibria," Chem. Geol. **117**, 167–191 (1994).

247. L. A. Nikolaev, *Physical Chemistry* (Vysshaya Shkola, Moscow, 1979) [in Russian].

248. G. S. Nikolaev, A. A. Borisov, and A. A. Ariskin, "Calculation of the Ferric–Ferrous Ratio in Magmatic Melts: Testing and Additional Calibration of Empirical Equations for Various Magmatic Series," Geochem. Int. **34**, 641–649 (1996).

249. K. M. Nolan and S. A. Morse, "Marginal Rocks Resembling the Estimated Bulk Composition of the Kiglapait Intrusion," Geochim. Cosmochim. Acta **50**, 2381–2386 (1986).

250. C. J. Nye and M. R. Reid, "Geochemistry of Primary and Least Fractionated Lavas from Okmok Volcano, Central Aleutians: Implications for Arc Magma Genesis," J. Geophys. Res. **91**, 10 271–10 287 (1986).

251. M. J. O'Hara, "Primary Magmas and the Origin of Basalts," Scot. J. Geol. **1**, 19–40 (1965).

252. M. J. O'Hara and R. E. Mathews, "Geochemical Evolution in an Advancing, Periodically Replenished, Periodically Tapped, Continuously Fractionating Magma Chamber," J. Geol. Soc. London **138**, 237–277 (1981).

253. K. E. Olson and S. A. Morse, "Regional Al–Fe Mafic Magmas Associated with Anothosite-Bearing Terranes," Nature **344**, 760–762 (1990).

254. E. F. Osborn, "Role of Oxygen Pressure in the Crystallization and Differentiation of Basaltic Magma," Am. J. Sci. **257**, 609–647 (1959).

255. A. Yu. Ozerov, A. A. Ariskin, and G. S. Barmina, "The Problem of Genetic Relations between High-Aluminous and High-Magnesian Basalts of Klyuchevskoi Volcano, Kamchatka," Dokl. Acad. Nauk, Earth Sci. Sect. **350** (7), 1127–1130 (1996).

256. A. Yu. Ozerov, A. A. Ariskin, P. H. Kyle, *et al.*, "Petrological–Geochemical Model for Genetic Relationships between Basaltic and Andesitic Magmatism of Klyuchevskoi and Bezymyannyi Volcanoes," Petrology **5**, 550–569 (1997).

257. A. Yu. Ozerov, "The Evolution of High-Alumina Basalts of the Klyuchevskoy Volcano, Kamchatka, Russia, Based on Microprobe Analyses of Mineral Inclusions," J. Volcanol. Geotherm. Res. **95**, 65–79 (2000).

258. J. D. Pasteris, "Relationships between Temperature and Oxygen Fugacity among Fe–Ti Oxides in Two Regions of the Duluth Complex," Can. Mineral. **23**, 111–127 (1985).

259. L. L. Perchuk and V. I. Vaganov, "Thermal Regime of Crystallization and Differentiation of Basic and Ultrabasic Magmas," in *Contributions to Physicochemical Petrology* (Nauka, Moscow, 1978), Issue VII, pp. 142–173 [in Russian].

260. M. R. Perfit, D. A. Gust, A. E. Bence, *et al.*, "Chemical Characteristics of Island-arc Basalts: Implications for Mantle Sources," Chem. Geol. **30**, 227–256 (1980).

261. E. Petitpierre and P. Boivin, "CRYSTALLIZATION: A Computer Program for Modeling the Crystallization of a Magmatic Liquid," Comput. Geosci. **9**, 455–461 (1983).

262. T. Plank and C. H. Langmuir, "An Evaluation of the Global Variations in the Major Element Chemistry of Arc Basalts," Earth Planet. Sci. Lett. **90**, 349–370 (1988).

263. A. I. Polyakov and N. S. Muravieva, "Differentiated Rhyolite–Basalt Associations in Iceland and the Origin of Silicic Volcanic Rocks: A Model of Fractional Crystallization," Geokhimiya, No. 9, 1362–1379 (1981).

264. R. Powell, T. Holland, and B. Worley, "Mineral Equilibria Calculations with THERMOCALC," in *Abstracts of Mineral Equilibria and Databases Meeting, Espoo, Finland, 1997*, pp. 61–62.

265. D. C. Presnall, "The Join Forsterite–Diopside–Iron Oxide and Its Bearing on the Crystallization of Basaltic and Ultramafic Magmas, Am. J. Sci. **264**, 753–809 (1966).

266. D. C. Presnall, J. R. Dixon, C. H. O'Donnell, and S. A. Dixon, "Generation of Mid-Ocean Ridge Tholeiites," J. Petrol. **20**, 3–35 (1979).

267. K. Putirka, "Clinopyroxene + Liquid Equilibria to 100 kbar and 2450 K," Contrib. Mineral. Petrol. **135**, 151–163 (1999).

268. M. H. Reed, "Calculation of Multicomponent Chemical Equilibria and Reaction Processes in Systems Involving Minerals, Gases, and an Aqueous Phase," Geochim. Cosmochim. Acta **46**, 513–528 (1982).

269. J. Renner, B. Evans, and G. Hirth, "On the Rheologically Critical Melt Fraction," Earth Planet. Sci. Lett. **181**, 585–594 (2000).

270. J. R. Reynolds, Segment–Scale Systematics of Mid-Ocean Ridge Magmatism and Geochemistry, PhD Thesis (Columbia Univ., 1995).

271. K. Righter and I. S. E. Carmichael, "Phase Equilibria of Phlogopite Lamprophyres from Western Mexico: Biotite–Liquid Equilibria and *P–T* Estimates for Biotite-Bearing Igneous Rocks," Contrib. Mineral. Petrol. **123**, 1–21 (1996).

272. P. L. Roeder and E. Emslie, "Olivine–Liquid Equilibrium," Contrib. Mineral. Petrol. **29**, 275–289 (1970).

273. P. L. Roeder, "Activity of Iron and Olivine Solubility in Basaltic Liquids," Earth Planet. Sci. Lett. **23**, 397–410 (1974).

274. I. D. Ryabchikov, *Thermodynamic Analysis of the Behavior of Minor Elements during the Crystallization of Silicate Melts* (Nauka, Moscow, 1965) [in Russian].

275. I. D. Ryabchikov, "Magma Generation in the Mantle," in *Igneous Rocks: The Evolution of Magmatism during the Earth's History,* Ed. by V. I. Kovalenko (Nauka, Moscow, 1987), pp. 349–371 [in Russian].

276. I. D. Ryabchikov, "Simulating Peridotite Partial Melting," Geochem. Int. **31** (7), 14–26 (1994).

277. V. V. Ryabov, A. Ya. Shevko, and M. P. Gora, *Magmatites of the Noril'sk Region*, Vol. 1 *Petrology of Traps* (Nonparel', Novosibirsk, 2000) [in Russian].

278. R. O. Sack, "Spinels as Petrogenetic Indicators: Activity–Composition Relations at Low Pressures," Contrib. Mineral. Petrol. **7**, 169–186 (1982).

279. R. O. Sack and M. S. Ghiorso, "An Internally Consistent Model for the Thermodynamic Properties of Fe–Mg-Titanomagnetite–Aluminate Spinels," Contrib. Mineral. Petrol. **106**, 474–505 (1991).

280. R. O. Sack, I. S. E. Carmichael, M. Rivers, and M. S. Ghiorso, "Ferric–Ferrous Equilibria in Natural Silicate Liquids at 1 Bar," Contrib. Mineral. Petrol. **75**, 369–376 (1980).

281. R. O. Sack, D. Walker, and I. S. E. Carmichael, "Experimental Petrology of Alkalic Lavas: Constraints on Cotectics of Multiple Saturation in Natural Basic Liquids," Contrib. Mineral. Petrol. **96**, 1–23 (1987).

282. V. N. Sharapov and A. N. Cherepanov, *Dynamics of Magmatic Differentiation* (Nauka, Novosibirsk, 1986) [in Russian].

283. V. N. Sharapov, A. N. Cherepanov, V. N. Popov, and A. G. Lobov, "Dynamics of Basic Melt Cooling during the Filling of a Funnel-shaped Intrusive Chamber," Petrology **5** (1), 8–19 (1997).

284. Yu. M. Sheinmann, *Essaya on the Geology of the Earth's Deep Interiors* (Nedra, Moscow, 1968) [in Russian].

285. P. Shi, "Low-Pressure Phase Relationships in the System Na_2O–CaO–FeO–MgO–Al_2O_3–SiO_2 at 1100°C, with Implications for the Differentiation of Basaltic Magmas," J. Petrol. **34**, 743–762 (1993).

286. K. Shibata, "The Oxygen Partial Pressure of the Magma from Mihara Volcano, O-Sima, Japan," Bull. Chem. Soc. Jpn. **40**, 830–834 (1967).

287. Yu. V. Shvarov, "Calculation of Equilibrium Composition for a Multicomponent System," Dokl. Akad. Nauk SSSR **229** (5), 1224–1226 (1976).

288. E. C. Simmons, D. H. Lindsley, and J. J. Papike, "Phase Relations and Crystallization Sequence in a Contact-Metamorphosed Rock from the Gunflint Formation, Minnesota," J. Petrol. **15**, 539–564 (1974).

289. J. Sinton, C. Langmuir, J. Bender, and R. Detric, "What is a Magma Chamber?" Ridge Events **3** (1), 46–48 (1992).

290. T. W. Sisson and T. L. Grove, "Temperatures and H_2O Contents of Low-MgO High-Alumina Basalts," Contrib. Mineral. Petrol. **113**, 167–184 (1993).

291. V. P. Slater, C. K. Thompson, J. Nettles, *et al.*, "An Evaluation of the Igneous Crystallization Programs—MELTS, MAGPOX, and COMAGMAT: II. Importance of Magmatic f_{O_2}," in *Abstracts of LPS XXXIV, 2003*, pdf-1896.

292. D. Snyder, I. S. E. Carmichael, and R. A. Wiebe, "Experimental Study of Liquid Evolution in a Fe-Rich, Layered Mafic Intrusion: Constraints of the Fe–Ti Oxide Precipitation on the T–f_{O_2} and *T–P* Paths of Tholeiitic Magmas," Contrib. Mineral. Petrol. **113**, 73–86 (1993).

293. A. V. Sobolev, "Melt Inclusions in Minerals as a Source of Principal Petrological Information," Petrology **4**, 209–220 (1996).

294. A.V. Sobolev and M. Chaussidon, "H_2O Concentrations in Primary Melts from Supra-Subduction Zones and Mid-ocean Ridges: Implications for H_2O Storage and Recycling in the Mantle," Earth Planet. Sci. Lett. **137**, 45–55 (1996).

295. A. V. Sobolev, A. A. Migdisov, and M. V. Portnyagin, "Incompatible Element Partitioning between Clinopyroxene and Basalt Liquid Revealed by the Study of Melt Inclusions in Minerals from Troodos Lavas, Cyprus," Petrology **4**, 307–317 (1996).

296. A. V. Sobolev, A. W. Hofmann, N. Shimizu, *et al.*, "Primary Melts Reveal Small-Scale Heterogeneity in Convecting Mantle," Geochim. Cosmochim. Acta **66** (Suppl. 15A), A725 (2002).

297. A. Soesoo, "Fractional Crystallization of Mantle-Derived Melts as a Mechanism for Some I-Type Granite Petrogenesis: An Example from Lachlan Fold Belt, Australia," J. Geol. Soc. (London) **157**, 135–149 (2000).

298. R. S. J. Sparks, "Petrology and Geochemistry of the Loch Ba Ring Dyke, Mull (N.W.Scotland): An Example of the Extreme Differentiation of Tholeiitic Magmas," Contrib. Mineral. Petrol. **100**, 446–461 (1988).

299. E. Stolper, "A Phase Diagram for Mid-Ocean Ridge Basalts: Preliminary Results and Implications for Petrogenesis," Contrib. Mineral. Petrol. **74**, 13–27 (1980).

300. J. C. Stormer, Jr., "The Effects of Recalculation on Estimates of Temperature and Oxygen Fugacity from Analyses of Multicomponent Iron–Titanium Oxides," Am. Mineral. **68**, 586–594 (1983).

301. C.-O. Sun, R. J. Williams, and S.-S. Sun, "Distribution Coefficients of Eu and Sr for Plagioclase–Liquid and Clinopyroxene–Liquid Equilibria in Oceanic Ridge Basalt: An Experimental Study," Geochim. Cosmochim. Acta **38**, 1415–1433 (1974).

302. N. M. Sushchevskaya and T. I. Tsekhonya, "Distinctive Features of the Formation of Basalt Magmatism in the Mid-Atlantic Ridge Equatorial zone," Geochem. Int. **31** (12), 87–103 (1994).

303. N. M. Sushchevskaya, T. I. Tsekhonya, and A. A. Peive, "Distinctive Features of Magmatic Processes in the Mid-Atlantic, Southwest Indian, and North Weddell Ridges," Geochem. Int. **36** (3), 209–221 (1998).

304. N. M. Sushchevskaya, A. A. Peive, T. I. Tsekhonya, *et al.*, "Magmatic Petrology and Geochemistry of the Active Parts of the Romanche and St. Paul Fracture Zones and the Related Parts of the Mid-Atlantic Ridge," Geochem. Int. **33** (2), 39–61 (1996a).

305. N. M. Sushchevskaya, T. I. Tsekhonya, E. P. Dubinin, *et al.*, "Formation of the Oceanic Crust in Mid-Oceanic Ridges of the Indian Ocean," Geochem. Int. **34** (10), 869–880 (1996b).

306. N. M. Sushchevskaya, B.V. Belyatsky, T. I. Tsekhonya, *et al.*, "Petrology and Geochemistry of Basalts from the Eastern Indian Ocean: Implications for Its Early Evolution," Petrology **6**, 480–505 (1998).

307. S. Tait and C. Jaupart, "Compositional Convection in a Reactive Crystalline Mush and Melt Differentiation," J. Geophys. Res. **97**, 6735–6756 (1992).

308. S. Tait and C. Jaupart, "The Production of Chemically Stratified and Adcumulate Plutonic Igneous Rocks," Mineral. Mag. **60**, 99–114 (1996).

309. E. Takahashi and I. Kushiro, "Melting of a Dry Peridotite at High Pressures and Basalt Magma Genesis," Am. Mineral. **68**, 859–879 (1983).

310. C. R. Thornber, P. L. Roeder, and J. R. Foster, "The Effect of Composition on the Ferric–Ferrous Ratio in Basaltic Liquids at Atmospheric Pressure," Geochim. Cosmochim. Acta **44**, 525–532 (1980).

311. R. N. Thompson, "Phase–Equilibria Constraints on the Genesis and Magmatic Evolution of Oceanic Basalts," Earth Sci. Rev. **24**, 161–210 (1987).

312. C. K. Thompson, V. P. Slater, K. R. Stockstill, *et al.*, "An Evaluation of the Igneous Crystallization Programs—MELTS, MAGPOX, and COMAGMAT: I. Does One Size Fit All?" in *Abstracts of LPS XXXIV, 2003*, pdf-1881.

313. P. Thy and G. E. Lofgren, "Experimental Constraints on the Low-Pressure Evolution of Transitional and Mildly Alkalic Basalts: The Effect of Fe–Ti Oxide Minerals and the Origin of Basaltic Andesites," Contrib. Mineral. Petrol. **116**, 340–351 (1994).

314. C. E. Tilley, "Some Aspects of Magmatic Evolution," J. Geol. Soc. (London) **106**, 37–50 (1950).

315. M. J. Toplis and M. R. Carroll, "An Experimental Study of the Influence of Oxygen Fugacity on Fe–Ti Oxide Stability, Phase Relations, and Mineral–Melt Equilibria in Ferro-basaltic Systems," J. Petrol. **36**, 1137–1170 (1995).

316. M. J. Toplis and M. R. Carroll, "Differentiation of Ferro-Basaltic Magmas under Conditions Open and Closed to Oxygen: Implications for Skaergaard Intrusion and Other Natural Systems," J. Petrol. **37**, 837–858 (1996).

317. M. J. Toplis, G. Libourel, and M. R. Carroll, "The Role of Phosphorus in Crystallization Processes of Basalt: An Experimental Study," Geochim. Cosmochim. Acta **58**, 797–810 (1994a).

318. M. J. Toplis, D. B. Dingwell, and G. Libourel, "The Effect of Phosphorus on the Iron Redox Ratio, Viscosity, and Density of an Evolved Ferrobasalt," Contrib. Mineral. Petrol. **117**, 293–304 (1994b).

319. D. R. Tormey, T. L. Grove, and W. B. Bryan, "Experimemtal Petrology of Normal MORB near the Kane Fracture Zone: 22°–25° N, Mid-Atlantic Ridge," Contrib. Mineral. Petrol. **96**, 121–139 (1987).

320. A. H. Treiman and S. R. Sutton, "Petrogenesis of the Zagami Meteorite: Inferences from Synchrotron X-ray (SXRF) Microprobe and Electron Microprobe Analyses of Pyroxenes," Geochim. Cosmochim. Acta **56**, 4059–4074 (1992).

321. V. P. Trubitsyn and E. V. Kharybin, "Convection in Magma Chambers Produced by Inversion in Distribution of Sinking Crystals," Phys. Solid Earth **33**, 382–386 (1997).

322. R. M. Tyson and L. L. Y. Chang, "The Petrology and Sulfide Mineralization of the Partridge River Troctolite, Duluth Complex," Can. Mineral. **22**, 23–38 (1984).

323. K. Uto, "Variation of Al_2O_3 Content in Late Cenozoic Japanese Basalts: A Reexamination of Kuno's High-alumina Basalt," J. Volcanol. Geotherm. Res. **29**, 397–411 (1986).

324. M. Wadhwa, H. Y. McSween, Jr., and G. Crozaz, "Petrogenesis of Shergottite Meteorites Inferred from Minor and Trace Element Microdistributions," Geochim. Cosmochim. Acta **19**, 4213–4229 (1994).

325. L. R. Wager, "The Major Element Variation of the Layered Series of the Skaergaard Intrusion and Re-Estimation of the Average Composition of the Hidden Layered Series and of the Successive Residual Magmas," J. Petrol. **1**, 364–398 (1960).

326. L. R. Wager and G. M. Brown, *Layered Igneous Rocks* (Oliver, Edinburgh, 1967).

327. L. R. Wager and W. A. Deer, "Geological Investigations in East Greenland: III. The Petrology of the Skaergaard Intrusion, Kangerdlugssuaq, East Greenland," Meddelelser om Gronland **105** (4), 1–352 (1939).

328. D. Walker, T. Shibata, and S. E. DeLong, "Abyssal Tholeiites from the Oceanographer Fracture Zone: II. Phase Equilibria and Mixing," Contrib. Mineral. Petrol. **70**, 111–125 (1979).

329. J. S. Weaver and C. H. Langmuir, "Calculation of Phase Equilibrium in Mineral–Melt Systems," Comput. Geosci. **16**, 1–19 (1990).

330. W. B. White, "Numerical Determination of Chemical Equilibrium and Partitioning of Free Energy," J. Chem. Physics **46**, 4173–4175 (1967).

331. R. A. Wiebe, "Silicic Magma Chambers as Traps for Basaltic Magmas: The Cadillac Mountain Intrusive

Complex, Mount Desert Island, Maine," J. Geol. **102**, 423–437 (1994).

332. B. J. Wood and D. G. Fraser, *Elementary Thermodynamics for Geologists* (Oxford Univ. Press, Oxford, 1977; Mir, Moscow, 1981).
333. T. L. Wright and P. C. Doherty, "A Linear Programming and Least Squares Computer Method for Solving Petrological Mixing Problems," Geol. Soc. Am. Bull. **81**, 1995–2008 (1970).
334. H.-J. Yang, R. J. Kinzler, and T. L. Grove, "Experiments and Models of Anhydrous, Basaltic Olivine–Plagioclase–Augite Saturated Melts from 0.001 to 10 kbar," Contrib. Mineral. Petrol. **124**, 1–18 (1996).
335. A. A. Yaroshevskii, D. A. Ionov, Yu. V. Mironov, *et al.*, "Petrography and Geochemistry of the Ioko–Davyren Layered Dunite–Troctolite–Gabbro–Norite Pluton, Northern Baikal Area," in *Petrology and Ore-Bearing Potential of Natural Rock Assemblages* (Nauka, Moscow, 1982), pp. 86–117 [in Russian].
336. H. S. Yoder, Jr. and C. E. Tilley, "Origin of Basalt Magmas: An Experimental Study of Natural and Synthetic Rock Systems," J. Petrol. **3,** 342–532 (1962).
337. Y. Zhang, "Mechanical and Phase Equilibria in Inclusion-Host Systems," Earth Planet. Sci. Lett. **157**, 209–222 (1998).